Investigation of head-neck tapers in modular hip prostheses

Halimat-Shaddiya Yewande Raji

Submitted in accordance with the requirements for the degree of Doctor of Philosophy

School of Engineering and Materials Sciences

Queen Mary, University of London

September 2017

Supervisor: Professor Julia Shelton

Statement of Originality

I, Halimat-Shaddiya Yewande Raji, confirm that the research included within this thesis is my own work or that where it has been carried out in collaboration with, or supported by others, that this is duly acknowledged below and my contribution indicated. Previously published material is also acknowledged below.

I attest that I have exercised reasonable care to ensure that the work is original, and does not to the best of my knowledge break any UK law, infringe any third party's copyright or other Intellectual Property Right, or contain any confidential material.

I accept that the College has the right to use plagiarism detection software to check the electronic version of the thesis.

I confirm that this thesis has not been previously submitted for the award of a degree by this or any other university.

Signature: H-S Y Raji

Date:15/09/17

Abstract

Corrosion at the head-neck junction of total hip replacements is a poorly understood phenomenon with an incidence of 1 - 2 %. Concerns around taper junction corrosion have focused on design factors including changes in taper surface topography and geometry as well as operating conditions such as high bearing surface friction and fluid ingress-egress at the taper junction. Hence, this thesis considered 3 aspects of the head taper junction namely: (1) frictional torque at the bearing surface and below the taper junction for varying head sizes and bearing material combinations, (2) Cobalt and Chromium ion release from CoCr/Ti taper junctions, (3) FE analysis of tapers utilising variables including taper length, material, angle, and clearance under loading conditions representative of walking, hip simulator profiles and stair climb.

Bearing friction and the torque about the taper axis beneath the taper junction were positively correlated with the head size (R^2 = 0.57 $_{\text{bearing friction}}$, R^2 = 0.88 $_{\text{torque}}$) and average surface roughness (R_a) (R^2 = 0.66 $_{\text{bearing friction}}$, R^2=0.79 $_{\text{torque}}$) of the femoral head. Torque generated on large MoP bearings (0.93 ± 0.2 Nm) was found to be comparable to MoM (0.81 Nm). The median cumulative Cr release rate was at least 2 times greater than that of Co (0.0220 ppb/cycle Cr relative to 0.0109 ppb/cycle Co) due to the acidic environment utilised in the accelerated tests. No statistically significant difference in ion release was found, between the trunnions of different surface finishes.

Finite element analyses showed that the largest gaps generated at the mouth of the taper, were associated with smaller taper contact areas. Clearances within ±0.1° enabled the tapers to engage over comparable lengths and therefore did not show differences in taper opening, showing this was influenced by the taper engagement length rather than location (proximal or distal) of contact. Stair climb loading generated the largest taper gaps (80 μm) and surface stresses on the head taper (1200 MPa); these were greatest on the shortest

trunnion. Although the stair climb loading condition is not currently mandated in testing THR devices, its use could provide a more accurate prediction of taper performance *in vivo* and may be beneficial to ‘beyond compliance’ initiatives to improve implant performance.

Acknowledgements

Julia Shelton, I really appreciate your efforts with the endless proofreading and corrections. Thank you for providing me with the opportunity to undertake the doctoral research journey. I am a better person for it both personally and professionally.

I would like to express my gratitude to Corin Group plc for their financial support and supply of test components and to Wallwork Ltd for helping with experimental measurements.

To the SEMS technical support team: Douge Thompson, Dennis Ife, Thomas Baumard and Ben Milsom, thank you so much for helping with manufacturing, modifications and equipment troubleshooting. I wish you all the best karma in your future endeavours.

Shaz, thank you for inspiring and encouraging me to keep fit during this process.

Alison, Richard, Shah, Patricia, Mouna, Burcu, Claire, I can't thank you enough for listening and letting me vent when I needed to. Ang, Damarys, thank you for sharing your talents with me. It was by far the best part of the journey. To everyone who contributed to and partook in deep belly laughs and fond memories, my gratitude is immense.

Lastly, I would like to thank my family for their unwavering support and belief in me.

Thank you all.

Contents

List of Figures

List of Tables

Abbreviations

AAS	Atomic Absorption Spectroscopy
ALTR	Adverse Local Tissue Reaction
ARMD	Adverse Reaction to Metallic Debris
CoC	Ceramic-on-Ceramic
CoP	Ceramic-on-Polyethylene
DAQ	Data acquisition
EDX/EDS	Energy-Dispersive X-ray Spectroscopy
FAAS	Flame Atomic Absorption Spectroscopy
FEA	Finite Element Analysis
GFAAS	Graphite Furnace Atomic Absorption Spectroscopy
HXLPE	Highly crosslinked polyethylene
ICI	Inflammatory Cell Induced
ICP-MS	Inductively Coupled Plasma Mass Spectrometry
LHMoM	Large headed Metal-on-Metal
LHMoP	Large headed Metal-on-Polyethylene
MACC	Mechanically Assisted Crevice Corrosion
Mc	Million cycles
MoM	Metal-on-Metal
MoP	Metal-on-Polyethylene
PBS	Phosphate Buffered Saline
PSF	Pseudosynovial Fluid
ROM	Range of motion
ROS	Reactive Oxygen Species
SEM	Scanning Electron Microscopy
SF	Synovial Fluid
THR	Total Hip Replacement

Chapter 1. Introduction

Taper corrosion is a poorly understood phenomenon which was first reported in late 1980s (Gilbert et al., 2015a). However, there has been a resurgence in corrosion at the head neck junction stemming from large failure rates associated with large head metal-on-metal (LHMoM) devices where more than 25 % of components experienced failure in the form of adverse tissue reactions within the first decade (Eltit et al., 2017, Kurtz et al., 2013, Moga et al., 2013). The hypothesis for taper corrosion in LHMoM was that increased friction at the bearing surface, due to large head sizes and poor clearances, resulted in excessive torques and micromotion at the junction. Since then, the use of MoM components has reduced considerably; in 2016, MoP components accounted for approximately 60 % of the total primary THR procedures (National Joint Registry of England, 2016). The discontinued use of MoM along with the contraindications for CoP bearings suggests that the relative proportion of MoP components could increase in the future.

Higher friction factors have been reported in MoM devices (Brockett et al., 2007). They are also more susceptible to manufacturing precision. The phrase ‘if correctly engineered’ often precedes purported tribological advantages of MoM components (Isaac et al., 2006). Indeed, higher clinical failure rates have been reported in a widely implanted MoM THR system with clearances that were found to be out of tolerance so that very low or negative clearances resulted. It is hypothesised that this along with high acetabular cup angles may have contributed to edge loading and a breakdown of bearing surface lubrication thus increasing the bearing friction which is then transferred to the taper junction (Langton et al., 2016, Matharu et al., 2017). If edge loading does occur in MoP devices, it does not have tribological implications which increase friction (Fisher, 2011). For these reasons, it may have been thought that taper corrosion would not be a problem with MoP components. However, the first documented report of adverse tissue reactions due to taper corrosion was from MoP components (Morlock et al., 2016, Cooper et al., 2012b). Subsequently, there

have been several studies detailing the observation of MoP taper corrosion and associated pseudotumours in patients (Hussenbocus et al., 2015). Some of these reports have indicated an increase in the severity of corrosion and as well as more aggressive pseudotumours associated with MoP as compared to MoM devices (Eltit et al., 2017, Moga et al., 2013).

Research into taper corrosion has focused on issues related to taper surface topography, assembly conditions, trunnion flexural rigidity, changes in taper geometry (length and angle), head size and offset (Morlock et al., 2016, Hussenbocus et al., 2015, Jacobs, 2016). Of these factors, there is a consensus that increasing offset results in worse loading conditions at the taper junction. With respect to geometric and topographical features, if there was uniformity across manufacturers there may be reduced variability in performance. In the 1990s, attempts to ensure uniformity with the 'Euro taper' (ISO, document ISO/TC150/SC4 N117) failed because of the concern that it would encourage taper combinations which had not been previously evaluated together (Morlock et al., 2016, Scheuber et al., 2014). Indeed, in a 2015 review of the National Joint Registry for England and Wales, mixing tapers between manufacturers was found to occur in 3% of a sample population and associated with higher revision rates in CoP and MoP bearings (Tucker et al., 2015).

Regardless, even when the paired components are indicated for use, in extreme cases, taper junction failure has led to voluntary recalls by manufacturers even though the two cases were actually for modular neck tapers (Pivec et al., 2014). For other taper designs which remain on the market, the overall performance of tapers is variable; between 1-2% of tapers have been reported to corrode *in vivo* sometimes severely resulting in pain, adverse local tissue reactions and revision (Hussenbocus et al., 2015). It has become apparent that laboratory evaluations do not recreate the extent of *in vivo* taper corrosion (Hothi et al., 2017b, Whitehouse et al., 2015, Tan et al., 2015). This is certainly true of the lack of foresight with respect to the corrosion of smaller heads because it has been supposed,

perhaps based on the origin of the problem, that it is relevant only to large heads. However, smaller (28-32 mm) MoM and MoP heads also result in adverse tissue reactions due to taper corrosion (Lombardi et al., 2016, Tan et al., 2015, Triantafyllopoulos et al., 2016).

Tapers are currently only evaluated dynamically, through the ASTM fretting test; although this has been advantageous for measuring corrosion rates and evaluating the damage induced by long term loading (Schaaff, 2004), a constant load vector direction is used to conduct the test. It is therefore not able to replicate the toggling which has been observed in retrieved taper components (Langton et al., 2012). Toggling allows fluid ingress into the taper junction which may initiate either crevice corrosion or in the presence of micromotion, mechanically assisted crevice corrosion (MACC) (Morlock et al., 2016, Langton et al., 2012). Hip simulators are the gold standard for evaluating the tribological performance at the bearing surface of THRs *in vitro*, under loading and environment conditions comparable to the hip joint *in vivo*. The changing load vector which occurs during a simulator cycle makes them an attractive option for evaluating the performance of different taper designs.

Chapter 2. Literature Review

2.1 Total Hip Replacement devices

A hip replacement device is a prosthesis used to address diseased states of the hip joint including osteoarthritis, rheumatoid arthritis, congenital hip dysplasia and femoral neck fractures through a procedure known as total hip arthroplasty. Currently, there are approximately 90 000 primary procedures carried out annually in the UK (National Joint Registry of England, 2016) and the number of procedures in the US has been projected to reach 572 000 by 2030 (Kurtz et al., 2007).

The hip replacement device could be a total hip replacement (THR) or a hip resurfacing device. The former describes a combination of a head on stem which articulates with an acetabular cup that may include a shell (Figure 2-1). A total hip resurfacing device consists of a femoral component without a stem, that articulates with an acetabular component (Figure 2-1).

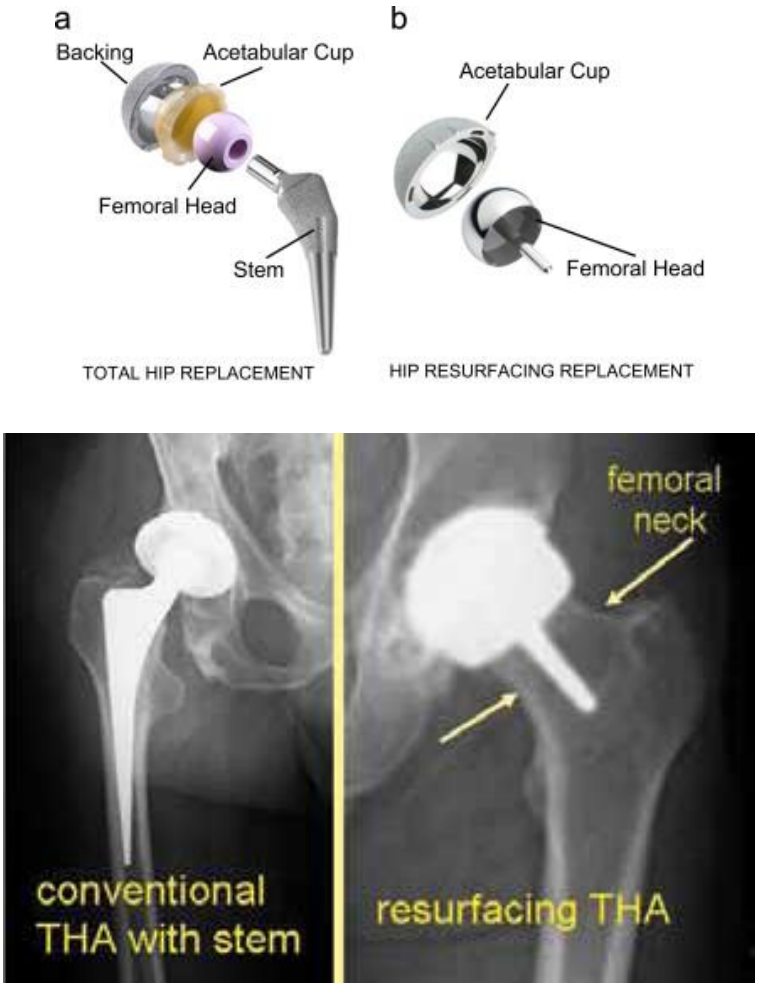

Figure 2-1a) A Total Hip Replacement and (b) a Hip Resurfacing device and their respective X-ray images (Mattei et al., 2011, Holzwarth and Cotogno, 2012)

Components of total hip replacement devices may be considered as monoblock or modular. Monoblock components (Figure 2-2) are manufactured as a unit without the possibility of disassembly whilst modular devices can be assembled and disassembled. Thus, any hip replacement may be modular or monoblock; designs have featured modularity within stems, between a head and a stem, within acetabular components and within the femoral head (Figure 2-3). Despite the variations in modularity, the most common type of femoral modularity is currently the head-neck or head-sleeve-neck junction. The head-sleeve-neck junction is essentially a head-neck junction with an adapter sleeve interposed between the head and neck, which is widely utilised at revision.

Figure 2-2 Mc-Kee Farrar prosthesis with a monoblock stem

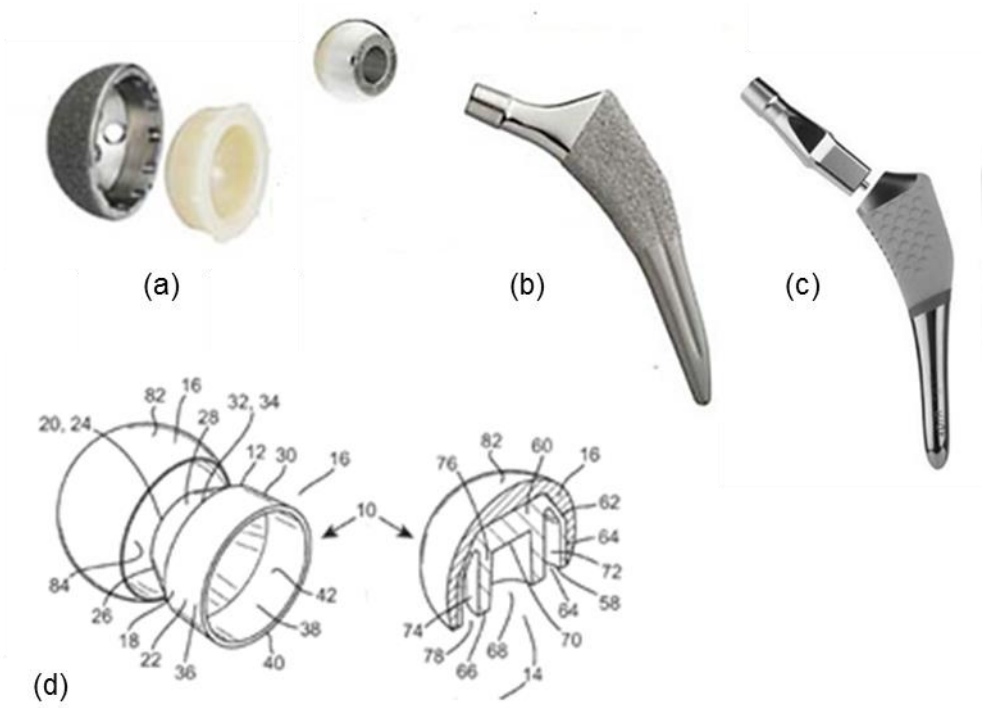

Figure 2-3 Different forms of modularity in total hip replacement (a) acetabular modularity (b) head-neck modularity (c) neck-stem modularity (d) femoral head modularity (Collins, 2011, Derar and Shahinpoor, 2015, Krishnan et al., 2013)

Modularity at the head-neck junction features a Morse taper (Figure 2-4). Stephen Morse invented Morse tapers in 1864 for joining two rotating parts in machine tooling (Hernigou et al., 2013). It is a type of self-holding taper wherein the components which constitute the junction are held together by friction with the intention of preventing relative motion between them (Oberg et al., 2012). Morse tapers were introduced to THAs in 1970s to provide choice with head-neck combinations optimised for their specific function. Also, modularity facilitates

the restoration of the hip centre by allowing alterations to be made to the offset, version and length of the femoral components independent of the stem fixation (Pastides et al., 2013). Furthermore, in the case of younger patients, hip replacement device may not outlast the patient; therefore, a revision procedure is often necessary. When a modular device is used, a well-fixed stem need not be necessarily removed to replace the bearing surface thus minimising bone loss (Goyal et al., 2014).

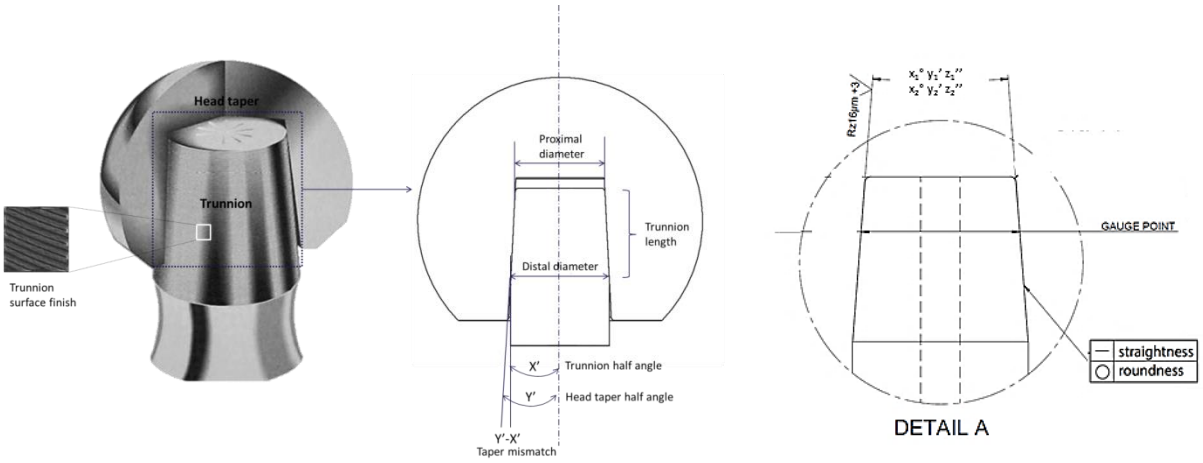

Figure 2-4 Features of a Morse taper between the femoral head and stem adapted from Hernigou et al. (2013)

2.1.1 Taper Design

Hip replacement designs feature a combination of different materials that are optimised for their specific function. Cobalt-chromium-molybdenum (CoCr) alloys or ceramics are used to manufacture femoral heads due to their high hardness, scratch and wear resistance (Swaminathan and Gilbert, 2012, Goldberg et al., 2002). Thus, head tapers are fabricated from CoCr or ceramics which could be Alumina or Zirconia-toughened alumina (Kurtz et al., 2013). These heads are paired with cobalt-chromium-molybdenum, titanium alloy or stainless steel (316L) trunnions. Titanium alloys are better suited for the fabrication of a stem than CoCr alloy or stainless steel alloy due to their relative modulus and reduction in the likelihood of stress shielding. Ti-6Al-4V is the most commonly used titanium alloy in hip

prostheses; however, the concern about the toxicity of vanadium and aluminium prompted the development of new alloys, Ti-12Mo-6Zr-2Fe (TMZF) and Ti-13Nb-13Zr (Raju et al., 2017, Wang, 1996). TMZF and Ti-13Nb-13Zr have lower modulus values than Ti-6Al-4V alloy, as well as higher tensile strength and toughness (Porter et al., 2014, Lee and Hwang, 2014, Wang, 1996). Recently, however, it has been suggested that the lower elastic modulus of newer titanium alloys may negatively impact the performance of the taper junction.

Taper sizes are specified with respect to the approximate proximal and distal diameters in mm. Hence available sizes include 8/10, 9/11, 10/12, 11/13, 12/14 and 14/16. There are also tapers with proprietary names including the V40, C-taper, Type-I, Type-II and PCA (Table 2-1). Contemporary designs feature smaller proximal and distal diameters as well as shorter lengths to avoid impingement of the prosthetic neck against the acetabular component and improve the range of motion (ROM) possible (Morlock et al., 2011). Hence, trunnion lengths have been reduced from 20 mm to below 10 mm and 12/14 and V40 tapers are more commonly used in place of 14/16 tapers (Morlock, 2015). Although two tapers may have the same proximal and distal diameter, the angle of approach from the bottom to the top diameter can vary (Bisseling et al., 2013) (Figure 2-5). A range of angles exist for Morse tapers used within implants (Hernigou et al., 2013) . The original Morse taper angle was a relatively small angle of 2.833°, but in current joint replacement devices, the taper angles range between 2 and 18° (Hernigou et al., 2013, Tan et al., 2015).

Table 2-1 The proximal and distal diameters of a range of taper designs: adapted from Triantafyllopoulos et al. (2016)

Taper design	Proximal diameter (mm)	Distal diameter (mm)
11/13	11.2±0.1	13.5±0.1
12/14	12.5±0.7	13.7±0.7
C-taper	12.4±0.4	13.8±0.7
V40	11.3±0.4	13.3±0.6
Type-I	11.7±0.9	12.7±0.9
PCA	12.3±0.7	13.3±0.5

Figure 2-5 Variation in a 12/14 taper (Hernigou et al., 2013)

Other design parameters included in taper specifications include surface finish, roundness and straightness (Hernigou et al., 2013), Figure 2-4. Machined profiles were introduced to metallic trunnions for use with ceramic heads in order that they undergo plastic deformation upon the mating of the taper resulting in increased contact area and a reduction in the tensile stresses at the interface, thereby increasing the fracture strength of the ceramic head (Drouin and Cales, 1994). Despite their initial origin, trunnions with threaded stems are commonly mated with both ceramic or CoCr head tapers (Arnholt et al., 2014, Munir et al., 2013). Consequently, with respect to surface profile, trunnions may be threaded (microgrooved) or smooth (Arnholt et al., 2014). A smooth trunnion has ground or polished surfaces, threaded trunnions are spiral machined to include microridges or microgrooves (Figure 2-6) (Gilbert et al., 2015a).

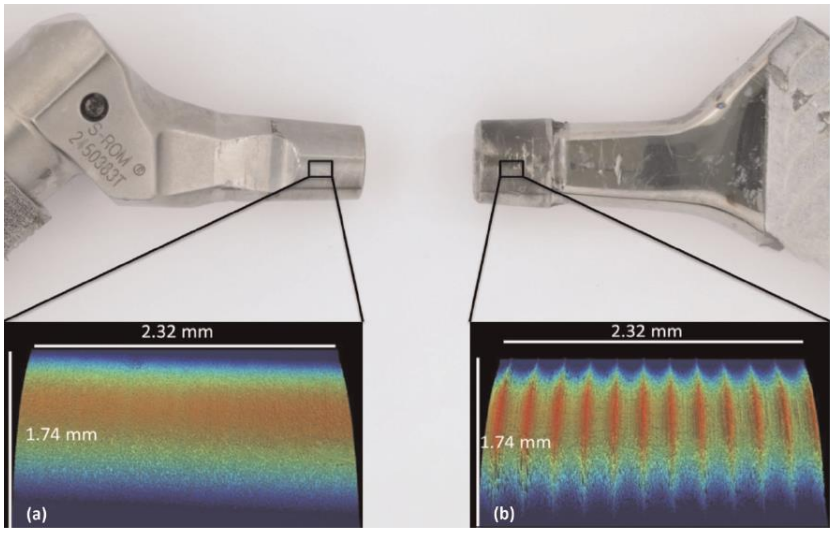

Figure 2-6 Smooth and rough trunnion; scale not shown in original image (Hothi et al., 2015)

The deviation of a line on the taper surface from a flat surface defines the taper straightness (Figure 2-7) (Underwood et al., 2012, Scheuber et al., 2014). A measure of roundness of the circumference of a cross section along the taper is defined as the taper roundness (Figure 2-7). Hence it measures the deviation at each level of the cone from a perfect circle (Underwood et al., 2012, Scheuber et al., 2014).

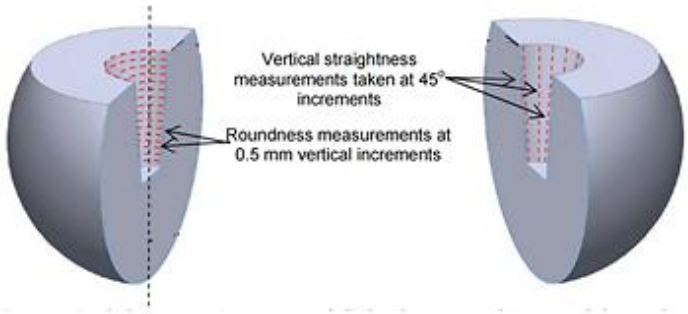

Figure 2-7A schematic of roundness and straightness measurements adapted from Underwood et al. (2012)

2.1.2 Taper Mechanics: loading and environment

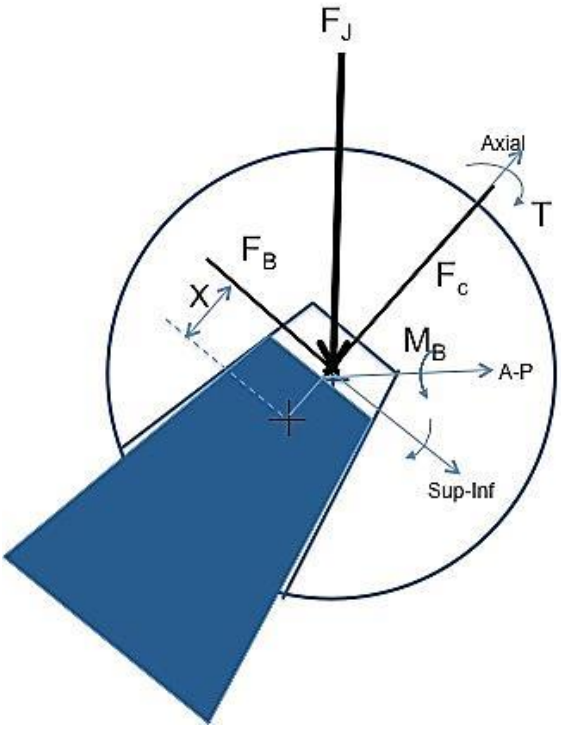

Figure 2-8 Forces at the taper junction M_B=bending moment, F_J=joint force, F_B= bending component of the joint force, F_c= axial compressive force along taper axis, T=torsional moment due to bearing friction, x= axial distance from the head centre to the point of taper support; adapted from Gilbert et al. (2015a)

Tapers are used to transfer the loads applied at the femoral head, along the taper axis through to the stem. The loads on a Morse taper on a THR device are compressive, torsional forces as well as bending moments (Figure 2-8). Compressive radial stresses arise from the radial component of the joint force, the impaction force and the press-fit stresses (Bishop et al., 2013). The joint force at the hip has been measured for various activities of daily living such as walking, sit-to-stand, stair climb, sporting activities (jogging) and also uncontrolled events such as stumbling (Figure 2-9). Press-fit stresses which are generated due to the surgical impact force along the axis of the taper and the axial component of the joint force, are responsible for the dissociation strength of the taper (Figure 2-10) (equation 1) (MacLeod et al., 2016, Bishop et al., 2013). These stresses consist of both normal and

shear stresses (Figure 2-10) wherein the shear stress is the product of the normal stress and the coefficient of friction at the taper junction.

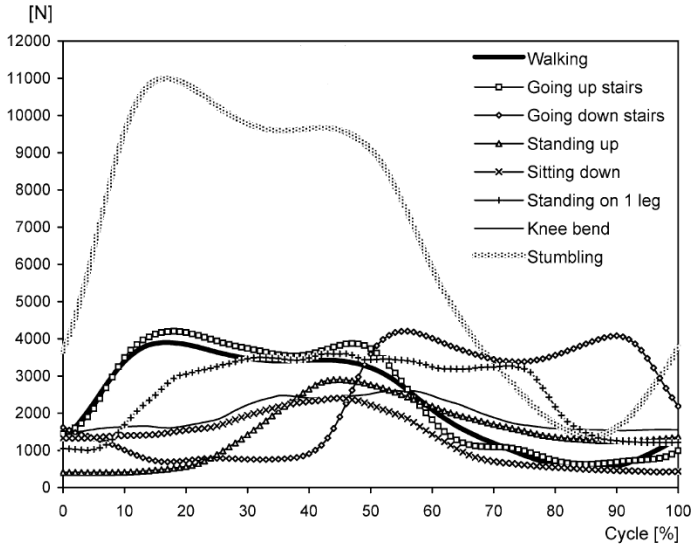

Figure 2-9 Peak resultant force for various activities; x axis measured as a percentage of total time taken to complete the loading cycle where walking = 1.10s, stair ascent = 1.59s, stair descent = 1.44s, sit-to-stand transfer = 2.49s, stand-to-sit transfer = 3.72s, single-legged stand=6.70s, knee bend=4.67s, stumbling=1.10s (Bergmann et al., 2001)

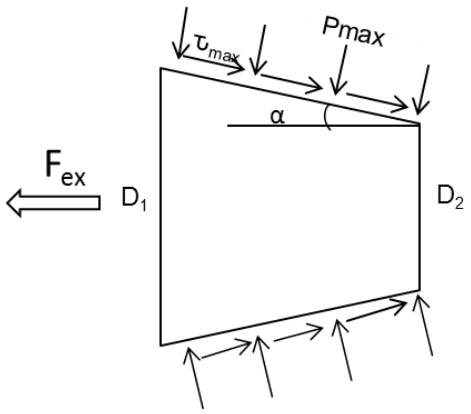

Figure 2-10 Schematic of extraction forces and stresses at a taper

$$F_{ex} = \mu A p \cos\alpha - A p \sin\alpha \quad (1)$$

where F_{ex} = extraction force

μ = coefficient of friction

p = mean taper pressure

A = contact area

Torsional moment is generated at the taper due to friction at the bearing surface and if aligned about the taper axis, can act as a removal torque where increased articular surface friction induces rotational micromotion about the neck axis (Schafer et al., 1998, Elkins et al., 2014). The off axis anatomy of the native hip will additionally induce a bending moment which will be experienced by the taper junction. Bending moments at the taper junction are a product of the transverse component of the joint force and the distance between the taper engagement position and the head centre ($F_B x$, Figure 2-8); however, they may also arise from bearing surface friction (Gilbert et al., 2015a).

The taper environment is the same as the rest of the implant which is surrounded by extracellular tissue fluid. This environment contains organic and inorganic components (Figure 2-11) at a neutral pH of 7.2 to 7.4. However, as a result of inflammation and infection, the pH could become more acidic or alkaline respectively (Davies et al., 2005).

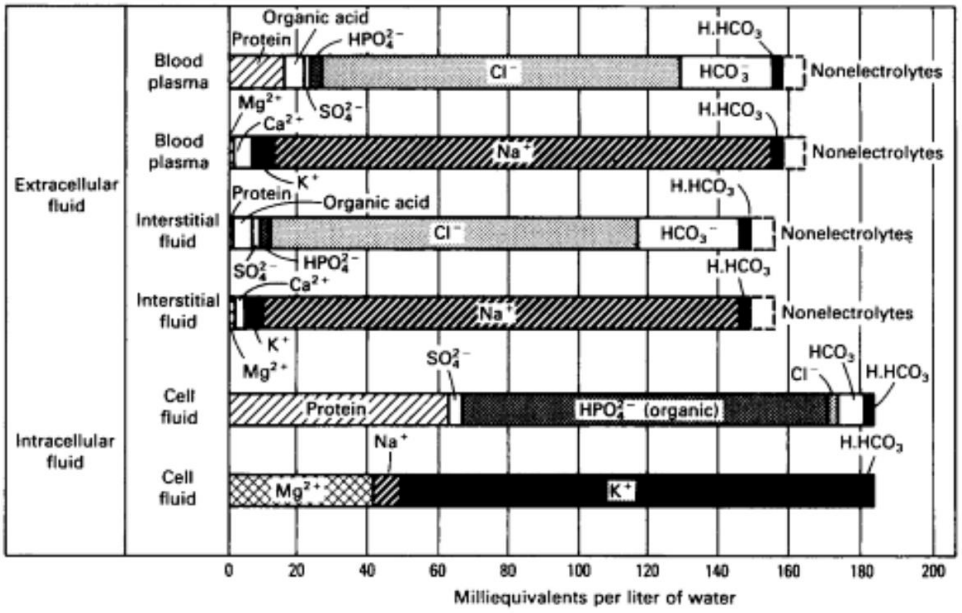

Figure 2-11 Ionic concentration of fluids *in vivo* (Davis, 2003)

Metals used in implants are artificially over-passivated to build up a protective oxide film before implantation (Zeng et al., 2015). These passive layers are typically 1 – 4 nm thick and serve as kinetic barriers to limit corrosion reactions in biological environments (Mali, 2016, Goldberg and Gilbert, 1997). During implantation, the oxide layer may be damaged. However, it has been reported that *in vivo*, a Ti alloy component oxidises preferentially to a CoCr alloy component and the oxide layer formed on the former will be much thicker resulting in increased hardness and protection of the substrate metal from abrasive damage (Moharrami et al., 2013).

2.2 Challenges with Femoral Modularity

During its service life, an implant undergoes cyclic loading (Goldberg et al., 1997). Depending on the fit of the components at the taper junction, relative motion, initiated by either the compressive joint force or the moment about the A-P axis (Figure 2-8), may ensue (Elkins et al., 2014, Gilbert et al., 2015a). Micromotion which occurs parallel to the axis of loading along the taper surfaces of the order of 10-100μm, results in fretting (Figure 2-14) (Viceconti et al., 1997). This oscillatory motion has been described as being capable of

removing the passive layer by fracture of the oxide layer present on the taper surfaces, which results in the production of particulate debris capable of stimulating inflammatory reactions or causing third body wear at the bearing surface (Bobyn et al., 1994, Goldberg et al., 1997).

The assembly of the head and trunnion creates a crevice at the taper junction. Cyclic physiological loading in the presence of fluid, may generate a wicking action which could draw fluid into the taper junction (Jani et al., 1997). Therefore, stagnant fluid is able to collect within crevices which can initiate crevice corrosion. Corrosion is a destructive electrochemical reaction between a metal and its environment. Although there are different types of corrosion, some forms of corrosion have been identified as pertinent to orthopaedic alloys including pitting, crevice, galvanic, intergranular, stress-corrosion cracking and corrosion fatigue (Hansen, 2008).

Crevice corrosion occurs in the presence of restricted areas on metal surfaces which form crevices which are just wide enough to permit fluid entry yet sustain a stagnant zone (Fontana, 2005). At the start of the process, oxidation and reduction reactions are balanced. Every liberated electron from the oxidation reaction is recruited in the reduction process; consequently, oxygen levels decrease with continuous reduction reactions in the crevice (Fontana, 2005). Continued oxygen consumption in the crevice results in depleted oxygen levels and the restrictive crevice geometry prevents the exchange of fresh fluid to renew the oxygen concentration (Cartner et al., 2016). Metallic dissolution continues within a crevice (equation 2), the metal ions also react with water (hydrolysis) (equation 4) which increases the acidity by the generation of hydrogen ions (Sridhar et al., 2005). Reduction reactions will also occur outside of the crevice resulting in an influx of anions from the adjacent environment into the crevice (Bryant and Neville, 2016). As a result of all these reactions, the crevice solution becomes concentrated with metallic chlorides. The metal chlorides can also undergo hydrolysis to form metal hydroxides and hydrochloric acid (HCl) (equation 5)

resulting in a further reduction in pH; active corrosion of the bulk metal occurs when the pH of the crevice solution is high enough to breakdown the passive film (Bryant and Neville, 2016). The reduction of pH can also lead to pitting and etching of the surfaces (Cartner et al., 2016) where etching is also a form of corrosion attack (Collier et al., 1992).

$$M \rightarrow M^{n+} + ne^{-}(\text{oxidation}) \quad (2)$$

$$O_2 + 2H_2O + 4e^{-} \rightarrow 4OH^{-}\ (\text{reduction}) \quad (3)$$

$$M^{+} + H_2O \rightarrow MOH + 3H^{+}(\text{hydrolysis}) \quad (4)$$

$$M^{+}Cl^{-} + H_2O \rightarrow MOH + H^{+}Cl^{-}(\text{hydrolysis}) \quad (5)$$

With respect to THR devices, a model of mechanically assisted crevice corrosion (MACC) (Figure 2-12) has been postulated. MACC describes a corrosion process initiated by relative movement at the interface due to mechanical loading and the interactive effects of fluid ingress into a crevice such as the taper junction (Pansard et al., 2012, Cartner et al., 2016, Goldberg and Gilbert, 1997). After the fracture of the passive layer, the base metal is exposed to the corrosive physiological fluid. Repassivation occurs using dissolved oxygen in solution. Continuous loading sustains the depassivation-repassivation eventually depletes the dissolved oxygen in the crevice (Goldberg et al., 1997), thus initiating the crevice corrosion mechanism described above. According to Van Citters et al. (2015), the susceptibility of a taper junction to crevice corrosion is defined by a scaling factor which is related to the square of a crevice depth divided by its width. Wherein, a large scaling factor is related to a deeper crevice and thus is associated with a reduced pH. Further, the oxide of CoCr becomes thermodynamically unstable at a pH below 3.5 and less likely to reform causing active corrosion of the base metal (Cartner et al., 2016).

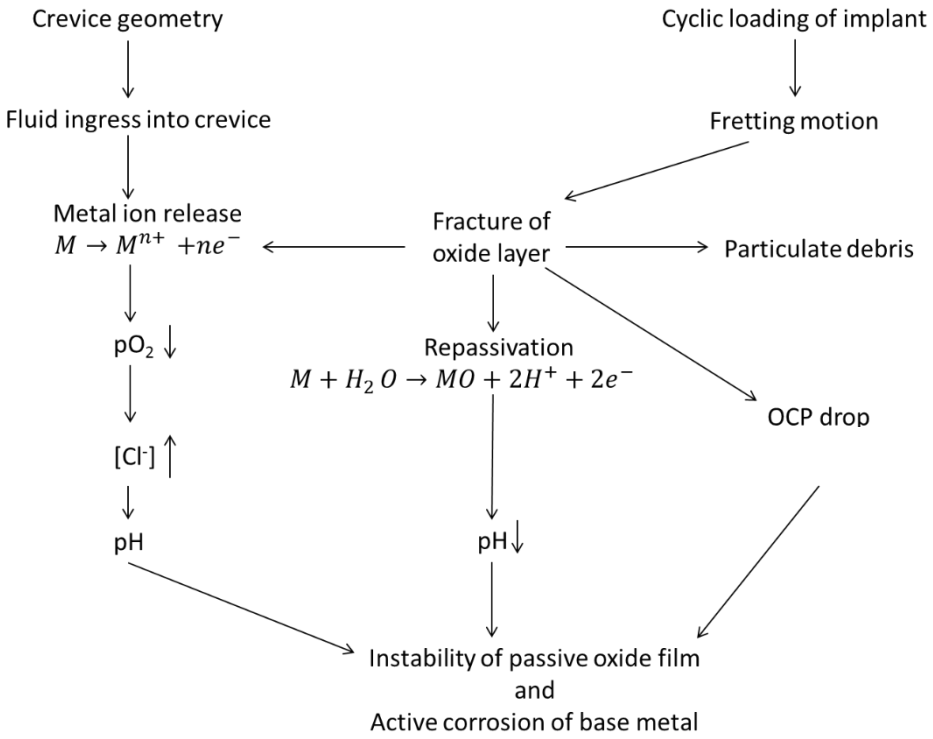

Figure 2-12 MACC model (Goldberg et al., 1997, Mali, 2016)

2.2.1 Taper corrosion

Head-neck taper corrosion was identified as a clinical concern in the 1980s and is the most common site of corrosion in single-site femoral component modularity in primary and revision THR procedures (Liodakis et al., 2015). Earlier reports of corrosion were attributed to less rigorous design tolerances, material processing and manufacturing techniques (wrought or cast) (Lavernia et al., 2015). Subsequent improvements coupled with the introduction of MoM hip implants resulted in a shift in the focus from the taper junction to MoM bearing interface (Lavernia et al., 2015, Cooper, 2014). However, recent retrieval studies have brought renewed focus on fretting and wear at the taper (Lavernia et al., 2015) due to an increase in failure rates of large-diameter metal-on-metal bearings. Modern taper corrosion has been reported as one of the causes for hip implant failure (Witt et al., 2014). Its occurrence is widely variable with reported incidences of between 0 and 95% (Pourzal et

al., 2016, Liodakis et al., 2015, Cooper, 2014, Matthies et al., 2013); although the higher rates have been broadly associated with large-diameter metal-on-metal bearings.

Most of the studies with femoral modularity solely at the head-neck junction have shown that when corrosion is observed, it is often on the head taper. Where corrosion is observed on the stem, it is less severe. Generally, on the taper assembly, there is a higher degree of corrosion observed distally where there is exposure to physiological fluid (Tan et al., 2015, Triantafyllopoulos et al., 2016). Triantafyllopoulos et al. (2016) reported more severe fretting proximally on the trunnion and Del Balso et al. (2015) found that the central zone of the female taper showed increased fretting damage because it is the region where contact of the taper occurs.

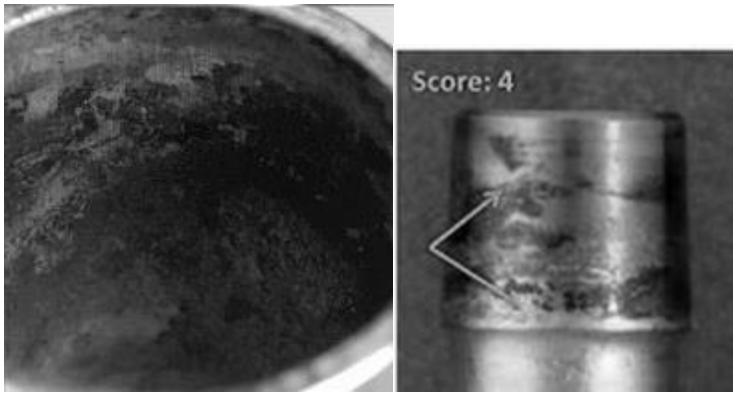

Figure 2-13 Head taper and trunnion corrosion (Higgs et al., 2016)

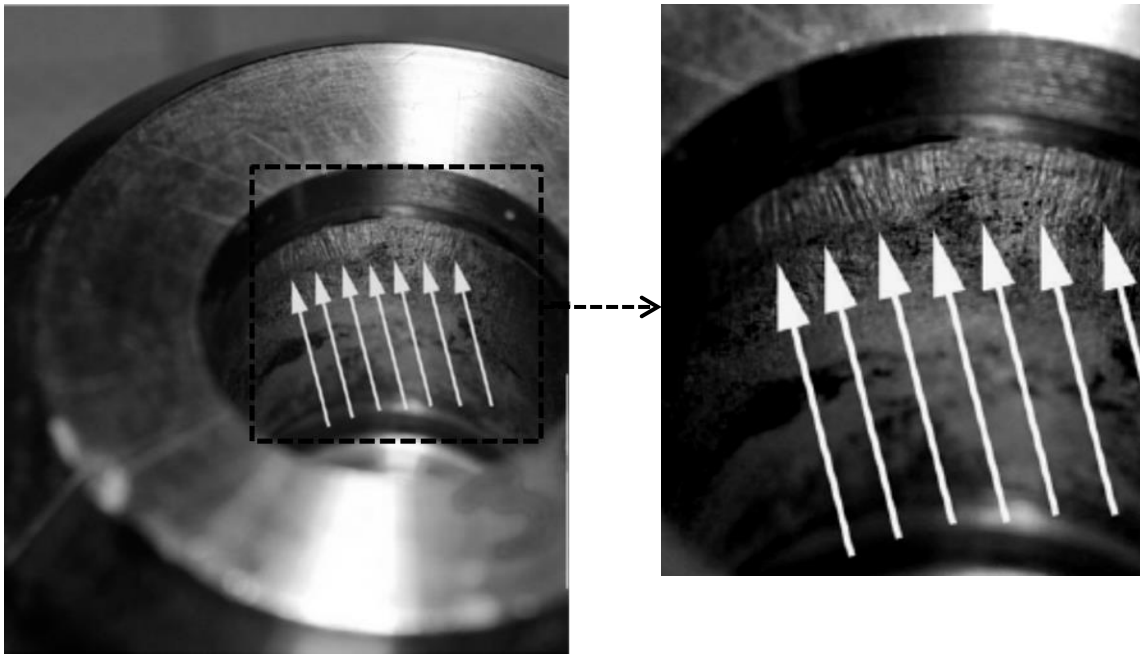

Figure 2-14 Fretting marks on a 36 mm CoCr femoral head (Morlock et al., 2016)

2.3 Effect of corrosion

Corrosion may be observed at modular junctions as either material loss or deposition (Witt et al., 2014). It generates ionic and particulate metallic products with associated increases in metal ion levels (Goyal et al., 2014) and adverse local tissue reactions (ALTR). Ionic products from CoCr alloys are predominantly Co^{2+} (Liao et al., 2013). The taper interface releases a significant amount of corrosion products (Lavernia et al., 2015) from either the male or the female taper (Matthies et al., 2013). Male tapers have been found to have negligible material loss. Matthies et al. (2013) reported a mean volumetric loss of 0.34 mm^3 from 36 femoral stems from titanium and cobalt chrome alloys; the group indicated that the mean volume of material lost from the head tapers was 3.6 mm^3 and concluded that the volumetric loss from the head taper is at least comparable to the loss from the acetabular bearing component but can be more than bearing wear. Although Langton et al. (2016) defined taper failure as head taper wear volume, of over 0.5 mm^3 with an asymmetric and circumferential wear pattern. Table 2-2 shows that the volumetric wear at the female taper

could exceed 20 times this value; in addition, this value may be considered conservative because the male tapers which were defined as having negligible material loss by Matthies et al. (2013) were in the range 0 – 0.83 mm^3.

Table 2-2 Range of volumetric material loss (mm^3/yr) †=mean± stdev *=not available

Bearing combination	Head taper	Male taper	References
MoM	0.46 –13.67	*	Langton et al. (2012)
MoM	0-4.29	0-0.36	Matthies et al. (2013)
MoM	0.593 - 4.871	0.005-0.006	Bishop et al. (2013)
MoM	1.96 ± 4.92†	0.02 ± 0.05	Witt et al. (2014)
	4.05 ± 5.48	1.28 ± 1.84	
MoM	0.0002 – 2.178	*	Hothi et al. (2015)
MoM	0.402 – 0.123	*	Brock et al. (2015)
*****	*	0.04 – 0.28	Bone et al. (2015)
MoM	0 - 3.45	*	Whittaker et al. (2016)
CoP MoP MoM	0–8.70	0–0.32	Kocagoz et al. (2016)
MoP	0.084	*	Hothi et al. (2017a)

Particulate corrosion products are found either at the taper interface or the entry to the taper junction (Figure 2-15a). The main solid corrosion product has been found to be chromium orthophosphate. Chromium orthophosphate particles are amorphous and translucent, irregularly shaped, green to yellow and range in size from submicron to 400 µm, (Jacobs et al., 1998); it has been found to be deposited loosely at the mouth of the taper junction thus able to migrate into the joint space (Figure 2-15b). Cobalt phosphate can also be found at severely corroded taper junctions. The thin layer (~ 20 µm) of crystalline oxides and chlorides formed inside the junction (Figure 2-15a) are susceptible to delamination from the surface (Hall et al., 2015). In the presence of Ti alloys, corrosion products can also include titanium oxides or hydroxides (Hall et al., 2015), which are seen as black, violet or white deposits which may be opaque or translucent (Jacobs et al., 1998). They are needle-

like, highly crystalline and can be an order of magnitude larger than cobalt and chromium particles (Hall et al., 2015).

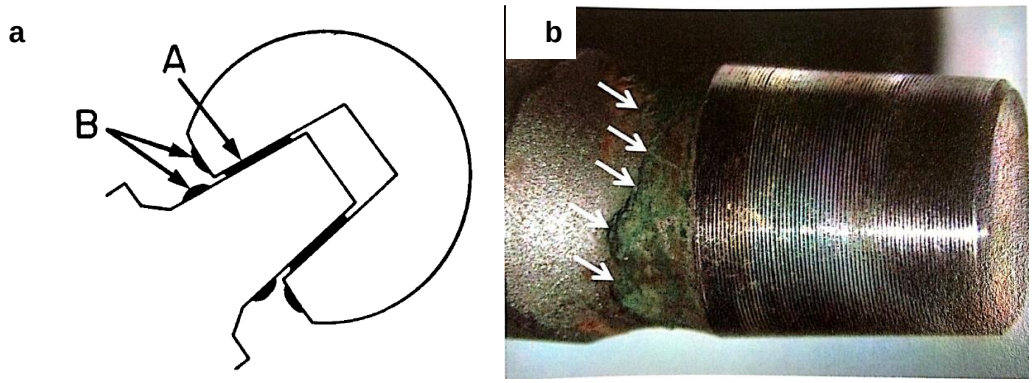

Figure 2-15 (a) Locations of corrosion products at a taper junction A= thin interfacial layer of mixed oxides and chlorides B=thicker deposits of chromium-orthophosphate hydrate-rich corrosion products (b) Chromium orthophosphate on a retrieved CoCr trunnion; adapted from (Jacobs et al., 1998, Hall et al., 2015)

The effects of both particulate and ionic corrosion products are widespread necrosis of the periprosthetic tissues, local synovitis, osteolysis, component loosening, and early failure (Hussenbocus et al., 2015, Jacobs et al., 1998). Adverse tissue reactions, also known as pseudotumours, have been identified a mechanism of failure in THR (Ricciardi et al., 2016) with symptoms including pain, fluid accumulation in the joint space, soft tissue necrosis and abductor muscle loss (Liodakis et al., 2015). Local tissue destruction coupled with abductor weakness sometimes additionally results in instability (Plummer et al., 2016). Implant fractures may occur (Berry et al., 2014), although these are extremely rare with devices with sole modularity at the head-neck junction. For dual modularity designs, they have been reported as the second most prevalent problem after ALTR with an incidence of 2.4 % reported in one dual modularity design (Cooper, 2014). The generation of debris at the taper may result in the ceramic bearing failure if the particles were to migrate to the bearing surface and initiate a 3rd body wear mechanism (Huber et al., 2009).

Aside from localised effects, ionic and particulate corrosion products are feared to have systemic implications in remote organs. This is due to their dispersion via lymphatic and

haematogenous transport (Hall et al., 2015). Particles have been discovered in the liver, spleen, abdominal lymph nodes and placenta of patients with THRs (Osman et al, 2016). Divalent Co is most commonly found nonetheless, it can also exist in its trivalent state Co(III) (Valko et al., 2005). Systemic toxicity of cobalt has been reported to result in cardiomyopathy, depression, weight loss or gain, haemolytic anaemia, and local motor and sensory dysfunction (Cooper, 2014, Witt et al., 2014). The most common oxidation states of Cr are trivalent Cr(III) and hexavalent (Cr(VI)) (Afolaranmi et al., 2008). Cr(VI) has been reported to be highly genotoxic; however, it is detoxified by entering into the red blood cells and undergoing reduction to its trivalent state. The resulting Cr(III) exhibits reduced toxicity in comparison to Co(II) (Kwon et al., 2009, Posada et al., 2015).

Ultimately, a component which induces symptoms, produces elevated metal levels recorded in the blood or urine, and causes localised soft-tissue reactions may be considered to be corroded and will need to be revised (Cooper, 2014). The outcome of revisions when corrosion is present has been found to be significantly worse than revisions when observable corrosion is not present (Cooper, 2014, Liodakis et al., 2015). The female taper (for single taper designs) is known to corrode preferentially over the trunnion (Hothi et al., 2016b). Therefore, in revising the implant due to clinically significant symptomatic corrosion, a metal head is most commonly replaced with a ceramic head (Lanting et al., 2016). It has been suggested that the stem should be left *in situ* provided a taper lock can be achieved with a new head (Lanting et al., 2016) as the removal of a well-fixed stem would result in significant bone loss and soft tissue damage, delayed recovery as well as increased risks of femoral fracture (Goyal et al., 2014). Moreover, Goyal and associates showed that retaining a corroded yet well-fixed stem does not normally result in re-revision due to corrosion.

The revision of a corroded femoral component with a ceramic head has been shown to result in a rapid reduction in serum metal levels (Hussenbocus et al., 2015). Goyal and

associates (2014) also concluded that replacing a corroded head with a metal head does not appear to unfavourably affect the survivorship even when the stem is corroded.

2.4 Detection of taper corrosion

2.4.1 Clinical diagnosis

A painful THR may be suggestive of taper corrosion (Hussenbocus et al., 2015). However, it is difficult to ascertain this because other conditions such as bursitis, infection and loosening also present with pain (Pivec et al., 2014). Pivec et al. (2014) reported that corrosion presents as groin pain usually after a pain free period (1 – 2 years) with the patient feeling like their arthritis is returning. However, Pansard et al. (2012) countered the idea that an initial pain-free period is necessary when they reported a case of severe taper corrosion with no pain-free interval; therefore, a radiographic evaluation is required. Erosion of the bone adjacent to the taper junction is frequently reported due to increased ion exposure (Pivec et al., 2014, Moskal and Stover, 2015). Alternatively, an MRI with metal artefact reduction sequencing (MARS) protocols can be used to detect associated joint effusion or soft tissue masses; where an MRI is unavailable or contraindicated, an ultrasound may be used (Cooper, 2014). Tissue biopsies can be performed to confirm a diagnosis of an adverse reaction from taper corrosion (Cooper, 2014).

Further, Morlock et al. (2016) suggested that a Co/Cr ratio of more than 1.5 in conjunction with clinical symptoms is indicative of a malfunctioning taper. More commonly, the consensus is that elevated serum cobalt relative to chromium, with only minimally elevated serum chromium, indicates taper corrosion (Carli et al., 2015, Hussenbocus et al., 2015, Pivec et al., 2014, Plummer et al., 2016, Nodzo et al., 2017, McGrory et al., 2017). At a minimum, this represents a Co/Cr ratio greater than 1. Chromium is minimally elevated in serum as a result of the precipitation of chromium orthophosphate ($CrPO_4$) (McGrory and McKenney, 2016). These findings are different to the reported clinical findings from a heavily

wearing bearing surface of MoM THR wherein both ions increase in the same ratio (Jennings et al., 2016).

Ion analyses of serum, blood and urine have been performed predominantly utilising two methods namely Inductively Coupled-Mass Spectrometry (ICP-MS) or Atomic Absorption Spectroscopy (AAS).

An ICP mass spectrometer combines a high-temperature plasma source with a mass spectrometer wherein the ICP source ionises the atoms of the elements present in the sample and the ions are subsequently separated and detected by the mass spectrometer. The ICP is generated in a torch with three concentric quartz tubes using an induction coil and a radiofrequency (27-40 MHz) power supply (Montaser, 1998, Olesik, 2000). An oscillating current in the coil induces an intense magnetic field at the top of the torch (Thomas, 2004). A flow of argon is introduced between the two outermost tubes of the torch (Montaser, 1998). A high voltage spark is applied causing the argon atoms to be stripped of electrons. The electrons are accelerated by the oscillating magnetic field, colliding with more argon atoms, stripping off more electrons (Thomas, 2004). The continuous collision of atoms, ions and electrons, forms argon plasma of very high temperature (~10,000 K) (Sneddon and Butcher, 2002). The sample to be analysed is introduced into the central channel of the torch and thus the argon plasma (Levinson, 2001). This could be achieved by introducing an aspirated liquid or dissolved solid into a nebuliser or by the use of laser ablation of a solid sample (Vanhaecke, 2012). Once the sample aerosol is introduced into the ICP torch (Figure 2-16), the elements in the aerosol are converted into gaseous atoms and collisions between the atoms of the analyte and the electrons result in ionisation towards the end of the plasma. The ions are analysed in a vacuum via mass spectrometry and are separated by their mass-to-charge ratio (Vanhaecke, 2012). A detector receives an ion signal proportional to the concentration. The concentration of a sample can be determined through calibration with reference standards (Wang, 2010).

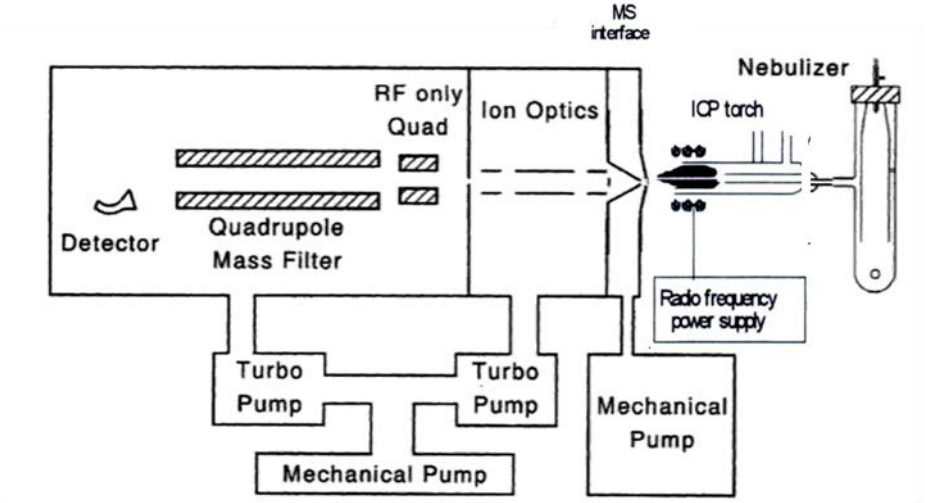

Figure 2-16 Schematic of ICP-MS instrument (Olesik, 2000)

In atomic spectrometry, the interaction of the sample with light provides qualitative and quantitative information about its constituent elements. A sample of interest is atomised by heating so that the atoms of the analyte absorb energy and are excited to a higher energy level (Levinson, 2001). The constituent elements can thus be identified and quantified by the absorption of specific wavelengths of light since there is a direct relationship between the amount of light absorbed and the concentration of the element in the light path (Levinson, 2001). Common atomisers used to excite the atoms are flame and furnace electrothermal (graphite furnace) (Sneddon and Butcher, 2002). These correspond to the Flame Atomic Absorption Spectroscopy (FAAS) and Graphite Furnace Atomic Absorption Spectroscopy (GFAAS) (Figure 2-17) techniques respectively.

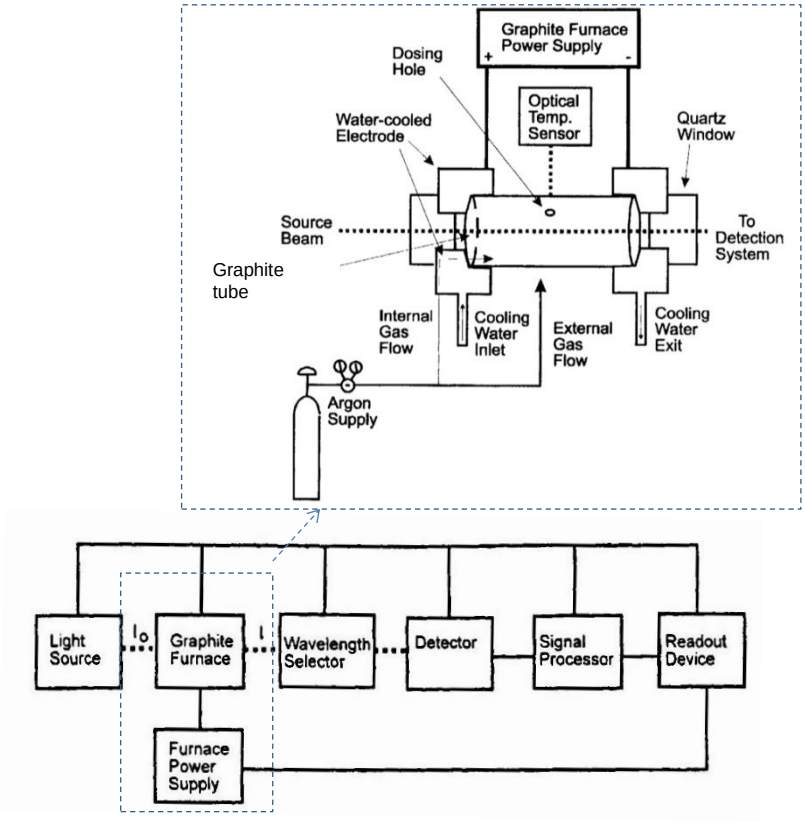

Figure 2-17 Schematic of GFAAS instrumentation adapted from Sneddon and Butcher (2002)

In the GFAAS technique, an incident light is used from a hollow cathode lamp or electrodeless discharge lamp (Schlemmer and Radziuk, 1999), corresponding to the excitation wavelength of the analyte of interest. A hollow graphite cylinder is placed in the path of the light. The analyte is introduced into the graphite tube through a dosing hole in the centre of the tube via a micropipette. The graphite tube is purged with an inert gas such as argon and a current heats the tube in stages to dry or evaporate, ash and atomise the sample at increasing temperatures up to 3000°C (Nadkarni, 1991). Atomisation of the sample generates a transient absorption signal (Figure 2-19) since absorbing atoms of the analyte diminish the intensity of the incident radiation I_o (Nadkarni, 1991). The reduction in intensity is dependent upon the absorption coefficient or absorptivity '*a*', the concentration of atoms '*c*' and to the length of the absorption volume or path length of the atomisation cell '*b*'

(Figure 2-18). The original radiation intensity is reduced by a logarithmic function so that the absorbance:

$$A = \log I_o/I = abc$$

where '*a*' and '*b*' are constants

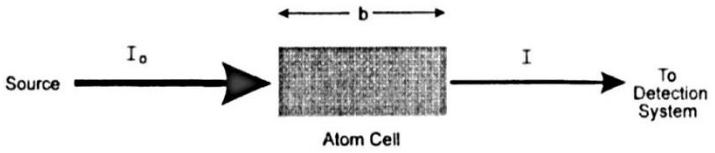

Figure 2-18 Schematic showing the incident and diminished intensities I_o and I and the path length b (Sneddon and Butcher, 2002)

The absorbance A has a linear correlation to concentration *c* that becomes non-linear at higher concentrations (Levinson, 2001). The relationship is used in calibrating the instrument by measuring the absorbance values of standard concentrations (Levinson, 2001). A calibration curve is generated and concentrations of samples of interest can then be calculated from their absorbance values.

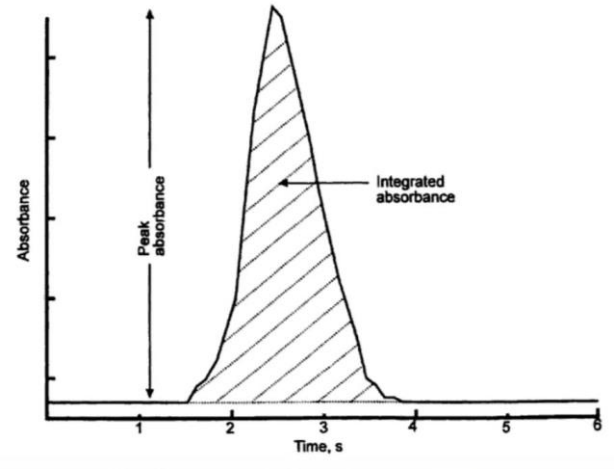

Figure 2-19 A transient GFAAS absorption signal (Butcher and Sneddon, 1998)

Alternatively, flames of air-acetylene or nitrous oxide-acetylene could be used as an atomisation source wherein the sample is nebulised into the flame This mode is termed Flame Atomic Absorption Spectroscopy (FAAS) (Pansu et al., 2001). In comparison to GFAAS, FAAS, requires a larger sample volume for analysis (~ml) (Levinson, 2001). As shown in Table 2-3, ICP-MS has detection limits an order of magnitude lower than AAS, and ICP-MS is capable of analysing multiple elements.

Table 2-3 Comparison between AAS, GFAAS, ICP-MS techniques (ThermoElemental, 2001)

		ICP-MS	AAS	
			GFAAS	FAAS
Detection limits (ppb)	Co	0.0001-0.001	0.5	5
	Cr	0.0001-0.001	0.025	6
Dynamic range		108	102	103
Precision (%)	Short term	0.5-2	0.5-5	0.1-1
	Long term	2-4	1-10	2-beam: 1-2 1-beam: <10
Sample throughput		All elements in < 1 minute	3-4 minutes per element	10-15 seconds per element

2.4.2 Laboratory evaluation

The occurrence and extent of corrosion can be confirmed in retrieved components using macroscopic and microscopic visual techniques including optical or electron microscopy (Whittaker et al, 2016). Along with electron microscopy, energy-dispersive x-ray spectrum (EDS) analysis can be used to confirm the elemental composition of corrosion deposits. Using imaging techniques, corrosion damage can be characterised by different surface features; these features include the transfer of machining features of the male taper onto the female taper surface known as *imprinting*. Pitting corrosion presents with several pits (Figure 2-20a) and intergranular corrosion (Figure 2-20b) exhibits material loss along grain boundaries (Hall et al., 2015).

Goldberg method (Table 2-4) is a semi-quantitative technique of evaluating, the extent of fretting and corrosion observed in components. This technique was introduced in 1993 and

classifies the damage due to corrosion by assigning values from 1 to 4 where 1 indicates no visible corrosion and 4 indicates severe corrosion; a 2002 modification of the scoring technique included fretting as well as corrosion (Gilbert et al., 1993, Knutsen et al., 2015, Goldberg et al., 2002). It has been suggested that there is a correlation between the Goldberg score and the volume of material lost at the taper junction (Matthies et al., 2013, Racasan et al., 2015). In characterising corrosion in an explant, the volume of material lost can be measured using a variety of techniques including out-of-roundness measuring machines (such as the Talyrond 365, Taylor Hobson, Leicester, UK), optical profilers and coordinate measuring machines (CMM). The CMM is capable of measuring of measuring linear differences to better than 2 µm, and volumetric loss to within 1 mm^3 but it is limited by the diameter of the stylus which may be unable to penetrate the depth of the crevice as shown in Figure 2-21 (Van Citters et al., 2015, Cook et al., 2015). Hence, more recently, the use of an optical CMM – Redlux Ultraprecision Optical CMM (RedLux Ltd, Southampton UK) has become prevalent. In contrast to contact CMM, the optical CMM produces a high resolution 3D map of the part's form.

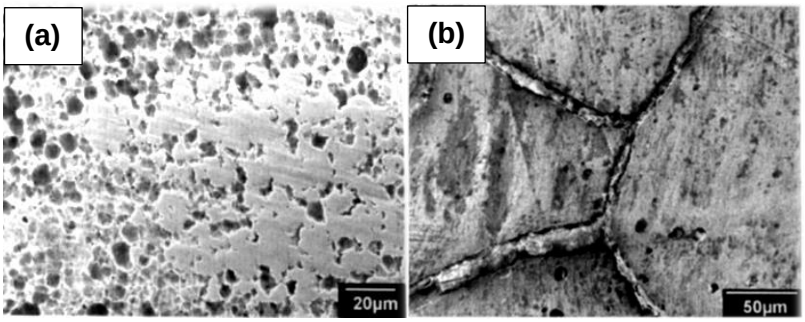

Figure 2-20 Corrosion patterns on CoCr: A=intense pitting corrosion, B =intergranular corrosion, etching and pitting (Hall et al., 2015)

Table 2-4 The Goldberg assessment visual scoring criteria for evaluating fretting and corrosion (Di Prima et al., 2015)

Severity	Score	Goldberg criteria	
		Corrosion	**Fretting**
None	1	No visible corrosion observed	-
Mild	2	<30% of taper surface discoloured or dull	Single band or bands of fretting scars involving three or fewer machine lines on taper surface
Moderate	3	>30% of taper surface discoloured or dull <10% of taper surface containing black debris, pits, or etch mark	Several bands of fretting scare or single band involving more than three machine lines
Severe	4	>10% of taper surface containing black debris, pits or etch mark	Several bands of fretting scars involving several adjacent machine lines or flattened areas with nearby fretting scars

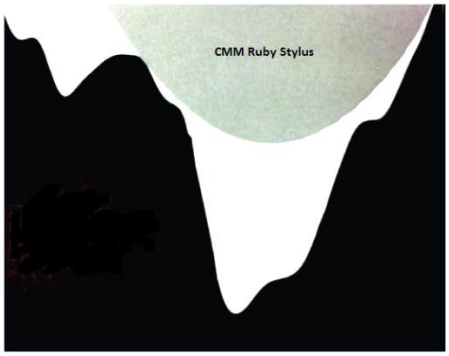

Figure 2-21 CMM probe relative to a crevice depth adapted from Van Citters et al. (2015)

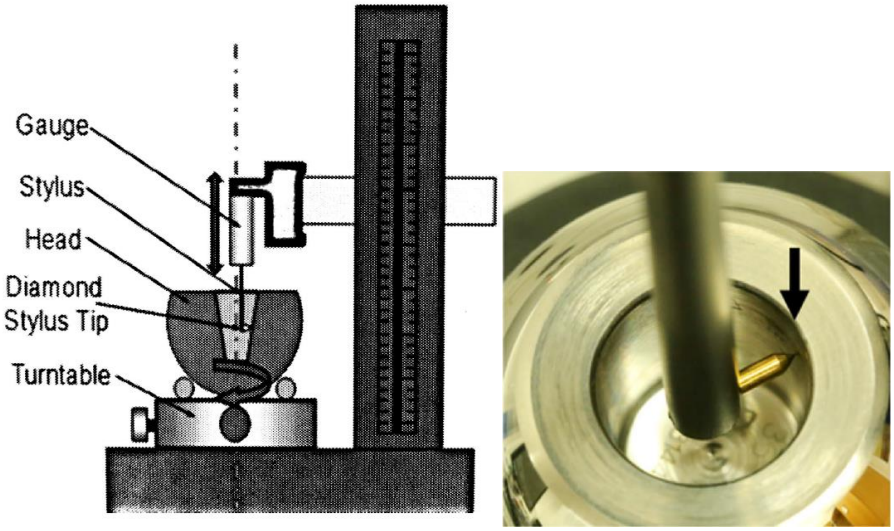

Figure 2-22 Schematic representation of Talyrond 365 out-of-roundness measuring equipment during head taper measurement adapted from Racasan et al. (2015), Whittaker et al. (2016)

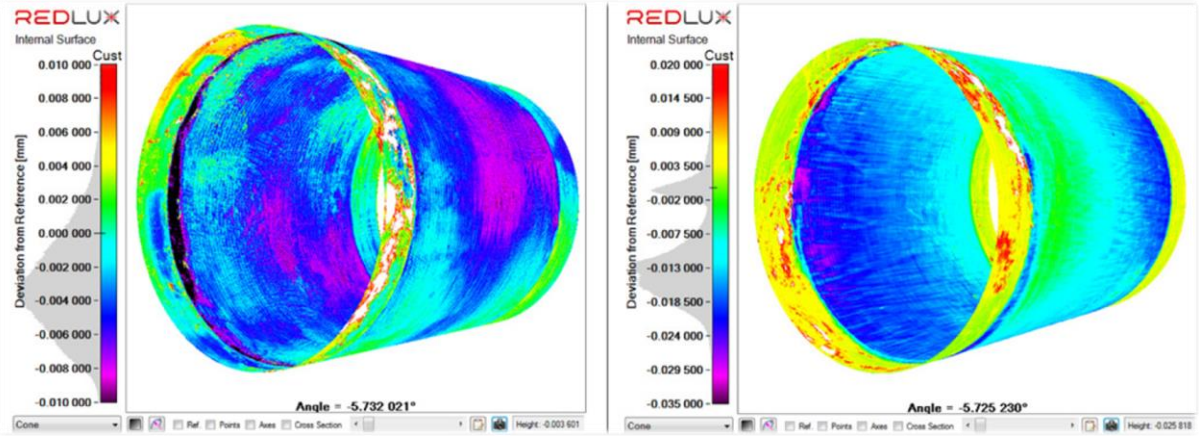

Figure 2-23 An example of material loss measurements from head tapers on an optical CMM (Cook et al., 2015)

2.5 Factors affecting taper corrosion

The potential for corrosion at a particular modular junction is multifactorial. This could be implant design, biological, patient related or factors due to surgical implantation. The duration exposed *in vivo* has also unsurprisingly been reported to show a significant influence on the severity of corrosion (Walker et al., 2016, Higgs et al., 2016). However, in a retrieval study evaluating the severity of corrosion for oxidised zirconium (OxZr) and CoCr

heads, Cartner et al. (2013) concluded that there was no correlation between the severity of corrosion and time. When fretting was considered in isolation, it was suggested that there is no correlation with time because fretting marks are removed as time progresses (Goldberg et al., 2002). However, whilst time *in vivo* was associated with both male and female fretting but not corrosion (Triantafyllopoulos et al., 2016), Nassif et al. (2014) did not find any correlation between fretting or corrosion and time *in vivo*.

2.5.1 Implant Design Factors

2.5.1.1 Head size

The recent concern related to taper corrosion was raised as a result of the increased failure of large diameter MoM bearings. Large heads (≥ 36 mm) were introduced due to their increased stability (Figure 2-24); the use of heads larger than 32 mm reduced dislocation rates by between 35 - 43 % (Ullmark, 2016). Large heads have also been reported to achieve a larger ROM at the bearing interface (Morlock et al., 2011), although this in part depends on the neck diameter and cup design (Figure 2-25).

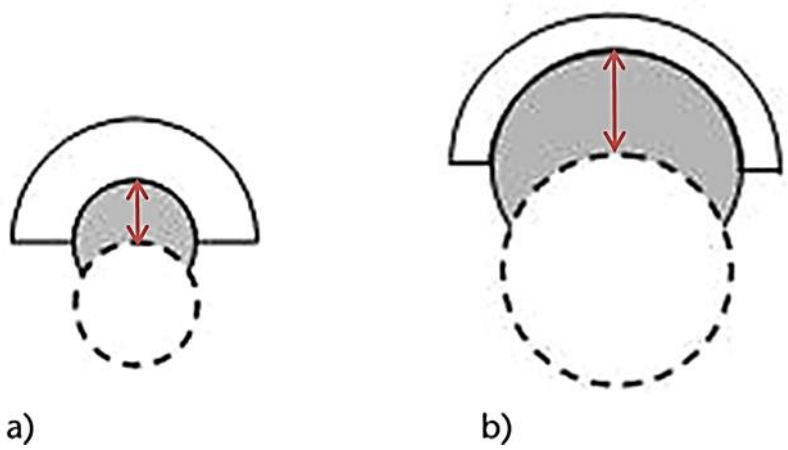

Figure 2-24A (a) smaller femoral head may dislocate after only a short distance (b) A larger head must travel a greater distance; distance before dislocation indicated by the red arrows (Ullmark, 2016)

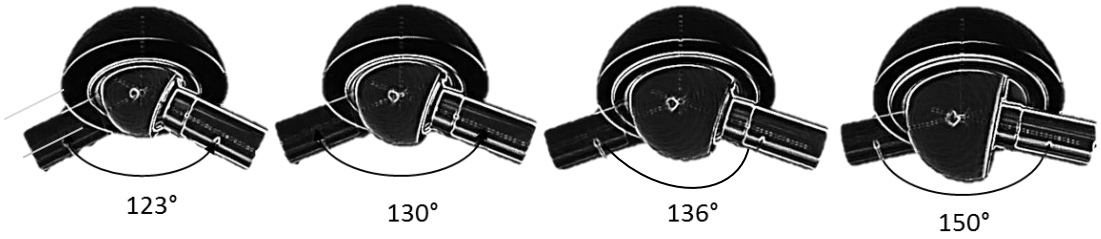

Figure 2-25 Increased range of motion for increasing head size; adapted from Altimed JSC (2012)

For a given bearing material combination and load, larger heads will generate higher friction moments at the bearing surface since the bearing surface torque (T_t) is proportional to femoral head radius (equation 6).

$$T_t = fLR \quad (6)$$

L= peak load, R=radius of femoral head, f= friction factor

Bearing surface torque in turn can transmit larger shear forces to the taper junction and it has been proposed this could damage the oxide layer and initiate MACC (Ullmark, 2016, Witt et al., 2014). It has been reported that torque influences fretting and corrosion more than axial load (Tan et al., 2015). However, there are conflicting reports of the effect of head size (Table 2-5) wherein some have found that larger heads result in higher taper wear and corrosion (Whittaker et al., 2016, Dyrkacz et al., 2013), whilst others found no relationship between the occurrence or severity of corrosion and head size (Cartner et al., 2013) with heads as small as 28 mm showing mild as well as severe corrosion (Tan et al., 2015).

Table 2-5 Summary of studies reporting the effect of head size on taper fretting and/or corrosion

Study	Material combination	Conclusion	Reference
Retrieval	CoCr/Ti CoCr/ FeCrNiMnMoNNb	• Head size did not correlate with metal ion release from the unstable tapers	Meyer et al. (2012)
Retrieval	CoCr/CoCr	• 36 mm heads corroded more than 28 mm heads	Dyrkacz et al. (2013)
Retrieval	CoCr/CoCr CoCr/Ti	• Increased head size did not correlate to higher corrosion scores	Cartner et al. (2016)
Retrieval	CoCr/CoCr CoCr/Ti	• A 5 mm increase in femoral head size caused a 26% increase in taper wear rate	Whittaker et al. (2016)
Retrieval	CoCr/CoCr CoCr/Ti CoCr/TMZF	• Fretting and corrosion of male and female tapers were not affected by head size	Triantafyllopoulos et al. (2016)
Review	CoCr/SS	• Torsional forces at the trunnion increase as head size increases • A large head on a narrow taper increases the risk of corrosion at the head-neck due to increased torque	Morley et al. (2012)
FEA	CoCr/Ti CoCr/TMZF	• Large maximum micromotion was observed when large head is used	Theodore et al. (2013)
In vitro	CoCr and OxZr heads	• No relationship between mean Goldberg score and head size	Cartner et al. (2013)

2.5.1.2 Bearing material combination

The materials utilised in bearing pairings will result in changes in the friction at the bearing surface which may also have implications for the stability of a taper junction (Donaldson et al., 2014). As indicated in equation 6, the frictional torque at the bearing surface is a function of the friction factor. The friction factor is a dimensionless parameter which is similar to the coefficient of friction, which facilitates comparisons of the effect of material combinations, implant size and design, lubricant, and load and motion profiles (Jin et al., 2006b). For a given femoral head diameter and maximum load, MoM bearings will generate higher torques since these components have been shown to result in higher friction factors (Figure 2-26).

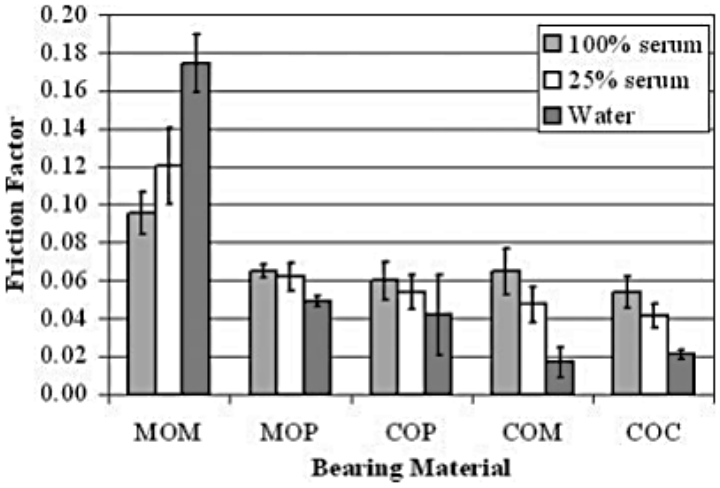

Figure 2-26 Friction factor measured for different bearing combinations and lubricants (Brockett et al., 2007)

Bearing friction is dependent upon lubrication conditions at the bearing surface and poor lubrication will result in increased torque (Panagiotidou et al., 2015). The type of lubrication at the bearing surface of hip implants is described by the lambda ratio (λ) (equation 7), where $\lambda \leq 1$ refers to boundary lubrication, $1 < \lambda < 3$, mixed lubrication and $\lambda > 3$, full fluid lubrication. The lambda ratio depends on material (elastic modulus and Poisson's ratio), geometrical (radius) and surface properties (composite surface roughness) of the bearings, lubricant properties (viscosity) at the bearing surface as well as operating conditions at the articulating surface (load and entraining velocity) (equation 10). The minimum film thickness h_{min} defines the relationship between the material, geometrical, and lubricant properties as well as the operating conditions (equation 8 – equation 12).

$$\lambda = \frac{h_{min}}{R_a{}'} \tag{7}$$

Minimum film thickness:

$$h_{min} = 2.798R\left(\frac{\eta u}{E'R}\right)^{0.65}\left(\frac{w}{E'R^2}\right)^{-0.21} \tag{8}$$

η (lubricant viscosity), R (equivalent radius), w (vertical load)

$$1/R = 1/R_1 - 1/R_2 \tag{9}$$

where R_1 = femoral head radius R_2= acetabular cup radius

Entraining velocity:

$$u = \frac{\omega d}{4} \tag{10}$$

ω (flexion-extension angular velocity), d (femoral head diameter)

Equivalent modulus:

$$E' = 2\Big/\left[\frac{1-v_{head}{}^2}{E_{head}} + \frac{1-v_{cup}{}^2}{E_{cup}}\right] \tag{11}$$

v_i(Poisson's ratio), E_i(Elastic modulus)

Composite roughness of the head and cup:

$$R_a{}' = \sqrt{R_{a(head)}{}^2 + R_{a(cup)}{}^2} \tag{12}$$

The Stribeck curve (Figure 2-27) indicates how operating conditions such as lubricant viscosity, sliding speed and load, influences the type of lubrication and consequently, the friction and wear properties at a bearing surface (Malik and Malik, 2015). A higher friction factor is associated with boundary lubrication than mixed and fluid film lubrication with the potential to increase the torque transmitted to the taper. Ideally, CoC and MoM components operate in full fluid film or mild mixed lubrication; MoP bearing combinations however operate in a mixed or boundary regime as a result of their rougher surface finish (Brockett et al., 2007). It is important to note that the Stribeck curve describes idealistic conditions, lubrication at the bearing surface may be affected by gait conditions such as stop-start or microseparation as well as design features such as low head-cup clearance (Hadley, 2012, Damm et al., 2013).

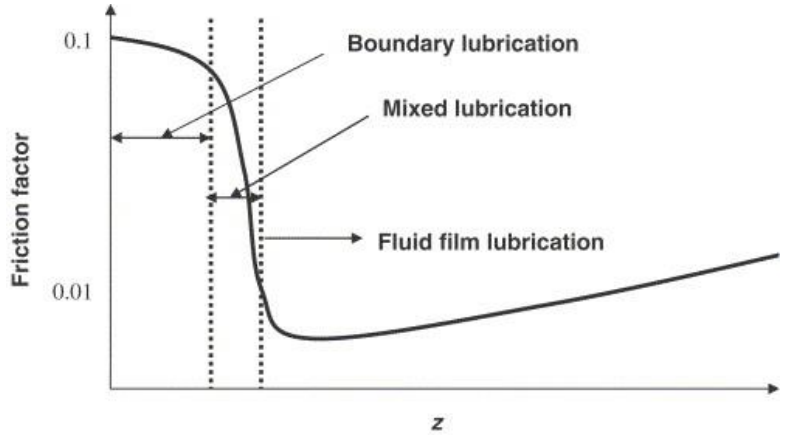

Figure 2-27 Stribeck curve where $z = \frac{\eta u R}{L}$ where η = viscosity of the lubricant, R =femoral head radius, u = entraining velocity of the bearing surfaces and L = load (Jin et al., 2006b)

Despite the theoretical relationship between friction factor and lubrication with torque and the supposed influence of torque on passive oxide layers, Latham et al. (2013), found no difference between MoM and MoP bearings with respect to corrosion. Moga et al. (2013), report that there is no significant difference in fretting and corrosion in head tapers and no statistical difference in trunnion fretting damage occurred between the two bearing combinations.

2.5.1.3 Head offset

A neutral (0 mm) offset is a condition where the head centre is coincident with the trunnion gauge point (Cartner et al., 2016). Deviations may occur such that the head centre sits proximal or distal to the trunnion gauge point at positive and negative offsets respectively. In the literature, reported offset options range from -3 to +12 mm (Cartner et al., 2016, Martin et al., 2016, Del Balso et al., 2015). The ability to vary the offset is one of the main benefits of modularity at the head-neck junction. During the surgical procedure, the femoral offset can be altered, independent of femoral stem fixation in order to restore the assumed physiological centre of the hip joint (Del Balso et al., 2015).

Head offset has been reported to influence fretting at the taper junction in retrieval analyses as well as following *in vitro* evaluations, as indicated in Table 2-6. In a retrieval

study,Del Balso et al. (2015) observed that the largest head offset showed the highest fretting. In laboratory evaluations, Gilbert et al. (2009) also found increased fretting damage in +6 mm offset heads as compared to heads with neutral offset whilst Panagiotidou et al. (2015) showed that larger offset heads result in increased in fretting corrosion currents. The increase in fretting with higher offsets has been associated with larger bending moments at the junction as well as a change in the motion at the junction from pistoning to rocking, where rocking increases micromotion (Panagiotidou et al., 2015, Donaldson et al., 2014). Rocking associated with increased offset was first described by Gilbert et al. (2009) where taper assemblies with a + 6 mm offset displayed large lateral motion.

Table 2-6 Summary of studies reporting the effect of head offset on taper fretting and/or corrosion
***Oxidized zirconium, **Biolox Delta**

Study	Material combination	Conclusion	Reference
FEA	CoCr/Ti	• Fretting work done is sensitive to head offset	Donaldson et al. (2014)
In vitro	CoCr and OxZr* heads	• There is a parabolic relationship between mean corrosion scores and head offset	Cartner et al. (2013)
In vitro	CoCr/Ti CoCr/CoCr Ceramic**/CoCr	• Higher offsets produced higher fretting corrosion currents due to increased bending moments • Ti stems showed the highest corrosion currents • Using ceramic heads did not prevent corrosion currents	Panagiotidou et al. (2015)
Retrieval	CoCr/Ti CoCr/CoCr	• + 8 mm heads showed greater total fretting scores than -3, +0 and + 4 mm offsets	Del Balso et al. (2015)
Retrieval	CoCr/Ti CoCr/CoCr CoCr/TMZF	• a 1 mm increase in head offset resulted 20% increase in the Goldberg score	Higgs et al. (2016)

2.5.1.4 Taper material combination

Historically, corrosion was attributed to less rigorous design factors including design tolerances, material processing and manufacturing techniques (Lavernia et al., 2015) as well as the use of dissimilar alloys. In a multicentre retrieval study,Goldberg et al. (2002) reported a higher incidence of corrosion in mixed alloy couples (CoCr/Ti). However, as early as 1998, it was reported that severe and extensive corrosive attack also occurred in same alloy combinations (CoCr/CoCr) (Jacobs et al., 1998) which has continued to be reported in more recent studies (Pourzal et al., 2016). It has been suggested that galvanic corrosion may not

be the predominant factor for ion release from the tapers (Table 2-7) (Levine et al., 2013, Reclaru et al., 2002).

The use of ceramic heads on metal trunnions has been shown to reduce both fretting and corrosion at the head-neck junction with a single modular feature since only the trunnion is then susceptible to passive oxide layer damage (Kurtz et al., 2013). However, it should be considered that larger diameter ceramic heads paired with ceramic cups, under poor lubrication regimes, have been reported to generate greater frictional torque than MoM bearings of the same diameter (Girard, 2015) which may thereby compromise the stability of the head-neck taper.

Table 2-7 Summary of studies reporting the effect of material combination on taper fretting and/or corrosion; *Zirconia

Study	Material combination	Conclusion	Reference
In vitro	CoCr / SS CoCr /CoCr CoCr/Ti	• The anodic current at the taper is more dependent on the polarisation potential of the materials than the galvanic coupling of dissimilar materials • CoCr/SS has the best corrosion resistance for the range of polarisation tested	Zhu and Windler (2003)
In vitro	CoCr/SS	• The CoCr/SS combination exhibits negligible galvanic corrosion with no risk of initiating crevice corrosion	Reclaru et al. (2002)
In vitro	CoCr /SS CoCr / CoCr	• Fretting was initiated at lower loads in CoCr/SS couples in comparison to CoCr/CoCr	Gilbert et al. (2009)
Retrieval + *in vitro*	Retrievals: CoCr/Ti CoCr/CoCr Ti/Ti	• There was an absence of surface corrosion for same alloy combinations • Corrosion increased in mixed alloy combinations	Cook et al. (1994)
	In vitro: CoCr /Ti CoCr/CoCr Zr* /Ti Zr /CoCr	• There was an increase in the production of wear debris in the CoCr/Ti combination	
Retrieval + *in vitro*	CoCr/CoCr CoCr/Ti CoCr/Ti	• No corrosion was observed in the same alloy retrievals or the factory made mixed alloy combination but corrosion was observed on the mixed alloy combinations which were retrieved	Lieberman et al. (1994)
Retrieval	CoCr/CoCr Ti/Ti CoCr/Ti	• Mixed alloy combinations had significantly higher head and neck corrosion scores than same alloy combinations	Goldberg et al. (2002)
Retrieval	CoCr/CoCr Ti/Ti CoCr/Ti	• None of the CoCr/CoCr or Ti/Ti corroded • 56.6% of CoCr/Ti corroded	Collier et al. (1991)
Retrieval	CoCr/CoCr CoCr/ Ti	• Significant corrosion was observed in both metal combinations	Gilbert et al. (1993)

2.5.1.5 Taper Dimensions

The taper dimensions that have been associated with the susceptibility to corrosion include the diameter, length, angle of the male and female tapers as well as the clearance between the two tapers. Some of the effects of geometrical features reported in the literature are summarised in Table 2-9.

2.5.1.5.1 Angular mismatch

Taper mismatch, also known as taper clearance, is defined as the difference between the head taper and trunnion angle (Jani et al., 1997). The mating of two tapers at a junction can result in zero, positive or negative mismatch. The extent of the mismatch controls the contact area and the position of contact between the components. Therefore, a positive mismatch (or clearance) represents a head angle greater than the trunnion angle and creates a proximally contacting taper, with contact occurring towards the innermost region of the taper, Figure 2-28a. This is in contrast to a distally contacting taper created by a negative mismatch wherein there is a smaller angle at the head taper angle than the trunnion (Jani et al., 1997) and contact occurs over the outermost region of the interface (Figure 2-28b).

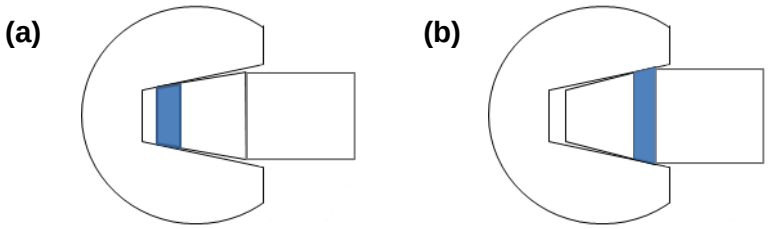

Figure 2-28 Schematic of (a) proximal contact (b) distal contact

There is an indication that tapers utilised in THRs are designed to contact proximally. The earliest use of Morse tapers in THR was to combine an Alumina femoral head with a metal stem (Johnston et al., 2007). A proximal contacting taper construct with a ceramic head prevents large tensile stresses occurring at the entrance of the taper (Figure 2-29); this reduces the risk of head fracture (Cales and Stefani, 1998). Johnston et al. (2007) indicated

that a taper angle of 5°38’22’’ was chosen to minimise tensile strains in the femoral head, although, larger angles are currently being used by many manufacturers. The design feature of proximal contact appears to have been assimilated into all-metal taper designs (Hernigou et al., 2013) since implant manufacturers design stems suitable for both ceramic and metal heads in order to minimise stock (Langton et al., 2012).

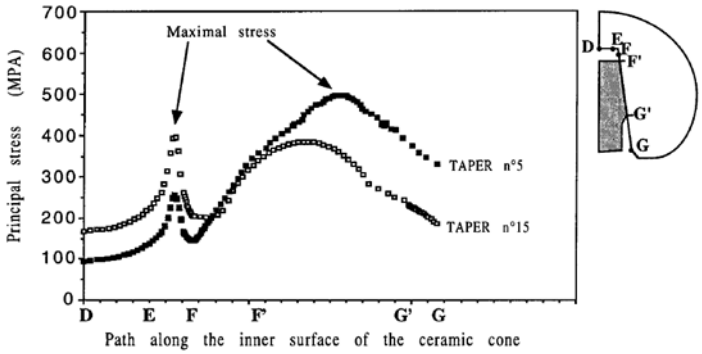

Figure 2-29 Variation of principal stress along 12/14 5° ceramic head tapers (adapted from (Cales and Stefani, 1998)

It is broadly assumed that the fretting damage at the taper can be controlled by adequate angular tolerance of the components (Abdullah, 2010) and it has been suggested that the taper mismatch should be larger than the female taper by 0 - 5 minutes (Abdullah, 2010, Johnston et al., 2007). However, Parekh et al. (2016) concluded from their FE study that within a tolerance of ±0.015^{o}, both positive and negative angular mismatches generate similar contact pressures and micromotion. With respect to corrosion, distal contact would not permit fluid into the taper interface (Figure 2-30a) and therefore would limit the initiation of crevice corrosion. However, a distally contacting taper may allow crevice corrosion to occur if fluid is drawn in by wicking during gait (Jani et al., 1997). In contrast, a proximally contacting taper would be more open to joint fluids (Figure 2-30b) such that the depleted oxygen condition encouraging crevice corrosion would not occur (Jani et al., 1997). However, in a retrieval study of ceramic and metal heads, Kocagöz et al. (2013) found no correlation between the taper mismatch and the visual corrosion scores.

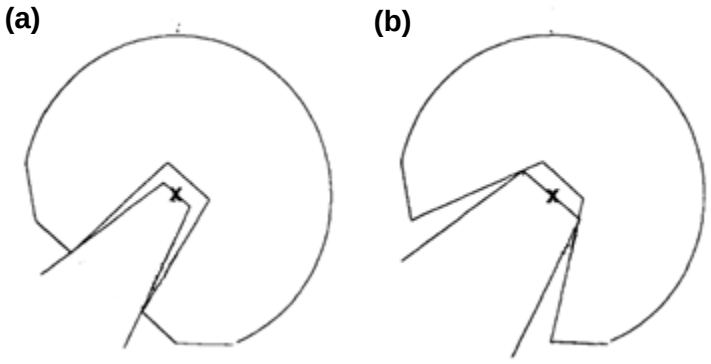

Figure 2-30 a) Distal contact with a closed junction (b) Proximal contact showing an opened taper junction in contrast to adapted from Jani et al. (1997)

2.5.1.5.2 Taper diameter

Trunnions with smaller diameters provide a larger impingement-free ROM (Figure 2-31). However, slimmer trunnions have a smaller total surface area for the interference fit and this could result in increased micromotion at the junction (Hussenbocus et al., 2015). Moreover, the use of a thinner trunnion with a larger head could compromise the taper integrity due to the combination of high frictional torque and smaller surface area (Morley et al., 2012, Morlock et al., 2011).

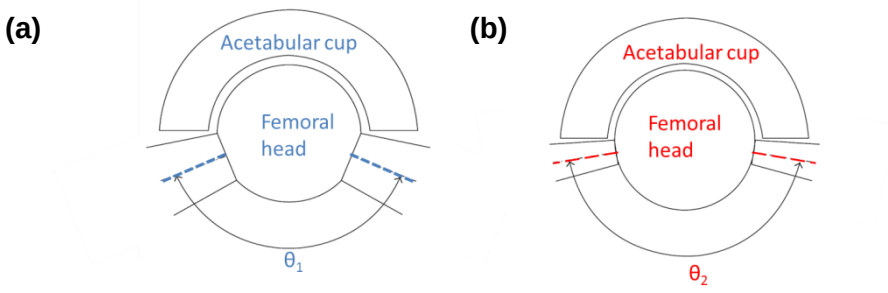

Figure 2-31 Schematic showing the increase in range of motion due to thinner taper in comparison to a thicker one

2.5.1.5.3 Trunnion length

The reduction in length of a trunnion means that they can sit entirely within the head taper (Figure 2-32). This reduction in length has been associated with edge loading at the trunnion base and may result in increased stresses and subsequent damage of the head taper (Tan et al., 2015, Esposito et al., 2014, Hussenbocus et al., 2015). The combination of edge loading with a low taper angle, causes large shear forces (Tan et al., 2015), which may facilitate corrosion by initiating the damage of the oxide layer. For longer trunnions, however, the surface area available to support the loading may not constitute the actual area under loading. Indeed, shorter tapers may exhibit comparable contact areas to longer tapers (Jauch-Matt et al., 2017).

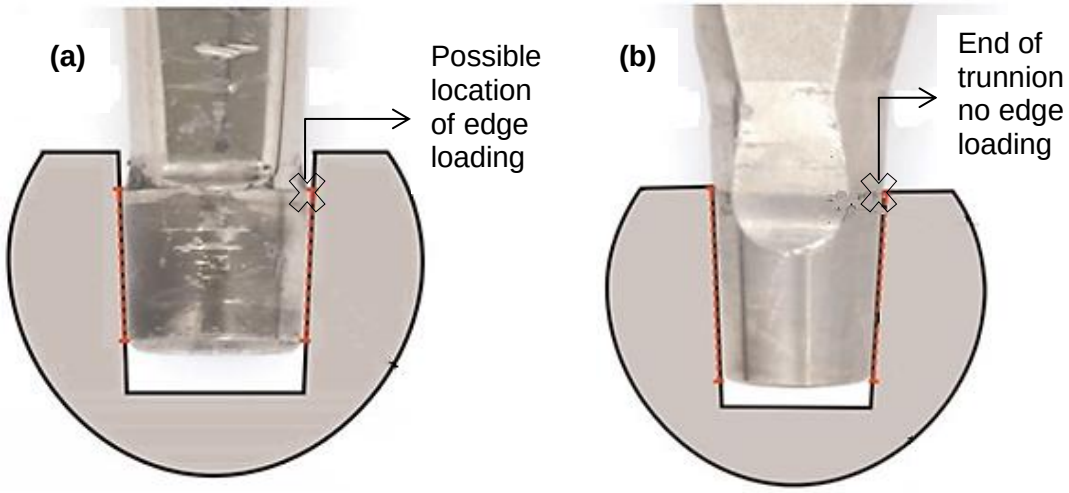

Figure 2-32 Engagement of a (a) short trunnion and (b) longer trunnion along a head taper adapted from Hothi et al. (2015)

2.5.1.5.4 Flexural rigidity

Trunnion rigidity defined in equation 13, has been identified as one of the strongest predictors of corrosion (Porter et al., 2014). In an evaluation of retrieved head tapers, Higgs et al. (2016) showed that head tapers paired with more rigid trunnions exhibited less fretting and corrosion damage.

$$Trunnion\ flexural\ rigidity = E \times I = E \times \left(\frac{\pi \times (ND)^4}{64}\right) \qquad (13)$$

Where E =modulus of elasticity

I = moment of inertia of the cross section about the bending axis

ND = neck diameter

The neck diameter ND relates to the proximal (D_1) and distal (D_2) diameters (Porter et al., 2014) as shown in equation 14 below

$$ND = D_1 - \frac{{D_1}^2+2D_1D_2+3{D_2}^2}{4\left({D_1}^2+D_1D_2+{D_2}^2\right)}(D_1 - D_2) \qquad (14)$$

The flexural rigidity of a trunnion is dependent upon both material and geometric characteristics. For a given material, a thinner taper would be more likely to deform more under loading resulting in the opening of the distal junction and subsequent fluid ingress (Brock et al., 2015). There is a large variability in the flexural rigidity of trunnions (Porter et al., 2014), due to the variability in the elastic modulus used (Table 2-8), as well as the variation in taper geometry. The use of shorter and thinner trunnions has been utilised recently in addition to the manufacture of stems with lower modulus alloys such as TMZF leading to decreased trunnion rigidity. Flexural rigidity values of 91 – 873.2 Nm^2 have been reported by Goldberg et al. (2002) whilst Porter et al. (2014) reported a range of 80 – 623 Nm^2. More recently, Higgs et al. (2016) reported even lower trunnion flexibility ranging from 84.5 – 402.6 Nm^2

Table 2-8 Modulus of elasticity of common femoral stem alloys (Porter et al., 2014, Wang, 1996)

Alloy	Elastic modulus (GPa)
TMZF	74-85
Ti-13Nb-13Zr	79-84
Ti-6Al-4V (Ti)	110-116
Orthinox (316L) (SS)	210
CoCr	230-240

Table 2-9 Some studies reporting the effect of taper geometry on taper fretting and/or corrosion

Study	Material combination	Conclusion	Reference
Retrieval	CoCr/CoCr Ti-6Al-4V/Ti-6Al-4V CoCr/Ti-6Al-4V	• With necks, flexural rigidity was inversely related to head and neck corrosion scores • Flexural rigidity of the neck was independent of neck or head fretting scores • Neck length had no effect on fretting or corrosion of the head and neck	Goldberg et al. (2002)
In vitro	CoCr/Ti CoCr/CoCr Zr/Ti Zr/CoCr	• Wear debris generated at the taper interface increased with increasing taper mismatch	Cook et al. (1994)
Review	-	• The loosening torque on thinner tapers is reduced	Morlock et al. (2011)
FEA	Ti/Ti CoCr/Ti Ti/CoCr CoCr/CoCr	• The peak stress and gap opening at the taper engagement level depends on the material coupling: Ti causes a larger gap due to its lower modulus. • CoCr/CoCr combination gaps less under bending but peak high stresses; localised high stresses accelerate corrosion	Chu et al. (2000)
	CoCr/Ti	• Fretting work done is sensitive to taper angle clearance	Donaldson et al. (2014)
	CoCr/Ti	• Micromotion increased on the male component with increasing tolerance	Shareef and Levine (1996)

2.5.1.6 Surface Roughness at Taper Junction

The plastic deformation of the surface asperities has been assumed to increase the contact area at the junction. However, if surgical impaction does not result in the plastic deformation of the asperities, then the contact area at the junction will be considerably smaller than the apparent area (Munir et al., 2013). Indeed, it has been suggested that the roughness features may initiate a corrosion mechanism (Table 2-11). Rough trunnions are seen to imprint upon female tapers when the taper components are dismantled, although there are conflicting reports regarding their effect. Imprinting of threads during assembly may initiate local corrosion process (Van Citters et al., 2015). Upon impaction of the head on a trunnion, the mating of a rough trunnion with a smooth head taper results in the damage of the head taper oxide layer as well as plastic deformation of the thread peaks; the resulting gaps may be 10-15 μm deep and thereby create a crevice which collects fluid and allows corrosion to proceed (Van Citters et al., 2015). In addition, surface ridges may enable fluid to travel along the continuous machined microthread thereby perpetuating corrosion

(Hussenbocus et al., 2015). The stability of the taper may be lower for a rough compared to a smooth trunnion; the dissociation force at the taper junction was found to be 22 - 35 % lower when the roughness, R_a, of the trunnion was increased from 1 to 4.2 µm (Yavari and Idris, 2016). Conversely, Pourzal et al (2016) reported that sharper trunnion peaks resulted in lower stem damage in both the same and mixed alloy couplings whilst Arnholt et al. (2015) did not find a correlation between trunnion morphology and fretting and corrosion damage at the taper interface.

It is possible that the lack of consensus on the effect of trunnion topography is because there is no standard for taper roughness profiles for either male or female tapers. A single manufacturer may adopt different profiles, as shown in Figure 2-33. In a comparison of 7 commercially available stems from 5 manufacturers, varying roughness features, including such as thread height and pitch were observed (Munir et al., 2013). Different thread heights and peaks will result in different contact points over the length of the taper interface and load distribution between the head taper and trunnion.

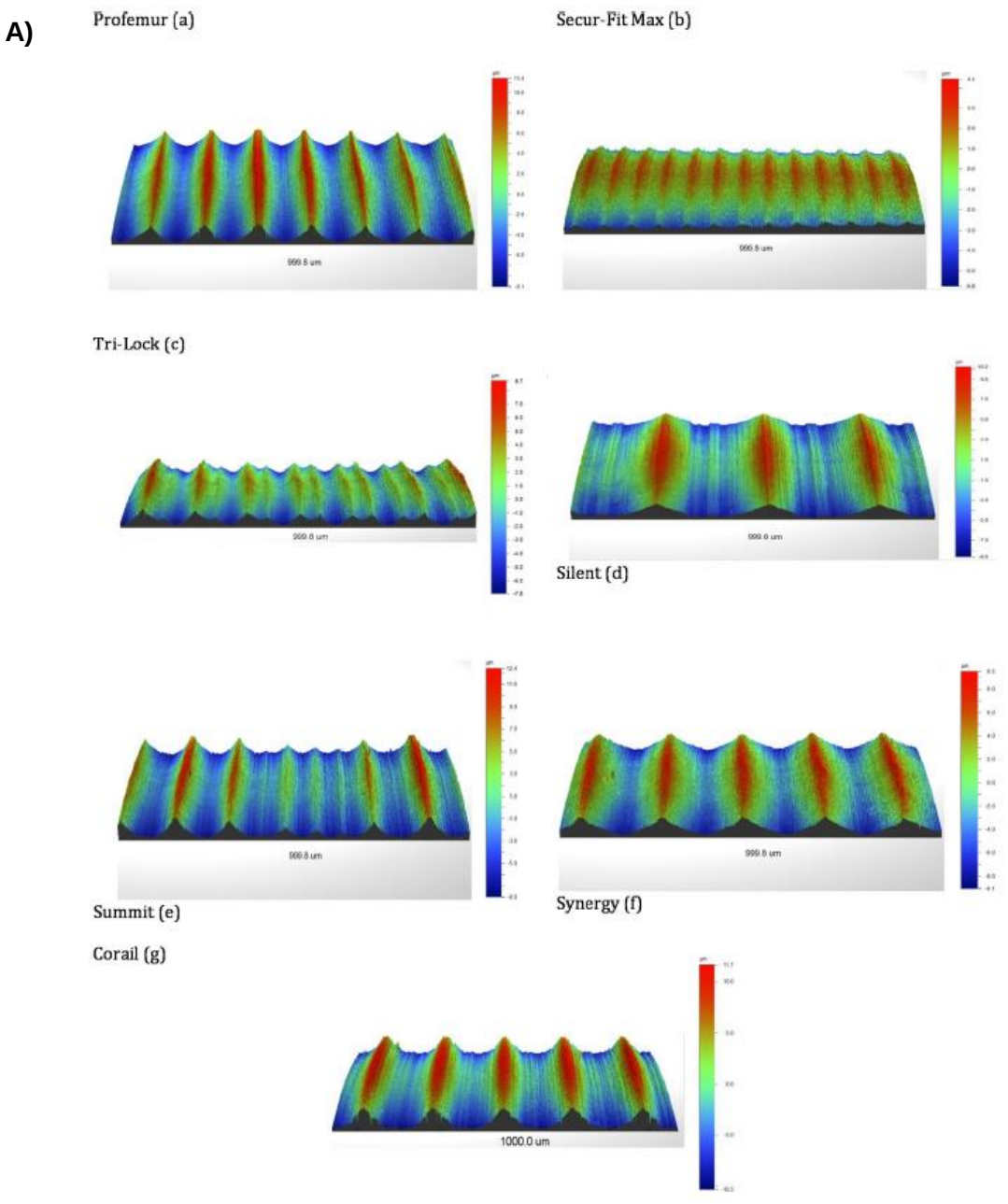

Figure 2-33 (A) Variations in surface topography of 7 trunnions from 5 manufacturers Profemur (Wright Medical), Secur-Fit Max (Stryker), Tri-Lock, Silent, Summit, Corail (DePuy Synthes), Synergy (Smith and Nephew) (B) Thread profile of some of the trunnions (Munir et al., 2013)

There is also appears a lack of consensus on the variables (Table 2-10) used to characterise the surface roughness of trunnions. Munir et al. (2013) reported the average surface roughness values whereas, Drouin and Cales (1994) reported peak (maximum) roughness values. In recent studies, the machining mark height and spacing have been reported (Figure 2-34) with suggestions that this is a more meaningful method of characterising the taper junction topography (Lundberg et al., 2015, Pourzal et al., 2016). It is foreseeable that sharper peaks and thus reduced 'machining mark spacing' would increase the stresses on the oxide layer leading to damage. Deeper troughs (increased R_v) may be more likely to encourage crevice corrosion because oxygen may be depleted in these regions. An understanding of how the roughness variables are likely to influence the corrosion process and ensure uniformity the characterisation of surface topography accordingly, is required.

Table 2-10 Roughness parameters; adapted from (Munir et al., 2013, Gadelmawlaa et al., 2002)

	Definition	
R_p	The maximum height of the profile above the mean line within an assessment length (µm)	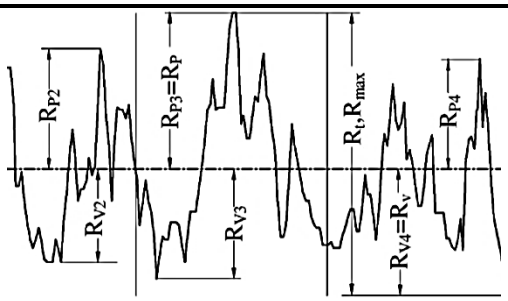
R_v	The maximum depth of the profile below the mean line within an assessment length (µm)	
R_{max}	Vertical distance between the highest peak and the lowest valley along an assessment length (µm)	
R_a	Arithmetic average height (µm)	

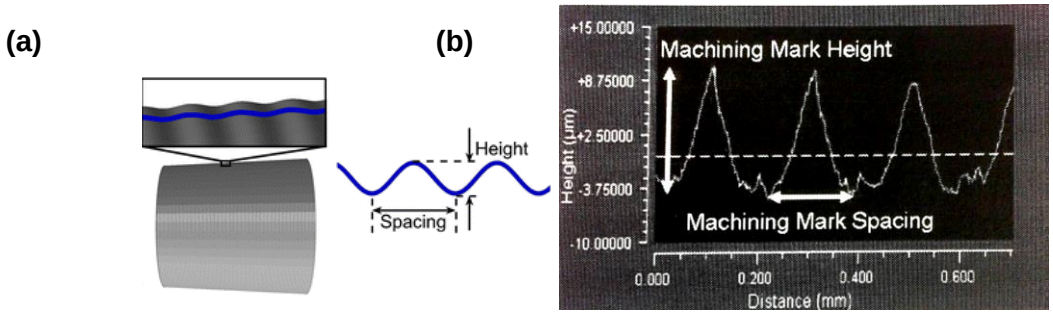

Figure 2-34 Machining mark height and machining mark spacing roughness features (Pourzal et al., 2016, Lundberg et al., 2015)

Indeed, there could be a compounded effect of increased head taper roughness which is not normally reported. Surface profiles are normally only stated for the stem taper (Bishop et al., 2013) but head tapers may display a surface roughness values (R_a) greater than those associated with rough trunnions (Whittaker et al., 2016). Manufacturing controls on the surface finish of head tapers appear to have become less stringent and this increase in surface roughness on the female taper has been associated with increased trunnion and head taper damage in mixed alloy couplings (Pourzal et al., 2016). Langton et al. (2016) found a random yet wide variation in the surface finish of head tapers; although there was no apparent correlation between the surface finish of the head taper and the date of manufacture of the femoral head. This suggests that the feature is not a systematic design change.

Trunnion angle, diameter, length and roughness are often reported in combination but, tapers can differ by each of these variables. Therefore, it is difficult to isolate the singular effects of all 4 variables during retrieval studies. For example, retrieval studies have compared the taper performance of S-ROM and Corail stems. These have shown that the Corail stems perform worse (Brock et al., 2015, Hothi et al., 2016b). Although both are manufactured by the same company, the S-ROM stem has a longer (14 mm along the medial-lateral plane) 11/13 trunnion, with a 6° angle and characterised as a smooth taper. In comparison, the Corail stem has a 5.6° 12/14 trunnion that is 10 - 10.5 mm long and classified as rough (Hothi et al., 2015) making the determination of which variable influences this behaviour challenging. When surface roughness and trunnion angle were matched in another study comparing the C-Taper to V40 trunnion design, it was concluded that there was no difference in fretting and corrosion scores on the head taper (Higgs et al., 2016). This may suggest that diameter and length are more important predictors of corrosion.

Table 2-11 Summary of studies reporting the effect of surface roughness on taper fretting and/or corrosion

Study	Material combination	Conclusion	Reference
In vitro	CoCr/Ti	• The surface roughness of the head taper was inversely related to head/neck contact area • Fretting corrosion increased where rough neck tapers were used • The passive film was disrupted on the rough neck tapers	Panagiotidou et al. (2013)
In vitro	CoCr/Ti	• Smooth tapers had higher pull-off forces compared to rough tapers	Jauch-Matt et al. (2017)
In vitro	SS/SS	• The highest pull out force was observed at smoother surface roughness (R_a)	Yavari and Idris (2016)
Retrieval	CoCr/CoCr CoCr/Ti	CoCr/CoCr: • Higher trunnion peaks were associated with lower stem taper damage scores CoCr/Ti: • Head taper roughness was associated with increased male and female taper damage • Higher trunnion peaks was associated with lower trunnion damage	Pourzal et al. (2016)
Retrieval	CoCr/Ti CoCr/CoCr	• Rough trunnions did not exhibit increased *in vivo* fretting corrosion or material loss	Arnholt et al. (2015)

2.5.2 Biological

Varying organisms have been suggested to result in different influences on the corrosion of metals (Videla and Herrera, 2005), namely: (i) the adherence of microorganisms to metal surfaces may modulate corrosion by changing the electrochemical conditions at the interface between the metal and the electrolyte, (ii) biofilms may reduce corrosion by enhancing the adherence of the passive film to the metal or act as diffusion barriers, (iii) the detachment of the biofilm could cause the passive layer to also detach and expose the substrate metal to the corrosive fluid, (iv) the bacterial colonisation of an implant surface could result in the depletion of oxygen thereby resulting in increased anodic dissolution, (v) the effect of localised colonisation relative to non-colonised regions could be a variation in potential differences along the metal surface thereby generating corrosion currents.

In addition to the knowledge of microbial induced corrosion, *in vitro* studies of have shown that osteoblasts, fibroblasts, and phagocytic cells are able to adhere and differentiate on stainless steel, titanium and CoCr on metal substrates in foil and disc form and directly corrode the surface leaving behind resorption pits or displaying increased levels of metal ion levels bound to cellular structures such as the cytoplasm and nuclear structures (Cadosch et

al., 2010, Cadosch et al., 2009, Hiromoto et al., 2002). Osteoblasts have been reported to increase the dissolution rate of CoCr (Harmand, 1995) but reports of cell induced corrosion have also been attributed to inflammatory cells. This mode of corrosion has been observed on retrieved Ti-6Al-4V and CoCr alloys and has been shown to occur regardless of implant design or metallurgy (wrought or cast) but has not been correlated with time *in situ*, severity of corrosion, patient gender or age, head size or metal ion levels; it has however, been shown to be correlated with aseptic loosening (Di Laura et al., 2017, Sivan et al., 2015).

Particulate and ionic forms of Co and Cr are able to trigger inflammatory reactions. In response, phagocytic cells release reactive chemical species in the form of hydrogen peroxide (H_2O_2) which is able to permeate the cell's membrane through to the oxide layer (Mu et al., 2000). Gilbert et al. (2015b) and Tengvall et al. (1989) showed that H_2O_2 increased the rate of corrosion of both CoCr alloy and Titanium; the oxide layer on a commercially pure titanium discs were found to be hyperoxidised by H_2O_2 which has been suggested to induce the release of titanium ions. However, the purported negative effect of H_2O_2 as a reactive oxygen species (ROS) is countered by Lin and Bumgardner (2004), who suggested that the release of ROS reduces corrosion by enhancing surface oxides when macrophages were cultured on CoCr plates.

Evidence of inflammatory cell induced (ICI) corrosion in hip replacements has been observed in retrieval studies where iron nodules were present in seemingly cell corroded explants (Gilbert et al., 2015b). Iron is abundant *in vivo* but does not exist in a free state due to its reactivity. However, part of the inflammatory sequelae involves the release of iron bound to storage proteins such as ferritin, by activated phagocytes (Cerquiglini et al., 2016, Gilbert et al., 2015b, Valko et al., 2005). The presence of iron and hydrogen peroxide can initiate a Fenton reaction (equation 15) which produces the hydroxyl radical ($^{\cdot}OH$). $^{\cdot}OH$ is a highly reactive species with a half-life of 10^{-9} s which is capable of indiscriminate reactions within a radius of 93Å (Thomas et al., 2009). Thus, it has been reported that the radical may

result in DNA damage (Valko et al., 2005). However, it is not currently clear if the hydroxyl radical is capable of damaging oxide layers or the underlying substrate metal.

$$Fe^{2+} + H_2O_2 -> Fe^{3+} + {}^{\cdot}OH + OH^{-} \quad (15)$$

A Fenton mechanism catalysed by iron sequestered from cells has been described but there are reports of Fenton reactions being catalysed by transition metals including Co and Cr (Stohs and Bagchi, 1995, Valko et al., 2005). Thus, the absence of Fe does not prevent the reaction from occurring and the only requirement is the production of H_2O_2. As indicated, with respect to CoCr alloys, both cobalt and chromium are released. According to Chumakov et al. (2016), Cr has the potential to generate more ˙OH than either Co or Fe.

Cell induced corrosion has been reported to occur over an area of 2.4 – 27.8 mm^2; features indicative of the phenomenon such as the etching of cell morphology and presence of cellular remnants have been observed in a number of regions of joint replacement devices such as non-contact regions of articular surfaces and non-articular machined surfaces as well as at modular junctions including the acetabular liner taper crevices and head-neck taper junctions (Di Laura et al., 2017, Gilbert et al., 2015b). The latter is feasible if gaps as small as 1 µm develop at the taper junction (Gilbert et al., 2015a).

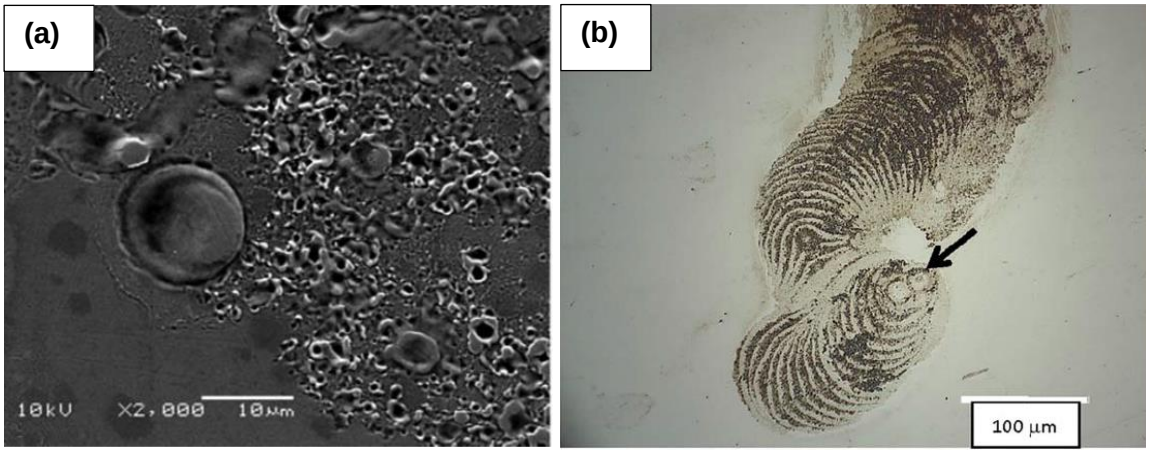

Figure 2-35a Isolated spots of corrosion on a modular head (b) Optical microscope image of a femoral head showing attack of a migrating cell (Di Laura et al., 2017, Gilbert et al., 2015b)

2.5.3 Surgical

Several studies have reported the correlation between surgical assembly conditions such as impaction forces and taper cleanliness with the performance of taper junctions, as summarised in Table 2-12. These factors are thought to influence the stability and integrity of the taper.

In a survey about the THR head impaction procedure, 25% of surgeons reportedly impacted with one heavy blow in line with the taper neck and 68% achieved taper fit with several blows in line with the taper neck (Ford et al., 2015). Due to the use of a minimally invasive approach, 5% did not pay attention to the direction of the impacted force (Ford et al., 2015). The effect of surgical impaction has been studied with respect to the pull-off force (indicative of taper strength) with the presumption that a high taper strength will result in reduced fretting as well as reduced likelihood of taper dissociation (Jauch-Matt et al., 2017). Pennock et al. (2002), found that the dissociation strength is determined by the largest impact force. A minimum force of 4 kN applied with a hammer has been recommended to lock a clean taper (Rehmer et al., 2012). Nonetheless, the applied impaction force may be

reduced to prevent intraoperative periprosthetic fracture especially in patients with poor osteogenic quality such as is common in elderly patients (Jacobs, 2016).

Minimally invasive and anterior approaches to THRs have become more prevalent (Jacobs, 2016) which increases the risk of off-axis impaction of the femoral head onto the trunnion. This leads to a reduction in the vector component of force that seats the taper (Pennock et al., 2002). Further, off-axis impaction may result in misalignment of the taper, crevice formation at the junction and subsequent fluid ingress (Jauch-Matt et al., 2017).

Contamination of a taper junction with bone chips has been shown in laboratory tests to result in increased micromotion at the junction although, this was evaluated at the neck-stem junction of a modular stem (Jauch et al., 2011). Lavernia et al. (2009) concluded that the contamination of a head-neck taper with blood and fat reduced the pull-out force required to separate the taper components by 20%. They subsequently showed that the dissociation strength of a clean taper is comparable to one that had been contaminated by blood and fat but was cleaned prior to impaction.

More recently, it has been suggested that artefacts previously attributed to ICI corrosion as described in 2.5.2, may have originated from the use of high-voltage based electrocautery or high-frequency based electrosurgical devices after the features were recreated by Campbell et al. (2017) as well as Aldinger and Pawar (2017). Further, Aldinger and Pawar (2017) suggested that the presence of iron deposits which was hitherto attributed to the cellular processes associated with the inflammatory sequelae was due to contact with the stainless steel electrosurgery device. Regardless of the source of these patterns observed in retrievals, the effect is the damage of the oxide layer thereby exposing the metal to corrosion.

Table 2-12 Summary of studies reporting the effect surgical condition on taper fretting and/or corrosion

Study	Material combination	Conclusion	Reference
FEA	N/A	• A high assembly load locks the taper and prevents the neck from experiencing rigid body motion during patient activities	Abdullah (2010)
FEA	Ti/Ti	• Relative motion was inversely proportional to impaction load	Bitter et al. (2013)
FEA	Ti/Ti CoCr/Ti Ti/CoCr CoCr/CoCr	• Impaction force was proportional to disassembly force. • The first impact was responsible for 90% of the taper strength; subsequent impacts contributed less • Off-axis impaction reduces the vector component of force which seats the taper • Multiple impactions with varying force has the same effect on taper strength as a single blow of the strongest force applied	Chu et al. (2000)
FEA	Ti/Ti	• Loading of the taper off-axis increases the micromotion on one side relative to the other	Shareef and Levine (1996)
In vitro	CoCr /SS CoCr / CoCr	• Assembling the CoCr/SS components dry did not stop fretting but increased the onset of fretting load in relation to wet assembly	Gilbert et al. (2009)
In vitro	CoCr/Ti	• A marked reduction in resistance to disassembly*** was observed when blood and fatty tissue were interposed between the junction	Lavernia et al. (2009)
Retrieval	CoCr/Ti-6Al-4Ni	• A defective fit of the head onto the stem would result in taper instability, accelerated corrosion and metallosis	Pansard et al. (2012)

2.5.4 Patient

Despite retrieval studies suggesting an incidence of head-neck taper corrosion of up to 90%, clinical manifestations of ALTRs are less than 5% (Jacobs, 2016). Therefore, there have been suggestions that individual patient variability may be due to genetic polymorphisms or adaptive immune responses (Jacobs, 2016). Further, it has been reported that women are more susceptible to adverse reactions for the same dose of metal debris (Langton et al., 2016, Cooper, 2014). The effect of patient weight has been identified as showing a positive correlation with fretting and corrosion (Higgs et al., 2016, Donaldson et al., 2014, Kurtz et al., 2013). Increased patient weight has been associated with increased moments and stresses at the taper junction (Higgs et al., 2016, McTighe et al., 2015) and Higgs et al. (2016) estimated that an increase in patient weight by 0.45 kg results in a 1% increase in propensity for taper damage. With increasing obesity rates, Figure 2-36, it seems likely that weight is likely to continue to be an issue. However, load due to patient weight or

activity has only been shown to influence micromotion in laboratory and FE analyses; weight or loading does not appear to influence clinical observations (Table 2-13).

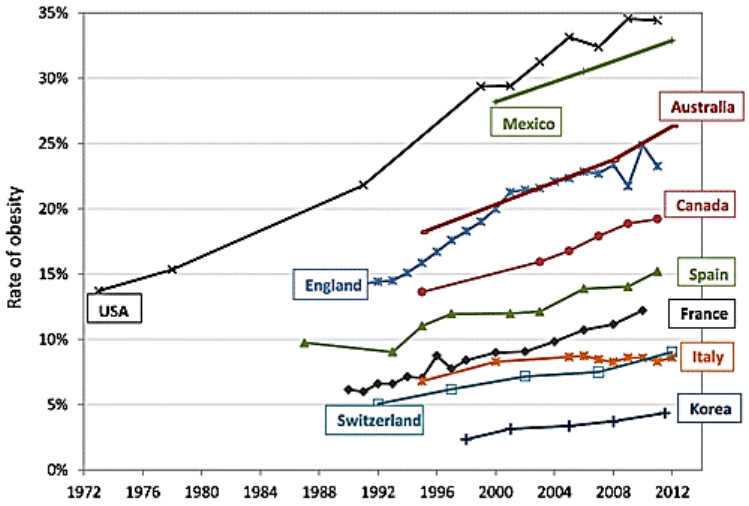

Figure 2-36 Trend of age and gender adjusted obesity rates over a range of countries, adapted from Morlock et al. (2016)

Table 2-13 Summary of studies reporting the patient specific effects on taper fretting and/or corrosion

Study	Material combination	Conclusion	Reference
In vitro	CoCr/CoCr CoCr/Ti-6Al-4V	• Micromotion between the stem and neck positively correlates with load levels (body weight or patient activity) • One-off high loads may result in micromotion at a taper junction which was previously stable.	Jauch et al. (2013)
FEA	N/A	• Micromotion at a taper junction is related to applied functional load.	Abdullah (2010)
FEA	CoCr/Ti	• Fretting work done is sensitive to patient weight but not factors such as gait variation, absolute taper dimensions (diameter, length) or contact length, impaction conditions (angle, force)	Donaldson et al. (2014)
Retrieval	CoCr/Ti Ti/Ti CoCr/CoCr	• No correlation between the amount of corrosion observed and age, weight, sex, patient activity or reason for revision	Collier et al. (1992)

2.6 Evaluating Modular junctions

The ability of modular junctions to perform as intended has been evaluated statically and dynamically. The standards for static evaluation of modular junctions are given in Table 2-14, although ASTM F2345 also entails the dynamic evaluation of a junction with a ceramic femoral head.

Table 2-14 Standards for static evaluations of modular junctions (Smith and Joyce, 2017)

ASTM F2009	Standard test method for determining the axial disassembly force of taper connections of modular prostheses
ASTM F2345	Standard Test Methods for Determination of Static and Cyclic Fatigue Strength of Ceramic Modular Femoral Heads
ISO 7206-10	Implants for Surgery – Partial and total hip-joint prostheses- Part 10: Determination of resistance to static load of modular femoral heads
ISO 7206-13	Implants for Surgery – Partial and total hip-joint prostheses- Part 13: Determination of resistance to torque of head fixation of stemmed femoral components

Uniaxial compression rigs are the standard for evaluating the susceptibility of a metallic modular junction to dynamic loading. The ASTM standard F1875 “Standard practice for fretting corrosion testing of modular implant interfaces: hip femoral head-bore and cone taper interface” addresses fretting of taper junctions in THRs. The standard highlights a short as well as a long-term evaluation of modular junctions (Schaaff, 2004). Short term tests which are recommended for evaluating design differences but groups who reported visual signs of corrosion have only been recorded after a minimum of 10 Mc (Aldinger et al., 2015, Jani et al., 1997) even though some retrievals have shown signs of corrosion as early as 8 months, equivalent to 1 Mc (Cooper et al., 2012a). The re-emergence of taper corrosion concerns has identified toggling as a mechanism for fluid ingress and facilitating corrosion. Thus, the use of a moving load vector, as is produced in hip simulators, may be better able to evaluate the taper junction.

Table 2-15 ASTM F1875-98 fretting test conditions (Schaaff, 2004)

		Frequency / Hz	Duration / Mc	Outcome	Purpose
Test	Short-term	1	1	Semi-quantitative measurement of corrosion rates	Evaluation of design differences in tapered junctions
	Long-term	5	10	Chemical analysis of the testing liquid and of the particulate debris	Study damage mechanisms

Hip simulators were developed to study the tribological performance of joint pairings in pre-clinical validation of THR devices (Affatato et al., 2006). Hip simulators were first developed in the 1960s (Smith and Joyce, 2017), with a number of designs currently used; some of which are given in Table 2-16. These simulators vary in their method of replicating joint biomechanics under physiological loading however, the results can provide confirmation of the material's performance for a given geometric design under a variety of operating conditions (Affatato et al., 2006). Although *in* vivo, the hip joint is subject to triaxial forces and rotations, in the development of hip simulators for wear testing, it was found that simplifying the motion from 3 to 2 axes was appropriate, provided they are 90° out-of-phase (Smith and Unsworth, 2000). A hip simulator will typically apply a set of motions and loads and a lubricant that creates tribological conditions comparable, but not necessarily identical, to those occurring *in vivo*. The load conditions applied are typically steady state gait, however, some simulators are capable of simulating stair climb and jogging, evaluating the breakdown of lubrication under stop-start conditions and incorporating electrochemical measurements (Hadley et al., 2013, Bowsher and Shelton, 2001, Affatato et al., 2008, Hesketh et al., 2013). The use of hip simulators to evaluate the performance of taper junctions has not been widely reported. These tests will need to be standardised to ensure uniformity in protocol and reporting. The use of unified standards for conducting wear tests and assessing wear of bearing surface components (ISO 14142 part 1 and 2) was established to allow comparable results across test facilities however, this has not been achieved and different simulators have reported different wear rates (Affatato et al., 2006).

Table 2-16 Characteristics of various hip simulators Flex/Ext: flexion-extension, Abd/Add: abduction-adduction, IER: internal-external rotation

	Motion Simulation		Peak Load / N	Reference
AMTI- Boston	Flex/Ext Abd/Add IER	(±25°) (±9°) (±20°)	4.5	Affatato et al. (2006)
HUT- 4	Flex/Ext Abd/Add	(46°) (12°)	2	
Mark II Durham	Flex/Ext IER	(+30°/-15°) (±10°)	2.9	
EW08 MMED (MATCO)	Flex/Ext Abd/Add	(±22.5°) (±22.5°)	2.1	
MTS Orbital simulator	Flex/Ext Abd/Add	(±23°) (±23°)	3	de Villiers (2014)
Prosim	Flex/Ext IER	(+30/-15°) (±10°)	4	Hadley et al. (2013)

2.7 Thesis Aims and Objectives

The aim of this thesis is to understand the behaviour of the head-neck taper interface in a range of conditions. This includes identifying the effect of head size on taper torque in MoP bearings and evaluating the effect of taper design factors (taper clearance, trunnion surface topography and length) on the separation of the taper interface as well as the metal ion release from the taper junction, under hip simulator load profiles experimentally and modelled using FE methods.

Objectives

1. Identify a suitable method for evaluating dynamic torques adjacent to the taper junction
2. Design and test taper junctions with proximal and distal contact conditions as well as defined surface roughness to be isolated from the bearing surface
3. Define and evaluate a range of clinically relevant taper clearances and trunnion lengths using finite element analysis (FEA) under appropriate loading conditions

Chapter 3. Torque measurement at the taper interface

3.1 Introduction

Torque is generated at a hip implant bearing surface, during activities which load the implant, as a result of friction at the bearing surface. This torque is transmitted through the implant and has been evaluated in relation to either the acetabular component or stem loosening both *in vivo* and *in vitro. In vivo,* the torque generated via instrumented prostheses has been evaluated by Schwachmeyer et al. (2013); whilst *in vitro*, torque has been evaluated using a range of methodologies, including friction simulators. Experimentally, the torque may be determined using strains as a proxy variable. Recent reports of increased corrosion at taper junctions have been proposed to be due to larger taper junction torques (Dyrkacz et al., 2013), which in turn lead to greater micromotion or fretting. However, the absolute magnitude of the torque transmitted through the taper junction has not been reported previously.

The torque experienced by implants is a function of the 3 axes of motion of a hip joint (Damm et al., 2013). Friction simulators and the ISO standard tests, often apply loads and motion in one plane only. Hip simulators incorporate multiple axes of motion as well as realistic dynamic loading cycles due to the changing position of the load vector through the cycle of an activity. The taper junction torque cannot be measured directly at the junction without altering or interfering with the dynamics. Consequently, torque measurements on the hip simulator can only be carried out at positions proximal or distal to the taper junction. The aim of the current study was to strains distal to the taper junction, while loaded on a hip simulator.

3.2 Materials and methods

3.2.1 Gauge placement

Three 17-4 stainless steel trunnion fixtures with 12/14 tapers were used to evaluate the trunnion strains resulting from the articulation of CoCr heads of varying sizes against acetabular components. A pair of 3 axis stacked rectangular rosettes and single axis gauges (UFRA-1-17-3L and UFLA-1-17-3L, Techni Measure, UK) were bonded using ethyl-2-cyanoacrylate glue (Loctite Superglue; Henkel Limited) at 4 positions around the circumference of a trunnion taper fixture. The rosette pair was placed on diametrically opposite sides and 90° to either of the rosette, a uniaxial linear gauge was positioned as shown in Figure 3-1. The trunnion fixture with the bonded gauges was covered in a polysulphide coating (M-coat-J; Vishay, UK) for moisture resistance.

3.2.2 Measurement setup

Two bridge configurations were used; a half bridge configuration to determine bending strains and full bridge to measure torque. An internal excitation voltage of 2.5 V, shunt resistance and bridge resistance of 100 kΩ and 120 Ω was applied. Data acquisition was applied at a rate of 10 Hz.

(a)

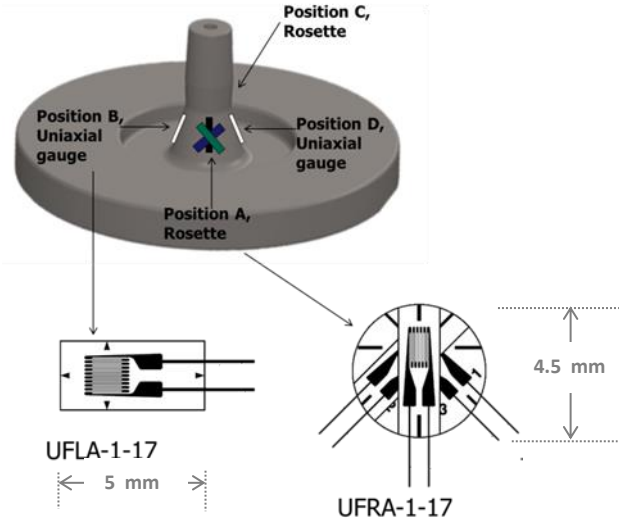

(b)

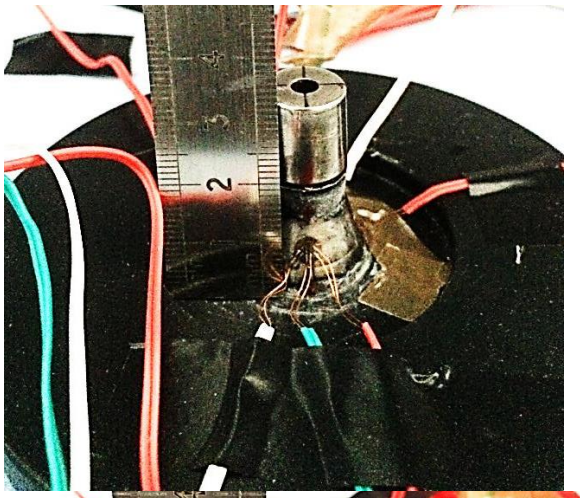

(c)

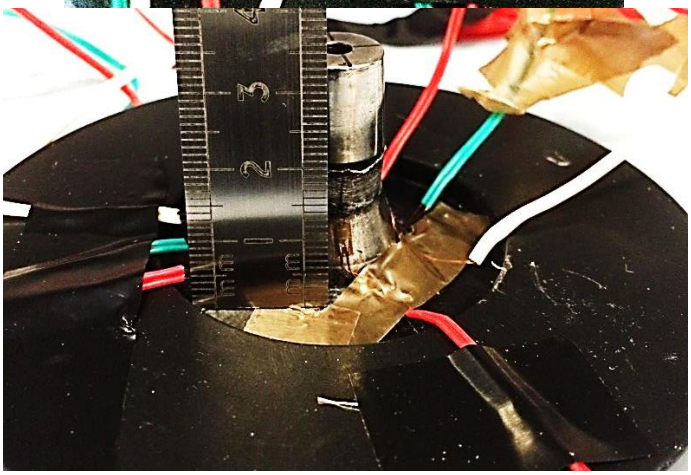

Figure 3-1 (a) Schematic showing the location of gauges on the trunnion fixture (b) A rosette positioned on the trunnion fixture (c) A uniaxial gauge positioned on the trunnion fixture

3.2.3 Test components

Tests were carried out on commercially available 28, 32, 40 mm as well as prototype 52 and 56 mm metal on polyethylene bearings; in addition to these, one 48 mm metal-on-metal (MoM) component was also evaluated (Corin Group PLC, Cirencester, UK).

Table 3-1 List of test components

		Head size / mm	Head offset / mm
Metal-on-polyethylene (MoP)	Commercially available	28	+3.5, +7
		32	+0
		40	
	Prototype	52	
		56	
Metal-on-metal (MoM)	Prototype	48	

3.2.4 Hip simulator setup

Testing was carried out on an eight station orbital hip simulator (MTS Systems, USA). Each component was subjected to a typical walking cycle with a maximum load of 3.0 kN at 60 rpm (Figure 3-2) using a lubricant of 25 % (v/v) newborn calf serum (1% w/v Sodium azide). Each test was repeated at least twice.

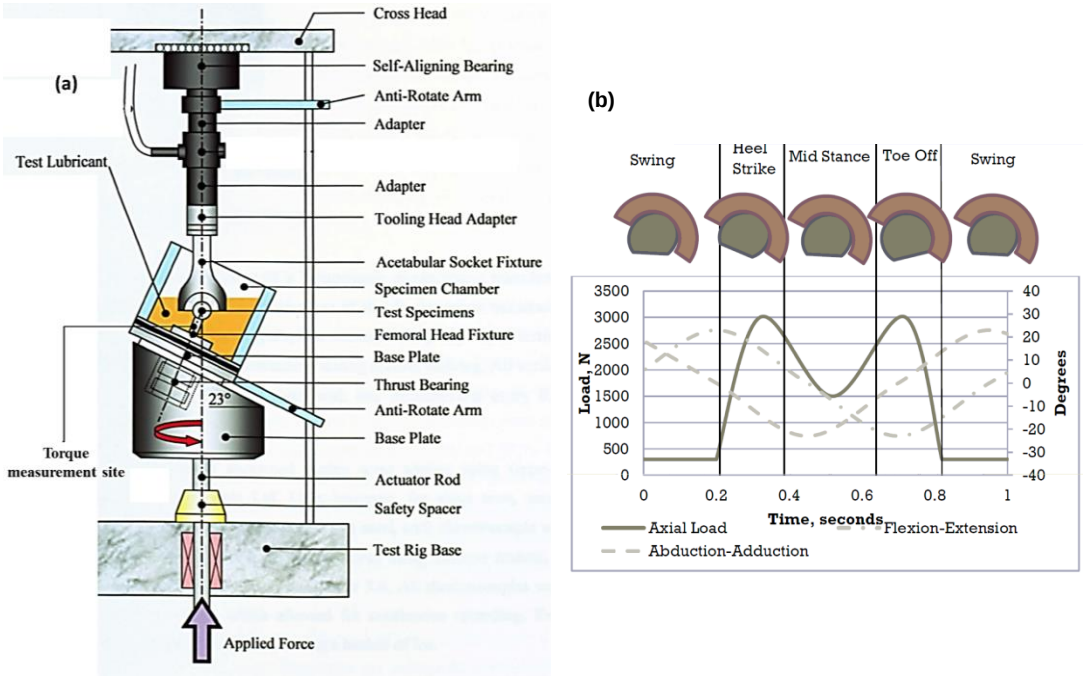

Figure 3-2 (a) Schematic of one station on the MTS hip simulator, adapted from (Bowsher, 2001) (b) loading cycle applied by the simulator

The components were also subjected to maximum sinusoidal loads of 250, 750, 1250, 2500 and 3850 N (minimum 0 N) at rotational speeds of 5, 10, 30 and 60 rpm, in order to investigate the influence of the load and fluid entraining velocity.

3.2.5 Validation of strain gauge measurements

Strain measurements were validated in 2 ways: (i) Comparing static strains to analytical solutions and (ii) Comparing static to dynamic results

3.2.5.1 Comparison of static strains to analytical solutions

The DAQ system was used to obtain the strains from a uniaxial gauge in the M-L plane which was connected in a quarter bridge configuration. The trunnion fixture was assembled with a 56 mm CoCr femoral head and the setup was loaded through a polyethylene cup using an Instron 5967 with 30 kN load cell (Figure 3-3a). The load was ramped up to 2.5 kN as shown in Figure 3-3b. The static moment was compared to analytical calculations.

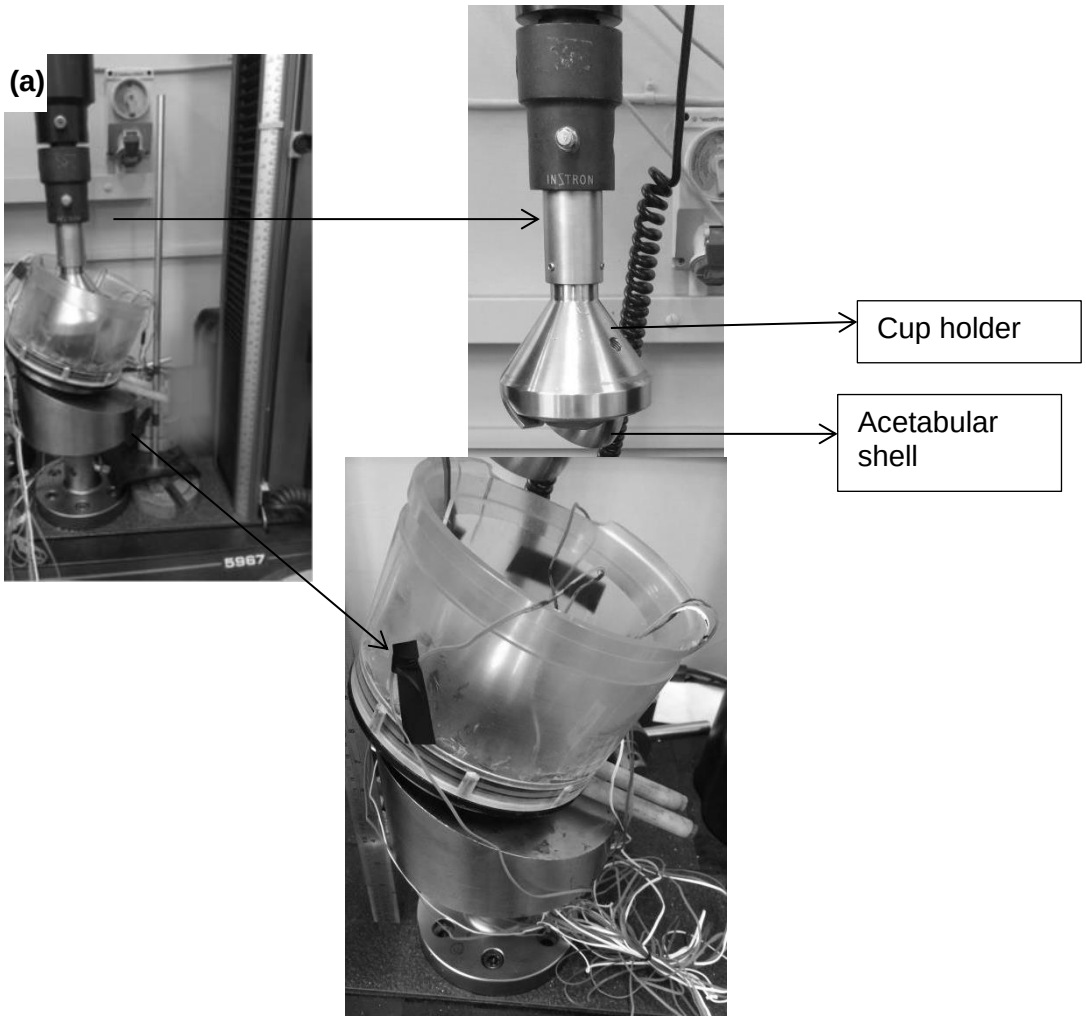

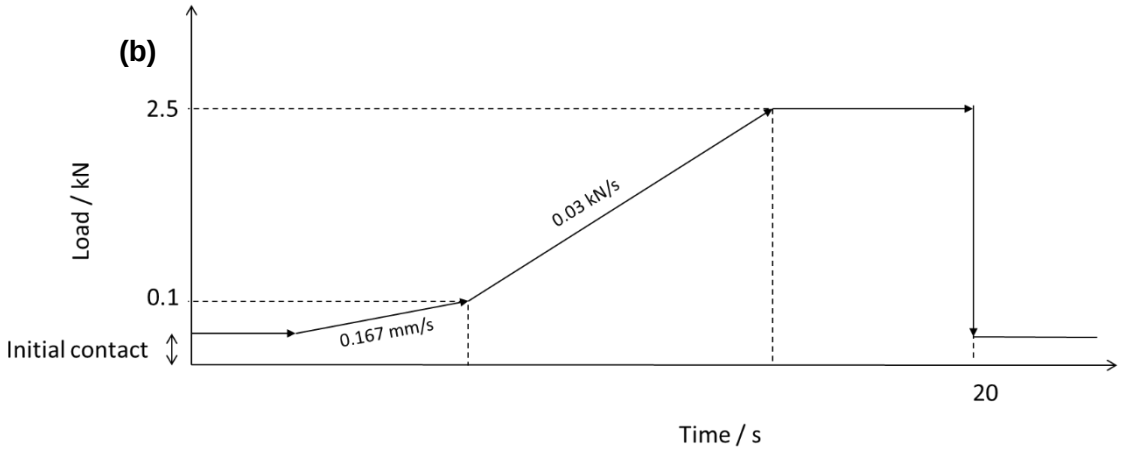

Figure 3-3 (a) Static measurement setup on Instron 5967 (b) load profile applied for static measurement

3.2.5.2 Comparison of static to dynamic results

A second uniaxial gauge was bonded diametrically opposite to the gauge in 3.2.5.1 to compare the bending strains obtained statically to the dynamic strains from a corresponding plane on the hip simulator test at a maximum load of 3 kN.

3.2.6 Single Axis Dynamic Compression

Dynamic compression testing was carried out using a commercially available stem with a 12/14 taper equivalent to the trunnion fixture used for testing on the hip simulator paired with a 40 mm CoCr head. The stem was fixed in acrylic cement; the stem orientation and cement level was determined using ISO 7206-4 (2010). The test was carried out on a single axis ElectroPuls E10000 (Instron, Buckinghamshire, UK) with a maximum and minimum sinusoidal load of 3.3 kN and 0.3 kN at 1 and 5 Hz replicating the ASTM F1875 fretting test for a duration of 3000 cycles. 2 pairs of uniaxial and rectangular rosettes were bonded around the circumference of the neck as shown in Figure 3-4 on diametrically opposite sides. The gauges were the same as those used on the hip simulator with the same bridge configurations.

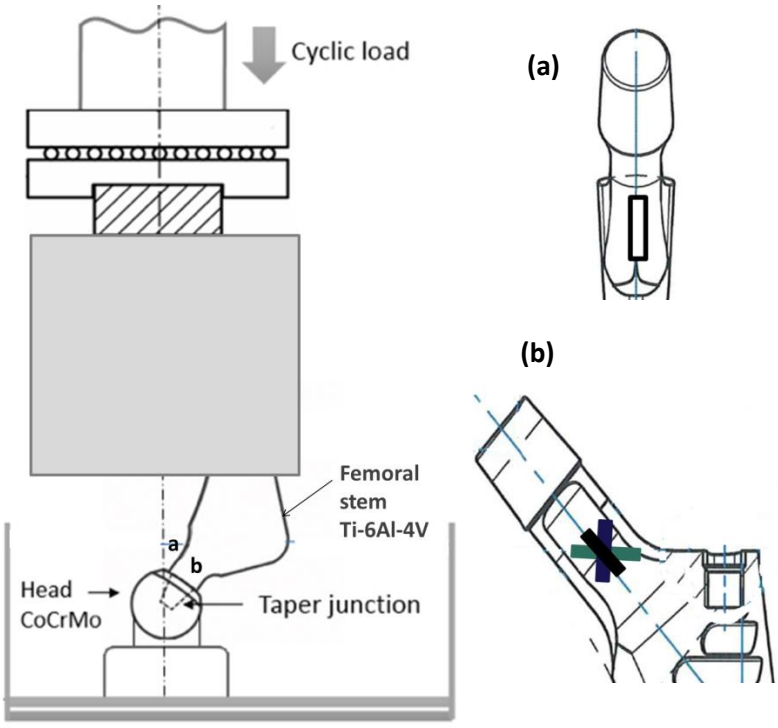

Figure 3-4 Left: Schematic of single axis dynamic compression setup, Right: Schematic of strain gauge positioning (uniaxial gauge in a, rosette in b) on the neck of the femoral stem beneath the trunnion

3.2.7 Positioning of bone chips on the trunnion

To determine the effect of contaminants on the torque measured, ovine cervical vertebrae was crushed into chips. A bone chip (0.02±0.002 g) was adhered to the trunnion lengthwise using cyanoacrylate. The cyanoacrylate was applied carefully to prevent it coating the trunnion surface and influencing the measurements. The adhesive held the bone chip in place whilst the taper was initially mated by hand. Taper lock was ensured using a peak load of 2 kN on the Instron as prescribed in ASTM F1875-98. Two positions were considered to evaluate any change in torque when the bone chip was located on the superior surface of the trunnion as compared to the posterior surface (Figure 3-5). The torque was evaluated at each position 3 times.

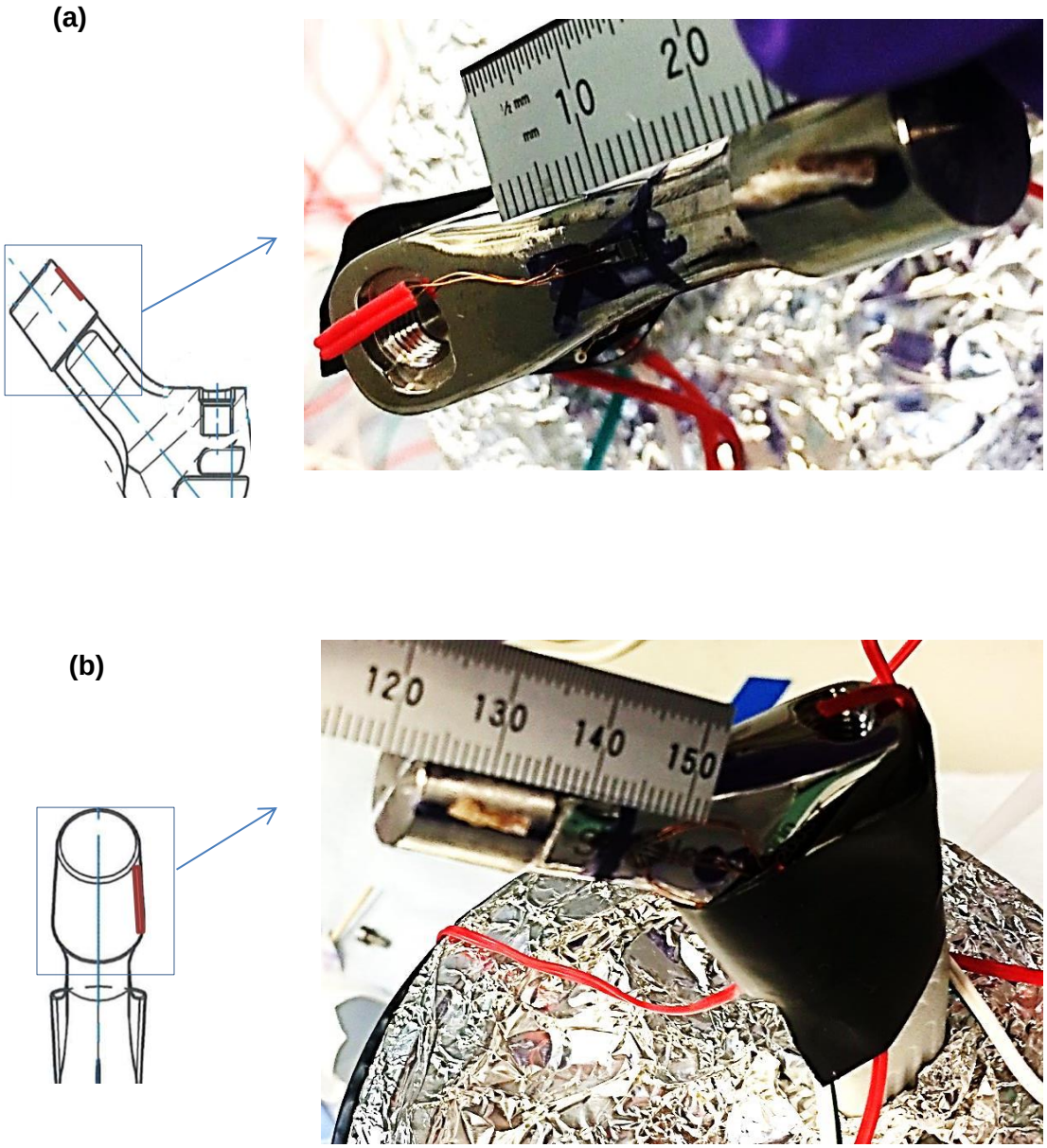

Figure 3-5 Locating the bone chip (a) superiorly (b) posteriorly on the trunnion surface of a Ti-6Al-4V stem

3.2.8 Pendulum friction simulator

Friction at the bearing surface was carried out on a pneumatically loaded pendulum friction simulator (Simulator Solutions, Manchester, UK), A friction simulator (Figure 3-6) applies a vertical load and a rotation in the flexion-extension. A load is applied from a loading frame through a motion arm; a femoral head is assembled to the motion arm in an inverse physiological orientation and a simultaneous flexion-extension profile is applied through the arm. The femoral head articulates against an acetabular cup, which is located on a moveable carriage mounted on pressurised hydrostatic bearings so that the system's friction is negligible. A piezoelectric transducer located anteriorly on the carriage measures the force transmitted from the frame to the carriage and thus the friction at the bearing surface (Brockett et al., 2007).

Prior to testing, each sample was cleaned based on ISO 14242-2 (2000). A ± 25° flexion-extension profile and a maximum load of 2 kN with a 300 N swing phase load (Figure 3-7) was applied at 1 Hz. Each test was performed in 2 directions: forward and reverse. The forward direction cycled from 0°;-25°;0°;25°;0° and the reverse direction 0°;25°;0°;-25°;0°, in order to minimise misalignment errors associated with the centres of rotations. The five metal-on-polyethylene bearing combinations were tested on a pendulum friction simulator. The bearing surface of the test components were lubricated with approximately 3 ml of 25 % new born calf serum. Each bearing size was tested 3 times; between each test, the lubricant was changed and the bearing surfaces were wiped clean.

For both directions, each test was run for 125 cycles and data was logged at 30 cycle intervals for 5 cycles. It has been found in previous studies that the data stabilises after 120 cycles (Brockett et al., 2007); therefore, the data used to calculate the frictional torque was the data logged between 120 and 124 cycles. The true torque at the bearing surface of each component was determined as the average of the frictional torques in the forward and reverse direction.

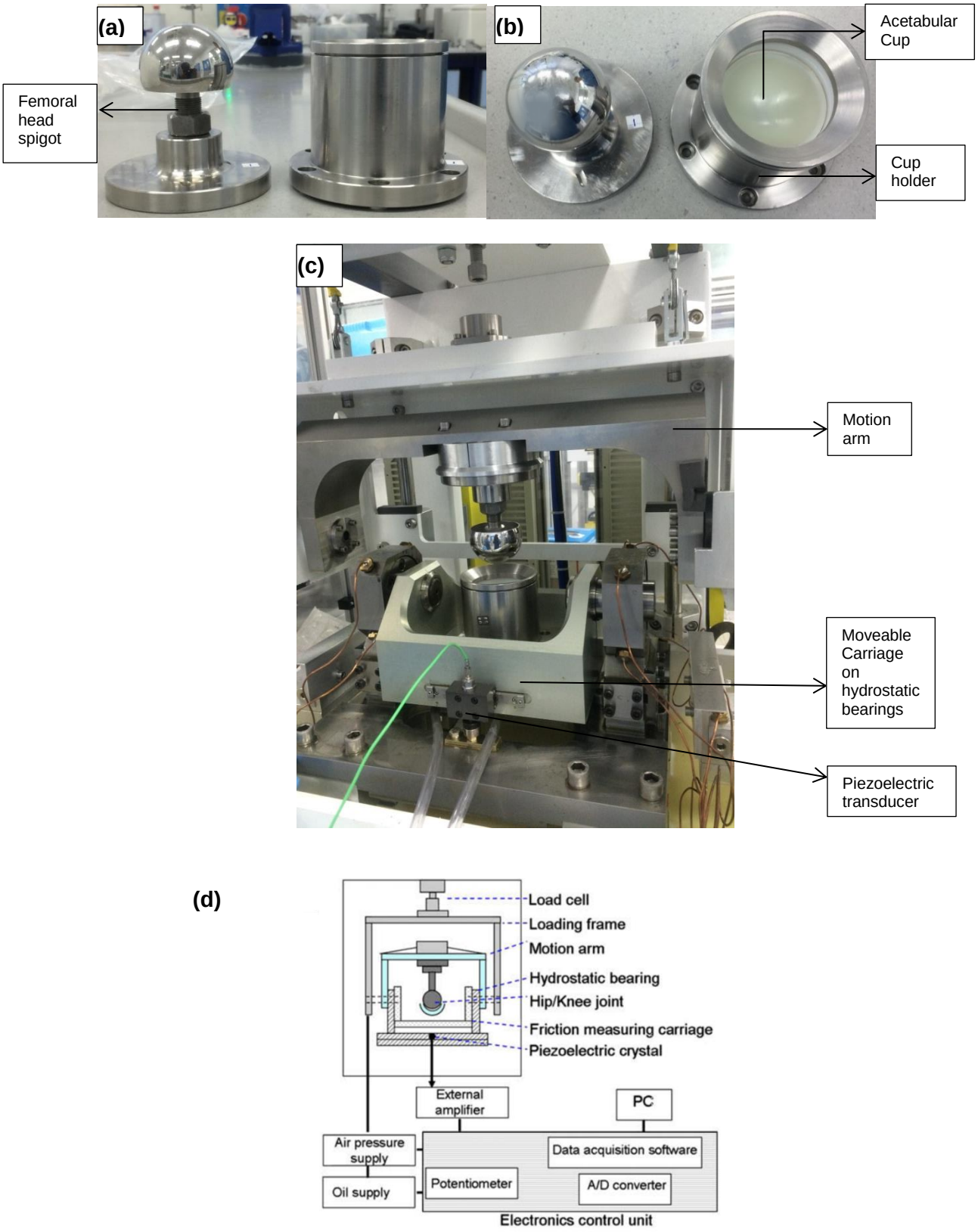

Figure 3-6 (a and b) Head and cup assembly setup for the friction simulator (c) The assembly of the bearing components mounted on the friction simulator (d) Schematic of friction simulator adapted from McCann et al. (2009)

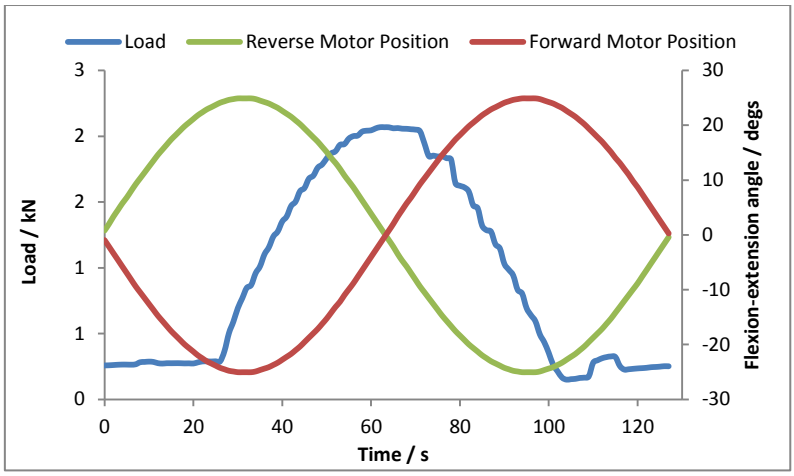

Figure 3-7 Load and rotational profile applied by the pendulum friction simulator

3.2.9 Roughness measurements

Roughness of the articulating surfaces of the femoral heads and acetabular cups was measured after testing using a ZeScope 3D optical surface profilometer (Zemetrics Inc, Tuscon, AZ) with a 20X objective lens.

ZeScope is an optical profilometer uses white light interferometry to generate a 3D image of the sample surface by comparing the optical path difference between light from a surface of interest and from a reference surface (Zygo, 2017). This is based on the superposition of light waves which are temporally and spatially coherent. The setup (Figure 3-8) comprises an LED light source which emits a beam of light to a beam splitter. Consequently, the incident beam is separated into two. The first beam is sent to a reference mirror, following a constant optical path whilst the other is sent to the sample of interest. Reflection of the split incident beams occurs at the reference mirror and samples respectively. The reflected beams are directed through the beam splitter to a CCD camera and superimposed. Interference occurs if the optical path difference is within the coherence length of the light source. For an optical path difference of an even number of half wavelengths, constructive interference results since the superimposed waves are in phase.

Where the optical path difference is an odd number of half wavelengths, the result is destructive interference since the waves are 180^{o} out of phase (Schneider et al., 2014). Since the reference mirror is of a known flatness, the optical path differences result from variations in topography at the sample surface (Zygo, 2017). Varying the z-coordinate (vertical position) of the sample results in varying interference intensities, this is recorded by a CCD camera. The inference intensity is a maximum, when the optical path difference is zero for a given x,y coordinate. Consequently, the z position at which the maximum interference occurred is recorded as the height for that x,y coordinate (Schneider et al., 2014). Provided the wavelength is known, the height differences across a surface can be deduced, in fractions of a wave. From these height differences, a 3D surface map is generated (Zygo, 2017).

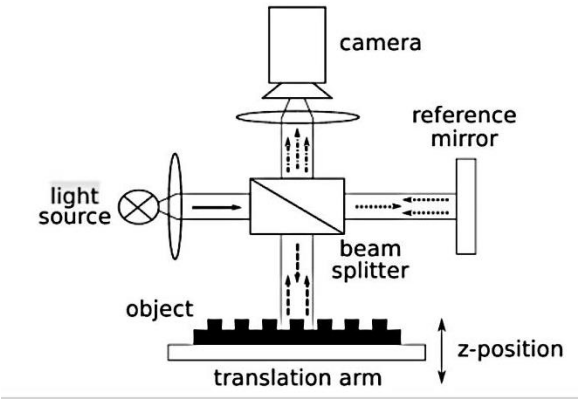

Figure 3-8 Schematic of principle of operation of white light interferometry (Schneider et al., 2014)

All components were cleaned prior to obtaining measurements. The roughness measure S_a was recorded as the R_a and a cut-off length of 0.8 mm was applied to remove components of longer wavelengths. The roughness of the smallest acetabular cup (28 mm) was not recorded because it required a lens with a longer working distance objective than was available.

3.2.10 Data analysis

Statistical analysis of all data was performed using a two-tailed student's t-test; significance was set at $p<0.05$.

3.3 Results

3.3.1 Validation of gauges

Assuming the location of the centre of the strain gauges was at 28.5 mm from the top of the taper (Figure 3-9) and that the applied load of 2.5 kN acted through the centre of the head, the bending moment generated could be estimated to be

Moment = F x lever arm (16)
F= 2.5 kN
Lever arm (x) = 28.5 cos 67 = 11.14 mm
Moment = 27.84 Nm

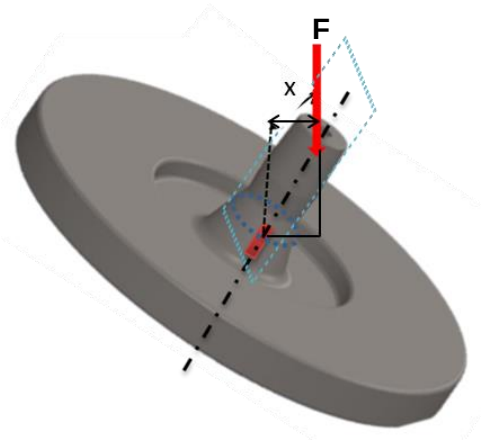

Figure 3-9 Schematic of analytical calculation

The difference between the static moment and the analytical results determined from equation 16 was within 10% (Figure 3-10a). Likewise, the difference in bending strains determined during the static and dynamic experimental setups was also within this limit (Figure 3-10b).

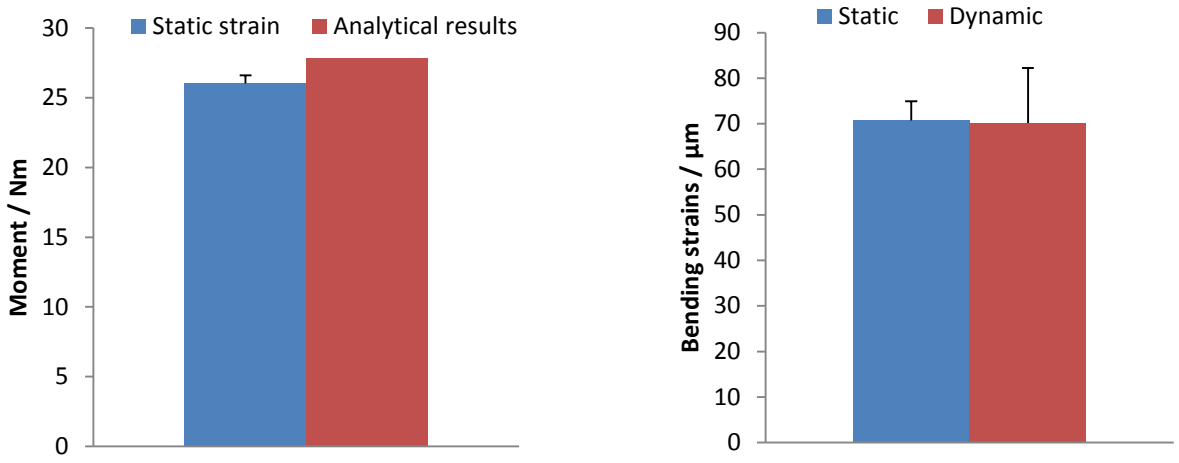

Figure 3-10 (a) Validation of the static moment with analytical results (b) Validation of the dynamic strains using static strains

3.3.1.1 Error estimation

The surface to which the strain gauges were bonded was conical and could be considered as a series of stacked concentric rings with varying radii. The strain gauge was assumed to be located at the midpoint of this surface. Any errors in locating the gauge vertically would result in an error in the estimation of torque since Torque is a function of R^3 (equation 19, Appendix A.4).

Assuming that the 5 mm long gauge was located at R_m (Figure 3-11), a radius of 8.3 mm was used, if the gauge was in fact located at positions 2 and 3, radii of 7.7 or 8.9 mm would be used. Therefore, the maximum error in torque measured experimentally is estimated at 19 %.

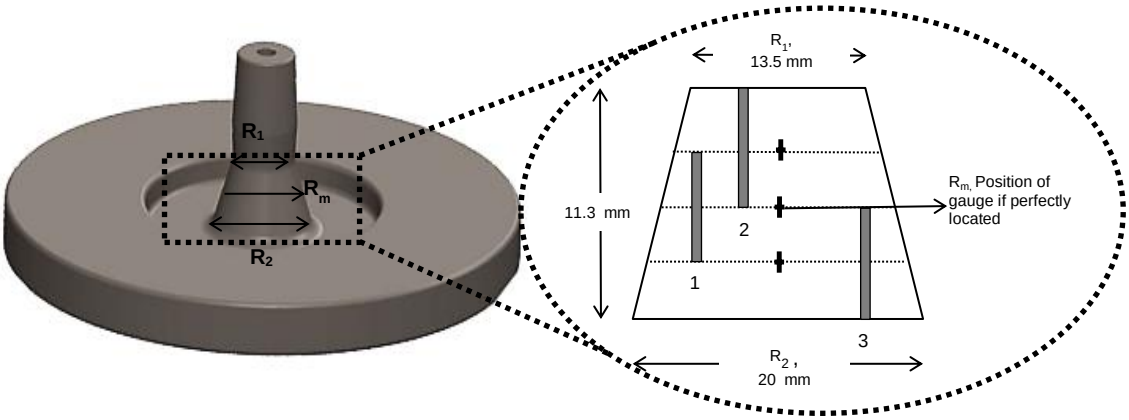

Figure 3-11 Schematic of placement error analysis

3.3.2 Hip simulator

The mean roughness (R_a) values of femoral heads and acetabular cups measured (Table 3-2) were found to be 0.062 and 1.08 μm respectively. Increasing head sizes resulted in increased taper torques measured from tests on the hip simulator. The significance of the head size over material combination was apparent (Figure 3-12). An increase in torque was measured when there was an increased head offset on the 28 mm head. The torque measured on the hip simulator showed a correlation with R_a of the femoral head (R^2=0.79, Figure 3-13), indicating that an increase of roughness influenced developed torques.

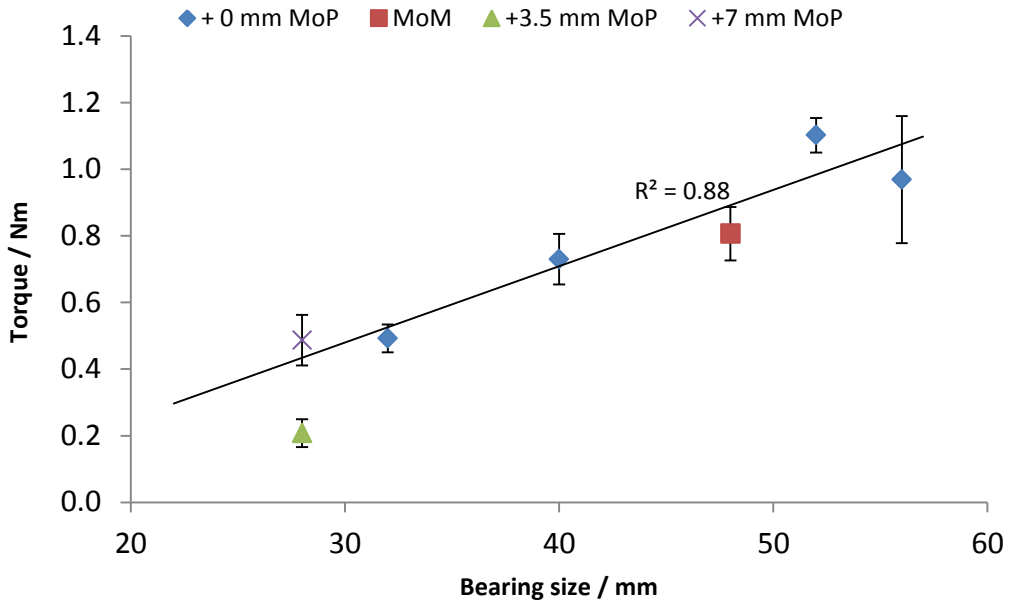

Figure 3-12 Relationship between head size and torque as measured on the hip simulator (error bars= ± SD)

Table 3-2 Average surface roughness, Ra (μm) of the femoral head and acetabular cup

	Femoral head	Acetabular cup
28	0.043	-
32	0.037	2.02
40	0.073	0.24
52	0.080	0.63
56	0.081	1.44

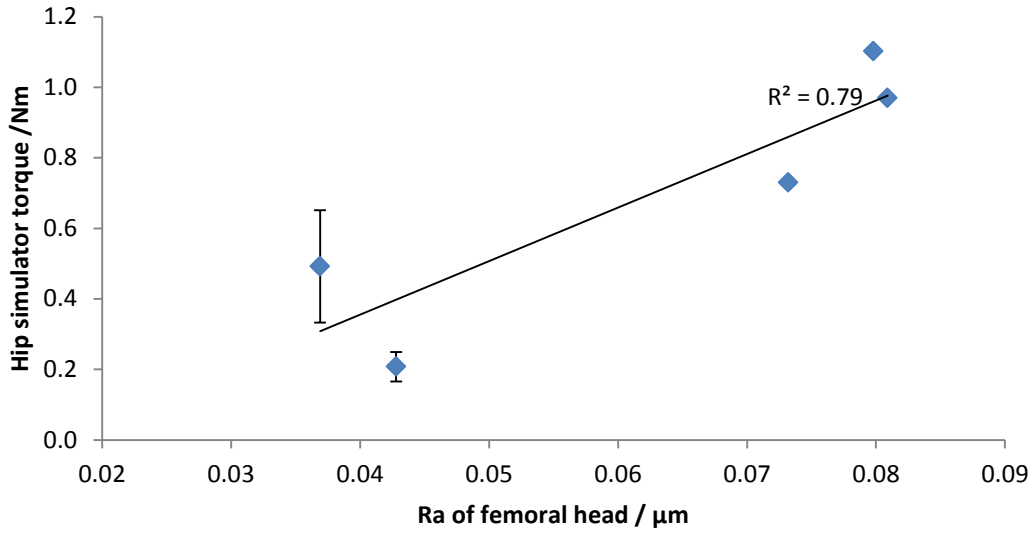

Figure 3-13 Increase in peak torque measured by the hip simulator as a function of femoral head roughness (R_a) (error bars= ± SD) (standard deviation not obvious on some data points due to small magnitude)

The maximum bending moment on the trunnion was an order of magnitude higher than the taper torques measured on the hip simulator. The maximum bending moment was higher in the X plane than the perpendicular Y plane and bending moments increased with head offset (28 mm combinations, Figure 3-14) but not head size (Figure 3-15).

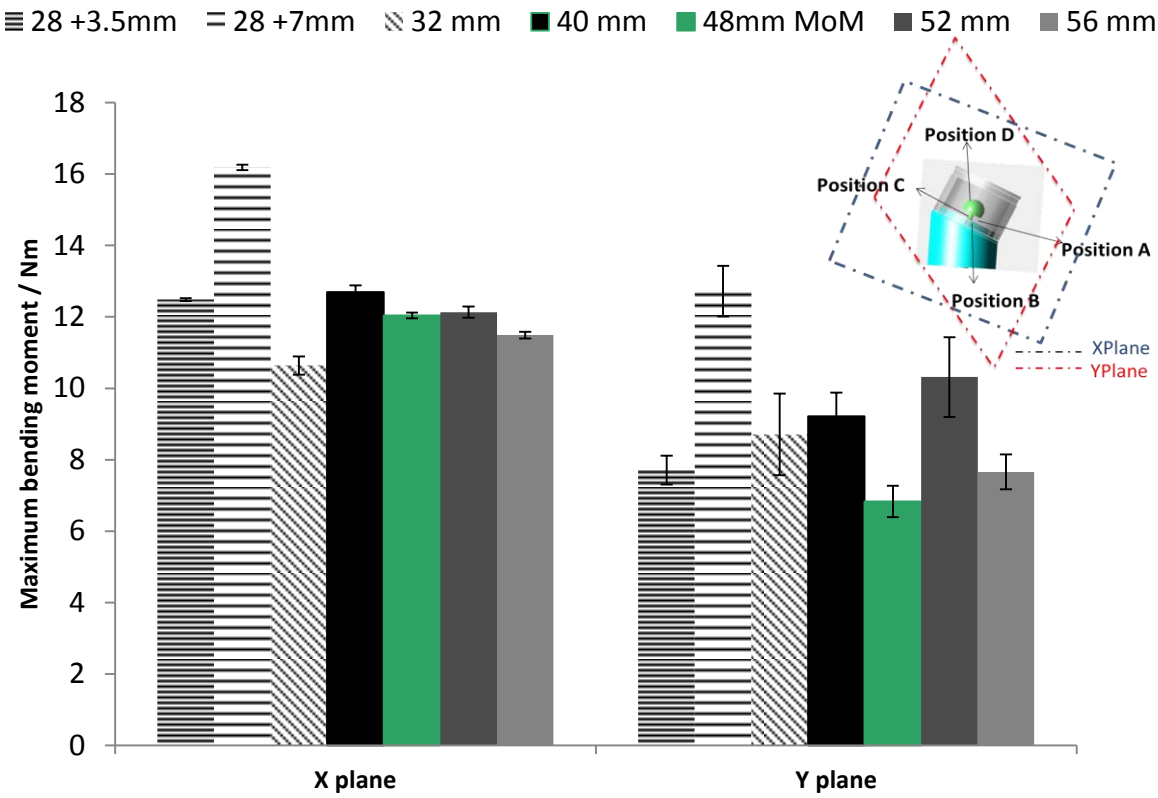

Figure 3-14 Variation of mean bending moments with head size (error bars = ± SD) in planes X and Y during loading cycles. X =frontal plane, Y =sagittal plane

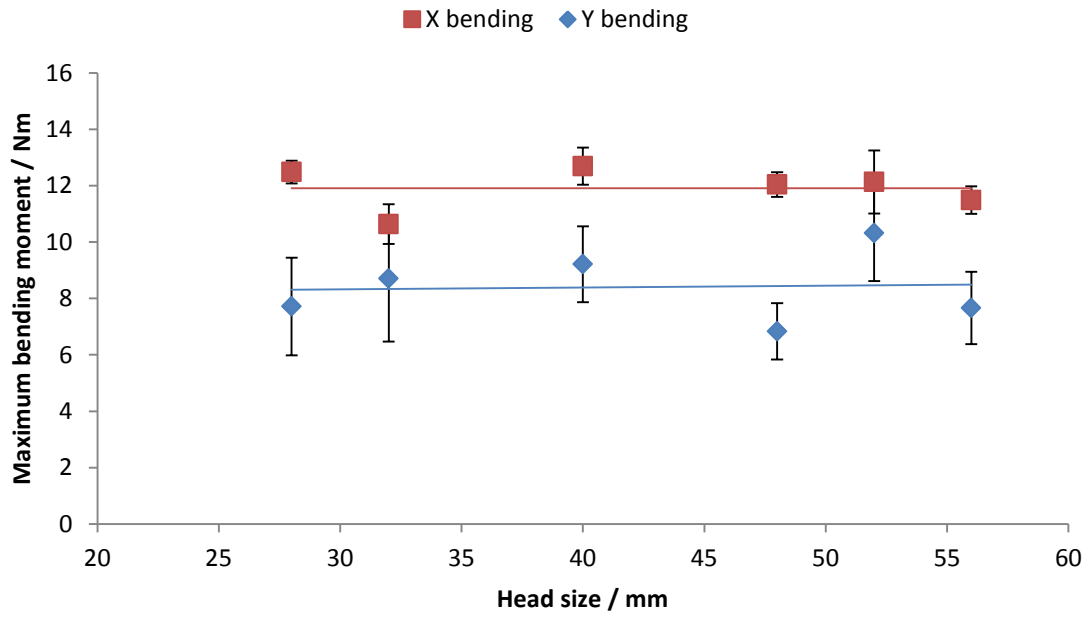

Figure 3-15 Relationship between head size and maximum bending moment on the hip simulator; error bars= ± SD

For all heads evaluated on the hip simulator, the torque developed below the taper was a function of load rather than speed of rotation or entrainment velocity (Figure 3-16).

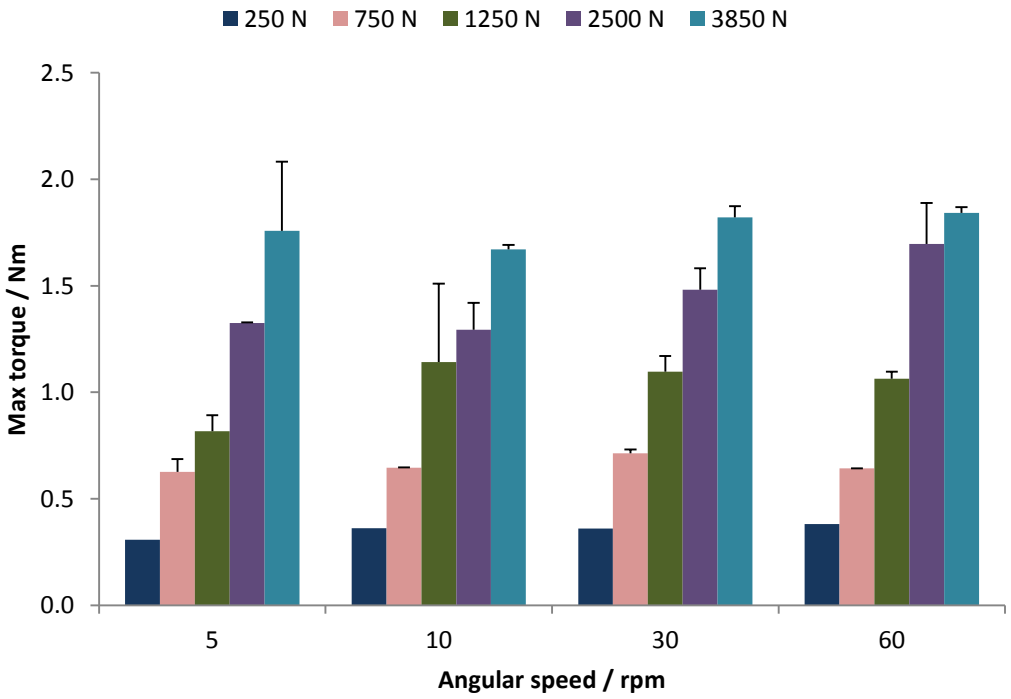

Figure 3-16 Maximum torque developed as a function of angular speed and peak applied load, for a 52 mm MoP bearing (error bars= + SD)

3.3.3 Single axis dynamic compression

The torque recorded following testing on the single axis rig was negligible (Figure 3-17). Both X and Y bending as well as torque reduced when the loading frequency was increased from 1 to 5 Hz. However, only the reduction in X bending from 1 to 5 Hz was statistically significant (p=0.02).

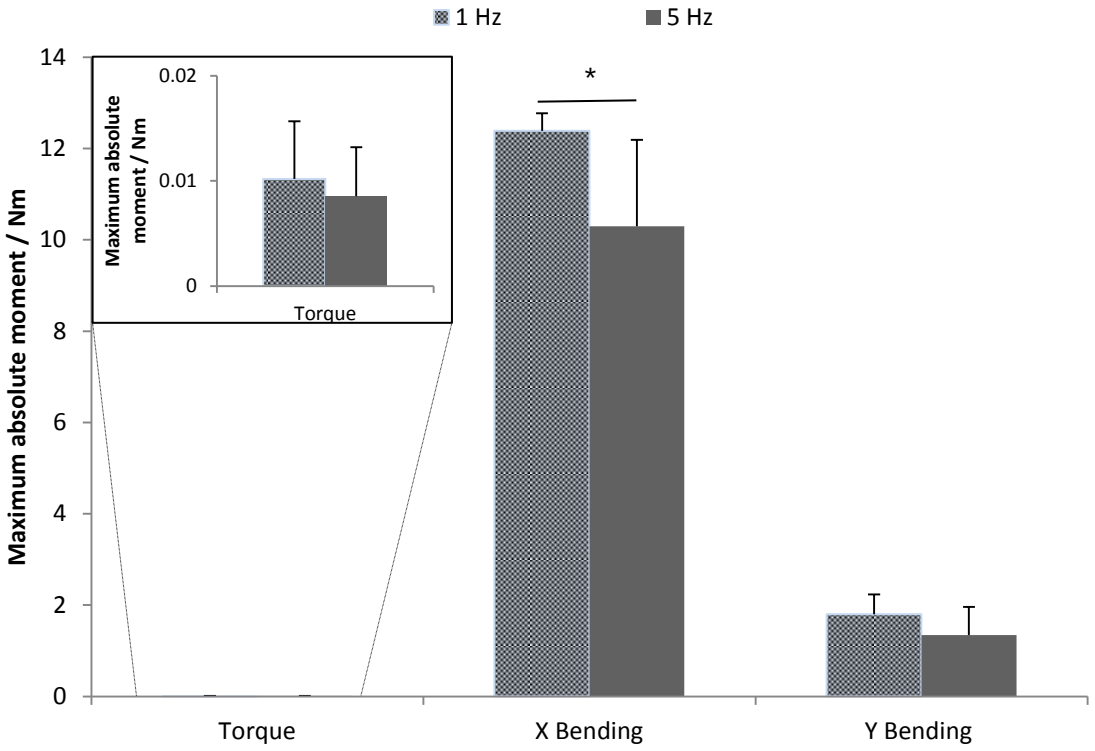

Figure 3-17 Peak moments measured beneath the taper junction using a 40 mm head on a single axis dynamic compression instrument (*=p<0.05, error bars= + SD)

3.3.4 Effect of contaminant on taper torque

Contaminating the taper with bone resulted in an increase in torque measured at the taper junction at both 1 and 5 Hz but this was not significant (p =0.51) (Figure 3-18). Considering the effect of bone chip placement at 5 Hz, it was observed that the torque measured higher at the posterior location but the difference was also not significant (p = 0.39) (Figure 3-19).

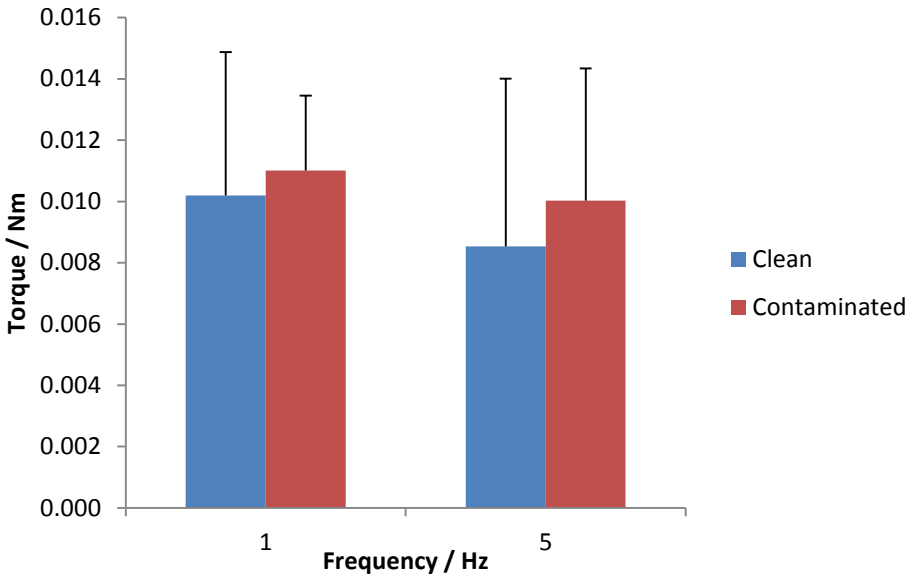

Figure 3-18 Effect of taper contamination on torque measured in uniaxial compression at 1 and 5Hz (mean +SD)

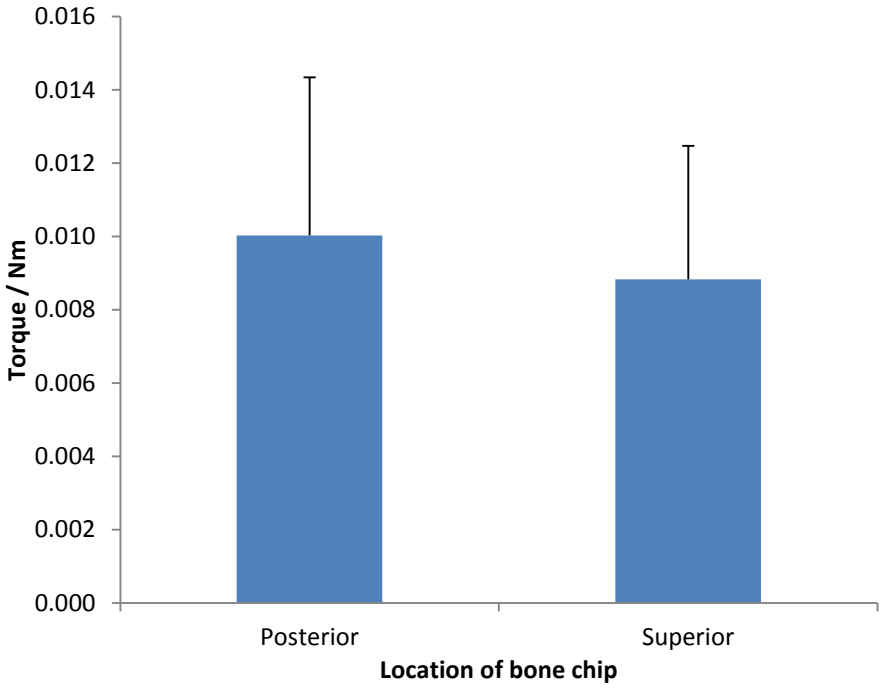

Figure 3-19 Effect of varying the location of contaminant on torque measured in uniaxial compression at 5 Hz (mean +SD)

3.3.5 Pendulum friction simulator

The pendulum friction simulator showed that the bearing surface friction measured was strongly correlated with the head size for the MoP combinations (R^2=0.63) (Figure 3-20) and the roughness of the femoral head (Figure 3-21).

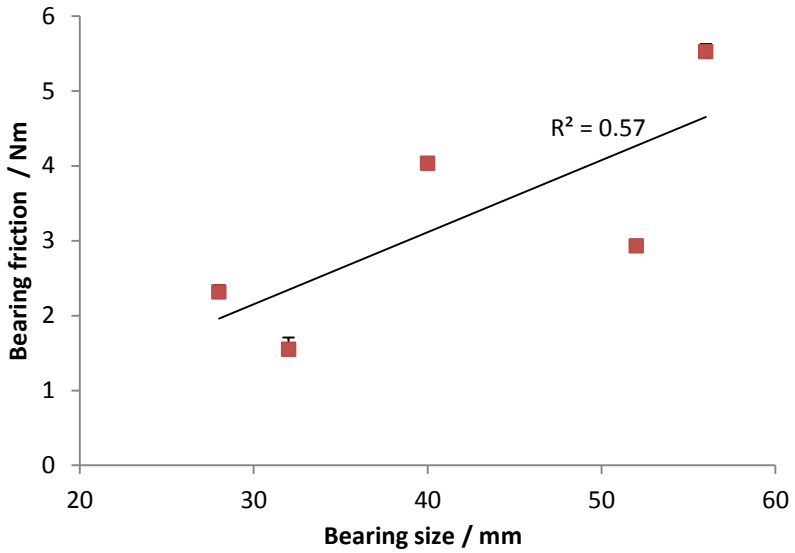

Figure 3-20 Bearing surface friction measured on the pendulum friction simulator (error bars= ± SD) (standard deviation not obvious on some data points due to small magnitude)

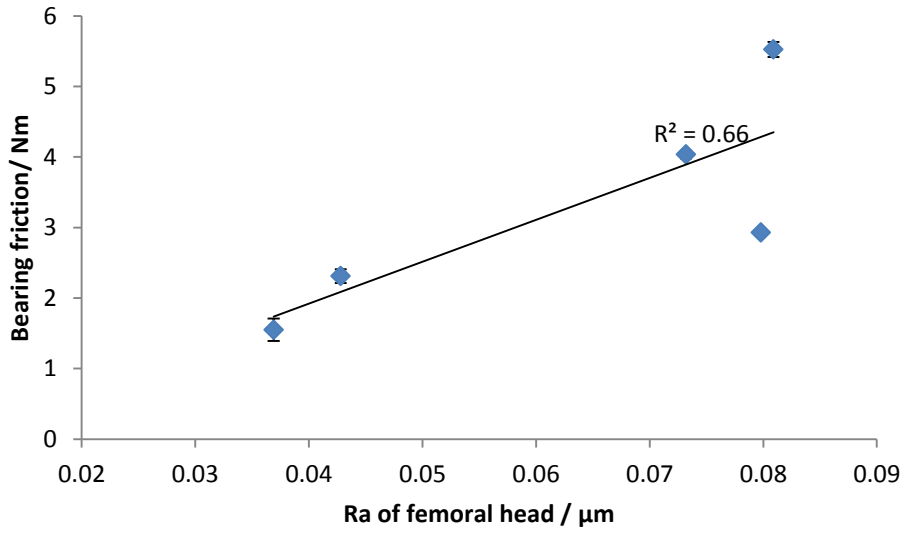

Figure 3-21 Increase in torque measured by the pendulum simulator as a function of femoral head roughness (R_a) (error bars= ± SD)(standard deviation not obvious on some data points due to small magnitude)

3.4 Discussion

3.4.1 Torque

Increasing torque and bearing surface friction with head size has been widely discussed (Panagiotidou et al., 2015, Dyrkacz et al., 2013, Hexter et al., 2013, Langton et al., 2012). The current study showed that the torque about the taper axis below the taper junction was positively correlated with the head size (R^2= 0.9), and that bearing surface friction also was strongly correlated with head size (R^2=0.6) (Figure 3-12 and Figure 3-20). A larger head size has been introduced as it provides increased stability and range of motion whilst generating a larger entraining velocity and thereby a greater minimum film thickness. However, the recent increase in the incidence of taper corrosion has been linked to increasing head sizes (Scholes and Unsworth, 2000). The mechanism by which this has been suggested to occur is due to instability initiated by increased torques at the taper junction (Damm et al., 2013). The contribution of head-cup clearance to the measured torques has not been evaluated; the effect of head-cup clearance on torque is only identifiable in measurement systems which generate internal-external rotation (Scholl et al., 2016a).

In the current study, large MoP bearings (52 and 56 mm) generated torque values higher than the 48 mm MoM bearing, suggesting that LHMoP may develop similar corrosion issues at the head taper due to bearing surface friction to those widely reported in MoM devices (Morlock, 2015, Langton et al., 2012). In MoP devices highly crosslinked polyethylenes (HXLPE) have enabled the use of large heads as a result of their greatly improved wear properties and thereby the possibility to use thinner liners. Although this was discouraged in conventional polyethylene due to the likelihood of wearing through the material, the introduction of HXLPE and vitamin E incorporated polyethylenes means liners are designed with thicknesses as low as 2.5 - 3.6 mm, compared to the 6 mm minimum recommended

thickness for conventional polyethylene (Rajpura et al., 2014, Girard, 2015, Moore et al., 2008, Exatech, 2012). HXLPE and vitamin E polyethylene bearings have been reported to generate large bearing surface friction (Meneghini et al., 2016, Burroughs et al., 2006). The increased friction in LHMoP is not just a concern due to the acetabular liner material. Thinner liners are susceptible to circumferential deformation following implantation *in vivo* which may in turn create even larger bearing surface torques as a result of the reduced clearances that may result (Shen et al., 2005).

It should be noted that the torques could be even higher *in* vivo since the absence of muscle forces during laboratory testing may in fact result in an underestimation of torsional loads generated (Duda, 2013). Further, the current results support the literature indicating that larger heads are more susceptible to corrosion due to large torques, MoP bearings as small as 28 mm have also been reported to exhibit corrosion at the taper interface (Tan et al., 2015). This reinforces the concept that there are multiple factors affecting taper corrosion.

3.4.1.1 Effect of lubrication regime and load profile on torque

A 52 mm diameter MoP bearing was used to evaluate the effect of lubrication and loading profile on torque. Based on the Hamrock and Dowson equation (Hamrock and Dowson, 1978), for a 52 mm diameter bearing with a measured composite roughness of 0.64 µm (Ra_{CoCr} = 0.08 µm, Ra_{PE} = 0.63 µm), the lambda ratio (2.5.1.2, equation 7) can be determined to lie in the region of 0.1 - 0.6 depending on sliding velocity, implying boundary lubrication will occur (Figure 3-22).

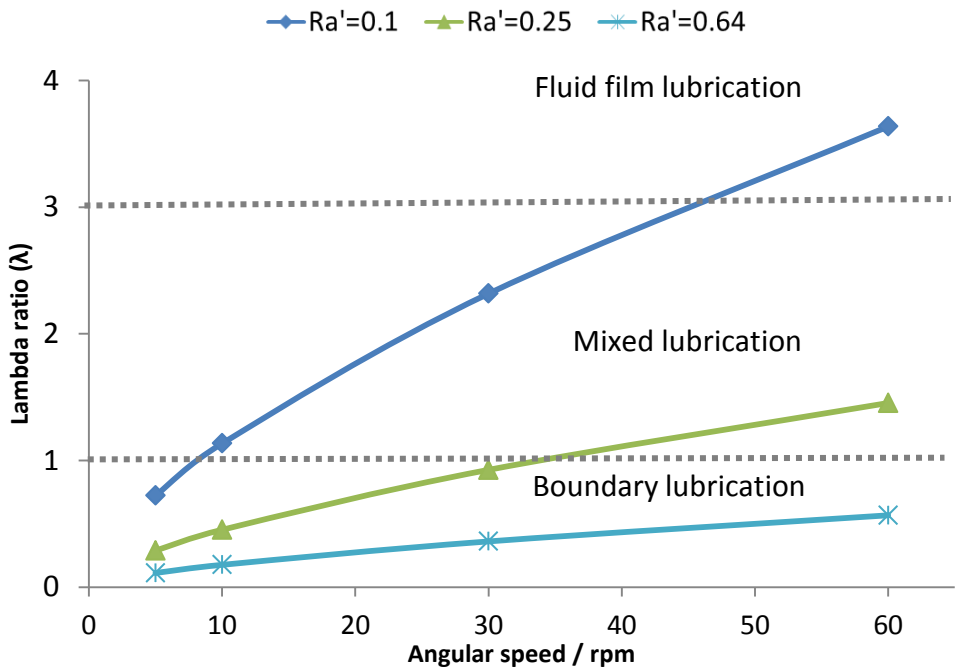

Figure 3-22 Relationship between lambda ratio and angular velocity for a 52 mm MoP bearing, tested using a maximum load of 3 kN, for a range of composite surface roughness

Metal femoral heads are polished during manufacture with an R_a typically specified as 0.02 ± 0.01 µm; even under low wearing conditions, R_a values have been reported to be between 0.018 – 0.035 µm from retrieved specimens (Taddei et al., 2016). Newly manufactured polyethylenes have higher roughness values, typically less than 2 µm; in service, the contact region polishes reducing the R_a to values that have been reported to be as low as 0.03 µm (Wang et al., 1995). However, in the current study, the lowest polyethylene roughness was measured on a 40 mm liner with an R_a value of 0.23 µm. The composite roughness (2.5.1.2, equation 12) therefore was, for the current tests, in the region of 0.24 µm indicating that the components could function in a mixed lubrication regime. If, however, the metal bearing surface was to be roughened by cement, bone or metal debris or in the event of a dislocation resulting in 3rd body abrasion (Day and Abboud, 2016), the head roughness could increase to values as high as 4 µm (de Villiers and Shelton, 2016) which results in further breakdown of the lubrication and would result in an increase in bearing

surface friction and torque transmitted to the taper junction. MoP devices will never operate in full fluid film lubrication as the liners cannot be polished to achieve such low roughness.

It was shown that the torque generated below the taper at the base of the fixture was more sensitive to the load applied (250 to 3850 N) than the change in entraining velocity (Figure 3-16). This could be as a result of the lubrication regime remaining within the boundary lubrication regime where the friction at the bearing surface is determined by asperity contact rather than being influenced by the small increase in film thickness due to a larger entraining velocity. The torque measured on the hip simulator was also found to depend on the loading profile. A lower torque was recorded when loaded with a walking cycle (1.1 Nm, Figure 3-12 for a 52 mm diameter head) in comparison to the sinusoidal loading where the maximum torque measured was approximately 1.5 Nm. This difference may be attributed to lubrication recovery the during the swing phase of a walking cycle profile (Damm et al., 2013). During the swing phase of the gait cycle, the bearing components separate resulting in a drop in pressure below ambient conditions. This results in fluid ingress into the bearing surface (Wroblewski et al., 2012), thus reducing the torque by 27 %.

3.4.1.2 The effect of contaminant on torque

It has been suggested that the presence of contaminants such as blood, fat and bone fragments at the taper interface during the surgical process could encourage fretting and/or corrosion by increasing micromotion at the junction (Lavernia et al., 2009). However, it was apparent from the current study, that the presence of bone fragments at the taper junction created resistance in initially mating the taper by hand. There are variations in the number of blows as well as the impaction force, reported by surgeons in mating the taper (Lavernia et al., 2009, Scholl et al., 2016b). Although impaction may overcome the initial resistance more readily than by hand, it is assumed that the head is placed on the trunnion by hand prior to

impaction wherein the surgeon should perceive the resistance at the junction and subsequently remove it. However, the resistance encountered could be less with smaller fragments.

The force required to separate the taper surfaces has been shown to be significantly lower when the CoCr/Ti taper was smeared with fat (Krull et al., 2017, Lavernia et al., 2009). Although bone is grouped in with the surgical debris that may contaminate the taper (Weisse et al., 2008, Lavernia et al., 2009), its effects appear to not have been evaluated with respect to metal heads. A reduction in static fracture load by up to 90 % was observed when Alumina/Ti taper interface was contaminated with human trabecular bone chips (Weisse et al., 2008). Whilst the bone chips may result in stress concentrations which cause fracture in a ceramic head taper, the current study did not show any significant impact in the torque measured at CoCr/Ti taper junction with and without embedded bone chips. Unlike fat and blood, the fat free bone chip would not have reduced the coefficient of friction at the interface. Also, the bone chip was located in only one position; it is possible that locating another bone chip along the same line could create a couple which may influence the torque measured. It should be noted however, that the current work isolated the effect of bone fragments. The combination of fragments with blood and/or fat may be different.

3.4.2 Bending moments

In comparison to *in vivo* telemetry studies, the bending moment obtained in this thesis is considerably larger (Dyrkacz et al., 2013). The difference may be attributed to the absence of muscle forces in laboratory testing. According to Duda (2013), the absence of musculature in testing will overestimate the moments obtained due to bending. The head sizes did not influence the bending moment when tested on the hip simulator (Figure 3-15); as the load magnitude and load position are both constant, meaning that the lever arm will remain unchanged in heads with no offset. However, *in vivo* where an increase in head size

as well as offset increases the lever arm (Fehring and Fehring, 2015), the bending moment will change.

The moment about the frontal (A-P) plane was consistently higher than the moment about the sagittal (M-L) plane on both the hip simulator and the uniaxial compression rig. This is consistent with the study by Bergmann et al. (2016) which utilised instrumented hip implants to evaluate the joint loads. Farhoudi et al. (2016) evaluated 3-D moments at the taper junction using analytical techniques, and also found that the peak bending moment about the anterior plane was between 3 and 8 times more than the peak bending moment about the lateral plane. However, the difference between the two moments is considerably larger in the uniaxial test setup. This is because the lever arm to the pair of gauges which measure the bending in the A-P plane is half of the neck thickness (6-7 mm) (Figure 3-23) which is considerably smaller than the lever arm in the M-L plane (15 mm) (Figure 3-23). In contrast, on the hip simulator, the lever arms lie on an ellipse with a minor diameter (in the sagittal plane) almost equal to the major diameter (in the frontal plane) such that the resulting moments are closer in magnitude.

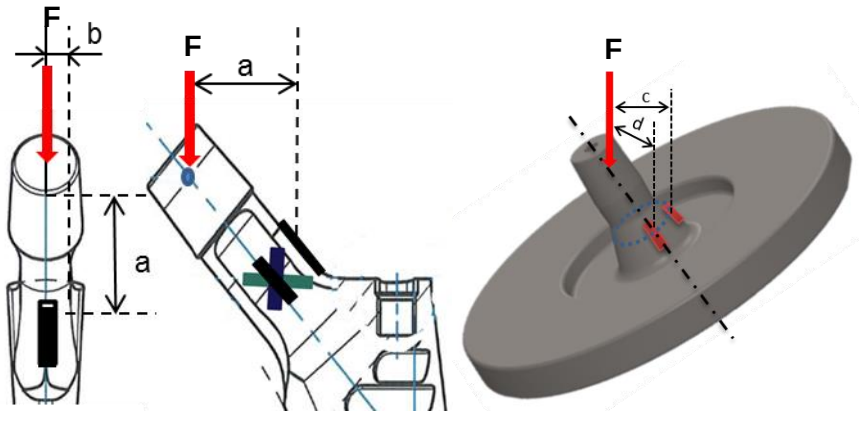

Figure 3-23 Force (red arrow) a=lever arm in M-L plane on the fretting test setup, b=lever arm in A-P plane on the fretting test setup c and d = lever arm in A-P (frontal) and M-L (sagittal) planes

The impact of loading frequencies was observed. ASTM F1875 fretting test prescribes 1 or 5 Hz as the frequency of testing depending upon the purpose and outcome of the study.

The frequency of walking is approximately 1 Hz, whilst other activities such as running, the frequency could increase to 4 Hz and 6 Hz has been reported in the clinical evaluation of human locomotion (Ferber and Macdonald, 2014). The results obtained on the uniaxial rig in the current study, showed that lower frequencies induce larger bending moments. Although higher frequencies may prevent the reformation of a passive oxide layer if the repassivation time is greater than the time between two load cycles (Viceconti et al., 1997), higher bending moments have been associated with increased wear and corrosion (Panagiotidou et al., 2013).

3.4.3 Comparison of methods

The evaluation of bending and torque on the uniaxial compression rig was undertaken to compare the loading conditions suggested in ASTM 1875 to the hip simulator. The aforementioned ASTM is the voluntary standard for evaluating the susceptibility of modular junctions to fretting. Comparatively, hip simulators focus on recreating wear conditions. Although fretting test imparts bending moments of comparable magnitude in the X plane, the observation of significantly larger torque and bending moments ($p<0.05$) in the perpendicular Y plane on the hip simulator (Figure 3-24) suggests that it develops more challenging loading conditions on the taper than uniaxial compressive loads. Since triaxial moments are generated, failure can occur about any plane. Therefore, the ASTM test appears to only suffice for a single plane. Moreover, if torsion is under estimated relative to *in vivo* conditions (Duda, 2013), then, the loading conditions imposed by the fretting test may be unlikely to recreate any failure mechanisms due to torques at the taper junction such as the bottoming out of the trunnion onto the head taper bore. A bottomed-out taper has been reported to cause greater wear (Koper et al., 2015, Buente et al., 2016). Similarly, torques about the taper axis could generate micromotion at the junction capable of depassivating the CoCr oxide layer at the junction (Jauch et al., 2013).

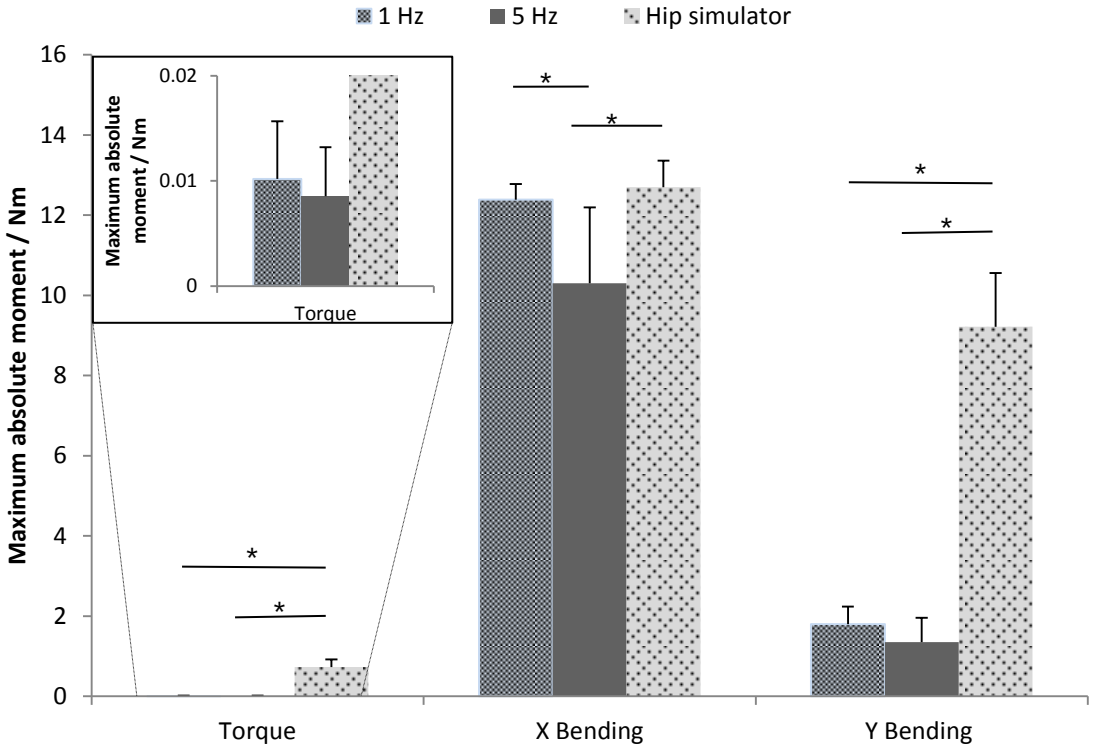

Figure 3-24 Comparison between single axis and hip simulator moments on a 40 mm femoral head (*=p<0.05, error bars= + SD)

3.5 Conclusions

1. The bearing surface friction and torque generated adjacent to the taper junction were sensitive to changes in bearing diameter.
2. The torques measured on 52 and 56 mm MoP were larger than the torque measured on 48 mm MoM. This observation reinforced the suggestion that taper corrosion initiated by large taper torques would not be limited to MoM bearing combinations.
3. Lower bending moments were measured just beneath the taper junction using the method specified by the ASTM F1875 than was measured on the hip simulator. In addition, the ASTM fretting test was found to apply negligible torques on the taper junction and therefore is not suitable for evaluating the contribution of torque to taper corrosion.

Chapter 4. Prediction of in vivo taper performance: The influence of loading and taper design variables

4.1 Introduction

The mating of a male and female taper creates a crevice which is controlled by the clearance between the angles. The precise taper angles, specified by individual manufacturers, exhibit inherent variability such that a nominal taper angle of 5° may range between 5.525° and 5.975° dependent on the manufacturer (Kocagöz et al., 2013, Brock et al., 2015). Therefore, manufacturer variations in male and female taper angles will generate different clearances.

Despite their apparent importance, no standard has been developed for the control of taper clearances. Indeed ASTM F1636-95e2 with specifications covering the dimensions and tolerances of male and female tapers has been withdrawn with no replacement (Parekh et al., 2016, Ashkanfar et al., 2017). In a retrieval analysis of THRs, Kocagöz et al. (2013) reported a taper clearance range of ±0.125° while there is anecdotal evidence that clinically, values up to 0.2° occur. The influence of clearances has previously been evaluated with respect to interface micromotion and stresses, establishing that within a relatively narrow (±0.015°) clearance, interface micromotion, or fretting, did not change between proximal and distal contacts (Parekh et al., 2016). Fluid ingress along with relative surface motion (micromotion) along the taper junction results in mechanically assisted crevice corrosion (MACC) (Hussenbocus et al., 2015). However, the effect of taper clearances on the taper gap opening (perpendicular to the surface) is yet to be established. This opening is important as it implies toggling, described as a mechanism which creates the opening of the taper junction allowing ingress of corrosive fluids (Langton et al., 2012). Under a loading condition

such that the vector changes direction relative to the taper, both proximal and distal contact conditions could result in separation at the taper junction and allow subsequent ingress of corrosive fluids into the taper.

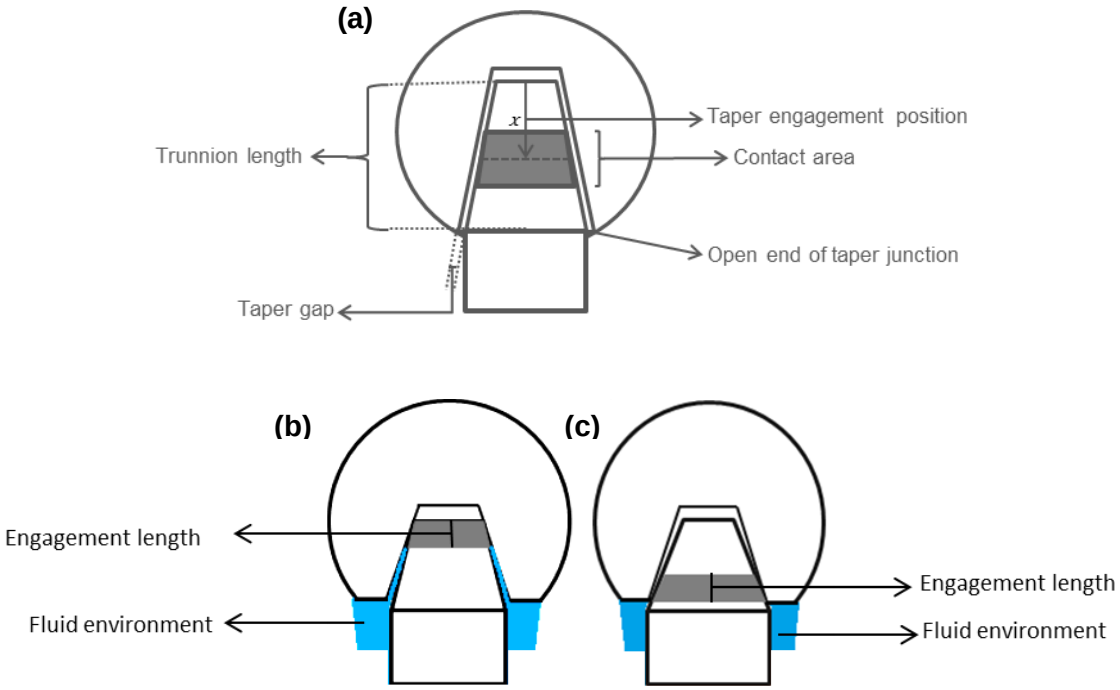

Figure 4-1 Schematic of taper junctions showing (a) taper contact variables, and contact regions described as (b) proximal and (c) distal

The current study is designed to computationally evaluate the effects of loading and clearances on the taper gap formation and surface stresses at the taper junction. The load profiles need to apply a changing load vector in the form of activities of daily living as well as profiles applied by commercially available hip simulators.

Recognition of the parameters that may influence corrosion can inform taper design and evaluation of taper performance. The influence of varying taper clearance on gap formation, defined as the relative movement at the entry of the taper interface normal to the taper surface (Figure 4-1a), which may influence fluid ingress, has not been previously studied. This leads to the test hypotheses that low taper clearance and distal contact will prevent taper gap opening under a moving load vector.

4.2 FE outline

Two FE models were generated:

i. A CoCr-steel taper assembly (CoCr femoral head and 17-4 steel trunnion fixture) to validate the computational model
ii. CoCr/Ti taper junction which has a clinically relevant trunnion material

4.3 Validation Model

4.3.1 Method

A 3D FE model of a 40 mm (+0 mm head offset) CoCr head, a 17-4 steel trunnion fixture and an acetabular liner was created using Abaqus/CAE v 6.13-1. The head-trunnion assembly and the liner were orientated at 23° and 35° respectively to the horizontal plane to recreate the hip simulator setup (Figure 4-2a). The components of the model were assigned individual material properties, as indicated in Table 4-1. After creating the geometry, the parts were only compatible with tetrahedral mesh. Meshing of the parts was achieved with C3D10 elements which are 10-noded quadratic tetrahedrons from the family of 3D stress elements. All materials were assumed to be linear elastic and homogenous. The head-trunnion and head-liner contact interactions were modelled using a finite sliding formulation with a surface-to-surface discretisation. At the head-liner interface, the coefficient of friction value used was 0.083 (Ong et al., 2009). At the head-trunnion interface, the friction coefficient for the CoCr alloy with 17-4 steel alloy has not been reported because it is not clinically relevant; for other relevant material combinations, the reported values have been between 0.15 and 0.21 (Elkins et al., 2014, English et al., 2016). For the present work, the higher value of 0.21 was used.

Table 4-1 Material properties on FE model (Jin et al., 2006a, AZoM, 2012)

Part	Material	E / MPa	v
Femoral head	CoCr	230 000	0.30
Trunnion	17-4 steel	200 000	0.29
Acetabular liner	HXLPE	1 000	0.40

4.3.2 Loading conditions

A load of 4 kN was applied to a node on top of the femoral head to mate the taper (Figure 4-2b). When loading was applied to lock the taper, the base of the trunnion fixture was constrained in all 6 degrees of freedom (Figure 4-2b). To mate the taper, the acetabular liner was excluded from the model during the impaction step by suppressing it and was subsequently reinstated to apply the hip simulator load profile.

After mating the taper, the assembled model was subjected to the hip simulator walking load profile (Figure 4-3a). The hip simulator load was applied at the base of the fixture such that the line of action of the force passed through the head centre (Figure 4-2b). Angular displacements applied by the hip simulator (Figure 4-3b) were applied to a reference point (RP1) at the centre of the head and coupled to the surface of the femoral head (Figure 4-4a). A 2nd reference point (RP2) located at the centre of the head was coupled to the trunnion surface as well as the articulating surface of the liner (Figure 4-4b and c). The backside of the acetabular liner was constrained in all 6 degrees of freedom. The hip simulator utilises an acetabular shell as a backing for the acetabular liner but this was not necessary to be included in the current model. The loads, rotations and boundary conditions applied were defined using Static/General step over a maximum of step time of 100 s. Static methods were used to simulate the mating of the taper because similar contact pressures have been shown between dynamic and static analyses (Ashkanfar, 2015). Loads and rotations were discretised into intervals over the loading cycle which allowed time variations of load and angular displacements.

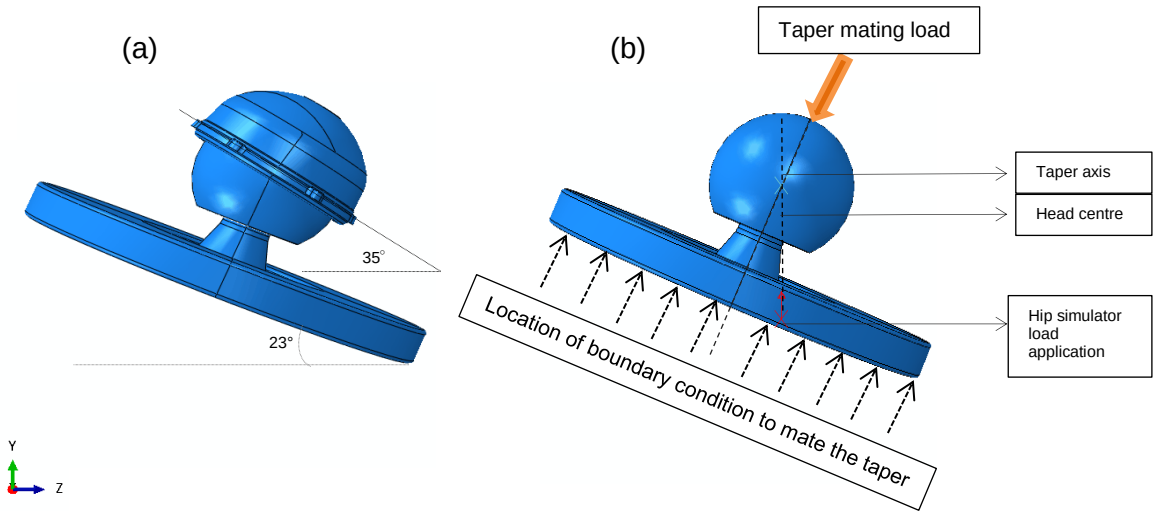

Figure 4-2 CoCr/17-4 steel model assembly (a) orientation (b) details of load and boundary condition application

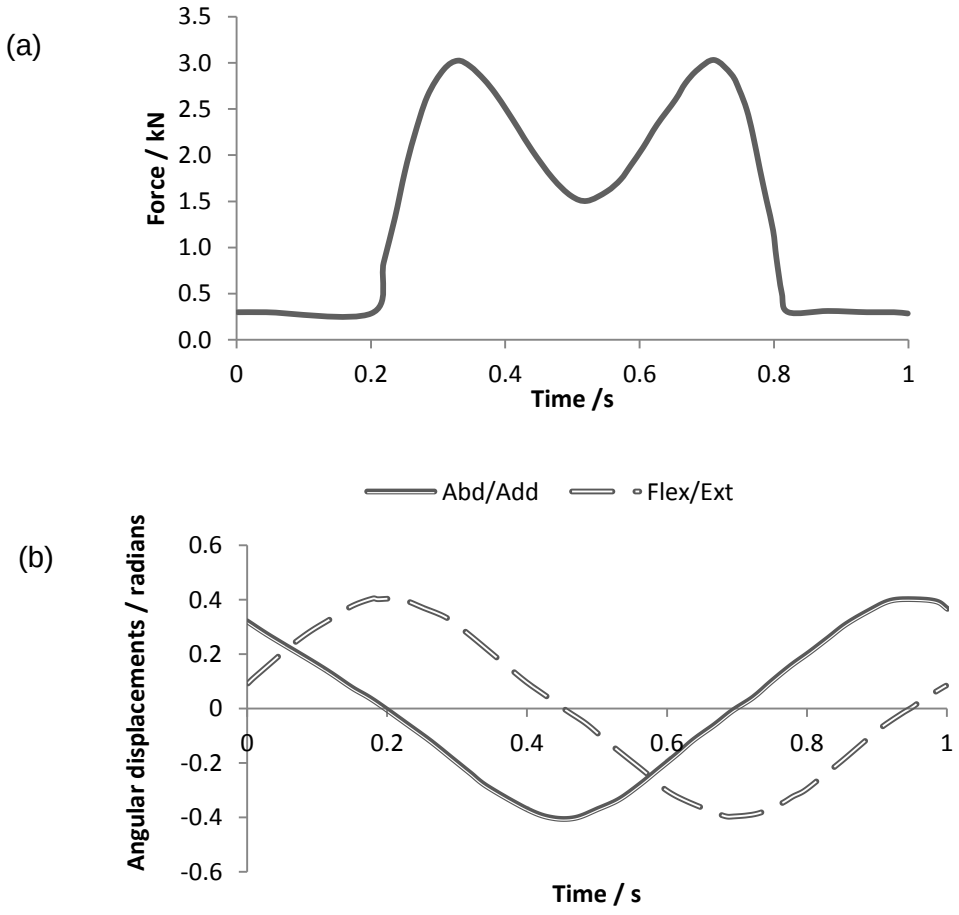

Figure 4-3 (a) Hip simulator load and (b) rotations

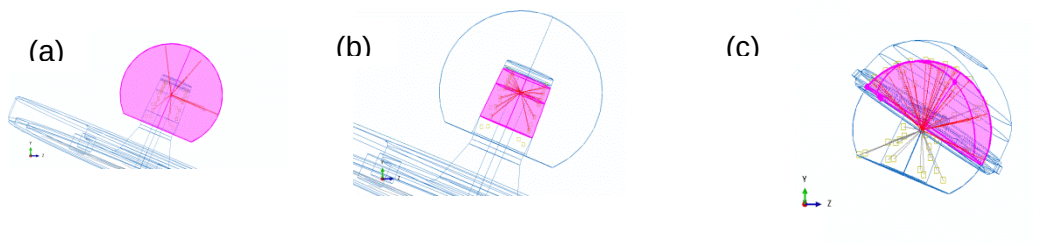

Figure 4-4 Reference point coupling with (a) femoral head, (b) trunnion, (c) articulating surface of acetabular liner

The FE model was validated by comparing the computational principal strains with the experimental strains measured from the strain gauge rosettes (Chapter 3) connected in a quarter bridge configuration.

The ideal placement position of a gauge would be 'b' (Figure 4-5). Computationally, the principal strain was taken as the average of strains determined at each node that make up that mesh line ('b'). To account for variations in lateral positioning of the gauge, the strain on 2 longitudinal mesh lines either side of the ideal position (d, e, f, g) were also determined from the FE model.

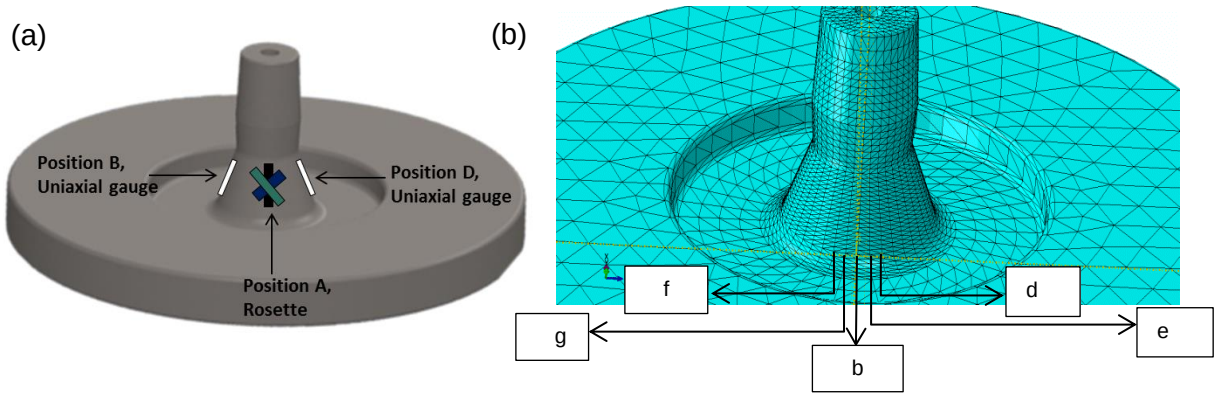

Figure 4-5 (a) Location of strain gauges in experiemental evaluation in Chapter 3; position C is diamterically opposite to A (b) Location of mesh lines for determining the principal strains computationally

4.3.3 Results

The principal strains recorded from the FE model was found to be tensile for position A (181 με) and compressive at position C (63 με). The largest difference between the mean principal strain determined in the FE model and the experimental value was 20με for the rosettes at both locations, Figure 4-6. The error that could be attributed to strain gauge position was estimated through the changing positions d,e,f,g. The greatest difference at position A was 20 με assuming the gauge was located at 'g'. The computational compressive principal strains were less variable with a 10 με difference compared to experimental principal strains.

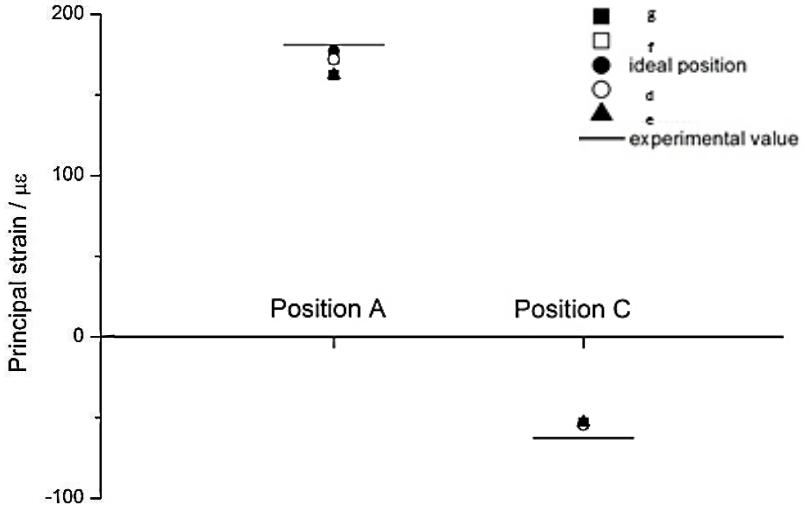

Figure 4-6 Experimental and computational principal strains at corresponding locations; positions A and C are as shown in Figure 4-5a

The results validate that the FE model was simulating the experimental conditions and could therefore be developed to study changes at the taper interface.

4.4 CoCr/Ti Model

A 3D FE model of a 40 mm (+0 mm head offset) CoCr head and a Titanium alloy trunnion (Ti-6Al-4V) was created. The femoral head was assigned material properties, as indicated in Table 4-1. The Ti-6Al-4V trunnion was assigned the following properties: E = 116 000 MPa and v = 0.31. Both parts were meshed with C3D10 elements. The contact interaction between the head taper and trunnion was modelled using a finite sliding formulation with a surface-to-surface discretisation and a constant friction coefficient of 0.21 (English et al, 2016).

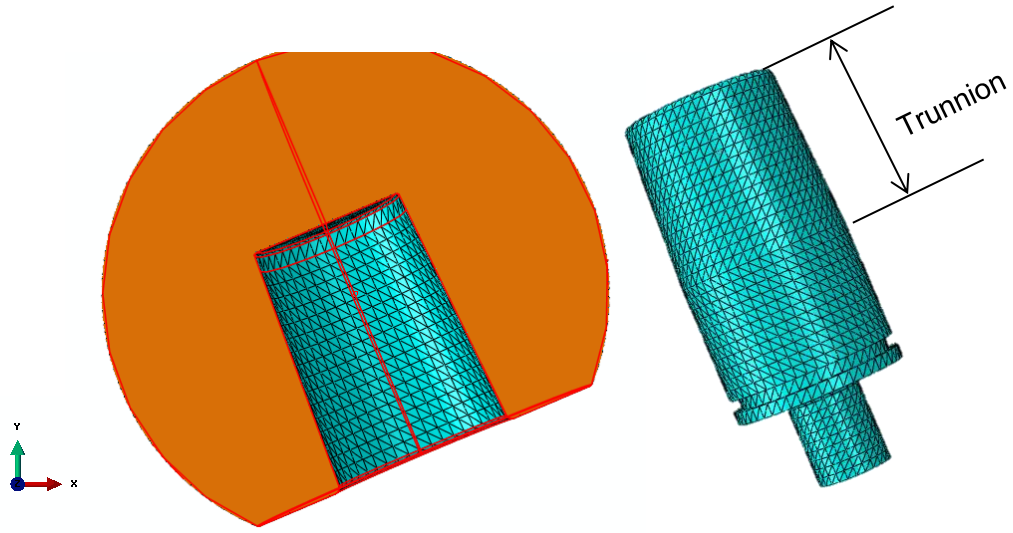

Figure 4-7 Mesh distribution on the femoral head and a Ti-6Al-4V trunnion

4.4.1 Loading conditions

A load of 4 kN was also applied to a node on top of the femoral head to mate the taper (Figure 4-8a) followed by functional loads representative of activities of daily living as well as profiles applied by commercial hip simulators. Modelling the impaction through a single node is a simplification but prevents the need to account for differences in cross section of surgical impactors, location of impaction and off-axis surgical impaction. When loading was applied

to lock the taper, the trunnion base (Figure 4-8a) was constrained in all 6 degrees of freedom over an area of 115 mm^2.

Four load profiles were modelled; 'walking' and 'stair climb' loading profiles were representative of activities of daily living as measured by an instrumented THR implant (Hadley, 2012). The 'orbital hip sim' load profile represented the loading cycle applied by an orbital hip simulator which undergoes biaxial rocking motion with angular displacements in flexion/extension (Flex/Ext) and abduction/adduction (Abd/Add) (Essner and Wang, 2010). The 'prosim' load profile simulated the loading profile exerted by a hip simulator which applies dual axes rotations, namely, Flex/Ext and internal/external rotation (IER) (Hadley et al., 2013). The loads for each of these profiles were applied to a reference point, coupled to the head taper and trunnion surfaces, located in the centre of the head (English et al., 2016) (Figure 4-8b). A second reference point was located in the head centre; this was constrained in 3 degrees of translation ($U_1=U_2=U_3=0$) and kinematically coupled to the surface of the femoral head, thereby precluding the need to include an acetabular liner in the model (English et al., 2016).

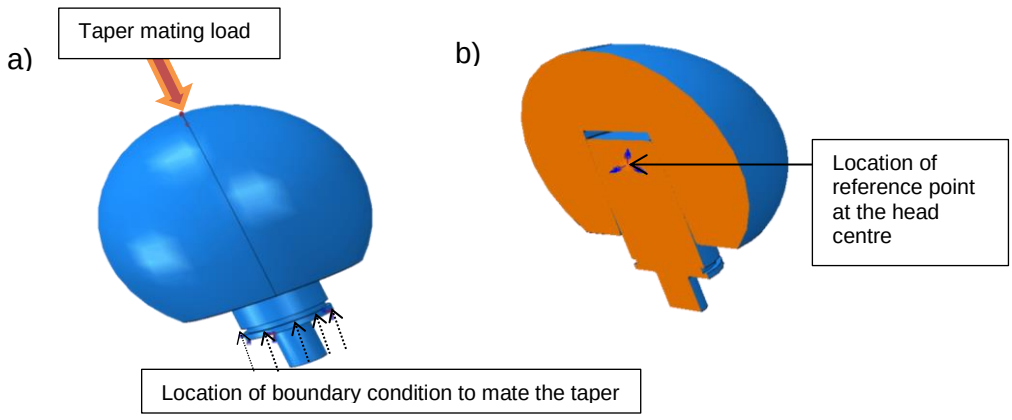

Figure 4-8 Location of loads and boundary conditions on the model

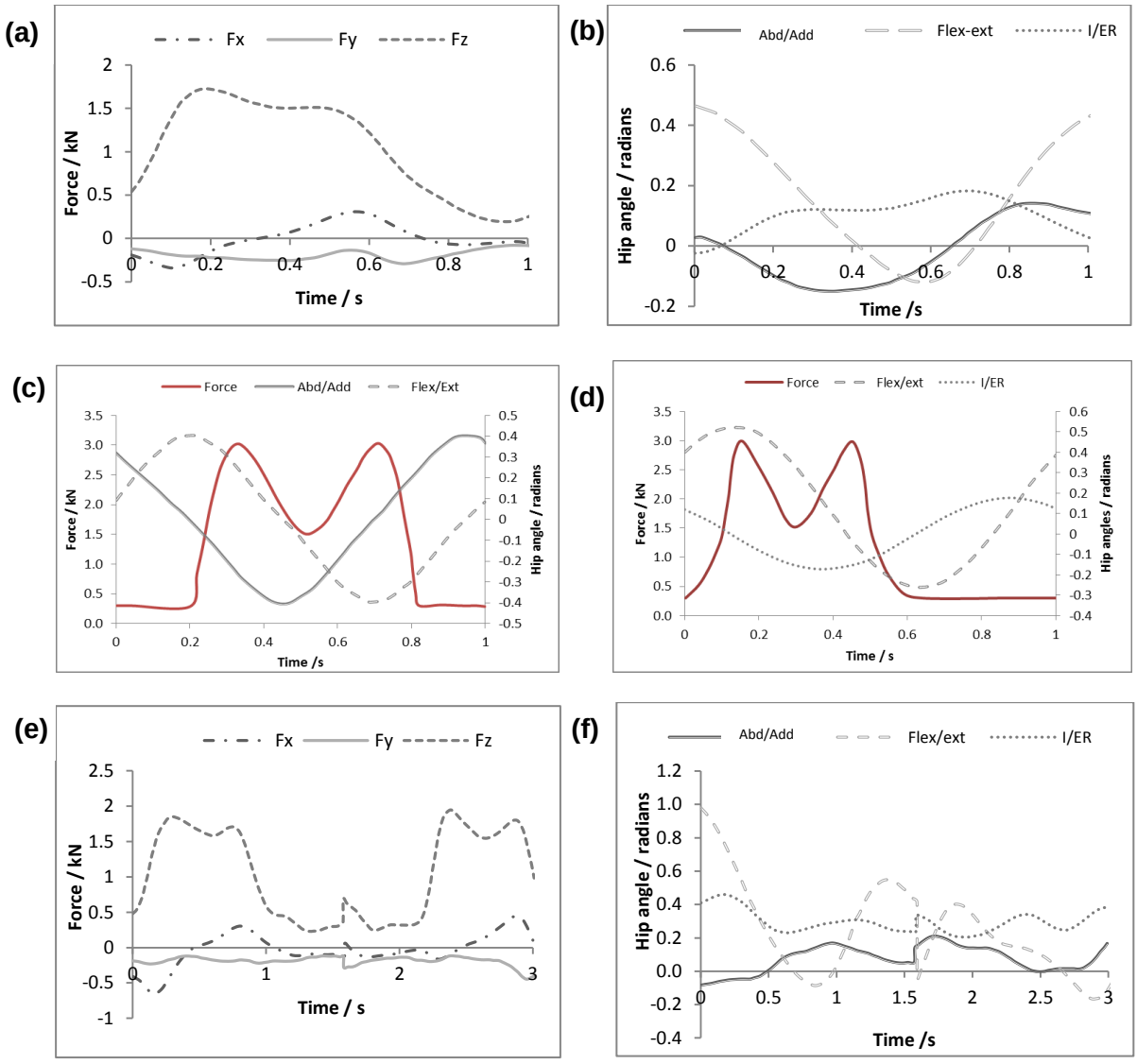

Figure 4-9 Forces and rotations applied to the femoral head during the simulation of (a and b) walking (c) Orbital Hip simulator (d) Prosim and (e and f) Stair climb (Hadley, 2012)

4.4.2 Variables

A range of variables were evaluated after tapers had been mated (taper lock). Maximum taper gap was defined as the largest normal separation between the two taper surfaces, measured at the open end of the taper junction, over a load cycle, Figure 4-1. Mean contact areas under loading and the peak von Mises stresses on the surface of the head and trunnion were compared under different loading and geometry variations. The contact area for the taper was defined as the sum of regions on the surface elements at the taper interface for which there was a contact force. This was recorded following mating of the

taper as well as being determined as the mean contact area over a loading cycle. Micromotion was recorded as either parallel or rotational. Parallel micromotion was defined as the maximum relative motion at the taper interface along the taper axis over a loading cycle. Rotational micromotion was the maximum relative motion over a loading cycle, tangential to the taper interface but orthogonal to the direction of parallel motion.

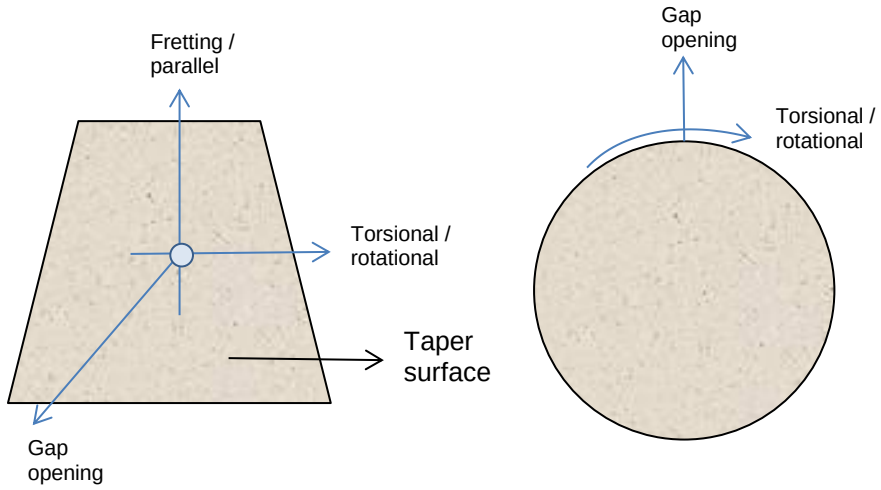

Figure 4-10 Schematic of variables depicting motion at the taper junction in front and plan views

Table 4-2 Matrix of variables evaluated

		Head taper angle°	Taper clearance°	Trunnion length / mm	Loading conditions	Trunnion material
Study	1	5.76	0.02 - 0.28	13.5	• Walking • Walking cycle applied by Orbital and Prosim hip simulators • Stair climb	Ti-6Al-4V
	2	5.76	-0.02 – -0.25		• Stair climb	
		2.9 8.7	0.02 - 0.28	15.5 13.3	• Stair climb	
	3	5.76	0.1	10.5 13.5 18	• Walking • Walking cycle applied by Orbital and Prosim hip simulators • Stair climb	
	4	5.76	0.02 - 0.28	13.5	• Stair climb • Modified stair climb	Ti-6Al-4V
	5	5.76	0.02 - 0.28		• Stair climb	Ti-6Al-4V CoCr
	6	5.76	0.1, -2.9		• Walking cycle applied by Orbital hip simulator	Ti-6Al-4V

4.4.3 Convergence study

Appropriate mesh densities for variations in trunnion length and angles were determined for the femoral head and trunnion via a convergence study using taper gap as the dependent variable. The angular variations were less susceptible to changes in mesh density; convergence of less than 2 % was achieved at approximately 160 000 elements with the exception of the 10.5 mm trunnion where it was achieved at approximately 190 000 elements.

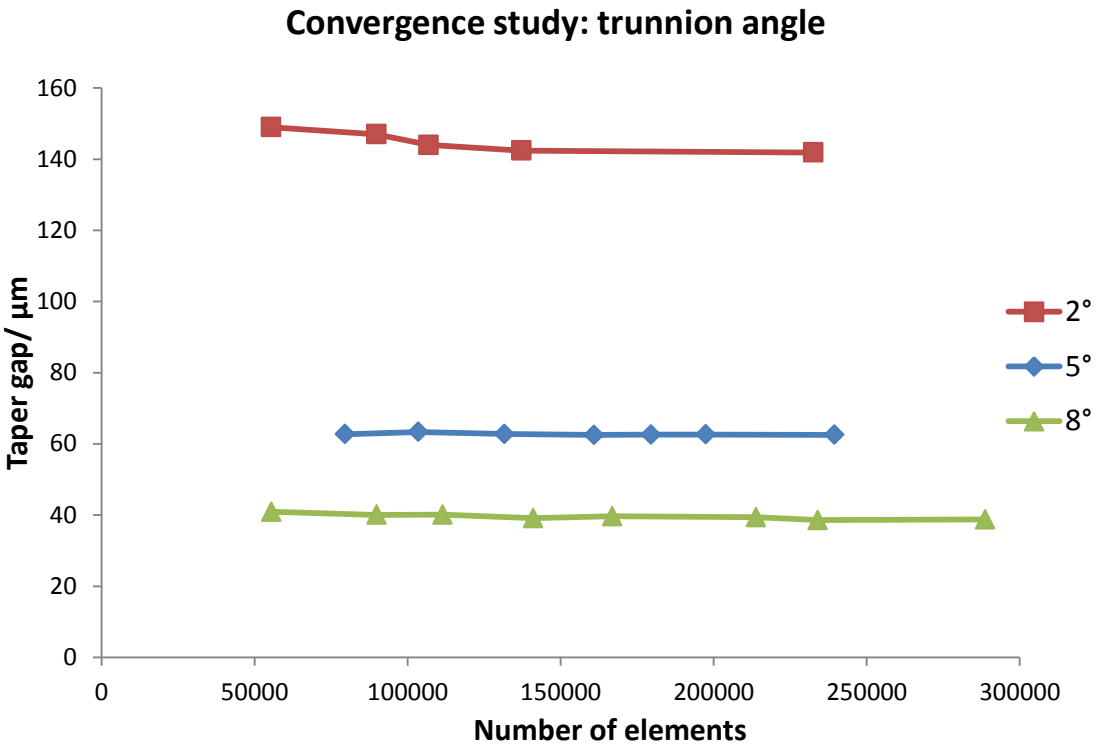

Figure 4-11 Convergence analysis for the variation in trunnion angles

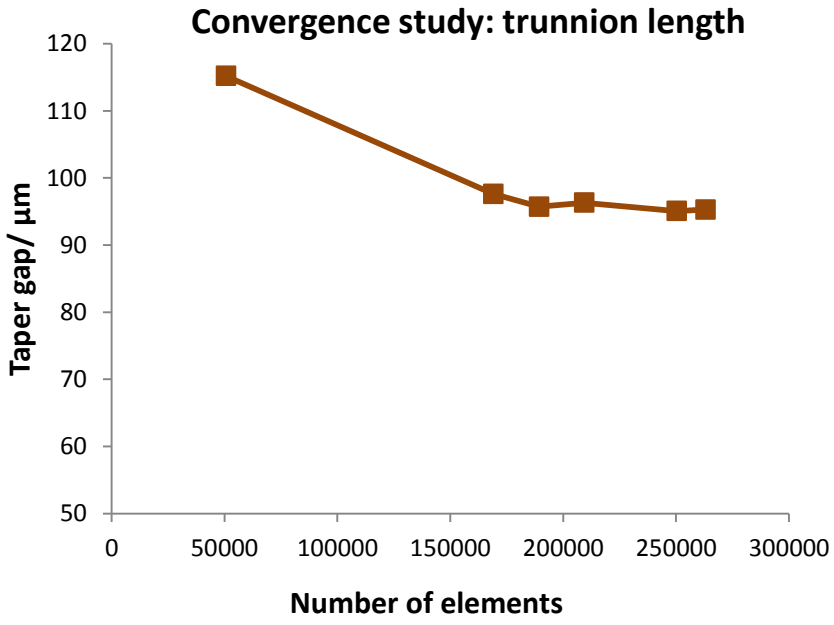

Figure 4-12 Convergence analysis for the 10.5 mm trunnion length

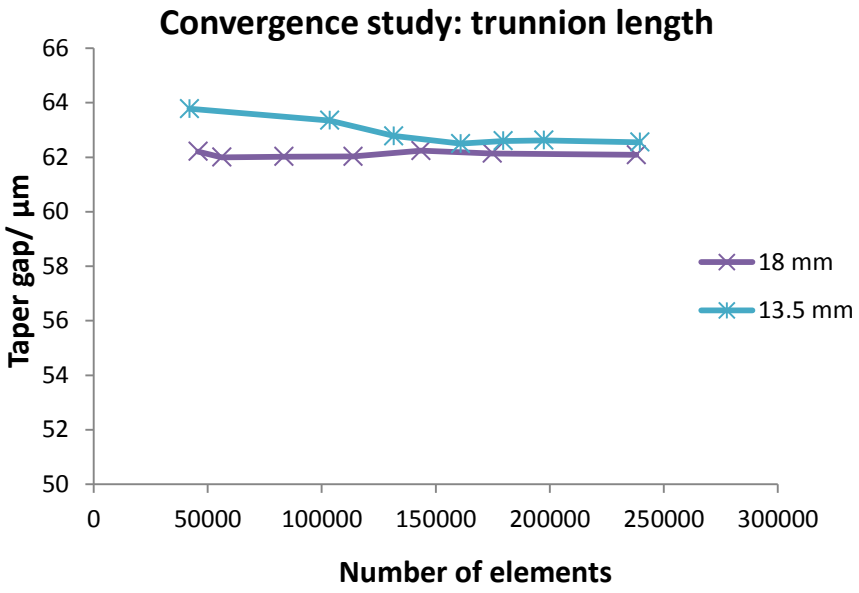

Figure 4-13 Convergence analysis for the 13.5 and 18 mm trunnion length

4.4.4 Study 1 - Effect of loading activity on taper conditions

The gap formed at the junction for 9 trunnion angles (5.48° - 5.74°) paired with a female taper at 5.76° was evaluated for loading activities: (1) walking cycle, (2) profile of a walking cycle applied by hip simulators and (3) stair climb (Figure 4-9). The taper angular variations chosen were representative of commercially available designs reported in the literature (Kao et al., 2016, Triantafyllopoulos et al., 2016, Kocagöz et al., 2013, Langton et al., 2012, Hernigou et al., 2013, Brock et al., 2015).

Results 1

Changing the taper clearances led to a range of contact areas as indicated in Figure 4-14. There was a reduction in mean contact area at the taper junction following loading conditions of both simulated stair climb and walking compared to the contact area after the taper was mated (Figure 4-14). The hip simulator conditions resulted in either an equivalent or an increase in the mean contact area (Figure 4-14) and showed an axisymmetric contact distribution (Figure 4-15a).

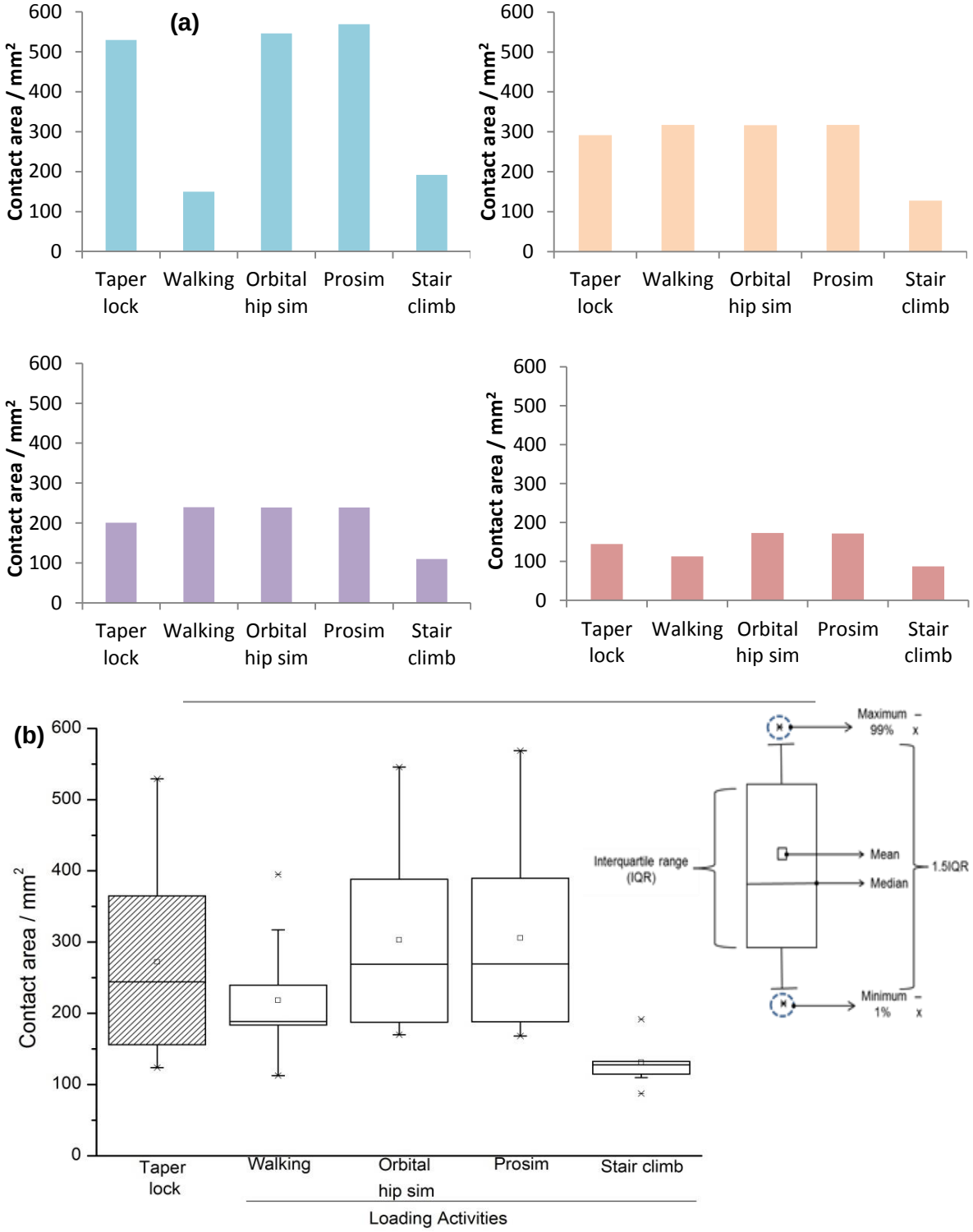

Figure 4-14 (a) Mean contact area developed in a range of loading activities for taper clearances of 0.08,0.19,0.21 and 0.28° (b) Summary of the influence of loading on the mean contact area after a loading cycle compared to the contact area generated at taper lock, presented for all taper clearances

In comparison to the axisymmetric contact, the contact area due to stair climb displayed an asymmetric pattern (Figure 4-15b). The contact distribution changed over the loading cycle (Figure 4-18). Considering all the positive clearances modelled, the mean contact area under stair climb load had a positive linear relationship with contact area after taper lock (Figure 4-16).

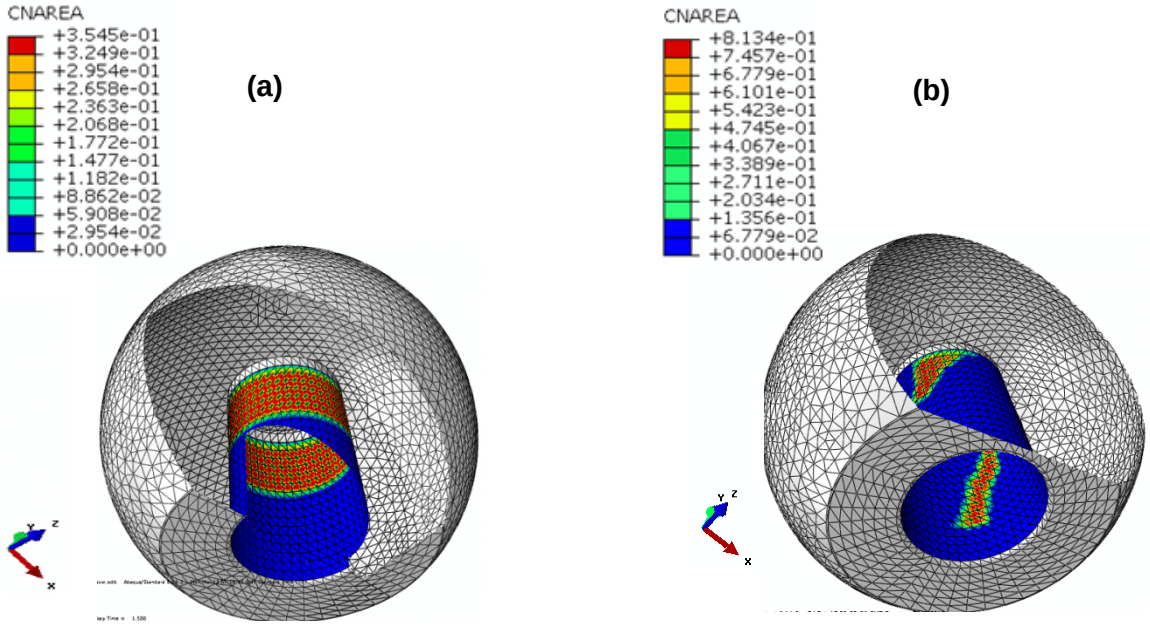

Figure 4-15(a) Axisymmetric contact area under 'hipsim' load profile at point of maximum taper gap (axisymmetric contact pattern for prosim profile and walking) (b) Asymmetric contact area on the femoral head during stair climb at point of maximum taper gap

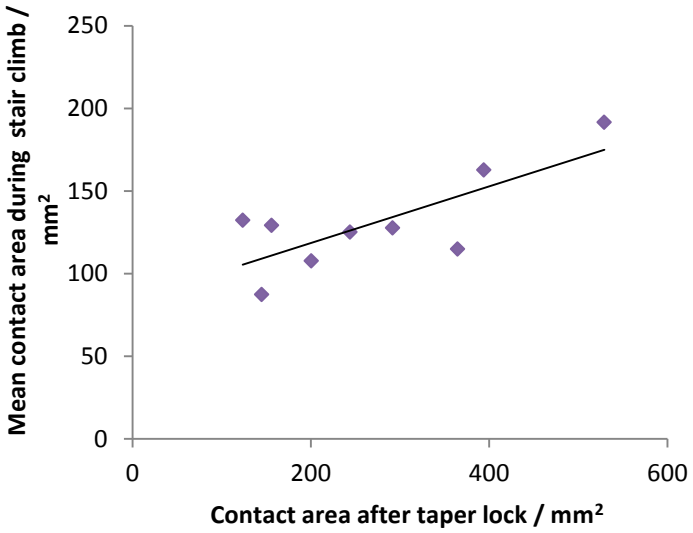

Figure 4-16 Relationships developed under simulated stair climb loading for a) contact area once the taper was mated with mean contact area at the taper junction after taper lock for all 5° proximal taper contact conditions

The maximum taper gap occurred at a load corresponding to 1.1 times bodyweight for a 75 kg mass (Figure 4-18). For all positive clearances modelled, the maximum taper gap generated was found to be inversely related to the contact area developed during the simulation of stair climb loading (Figure 4-19).

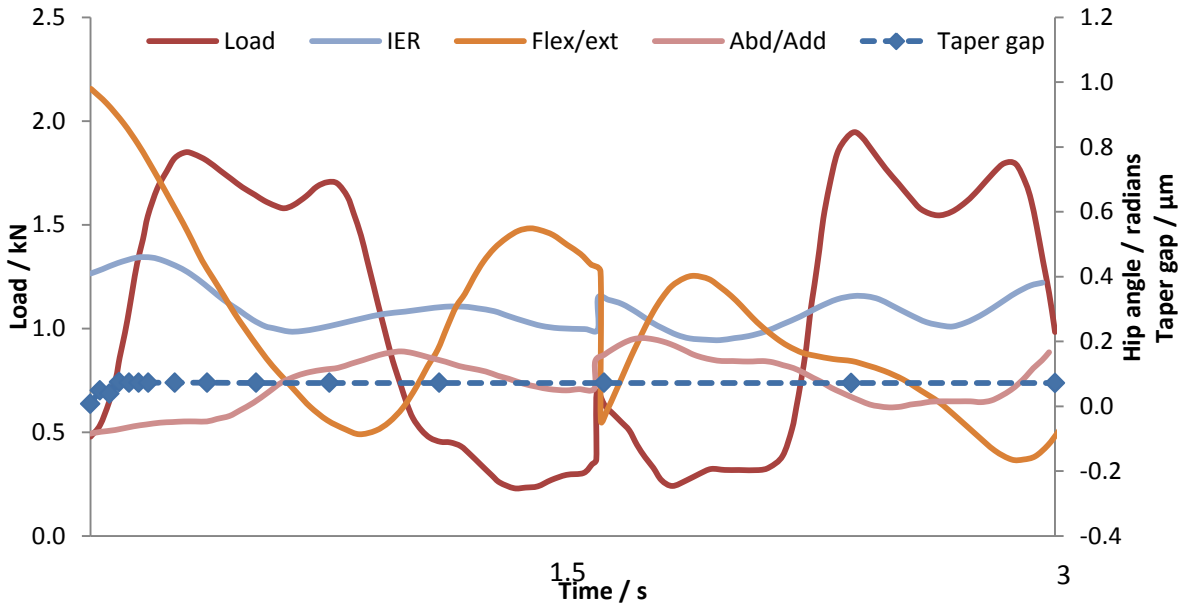

Figure 4-17 Example of a variation of taper gap with load and rotations under stair climb loading

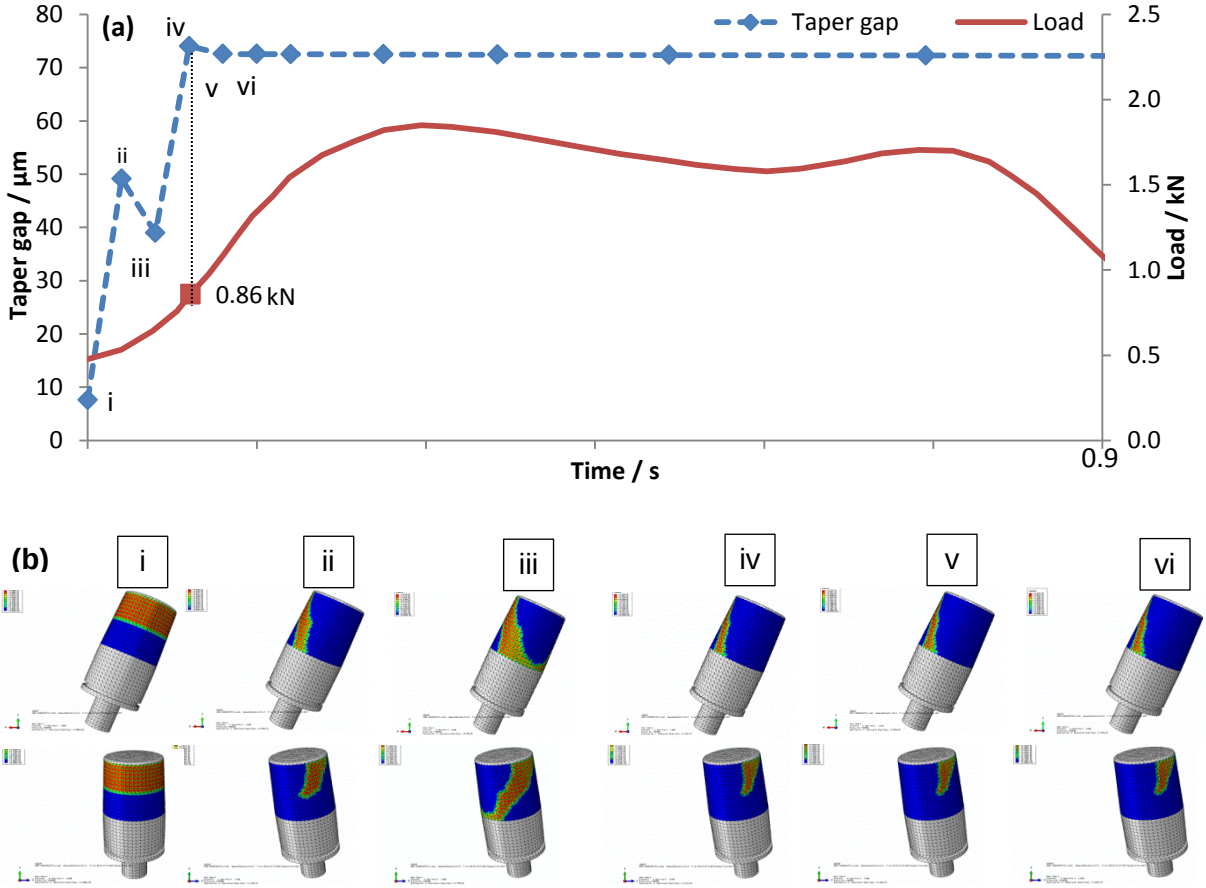

Figure 4-18 (a) More detailed view of Figure 4-17 showing the variation of taper gap with load and (b) changes in contact area distribution corresponding to taper gap magnitudes i to vi in (a) under stair climb loading

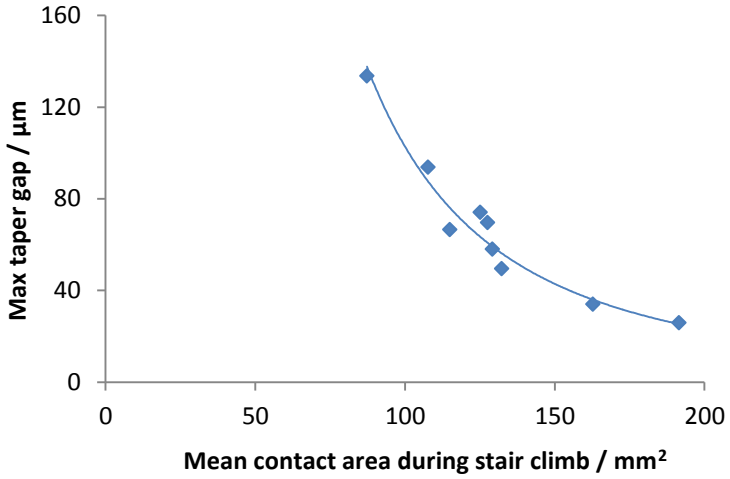

Figure 4-19 (b) Relationship between the maximum gap developed at the taper junction with mean contact area during stair climb for all taper clearances for a 5.76° head taper

Stair climb loading created the largest taper gap, the smallest contact area and largest surface stresses on the head taper were elevated compared to the other loading conditions (Table 4-3).

Table 4-3 Results for proximal taper contact conditions (mean of clearances modelled); maximum von Mises stresses at the trunnion did not change with loading activity

Activity	Max von Mises stress / MPa		Max taper gap / µm	Mean contact area / mm²
	Head taper	Trunnion		
Walking	250	86	13	219
Orbital hip sim	101		9	303
Prosim	107		9	306
Stair climb	950		67	131

Figure 4-20 confirmed that the load vector changed under hip simulator and stair climb loading conditions since the location of the maximum taper opening varied over the loading cycle. However, the location of the maximum taper gap moved a larger distance under stair climb loading even though the peak load applied by the hip simulator was 58 % higher (Figure 4-21).

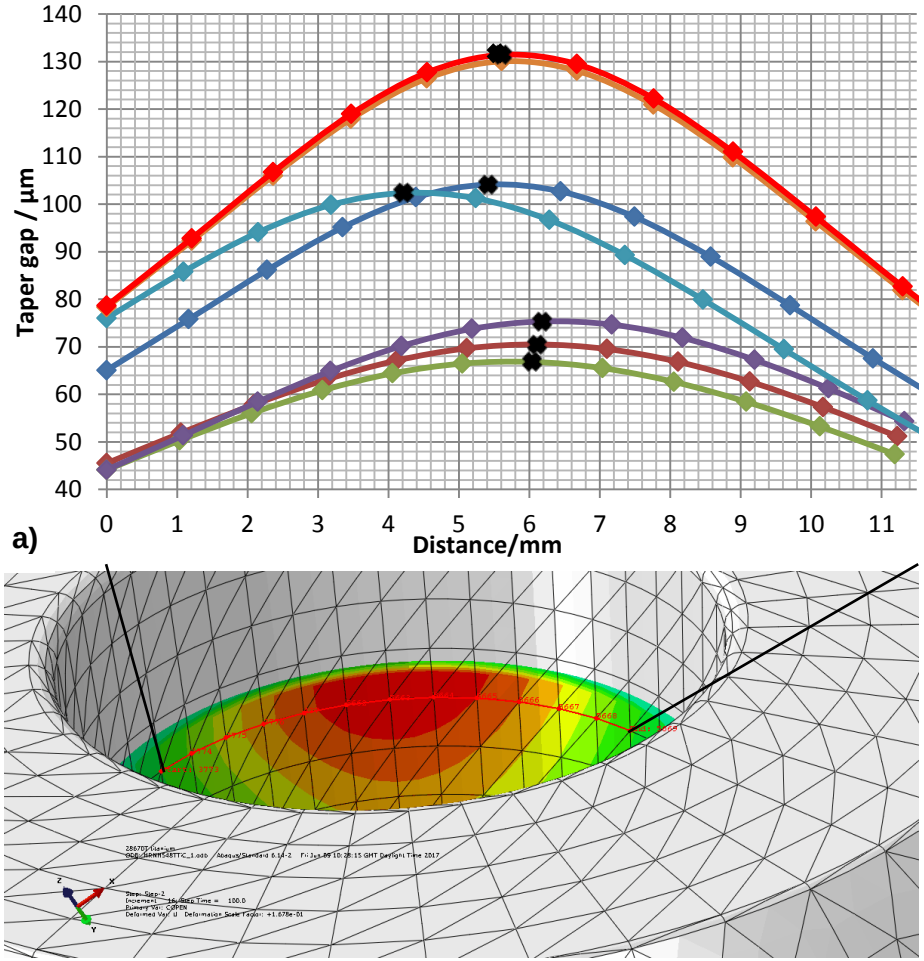

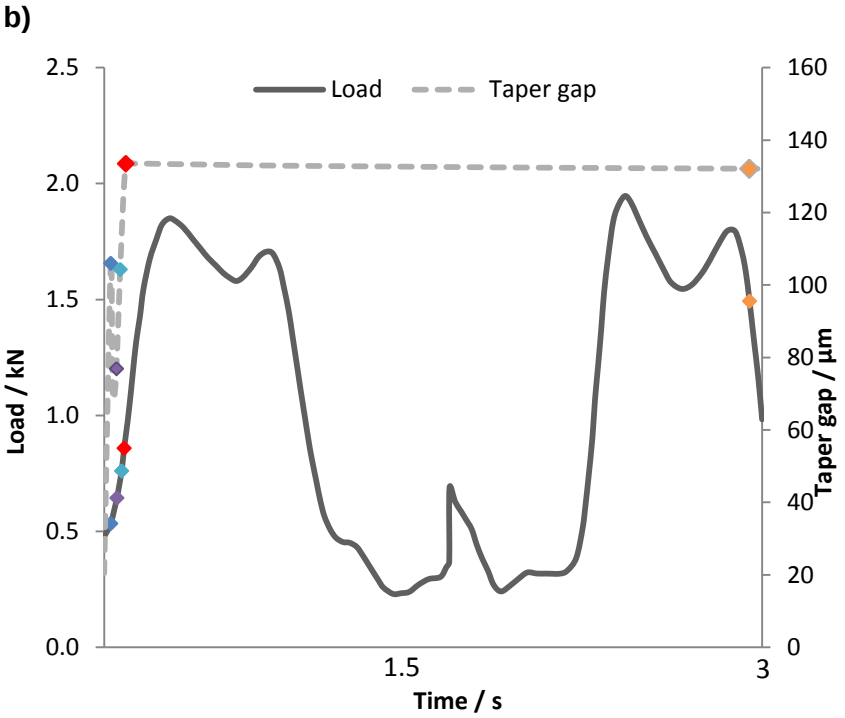

Figure 4-20 (a) Changes in the location of the maximum taper gap (marked x) on taper clearance 0.28°, the time points evaluated correspond to the load and taper gap highlighted in (b) which are colour coordinated; iii and iv are between i and v and are too close to be shown

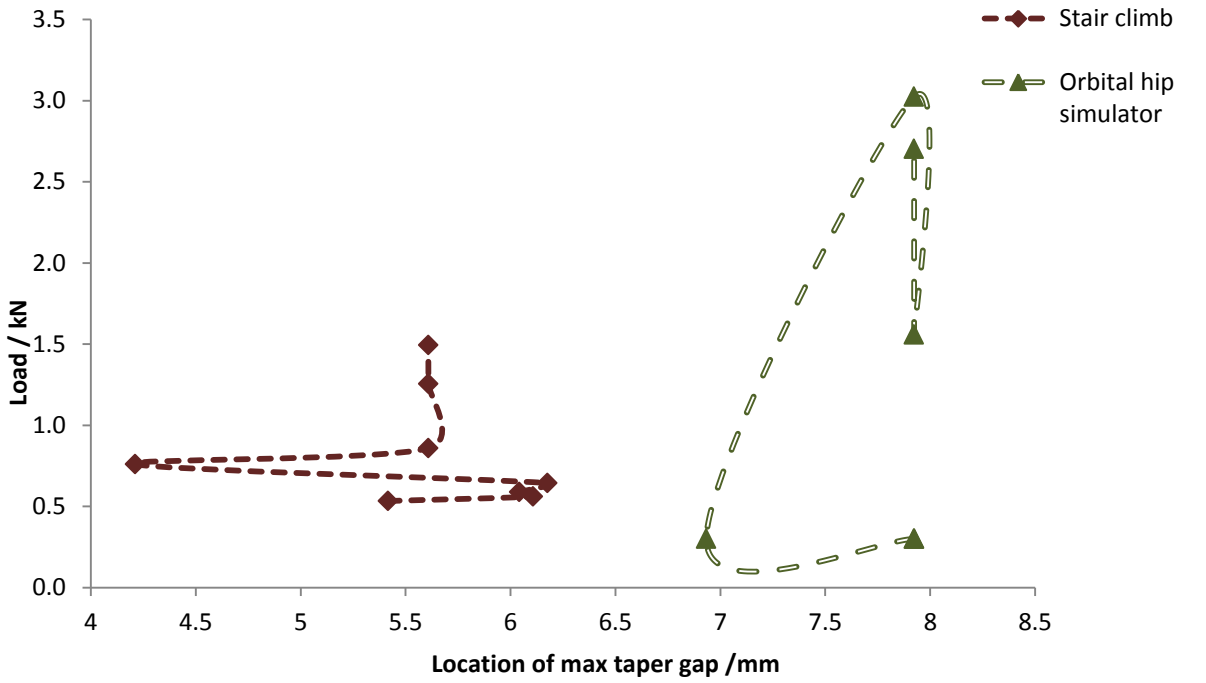

Figure 4-21 Location of the max taper gap at the interface for taper clearance 0.28° under orbital hip simulator and stair climb loading conditions

Further, it was observed that during stair climb loading, the plane of the maximum taper opening was the same as that of the highest surface head taper stresses. This, combined with the asymmetric contact pattern at the junction indicated that a toggling mechanism was being simulated during stair climb.

4.4.5 Study 2 – Variation in taper gap under proximal and distal contact conditions

Negative clearances of approximately -0.2° have been reported in commercially available THRs (Kocagöz et al., 2013); hence distally contacting tapers were introduced with clearance angles of -0.02° to -0.25°on a 5.76° head taper. These were evaluated under stair climb loading conditions only; the resulting maximum taper gap and taper engagement lengths were compared with the values obtained using the positive taper clearances.

The effect of angular clearances on taper gap at two other commercially relevant taper angles: 2 and 8° was also evaluated using stair climb loading (Figure 4-22).

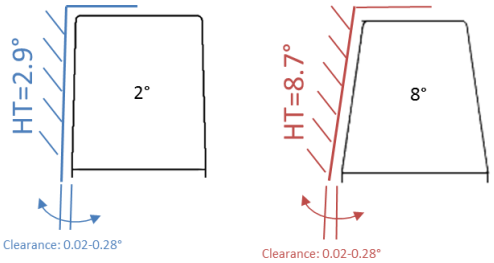

Figure 4-22 Schematic representation of taper angles and clearances modelled HT= head taper

Results 2

At taper lock, there was an axisymmetric contact pattern which varied over the length of the trunnion from the maximum area at -0.02° to the smallest area at -0.25° (Figure 4-23a). Under loading, this changed to asymmetric contact for all negative clearances. When the maximum taper gap was generated at a clearance of -0.25°, the smallest contact area was observed (Figure 4-23b) and the magnitude of the gap was approximately twice that of the lowest taper gaps (Figure 4-24a).

Overall, the maximum taper gap generated reduced with the taper clearance for 5° trunnions for both proximal and distal contact conditions along with the taper engagement lengths immediately after taper mating (Figure 4-24). Hence moving towards a condition of reduced taper clearances increased the length over which the taper was supported and reduced the maximum gap generated at the interface under loading. Within a range of ±0.1°, similar gaps were generated because the tapers engaged over comparable lengths.

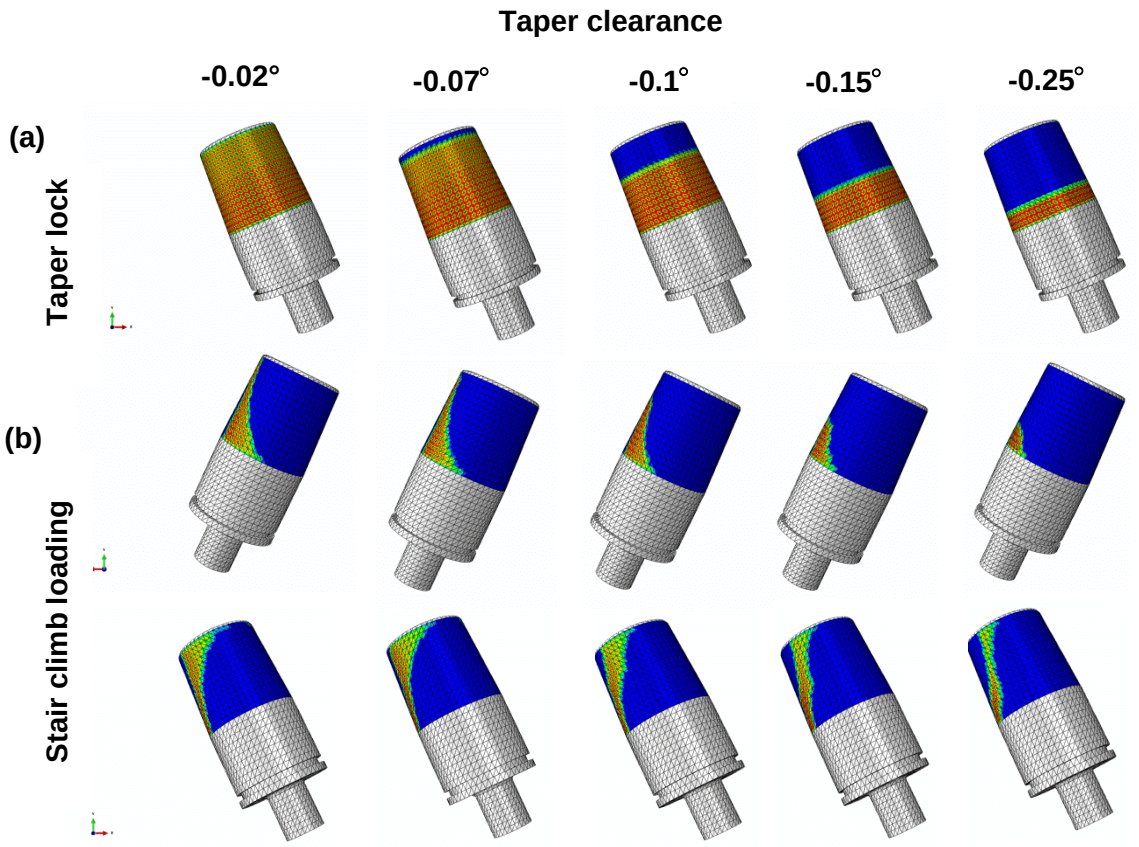

Figure 4-23 Change in contact area distribution from (a) symmetric after taper lock to (b) asymmetric under stair climb loading for the 5° taper with negative taper clearances; contact area depicted in (b) corresponds to the area distribution at the generation of maximum taper gap

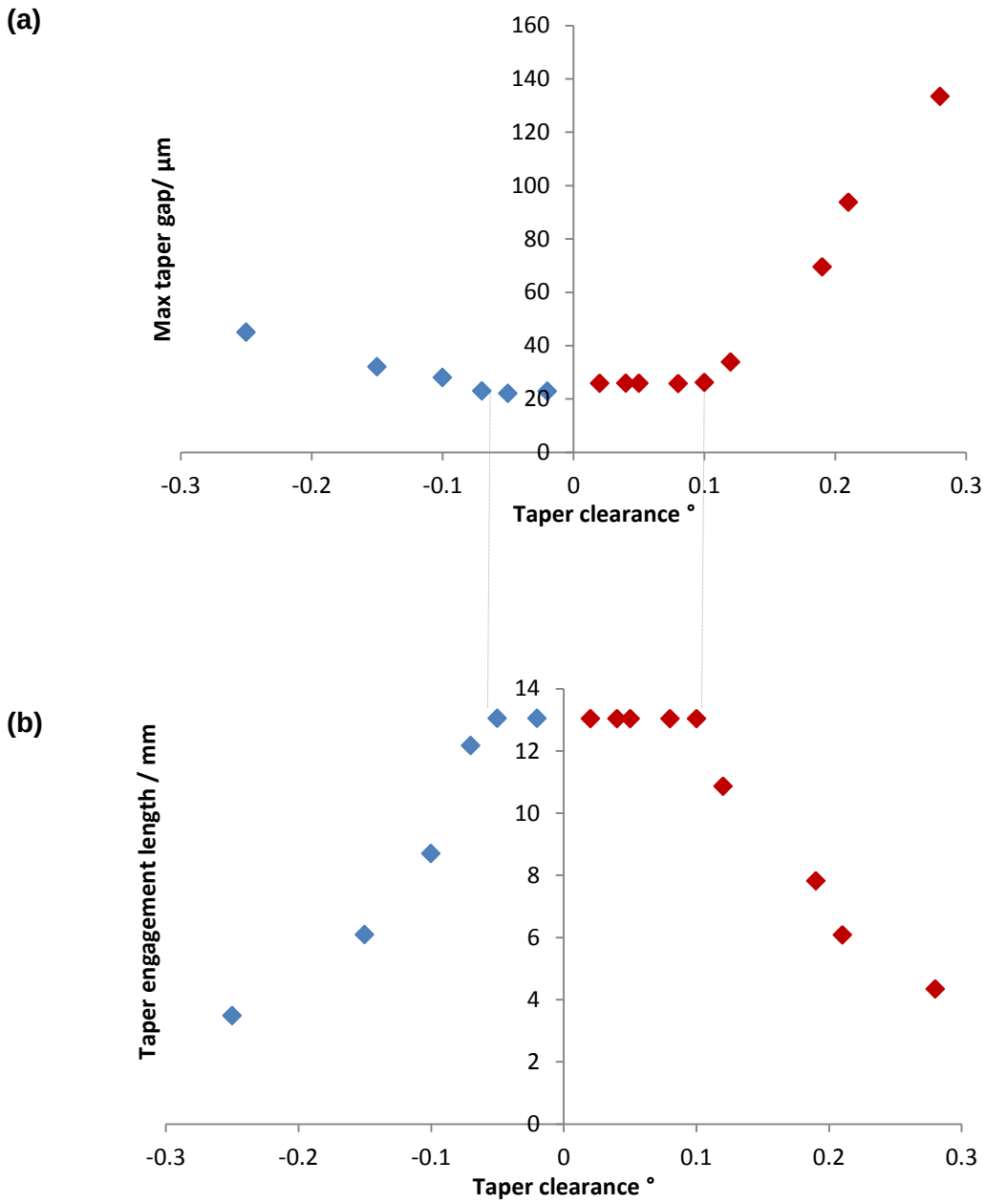

Figure 4-24 Change in a) taper gap b) engagement length under proximal and distal contact conditions for the 5° taper under stair climb loading, for a 13.5 mm long trunnion

For other commercially relevant taper angles, a reduction in clearance also resulted in a reduction in the gap formed at the taper junction (Figure 4-25); this was also due to an increasing taper engagement length (Figure 4-26). For a given clearance, the gap formed at the 2° taper was greater than the 8° taper. Further, comparing all 3 trunnion angles showed that the tightest proximal clearances resulted in the smallest gaps formed at the taper junction.

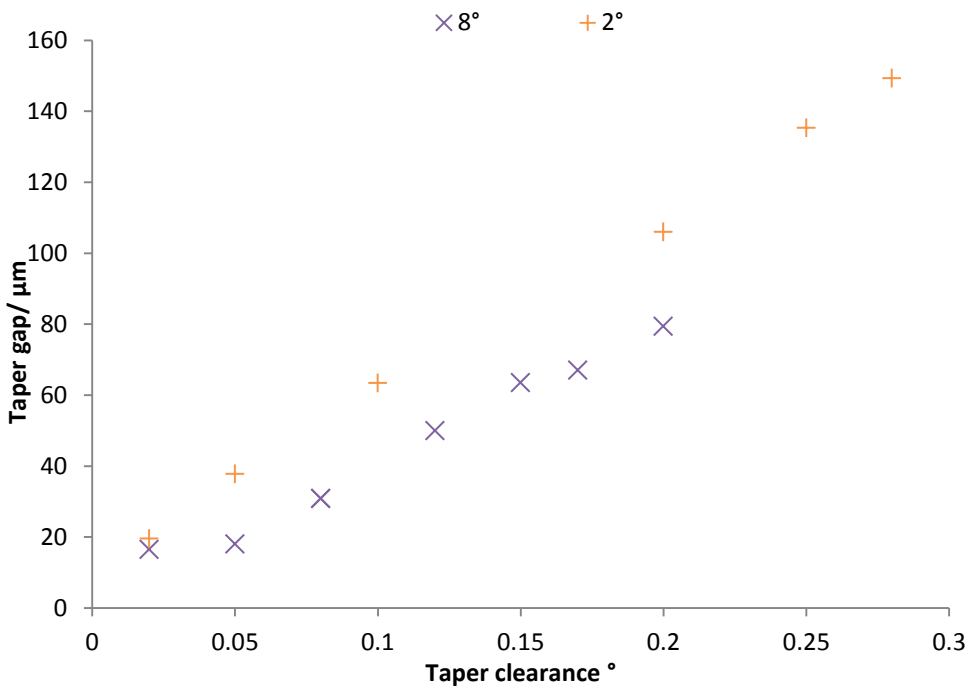

Figure 4-25 Relationship between taper clearance and taper gap formed under stair climb loading for 2° and 8° trunnions

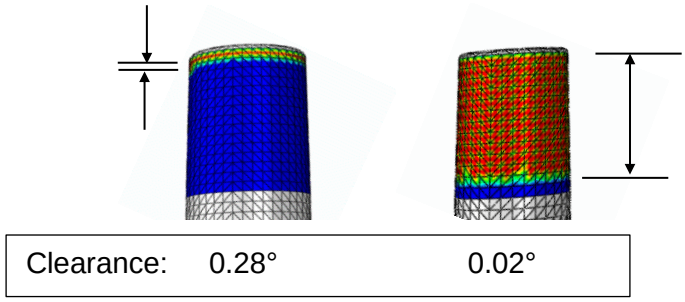

Figure 4-26 Engagement lengths for 2° trunnions with different clearances

4.4.6 Study 3 - Effect of trunnion length on taper gap

The taper gap generated was evaluated for 3 representative trunnion lengths: 10.5, 13.5 and 18 mm (Kao et al., 2016). The taper angles were kept constant using the same female taper angle of 5.76° and a male taper angle of 5.66°. Each taper was subject to walking, stair climb and the 2 hip simulator load profiles (Figure 4-9).

Results 3

Under walking and hip simulator loading profiles, the shortest trunnion length generated the lowest taper gap for the three trunnions evaluated, with comparable head taper stresses and contact areas. In comparison, under stair climb loading, the shortest trunnion generated a considerably larger maximum taper gap and peak von Mises stress at the head taper surface than the longer trunnions as well as the lowest contact area (Figure 4-27).

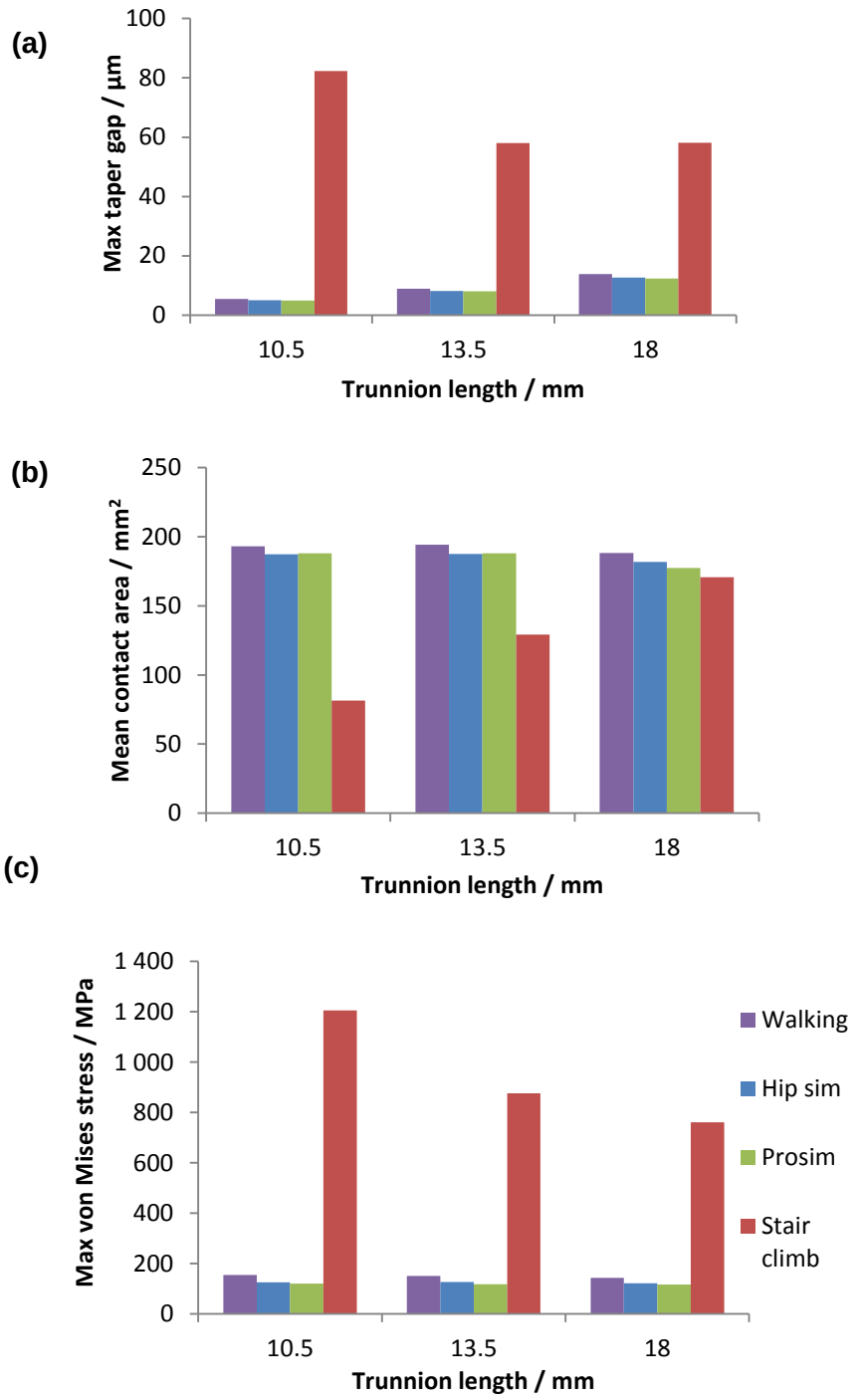

Figure 4-27 Effect of trunnion length on (a) maximum taper gap (b) corresponding contact area under physiological walking, 2 hip simulator profiles and stair climb activity (c) maximum surface stress at the head taper. All data relates to a taper assembly with a head taper angle of 5.76° and a trunnion angle of 5.66°, utilising a clearance of 0.1°

4.4.7 Study 4 - Evaluating a simplified stair climb load profile

The stair climb profile was modified by removing the IER component to recreate the d.o.f capabilities on an orbital hip simulator. This was evaluated on the proximal 5° tapers to determine its suitability as a simplified profile for approximating the effect of stair climb loading on taper junctions.

Results 4

Simplifying the stair climb loading profile to exclude rotation about the vertical axis (IER), did not have a considerable effect on the surface stresses at the head taper or the gap generated at the taper interface for 5° tapers which were designed for proximal contact (Figure 4-28).

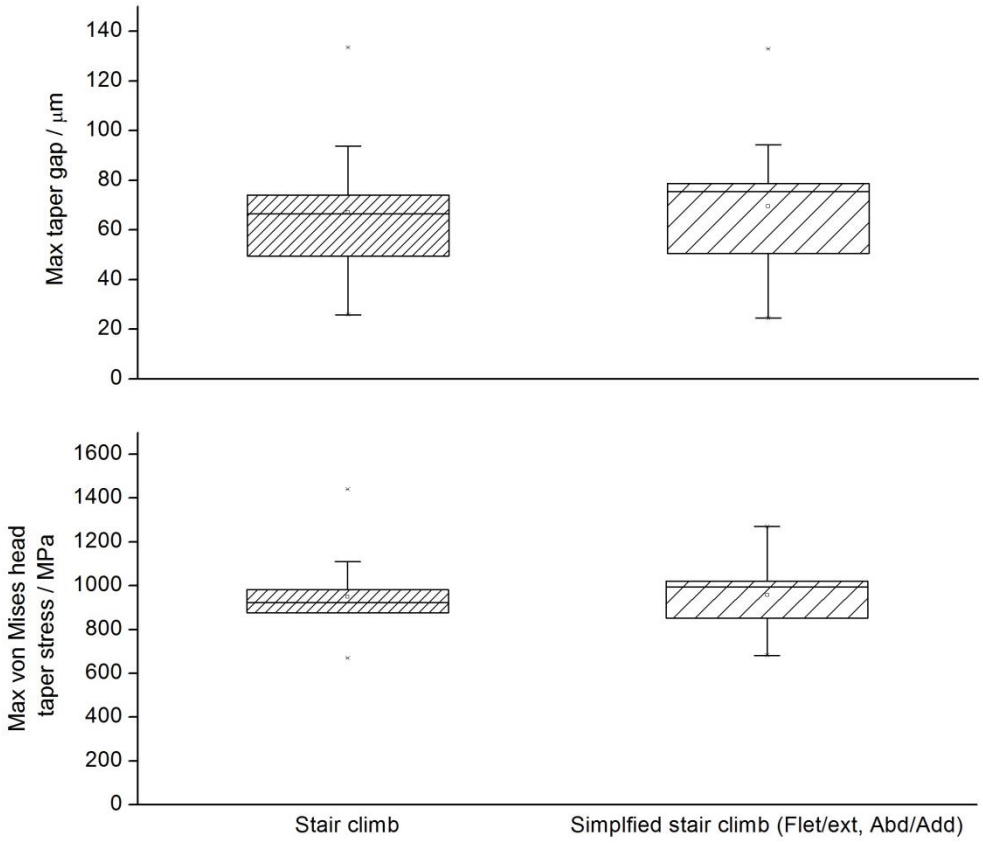

Figure 4-28 Comparing the surface stresses generated at the head taper and taper gap between stair climb loading and a simplified form with flex/ext and abd/add rotations only on proximally contacting 5° tapers

4.4.8 Study 5 – Effect of trunnion material on taper conditions

Under stair climb loading, a change in trunnion material from Ti-6Al-4V (E =110 GPa) to CoCr (E = 230 GPa) was evaluated with respect to taper gap and surface stresses at the head taper, for proximal contact conditions defined in 4.4.4.

Results 5

The mean gap at the taper interface on the 5° tapers with positive clearances (0.02 – 0.28°) increased by 4% on the taper assembly when a CoCr trunnion was modelled compared to the assembly with a Ti-6Al-4V trunnion. A 7% increase in the surface stresses was observed on the head taper when a CoCr trunnion was used (Figure 4-29).

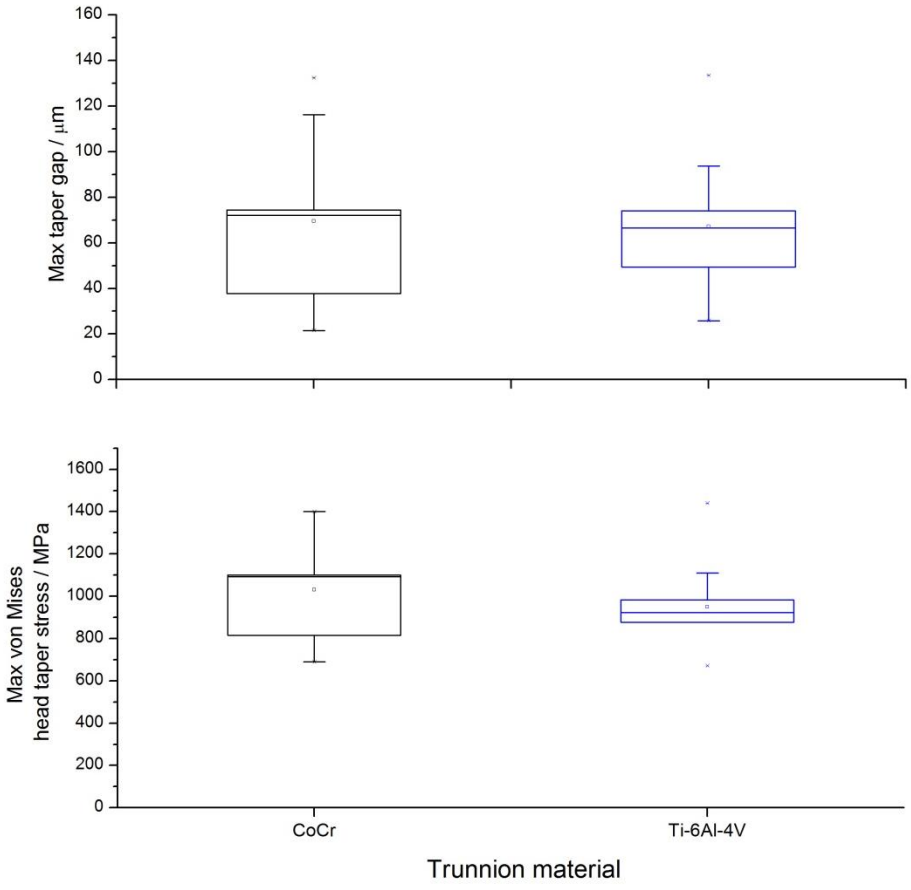

Figure 4-29 Comparison of the taper gap and surface stresses on the femoral head generated under stair climb loading for proximal 5° tapers between CoCr and Ti-6Al-4V trunnions

4.4.9 Study 6 - FE analysis of experimental variables

An evaluation was carried out to compare the micromotion and mean contact areas developed with the proximal and distal CoCr/Ti tapers (Figure 4-30) which had been designed and manufactured to be evaluated on the hip simulator. The proximal CoCr/Ti taper represented a range of clinically relevant angles on both male and female tapers. The distal CoCr/Ti taper was a combination of a commercially available femoral head taper and a non-clinically relevant trunnion to create an extreme negative clearance. The load profile applied to these tapers was implemented to replicate the orbital hip simulator. Two types of micromotion were evaluated per contact condition namely parallel and rotational displacements.

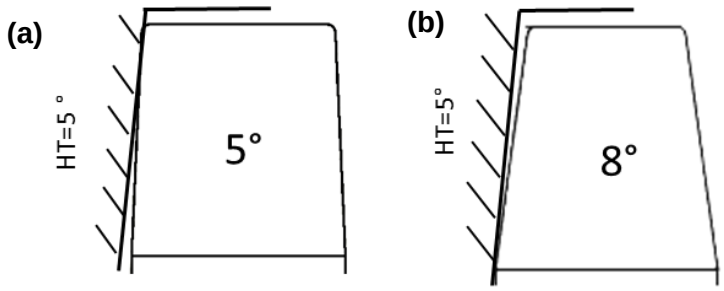

Figure 4-30 (a) proximal and (b) distal contact conditions evaluated on the hip simulator HT= head taper

Results 6

Upon impaction of the femoral head on the titanium trunnion, the engagement lengths of the proximal and distal tapers were 5 mm (Figure 4-31a) and 3 mm (Figure 4-31b) respectively. The proximal contact condition generated a mean contact area of 187 mm^2; in contrast, the distal contact condition generated a mean contact area of 9 mm^2 under the hip simulator load profile (Figure 4-32). This markedly lower contact area consequently generated increased rotational and parallel micromotion on the distal taper design as compared to the proximal taper contact model (Table 4-4). The more clinically relevant distal

contact tapers, with smaller clearances between -0.02 and -0.25° (section 4.4.5) were not evaluated experimentally because the intent of the experimental analysis was to create an extreme of distal contact. It was established from the model simulation that these generated a mean parallel micromotion of 4.52 µm and a mean rotational micromotion of 3.34 µm (Table 4-4).

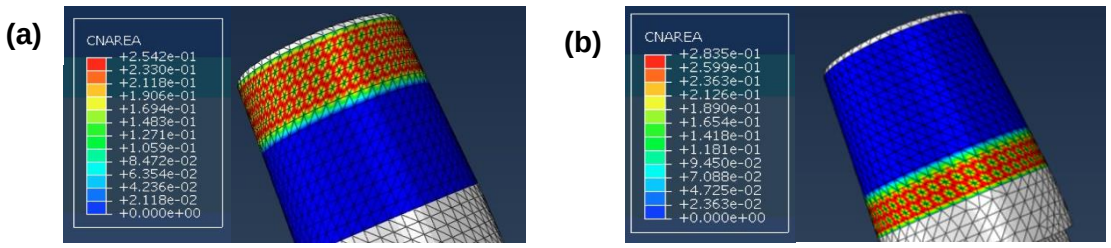

Figure 4-31 Contact distribution generated on the (a) proximal and (b) distal taper junctions evaluated on the hip simulator

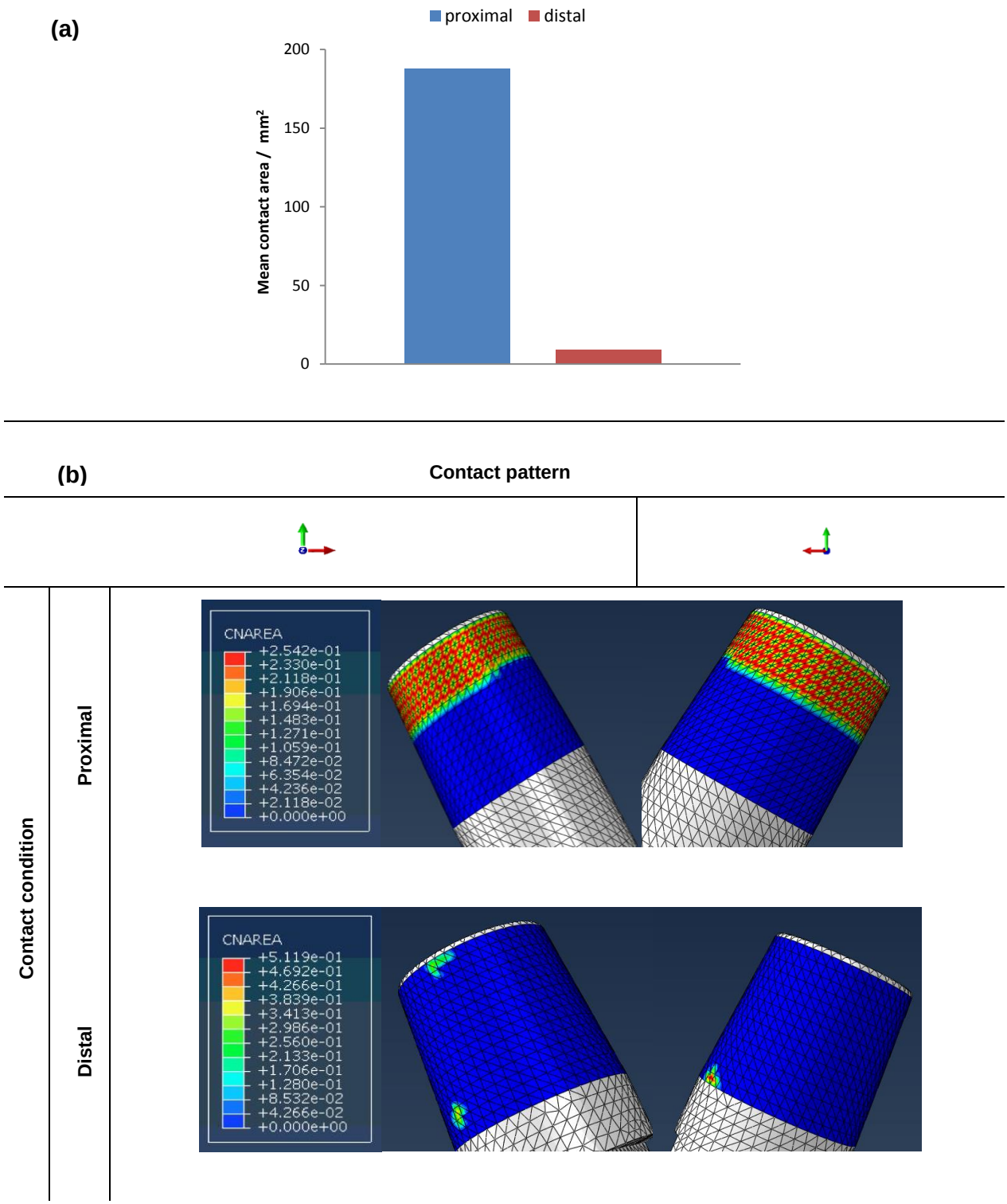

Figure 4-32 (a) Mean contact area over a hip simulator loading cycle (b) proximal and distal contact condition under hip simulator loading profile

Table 4-4 Evaluation of rotational and parallel micromotion generated on the hip simulator in proximal and distal conditions using FEA

	Taper clearance°	Micromotion / µm	
		Parallel	Rotational
Proximal	0.1	4.6	4.2
Distal	-0.02 – -0.25	4.5	3.3
	-2.9	395.5	569.8

4.5 Discussion

The FE modelling approach has proved successful in evaluating the effects of loading and taper clearances on both gap formation and surface stresses. The findings can be related to previously reported experimental and clinical findings. As an example, in retrieval studies (Hothi et al 2017) toggling has been suggested to both allow fluid ingress and produce 'tilting' of the trunnion in the head taper thus generating high surface stresses which exacerbates the potential for corrosion (Chu et al., 2000). In the present work evidence of the simulation of conditions that produce a toggling effect were observed in tapers (Figure 4-10 and Figure 4-14). Large gap opening values (9 – 150 μm) at the mouth, or distal end, of the tapers were observed depending on factors associated with trunnion length, taper engagement position, taper angle and taper clearance. Significantly, the effects were greatest under the simulated loading conditions of stair climbing.

It has been well established that orthopaedic metals develop corrosion resistant thin passive oxide layers of the order of 1 – 4 nm (Mali, 2016, Goldberg and Gilbert, 1997). However if this layer is compromised in a biological environment, the rate of corrosion can be increased by a factor of 10^8 (Goldberg et al., 2002). Although the premise of MACC is that micromotion due to cyclic loading, may abrade or fracture these oxide films (Gilbert et al., 1993), little is understood about these stress-induced mechanisms. The elevated von Mises surface stresses on the head taper established in the present work (Figure 4-27c), may create the conditions where this oxide layer is compromised thereby exposing the

underlying metal to the corrosive fluid which penetrates the taper junction. The introduction of rougher trunnions may further raise concerns about fracture of the oxide layer by increasing local surface stresses. A multiscale FE study (Lundberg et al., 2015) confirmed that the largest stresses were observed at the peaks of surface topography features. The current study established that trunnion surface stresses did not change substantially with variations of loading or taper design. This implies that whereas, changing conditions at the taper could have a detrimental impact on the passive oxide layer on the head taper, the trunnion oxide layer may remain intact. This could indeed provide an explanation for why head tapers are widely seen to corrode preferentially over trunnions in retrieved components (Higgs et al., 2013).

The use of a hip simulator loading profile which simulates a walking cycle, may be used in order to evaluate the response of a taper junction under a changing load vector. However, the present work has suggested that this loading condition may not provide a sufficient evaluation. Indeed, while the simulated walking cycle can be successfully used to estimate bearing surface wear, it is not capable of discriminating between different taper designs. In order to evaluate tapers, a more challenging activity may be required; stair climbing with its inherent increase in torsional loading (Bergmann et al, 2001), has previously been reported to differentiate the stability of different designs of cemented stems in the laboratory (Kassi et al., 2005). In the current study, stair climb loading generated the largest taper gaps and maximum surface von Mises stresses at the head taper (Table 4-3), as well as generating a movement that could be interpreted as representing toggling at the taper junction (Figure 4-10 and Figure 4-14). Replicating 3 axes of loading and rotation increases the complexity, cost and size of a hip simulator (Smith and Unsworth, 2000). Although the AMTI-Boston is able to replicate 3 axes of motion, most other hip simulators currently available are capable of producing 2 axes of motion (Table 2-16) in addition to single axis loading, this design has been shown to be sufficient for wear testing. The existing orbital hip simulators can be used

to approximate the effect of stair climb loading on taper junctions, much like simplified walking cycle profiles have been generated to simulate normal walking (Figure 4-28). However, this requires that the simulators' ROM to be increased. Currently, there are some simulators which are able to apply increased flexion with a flex/ext ROM of ±60° (Hadley, 2012).

Trunnion lengths have been reduced in current modular THRs providing impingement free ROM (Langton et al., 2012, Oehy and Bider, 2004). However, shorter trunnions have been reported to be associated with increased corrosion at the taper junction particularly at the taper base (distal end), which may be attributed to increased stresses at this location (Tan et al., 2015, Langton et al., 2012). The results of the present study showed that the stresses at the base of the shortest trunnion were indeed the largest and that under stair climb, the shortest taper (10.5 mm) produced a large taper gap (Figure 4-27). This raises concerns about short trunnion designs, indicating that there may be an explanation for the clinical findings.

Engineering drawings of tapers specify gauge points coincident on both male and female tapers. Although it is assumed that the taper will engage at this location, it is not known where the taper will actually engage after surgical impaction, due to manufacturing tolerances which lead to variability. The original design of tapers using ceramic heads was implemented for proximal contact to prevent large tensile stresses in the head thereby reducing the risk of head fracture (Cales and Stefani, 1998). However, metal taper junctions can be designed to engage distally (Kocagöz et al., 2013) without the risk of fracture. An experimental evaluation of the taper engagement position showed that the position of taper lock could be out of range of the position defined as the gauge point (Appendix A.2). FEA findings in this study indicate that regardless of taper angle, moving the taper engagement

point more distally, reduced the gap formed at the distal taper (Figure 4-25). This arrangement would be expected to reduce the transport of fluid into the junction.

Retrieval analysis has not found any clear correlation between taper clearance and damage due to fretting and corrosion (Kocagöz et al., 2013), although this may be due to the multiple factors that influence conditions in THRs. Under certain clearances in the current work, it has been shown that both proximal and distal contact conditions generate similar taper gaps if the length over which the taper engages is equivalent. Consequently, for the 5° tapers modelled in this study, a clearance of up to 0.1° maximised the engagement along the length of the trunnion, and thereby retained a maximum taper gap as small as approximately 20 μm. Ashkanfar et al. (2017) concluded that a similar taper mismatch (no more than 6′ or 0.1°) would minimise taper wear. Surprisingly, the taper gap generated at -0.25° was approximately twice the minimal taper gaps observed (Figure 4-23a). This showed that toggling developed under stair climb loading, could be detrimental the performance of such tapers too. However, at an equivalent clearance on the proximally contacting tapers (+0.25°), the maximum taper gap would be predicted to be more than double the value observed at -0.25° (Figure 4-23a).

Maximising the engagement length at a taper junction, thereby maximising the contact area, reduces the gaps that may be developed during loading. Increased contact area over the taper junction has been reported to be beneficial as it increases the stability at the taper junction (Hussenbocus et al., 2015). However, there has been no design limit for the contact area formed at the taper junction. A 1995 FDA recommendation for ceramic head tapers suggested that a stem taper must be in direct contact with at least 50% of the vertical length of the taper (FDA, 1995). Yet, in a study assessing the contact area at the taper interface, the proportion of area in contact for a 11 mm long trunnion, 12/14 taper was reported to be less than 20 % despite high impact loads of 8 kN (Witt et al., 2015). These area values

reported are similar to those generated following mating reported in the current study but do not represent the contact area that may occur during loading. However, the contact area under loading was found to be directly proportional to the area after taper mating under the most severe loading condition (Figure 4-19a) indicating that this initial measure remains useful. From the current modelling, the FDA recommendation of 50 % of the taper being in direct contact (after taper lock) would be predicted to generate a 57 μm gap at the taper whilst a 20 % area in contact at a mated taper interface would be predicted to generate taper gaps of over 90 μm under stair climb loading. Further experimental work is required to understand whether developing a threshold value of maximum taper gap generation under loading could reduce the onset of corrosion.

It was observed that in response to the application of a stair climb load profile, the use of a CoCr alloy for the trunnion resulted in increased separation at the taper interface (Figure 4-29). This might be expected to increase in surface stresses at the head taper as a larger gap would cause a greater tilt of the trunnion in the femoral head (Figure 4-33). The increase in both taper gap to allow for fluid ingress as well as elevated surface stresses which could damage the oxide layer, may provide support for the observation that clinically, CoCr/CoCr taper junctions also corrode (Gilbert et al., 1993), with no obvious advantages of utilising the same alloy and avoiding galvanic corrosion. Although the titanium alloy with the lower elastic modulus did not result in increased taper gap in the current work, there have been concerns around increased corrosion with respect to the TMZF alloy which has an even lower elastic modulus (74-85 GPa) with suggestions that this is due to its increased ‘flexibility’ (Walker et al., 2016, Tan et al., 2015, Raju et al., 2017). Flexural rigidity is a function of modulus and trunnion dimensions and is proportional to geometric properties to the fourth power (equation 12). Accordingly, the shorter 10 mm trunnion modelled in this study resulted in 42% increase in taper gap relative to the ‘mid length’ 13 mm trunnion. The gap formed at the taper junction was more sensitive to changes in dimension than modulus. Additionally, when reports of

taper corrosion are evaluated (Table 4-5), it can be deduced that increased trunnion rigidity does not prevent corrosion since the Ranawat-Burnstein MD Fit stem with a flexural rigidity almost 5 times that of the Accolade TMZF stem, was also found to corrode. In terms of frequency of reporting, the Ranawat-Burnstein MD Fit stem was only observed once; in Table 4-5, the M/L taper stem with more than twice the flexural rigidity of Accolade stem had the highest number of reports (n=20); the Prodigy stem, which is 347 % more rigid than the Accolade stem (Table 4-5), was reported 8 times in comparison to 14 reports of the Accolade stem. Nonetheless, a threshold might exist beyond which flexural rigidity could limit corrosion. Hothi et al. (2017a) reported clinically insignificant trunnionosis with 14/16 CoCr trunnions. Porter et al. (2014) presented a range of flexural rigidity of 14/16 CoCr trunnions as 561.03 - 623.20 Nm^2; although the stem evaluated by Hothi and colleagues was not quoted, it is possible that this threshold is above 500 Nm^2.

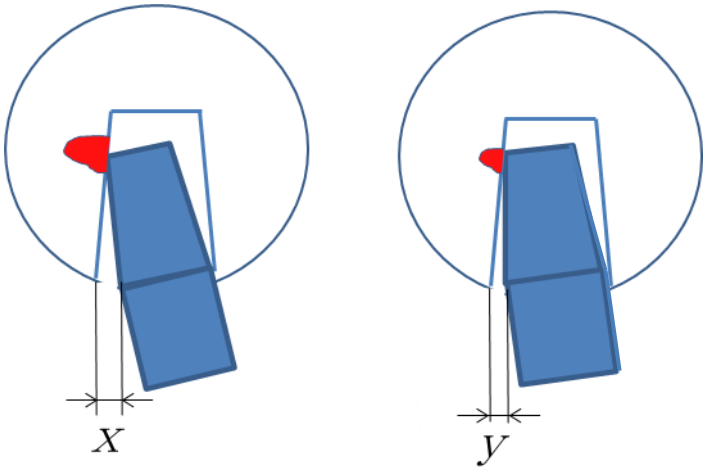

Figure 4-33 Schematic of increased tilting due to larger taper gap resulting in increased surface stresses at the head taper; where taper gap x > taper gap y and the red region represents the magnitude of surface stresses at the head taper

Table 4-5 Femoral stems associated with taper corrosion in case reports or retrieval studies (Porter et al., 2014, Eltit et al., 2017, Whitehouse et al., 2015, Walsh et al., 2012, Nodzo et al., 2017, Carli et al., 2015, Collier et al., 1991, Cooper et al., 2012b)

Femoral stem trade name	Taper size	Stem material	Flexural rigidity (Nm^2)	Manufacturer
Accolade	V40	TMZF	80.06	Stryker
Harris-Galante	6°	Ti-6Al-4V	89.37	Zimmer
S-ROM	11/13		108.98	DePuy
Taperloc	Type I		122.90	Biomet
Synergy	12/14		163.20	Smith & Nephew
PROFEMUR-Z	12/14		165.01	Wright medical
M/L Taper	12/14		165.32	Zimmer
ZMR	12/14		167.80 - 169.66	Zimmer
VerSys Fiber Metal Taper	12/14		168.61 - 169.03	Zimmer
Anatomic	6°	CoCr	185.94	Zimmer
Rejuvenate	V40		228.48	Stryker
VerSys Beaded FullCoat LHC	12/14		355.69	Zimmer
Prodigy	12/14		358.04	DePuy
VerSys Beaded FullCoat	12/14		363.11	Zimmer
VerSys Beaded FullCoat Revision	12/14		365.62	Zimmer
Ranawat-Burnstein MD Fit	Type II		377.19	Biomet

Consideration of design features at the taper junction is important if hip implants longevity is to be improved. In the current work, even the standard walking profile, or its simplified variants, has been shown to be insufficient to differentiate features that occur at taper junctions with relevant taper design variables. The mechanism that could be described as toggling was simulated during stair climb loading, as shown by differentiated maximum taper gap opening values and high localised von Mises surface stresses on the trunnion. The taper mean contact area may provide a design criterion that can indicate taper

performance; contact areas below 125 mm^2 over a stair climb loading cycle, lead to large gaps at the distal taper junction, which may be detrimental to taper performance. The use of a simplified stair climb profile with two axes of rotation, in line with the capabilities of the orbital hip simulator was established to be sufficient representation of a stair climb activity to generate gaps. The taper gap opening is dependent on the length over which the taper engages and not whether it engaged in proximal or distal contact; for 5° tapers, the engagement length was maximised and thus taper gap minimised within a clearance range of ±0.1°. These findings are significant in the future design evolution of taper junctions for use in the orthopaedic industry and their evaluation prior to implantation, impacting significantly on the benefits for patients.

Chapter 5. Method Development and Design

5.1 Problem Definition

It was proposed to use the hip simulator to study the effect of a moving load vector on the taper junction and its corrosion products whilst utilising metal-on-polyethylene bearing components.

5.2 Rationale for isolating the taper junction on LHMoP

Taper corrosion has also been reported in retrievals of MoP devices (Cook et al., 2013, Tan et al., 2015, Hothi et al., 2017a, Whitehouse et al., 2015) and Li et al. (2015) reported that a wear test on MoP devices (36 mm CoCr heads, 12/14 Ti-6Al-4V trunnions) showed visual signs of corrosion after 45 Mc of testing on a hip simulator. This appears to be a retrospective finding and although the material lost from the head taper was measured, the products from the taper were not collected nor characterised. Further, it is arguable that an *in vitro* evaluation using such an extended timeframe is not particularly useful.

Despite large headed metal-on-metal (LHMoM) devices being largely discontinued (Beadling, 2017), large heads are still regarded as advantageous in THR as they reduce the risk of dislocation (Crowninshield et al., 2004), even though they result in increased frictional torque at the bearing surface (Morlock et al., 2011). In MoP devices highly crosslinked polyethylenes (HXLPE) have enabled the use of large heads; Burroughs et al. (2006) showed that HXLPE exhibited a significant increase in frictional torque relative to conventional polyethylene. The introduction of vitamin E polyethylenes to counteract the oxidation of HXLPE (Rajpura et al., 2014), may exacerbate the bearing surface friction; Meneghini et al. (2016) reported increased frictional torque in highly crosslinked

polyethylene (HXLPE) with vitamin E in comparison to liners without the antioxidant when both polyethylene types were paired with large CoCr heads (Meneghini et al., 2016). Ultimately, the increased bearing surface friction may increase the forces and contribute to fretting and corrosion at the taper junction of LHMoP devices.

Corrosion results in the release of ionic and particulate matter which are capable of initiating inflammatory reactions in the body (Hussenbocus et al., 2015). It has been suggested that the taper products create a more severe reaction than wear debris from the bearing surface (Langton, 2014, Hart et al., 2013). Clinical retrieval studies have used ion analysis and quantified taper debris as an indicative measure of taper junction performance and degradation (Langton, 2014, Morlock et al., 2016). Although blood levels of Co and Cr have been measured and it is reported that an elevation of Co over Cr is indicative of taper corrosion (Plummer et al., 2016, Nodzo et al., 2017, McGrory et al., 2017), the concentration of ions released from the taper junction cannot be determined independent of the rest of the implant *in vivo*.

In laboratory testing, the taper junction needs to be isolated from the bearing surface in order to characterise the features associated with the taper (ionic and particulate products) independent of the bearing surface. It has been reported from retrievals, that the taper junction can contribute as much as a third of the total volumetric wear (Hart et al., 2013). Through this isolation, a different microenvironment can additionally be created around the taper to evaluate its effect on the taper junction rather than the lubricant necessary to develop appropriate tribological conditions at the bearing surface. Microenvironments around the taper junction whilst conducting uniaxial tests, have been previously reported; this was achieved by encasing the junction in an elastomeric sleeve (Aldinger et al., 2015, Jani et al., 1997) (Figure 5-1). By isolating the taper junction from the bearing surface on the hip

simulator, Pamu et al. (2012) showed the Co ions released from the taper junction were 2 orders of magnitude lower than the MoM articulating surface.

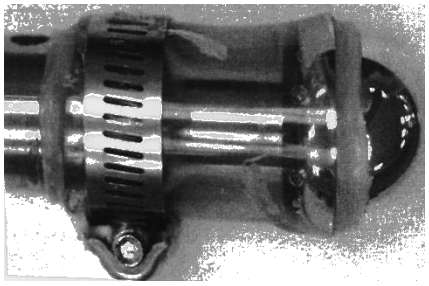

Figure 5-1 Taper junctions encased in an elastomer (Aldinger et al., 2015)

Further, an isolation mechanism could reduce the volume of fluid around the taper ensuring that small changes can be measured. The volume of fluid used to lubricate the bearing surface in hip simulator tests are typically up to 600 ml (Wang et al., 2004, Tateiwa et al., 2006, Royle, 2012); these large volumes of bearing surface fluid considerably dilute the concentration of ions released from the taper junction, meaning small differences in ion release between taper designs will not be differentiated. Whilst ASTM F1875 (1998) recommends a range of 5 – 100 ml, Aldinger et al. (2015) isolated the taper junction in 7 ml of fluid.

5.3 Gaiter isolation design

5.3.1 Design requirements

The requirements for the isolating mechanism were to:

1. Occupy the area between the head and the trunnion taper fixture when assembled
2. Not interfere with the engagement of the taper
3. Not obstruct the normal ROM at the bearing surface
4. Prevent lubricant exchange between the bearing surface lubricant and the fluid around the taper
5. Retains its structural integrity for the duration of no less than 0.3 M cycles which is the minimum number of hip simulator cycles run in a wear test before the lubricant is changed
6. Maintain its integrity at flash temperatures as high as 60°C measured at the bearing surface (Kurtz, 2010)
7. Utilise a sealing method that also meets requirement 6
8. Allow the microenvironment created at the taper to be evaluated at various time intervals without dismantling the setup

5.3.2 Design evolution

5.3.2.1 PTFE and Nylon 6-6 chambers

The motion path on the hip simulator makes it impossible to attach a chamber to the polar region of the femoral head as shown in Figure 5-1. Therefore, the first isolation chamber designed was manufactured from PTFE and was assembled as shown in Figure 5-2. The chamber featured proximal and distal concentric o-ring grooves (Figure 5-3) to seal

onto an internal surface on the femoral head and the base of the trunnion fixture respectively.

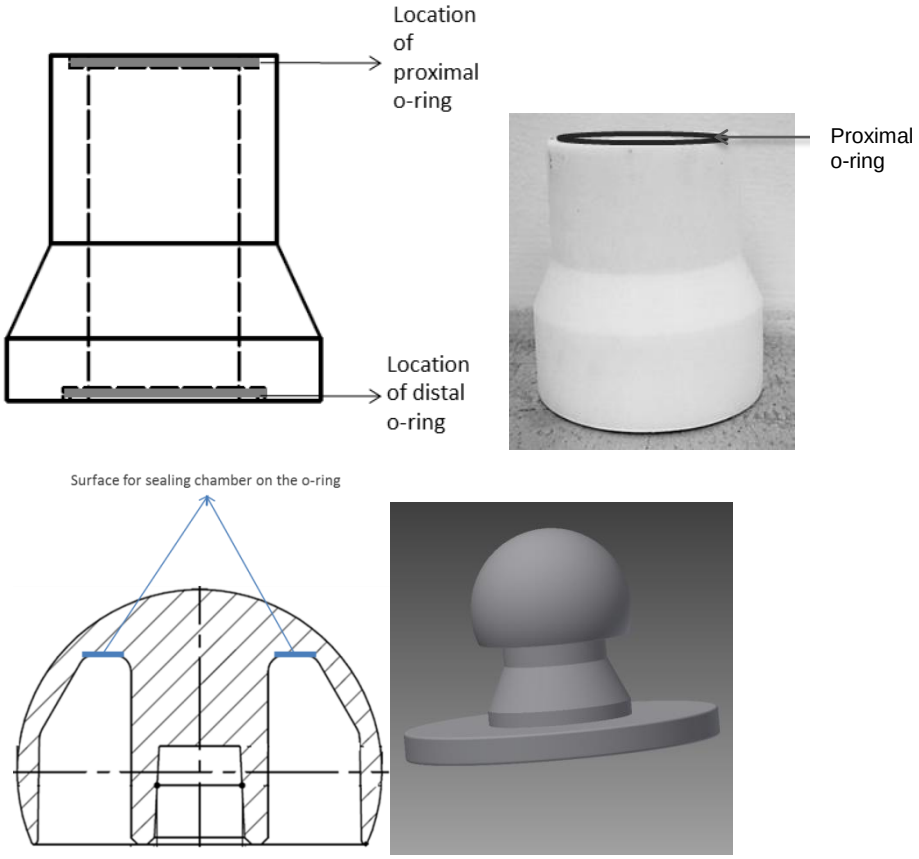

Figure 5-2PTFE chamber and associated components

The chamber was tested for structural integrity and fluid retention on a 56 mm CoCr head, UHMWPE liner and a shell under hip simulator loading conditions with 25 % bovine serum as the lubricant. Within the isolation chamber, a concentrated purple fabric dye was used so that any fluid leakage was apparent. The hip simulator was run for 0.25 Mc out of the required 0.3 Mc before it was observed that the dye leaked. Failure of the chamber was found to be caused by impingement of the PTFE chamber on the acetabular shell. This introduced a lateral force displacing the chamber during the test and allowing fluid egress. Whilst disassembling the components, it was noticed that the seal was intact as a significant force had to be applied to release the head from the taper suggesting that the method of fluid isolation would be appropriate if the lateral force is removed. Thus, the external

diameter of the chamber was reduced in a new prototype to prevent the impingement (Figure 5-3b). It was also observed that the PTFE had deformed around the proximal o-ring groove (Figure 5-3a). The 2nd prototype was therefore manufactured from nylon 6 (polycaprolactam) because of its increased stiffness (2.62 – 3.2 GPa; CES EduPack 2013) compared to PTFE (0.4 -0.552 GPa; CES EduPack 2013).

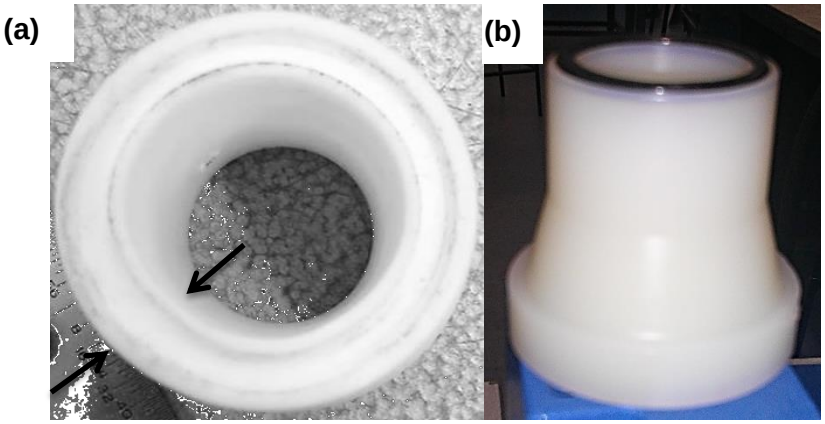

Figure 5-3 (a) deformed old isolation chamber (b) new prototype with reduced profile

A second test showed that the increased stiffness of nylon stopped the taper mating which rendered the design unsatisfactory. Also, it was decided that a taper isolation device which allowed the conditions in the microenvironment to be evaluated at different time intervals was highly desirable. Therefore, this was incorporated as an additional requirement. Further, the 56 mm heads were discontinued and therefore could not be supplied for these tests. However, it was important to retain the use of a large head to take advantage of higher demands on the taper junction. Rodriguez and Rathod (2012) reported that beyond 40 mm, there are no additional benefits of dislocation resistance. Therefore, 40 mm heads were ideal for use with a new isolation design.

The 40 mm and 56 mm heads have different profiles (Figure 5-4) which removed the proximal o-ring sealing surface.

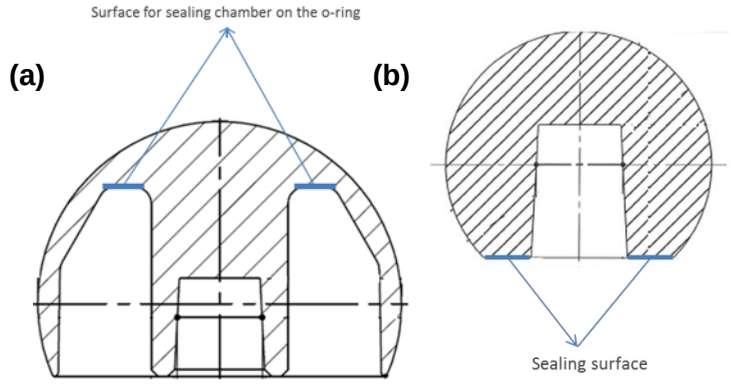

Figure 5-4 (a) 56 mm and (b) 40 mm head profiles

5.3.2.1.1 Silicone chambers

To eliminate the issue with the isolation chamber preventing the tapers mating, the 3rd chamber design was manufactured using silicone rubber. The mould components were manufactured as rapid prototype (ABS-M30 material) parts (Figure 5-5). Sylgard 184 silicone elastomer (Dow Corning Europe) was supplied as a two-part liquid component kit, a pre-polymer base (part A) and a crosslinking curing agent (part B) curable at both room temperature (RT = 25 ˚C) and elevated temperatures (Johnston et al., 2014). The uncured mixture of 10 parts base to 1 part curing agent was thoroughly degassed in a vacuum dessicator at low pressure to remove bubbles and poured into moulds to cure at 70°C. The resultant silicone chamber cured as a translucent structure (Figure 5-5). Sampling ports were incorporated into the silicone chamber by creating 2 holes using a biopsy punch, feeding silicone tubing through the holes to create an inlet and outlet port and sealing around the edge of the holes using silicone sealant to prevent leakage. The basal rim of the femoral head was sealed to the silicone chamber prior to being impacted onto the trunnion with a cyanoacrylate Loctite 406 used after the application of a primer, Loctite 770 (Henkel Ltd, Hertfordshire) (Figure 5-5) and the distal region of the chamber was sealed using a silicone sealant.

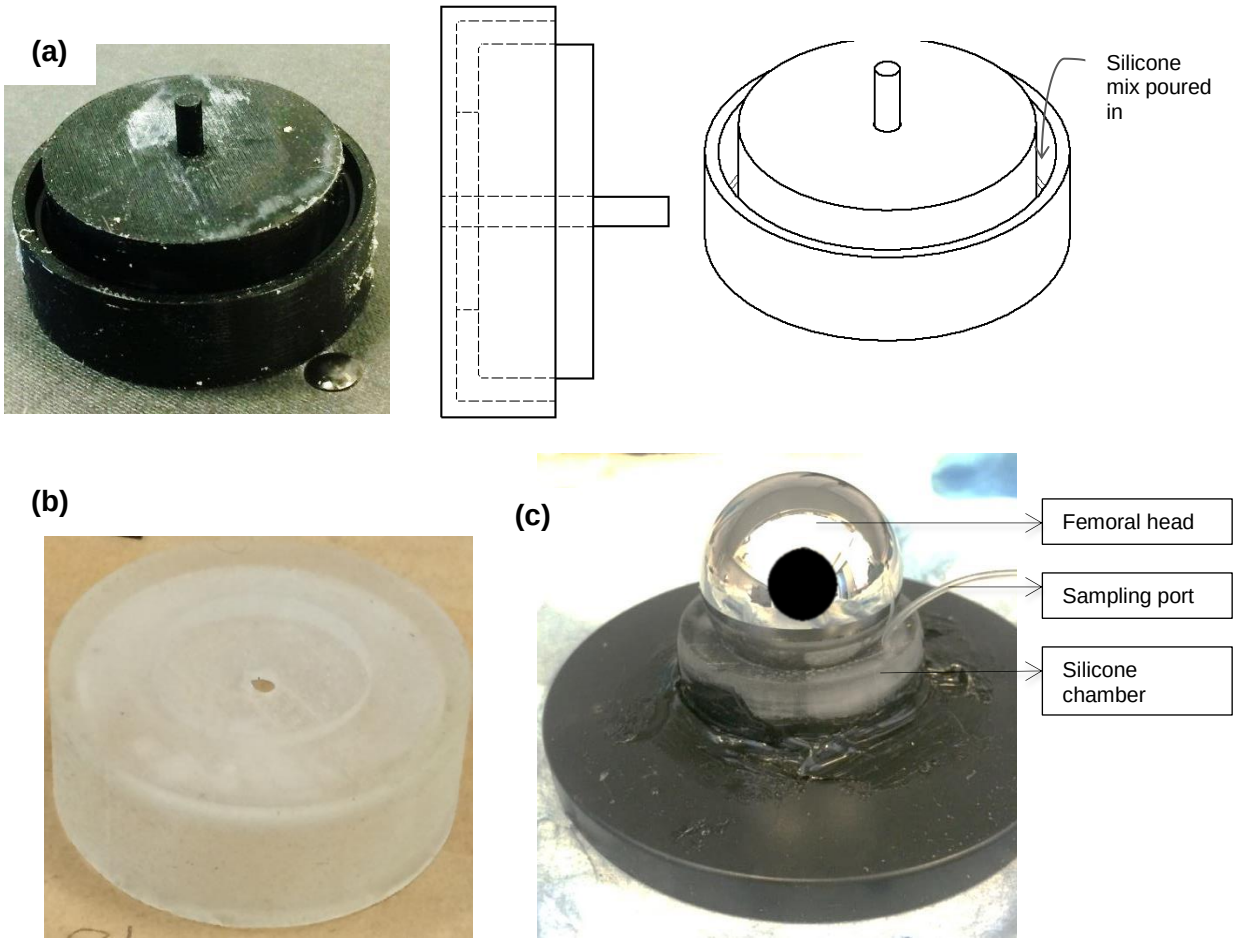

Figure 5-5 (a) 3-part rapid prototyped ABS mould (b) first silicone design created with PDMS (c) the initial PDMS design assembled on the 40 mm head; black circle drawn on to block light reflection

The assembly with a silicone chamber was evaluated on the hip simulator and it was found that it interfered with the assembly resulting in damage of the silicone chamber (Figure 5-6).

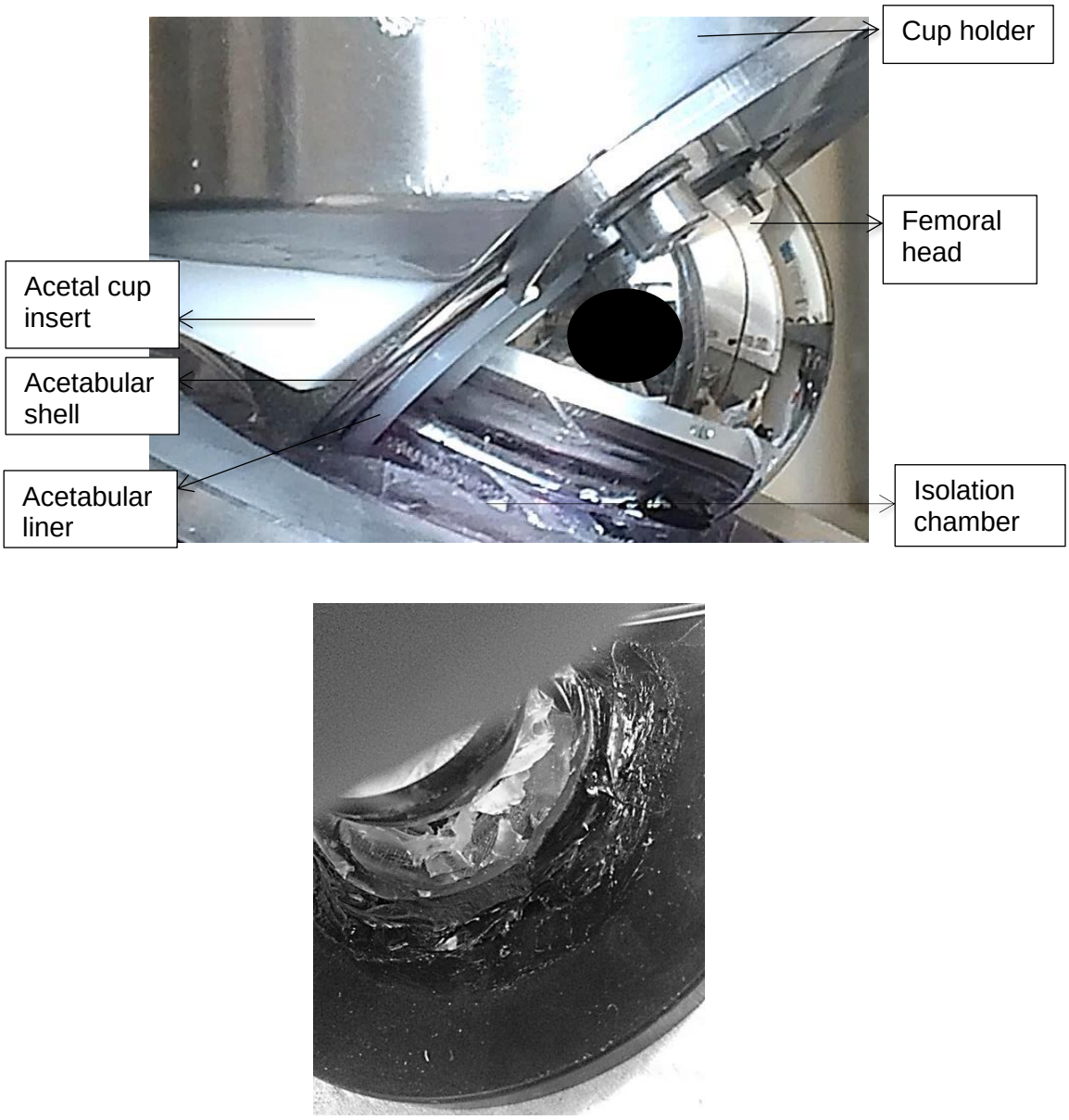

Figure 5-6 (a) Testing the initial design (b) Damage created on initial silicone design after running on the hip simulator; black circle drawn to block light reflection

5.3.2.1.2 Final isolation design

A new silicone taper isolation chamber was designed with a slimmer profile to prevent the interference of the chamber with the acetabular components during the motion of the hip simulator. The manufacture of the new chamber (Figure 5-7a) was outsourced to Beakbane Limited (Kidderminster, UK), as the design featured an inverted profile which required a split mould not achievable using rapid prototyping. The new design was adhered to the base rim of the femoral head using Loctite 406 with a 770 primer. The chamber was sealed at the distal end using a stainless steel plate with a 2 mm thick concentric o-ring bolted onto on the silicone chamber and the adaptable taper base via 6 M4 screws (Figure 5-7). Sampling ports were created on the manufactured part as described in 5.3.2.1.1.

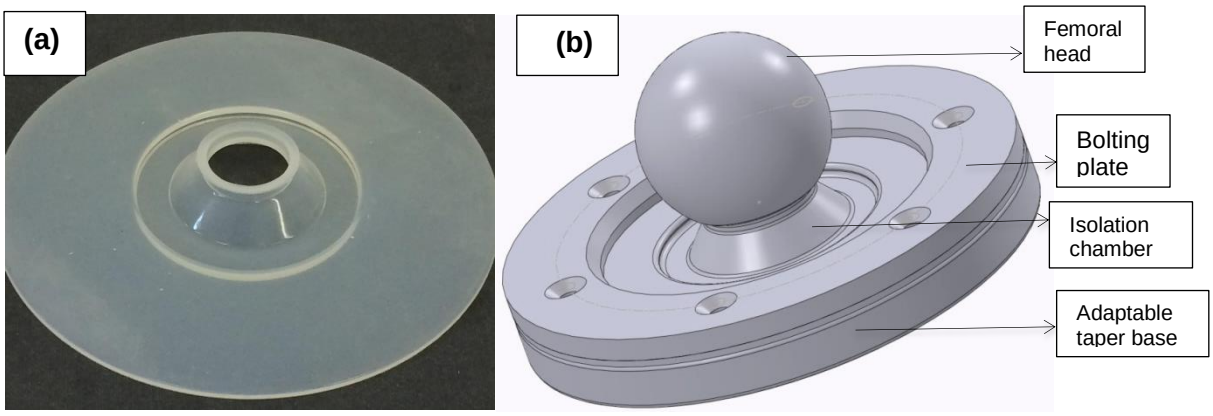

Figure 5-7 (a) Redesign of the isolation chamber with a slimmer profile (not showing the sampling ports) (b) Model of isolation chamber assembled

Further, the acetabular components were modified (see Appendix A.1) by removing 816 and 1172 mm^3 of the liner and shell respectively to ensure that the motion of the hip simulator did not interfere with the assembly.

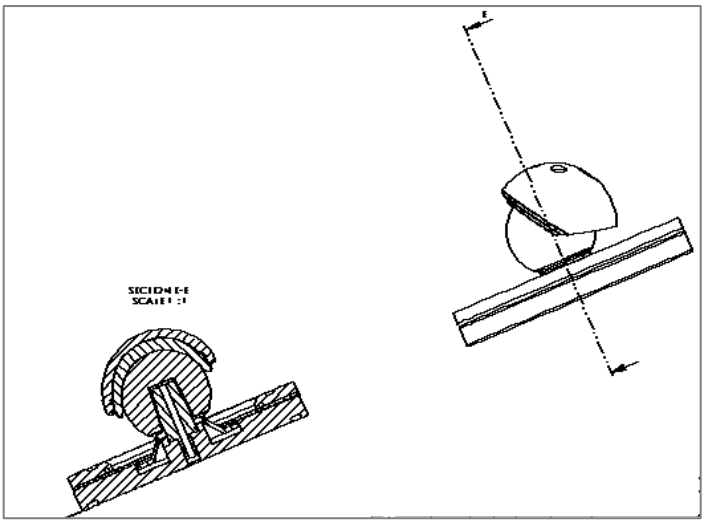

Figure 5-8 Assembly of the chamber on the head and trunnion on the modified acetabular components

5.4 Taper junction design

5.4.1 Material selection

The original trunnion fixture used on the hip simulator was a monobloc design manufactured from 17-4 steel which is not used clinically (Figure 5-9). The only region of interest in the current study is the taper and not the base of the fixture which constitutes a larger volume of material.

Figure 5-9 Monobloc trunnion fixture

Clinically, trunnions are fabricated from Ti-6Al-4V, 316L Stainless steel or CoCr alloy. Ti-6Al-4V alloys are attractive for use as hip stems because of their relatively low elastic modulus. A preliminary evaluation was carried out to compare two taper material

combinations, namely CoCr/17-4 steel and CoCr/Ti alloy under hip simulator loading. Royhman et al. (2014) showed that corrosion rate was inversely related to pH for both Ti6Al4V and CoCr alloys. Also, Virtanen et al. (2008) state that the rate of dissolution of wrought CoCr alloy was constant when the pH of saline was reduced from 7.4 to 2. Further, Nambu et al. (2015) reported that the pH in the taper of a dissociated modular femoral stem was 1.5 and Gilbert (2012) suggests the pH within modular tapers of hip replacement could be even lower than 1. Therefore the two CoCr female taper bores (40 mm heads) were filled with 0.5 ml of PBS, acidified to a pH of 1.6 before mating with either a 17-4 steel trunnion or a Ti-6Al-4V trunnion, which were otherwise identical, to create an aggressive test environment.

The components were tested on the hip simulator for 15 000 cycles, under standard gait cycle loading using 25 % serum as the lubricant at the bearing surface. The concentration of Cobalt ions released in the taper fluid was evaluated using Graphite Furnace Atomic Absorption Spectroscopy (GFAAS) (SpectrAA 220FS atomic absorption spectrometer with a GTA-110 autosampler, Varian, Oxfordshire, UK). All GFAAS measurements were performed using pyrolytically coated graphite partition tubes (Agilent, California, US).

The results showed that under same conditions, the Co/Ti combination released more Co ions into the taper fluid (Figure 5-10). It was resolved therefore that the worst case scenario would be created if the trunnion was manufactured from Ti-6Al-4V.

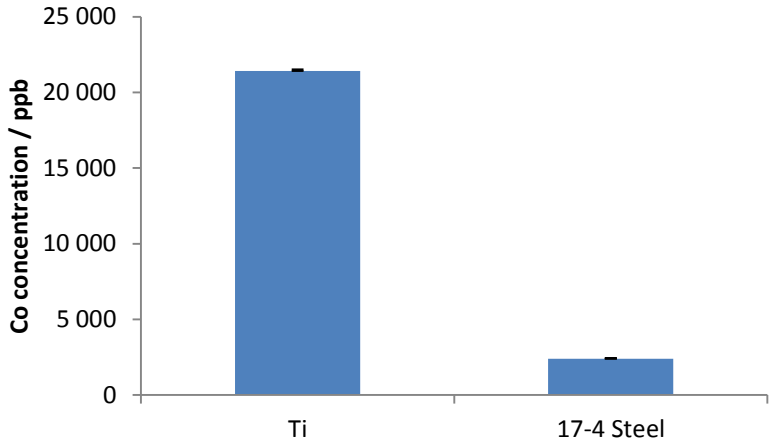

Figure 5-10 Comparing the cobalt release into the taper fluid after 15 000 cycles of testing on the hip simulator

An adaptable or modular trunnion design was introduced as it allows the trunnion to be varied independent of the substantial base fixture. The base fixture could be fabricated from Ti-6Al-4V, CoCr or steel. Titanium alloys have lower hardness and thus are susceptible to fretting (Antoniou and Radtke, 1997) particularly when it articulates against itself (Grupp et al., 2010) thus making it less suitable for a modular system. Grupp et al. (2010) showed that CoCr/Ti combinations reduced fretting in comparison to Ti/Ti but one of the variables of interest at the taper interface is Co release thus making any Co alloy unsuitable as a choice for the base. The 17-4 steel has been utilised previously under the hip simulator test conditions; Zartman et al. (2011) reported no issues associated with galvanic corrosion in the combination of steel and titanium and the combination poses no greater risk than for similar alloy combinations. Therefore, the final adaptable taper was designed to comprise of a Ti-6Al-4V trunnion and a 17-4 steel base (Figure 5-11). The 2 parts were designed for assembly by screwing a removable taper insert into the base. The 17-4 steel base was coated with PTFE (Fluorocarbon, Hertfordshire, UK) approximately 0.2 mm thick to prevent metal ion contamination from the large surface area. The taper inserts were designed with a left handed thread, in order to self-tighten under the motion of the hip simulator.

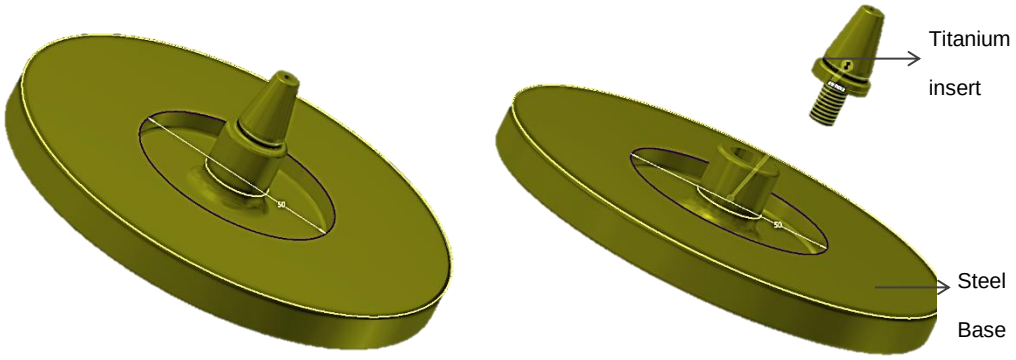

Figure 5-11 Adaptable taper design

5.4.2 Trunnion design evolution

The trunnion insert-base assembly was designed with a concentric 4 mm diameter hole through the whole assembly to facilitate the removal of the femoral head (Figure 5-12). Initial evaluation of the design on the hip simulator established that fatigue life of the trunnion insert was too low and led to early failure at the end of the threaded region. Therefore, the hole was removed to extend the fatigue life. However, this did not prevent some taper failures occurring.

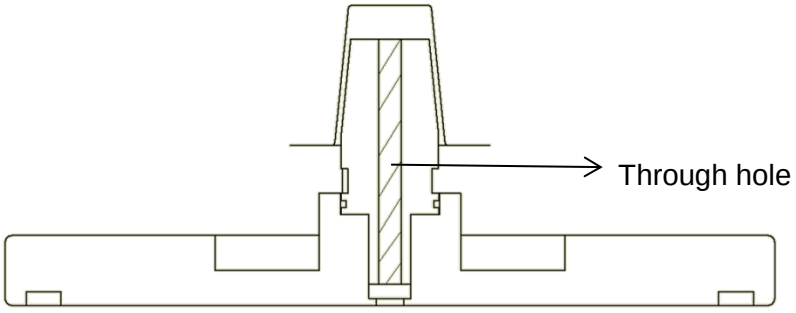

Figure 5-12 Adaptable taper assembly showing the concentric hole

It was identified that the continued failures were caused by a gap between the radius at the base of the insert above the thread and the thread on the base. An undercut feature was incorporated before the start of the thread (Figure 5-13)

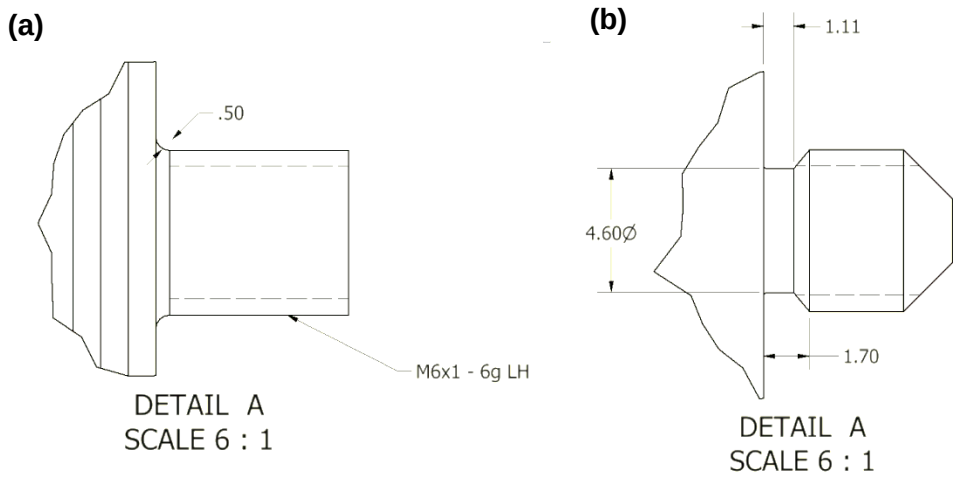

Figure 5-13 (a) Original trunnion base with no undercut feature behind the thread (b) Thread feature with undercut

5.4.3 Taper design variables

The taper design variables selected for experimental evaluation were both the contact location and trunnion roughness.

A proximal contact condition was designed through the mating of a head taper angle in the range 5.725 - 5.808° and a 5° trunnion angle (Figure 5-14). Although the 5° taper in clinical settings contacts both proximally and distally, no difference has been reported between the contact conditions (Kocagöz et al., 2013).

A distal contact was designed through mating a 5° head taper described above with an 8° trunnion (Figure 5-15). Although this was not clinically relevant, it was selected as an extreme condition to prevent fluid ingress into the taper interface. Smaller trunnion angles of 6 and 7° were considered to create this distal contact however the translation of the head centre could not be corrected by commercially available head offsets. These head offsets are manufactured in 4 mm increments. The proximal (5/5°) taper assembly utilised a +0 mm offset and the head centre could only be correctly located using an 8° trunnion on a -4 mm 5° head.

In a review of commercially available stems, Munir et al. (2013) categorised smooth (non-threaded) trunnions as having Rz values of between 6 and 7.5 μm and rough (threaded) trunnions with Rz values between 10 and 17.4 μm. Consequently, in the current study, 5° and 8° trunnions (Figure 5-14 and Figure 5-15) were designed and manufactured with smooth (Rz 6μm + 3) and rough surface (Rz 16μm + 3) topographies.

Four head-trunnion pairings were utilised namely: (i) proximal contact with a rough trunnion, (ii) proximal contact with a smooth trunnion, (iii) distal contact with a smooth trunnion and (iv) distal contact with a rough trunnion.

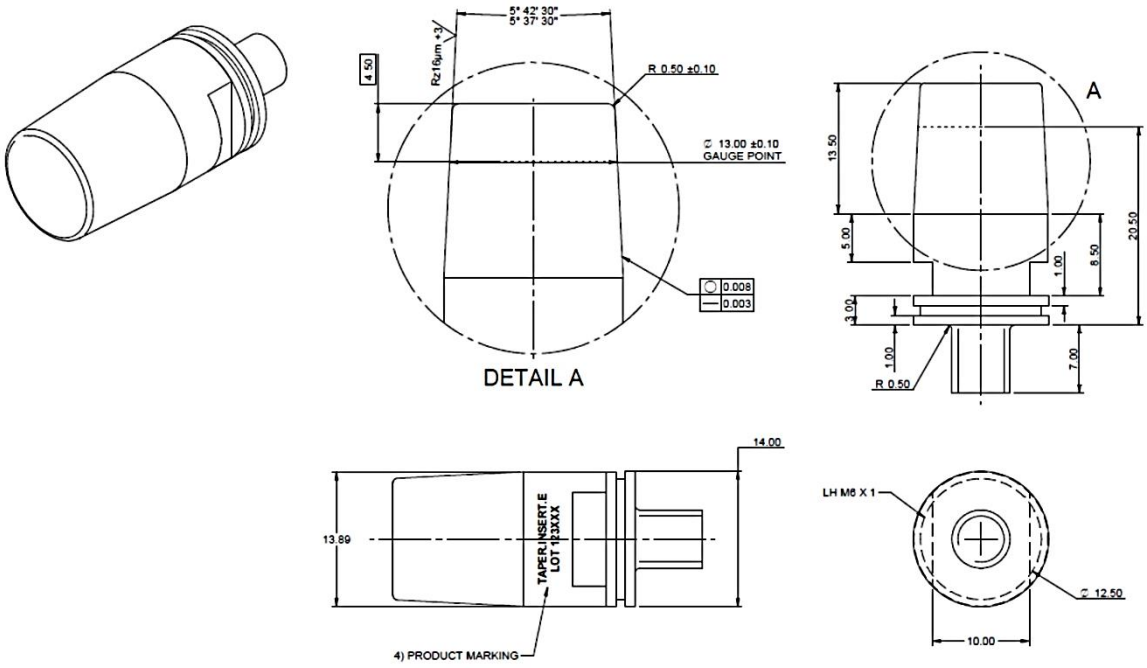

Figure 5-14 Engineering drawing of the 5° Ti-6Al-4V trunnion

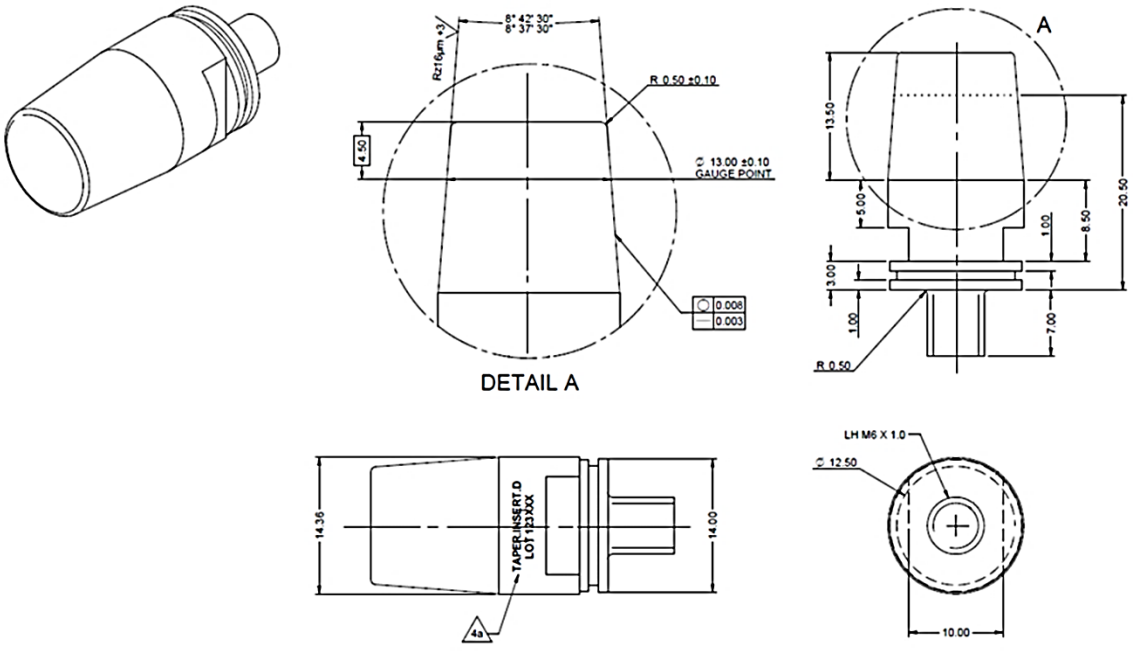

Figure 5-15 Engineering drawing of the 8° Ti-6Al-4V trunnion

5.5 Taper fluid selection

The taper junction has been evaluated in different fluids (Table 5-2); these are either physiologically representative or are selected to accelerate damage.

5.5.1 Physiological solutions

ASTM F1875(1998) recommends the chamber around the taper is filled with electrolyte 0.9 % sodium chloride (NaCl) in distilled water for short term tests; while for long term tests, 10 % solution of calf serum in 0.9 % NaCl in distilled water is recommended. Saline solutions such as Hank's, Ringer's, PBS and 0.9 % NaCl are used as 'artificial body liquids' because they have inorganic components which are present in physiological fluids including blood plasma and synovial fluid (Schaaff and Holzwarth, 2003, Beadling, 2017) (Table 5-1). Each of these solutions are different but can create an *in vitro* environment related to the *in vivo* conditions (Zheng, 2016, Bundy, 2005).

Table 5-1 Inorganic constituents of physiological fluids; units in mM

Solution	Na^+	K^+	Cl^-	Ca^{2+}	Mg^{2+}	HCO_3^-	HPO_4^{2-}	SO_4^{2-}	Reference
Blood	79-91	40-60	77-86	2.42	1.48-1.85	19.1-22.7	-	-	Turitto and Slack (2016)
Synovial fluid	133-139	3.5-4.5	87-138	1.2-2.4	-	-	-	-	
Plasma	134-145	3.5-5.2	100-108	2.12-2.72	0.7-1.5	25-30	1	0.5	Turitto and Slack (2016), (Zheng, 2016)
0.9% NaCl	153-154	-	153-154	-	-	-	-	-	Zheng (2016)
PBS	157	4.1	140	-	-	-	11.5	-	
Ringer's	113.6	1.88	115.3	1.08	0	2.38	0	0	Tas (2014)
Hank's	140.1-141.6	5.81-6.2	144.8-145.8	1.26-1.9	0.8-0.81	3.2-4.065	0.4-0.78	0.8-0.81	Tas (2014), (Zheng, 2016)

THR devices are also in contact with proteins. Implants have been shown to be covered with a layer of adsorbed protein immediately after insertion into the body (Karimi et al., 2012, Virtanen et al., 2008). The interactions of cations with proteins forms organometallic

complexes capable of influencing the corrosion rate (Karimi et al., 2012). There are varied reports on the effect of protein on corrosion; it is reported to be metal specific as well as dependent on the type and concentration of protein (Bundy, 2005).

The corrosion rate of CoCr alloy was found to be higher in 10% calf serum solution in saline than in saline (0.9% NaCl) alone (Hughes et al., 1990); Brown et al. (1988) reported an increase in Co and Cr ions released in 10% calf serum solution in saline (0.9% NaCl) as compared to the saline solution alone. Conversely, with 10% foetal calf serum solution in PBS, the corrosion resistance of Ti-6Al-4V increased relative to the pure saline condition (Khan et al., 1999). Yet, Nganbe et al. (2010) did not observe any corrosion after 1 Mc fretting test on modular neck devices run in bovine serum where both neck and stem body were manufactured from Ti-6Al-4V. Pamu et al. (2012) showed that following loading for 1 Mc on a hip simulator, the volume of ions released in new born calf serum from a head-trunnion junction was approximately 10 times lower than in Ringer's solution. At 2 Mc however, the ion release plateaued in serum but increased by 20 fold in the saline solution. Fibrinogen protein was found to increase the dissolution of cobalt powder after 16 hour exposure, but chromium dissolution was reduced relative to albumin. Comparatively, there was no change in the dissolution of titanium between the two proteins (Clark and Williams, 1982).

The fluids in contact with implants, have varying concentrations of protein, with interstitial fluid having a protein concentration of 4 g/L in comparison to 66.3 g/L in human serum (Karimi et al., 2012). Although it has been suggested that protein concentration may affect corrosion (Karimi et al., 2012, Beadling, 2017, Wang et al., 2004), Beadling (2017) found no significant difference in the static corrosion behaviour of CoCr alloy between 17 and 30 g/L protein concentrations. Further, proteinous lubricants such as calf or bovine serum have been added to saline; Beadling (2017) reported similar open circuit potential (OCP) in PBS

alone and bovine serum diluted to 17 and 30 g/L in PBS with no significant difference in breakdown potential.

5.5.2 Accelerated solutions

Accelerated test methodologies are required to create corrosion more quickly than under standard conditions (Meade, 1999) as testing for 10 Mc is too time consuming. The measured pH within modular tapers has been observed to be as low as 1 and 3 and the CoCr alloy is reported to be susceptible to corrosion at a pH lower than 3 (Gilbert, 2012, Aldinger et al., 2015). Therefore saline solutions have previously been acidified during *in vitro* evaluations; Aldinger et al. (2015) utilised saline at a pH of 1.5 in the taper microenvironment whilst evaluating fretting corrosion of CoCr heads.

CoCr alloy is susceptible to H_2O_2 (Gilbert et al., 2015b) but there have been conflicting reports on its effect on corrosion. Gilbert et al. (2015b) and Tengvall et al. (1989) showed that H_2O_2 increased the rate of corrosion of CoCr and Titanium alloys respectively. On the other hand, Lin and Bumgardner (2004), suggested that the release of ROS reduces corrosion by enhancing surface oxides. Liu and Gilbert (2017) suggest that the effect on H_2O_2 on corrosion of CoCr is dependent upon the prevailing pH and the group found that the addition of 30 mM H_2O_2 to PBS resulted in severe corrosion at physiological pH in comparison to lower pH. Reports of ICI corrosion speculated that corrosion occurs in response to Fenton reactions which may occur during inflammatory conditions in the implant environment, where H_2O_2 and iron are released as part of the inflammatory sequelae. Accordingly, H_2O_2 has been combined with iron salts to form Fenton reagents. Liu and Gilbert (2017) showed that there was a fivefold increase in corrosion current with Fenton reagent (10mM H_2O_2 + $FeCl_3$ + PBS) relative to PBS solution alone; a 30mM concentration of H_2O_2 in PBS resulted in an even larger corrosion current than Fenton reagent at the same pH of 7.4.

Viceconti et al. (1996) recommended that accelerated tests using $FeCl_3$ should be performed if crevice or fretting corrosion is a concern. $FeCl_3$ solution is characterised by increased acidity and chloride concentration than can be obtained under normal physiological conditions and can be used as a 'worst case' scenario because it is conducive to pitting and crevice corrosion (Shreir, 1976, Henthorn, 1981).

Table 5-2 Summary of test conditions used to evaluate taper junctions

Components	Test conditions	Outcome	Reference
4 ASTM F136 commercial cementless modular neck stem **4 ASTM F136 modular neck laboratory prototype**	*Environment:* Air (n=2) buffered Ringer's solution (n=3) $FeCl_3$ filtered solution (n=3) *Loading*: Uniaxial compression 200 to 2,100 N at 2 Hz to 1Mc	The commercial stems showed minimum fretting wear even in $FeCl_3$ solution. The Prototype stem with a smaller neck-body taper, showed extensive fretting wear in Ringer's and $FeCl_3$ solutions.	Viceconti et al. (1996)
28 mm CoCr heads 3 +8 mm (n=3), +16 mm (n=3)	*Environment:* 7 ml saline + HCl solution *Loading*: Uniaxial compression 534 to 5338 N at 5 Hz to 10 Mc	10 of 12 (heads and trunnions) showed severe corrosion (Goldberg score 4)	Aldinger et al. (2015)
CoCr (ASTM F-1537) discs	PBS with additions of HCl (pH 1, 3, and 7.4) and H_2O_2 (0.1 to 30 mM) OCP and polarization tests	Large increases in the corrosion susceptibility of CoCr when H_2O_2 is added to PBS or PBS with HCl (pH 1 or 3)	Gilbert et al. (2015b)
CoCr heads, (ASTM F1537, n=9) and 9 neck tapers (Ti-6Al-4V, ASTM F136, n=6) (CoCr ASTM F1537, n=3)	*Environment:* PBS solution *Loading*: Uniaxial compression Max 3200N at 3Hz to 1Mc	*Taper fluid v surrounding medium* Increased ion concentration inside the head in comparison to external solutions around the taper and neck. *Loaded v unloaded control:* Concentration of the taper fluid of loaded samples was significantly higher than taper fluid concentrations for unloaded controls.	Goldberg and Gilbert (2003)

50 CoCr (+8 mm) offset sleeved modular heads Ti-6Al-4V trunnions (n=6)	*Taper Environment:* bovine calf serum (n=3) Ringer solution (n=3) *Loading*: F/E 30°/15°,IER ±10°. Max 3 kN swing phase 0.3 kN at 1 Hz to 2Mc	Taper junction metal ion output: *Serum* 1.83 x 10^{-3} mm^3 (0.5 Mc) and 4.52 x 10^{-3} mm^3 (2 Mc) *Ringer's* 16.69 x 10^{-3} mm^3 (0.5 Mc) and 41.93 x 10^{-3} mm^3 (2 Mc)	Pamu et al. (2012)
CoCr head Ti-6Al-4V stem	*Taper Environment:* Lactated Ringer's *Loading*: 3300 N to 10 Mc	Ion concentration / µg 12/14 proximal: Co 25; Cr 7.5; Ti <2.5 10/12 proximal: Co 255; Cr 88; Ti 44 10/12 distal: Co 566; Cr 165; Ti 32	Jani et al. (1997)
CoCr heads CoCr and Ti-6Al-4V necks	*Taper Environment:* PBS Loading: 2000 N at 5Hz to 1.3 Mc	Co concentration *0.3 Mc* : 688 *0.75 Mc*: 440 *0.95 Mc*: 2036	Goldberg et al. (1997)
28 (+10.5mm) CoCr heads Ti-6Al-4V and CoCr necks	*Taper Environment:* 0.9% NaCl *Loading:* 0.3-3 kN at 10Hz to 5Mc (Ti) and 10 Mc (CoCr)	Ti: Impact 0.12; Hand assembly 0.85; Gentle impact -0.1 CoCr: Impact 0.06; Hand assembly 0.89; Gentle impact 0.29 Volume loss (mm^3)	Nambu et al. (2015)
26 mm SS (ASTM F138-13) heads **SS stems (ASTM F138, n=5)** **Ti-6Al-4V stems (ASTM F136, n=5)**	*Taper Environment:* 0.90% NaCl in distilled water *Loading:* 0.3-3 kN at 5Hz to 10Mc	Significant corrosive attack inside the head of the SS/SS, compared with SS/Ti which showed non- significant fretting corrosion attack at the bore	dos Santos et al. (2016)

5.5.3 Preliminary evaluations

To determine the fluid to be used in the taper microenvironment, two experiments were performed. The first was to carry out an evaluation of Fenton reagent by culturing macrophages onto polished CoCr discs. The second evaluation was carried out on the hip simulator with $FeCl_3$, acidified PBS and 25 % serum in and around the taper junction which was isolated from the bearing surface fluid by the manufactured silicon gaiter. PBS was chosen as the physiological saline solution because it has been used in previous studies (Table 5-2), was readily available and does not contain calcium and phosphate ions. The precipitation of calcium phosphate from physiological fluids has been reported to protect CoCr from passive dissolution (Lewis et al., 2006). The dissolution of $FeCl_3$ in ultrapure distilled and deionised water (resistivity 18.0 MΩ.cm) resulted in a pH of 0.95. PBS was acidified to a pH of 1.67 by serial addition of HCl. Therefore, the $FeCl_3$ and PBS [H+] solutions were chosen to create an aggressive environment which would accelerate the corrosive attack (5.4.1).

5.5.3.1 Study 1: Macrophage culture on polished CoCr discs

Human monocytes cell line U937 cells were seeded onto a 24.1 mm diameter polished CoCr disc. The cells were differentiated to macrophages by 50 nM PMA (Phorbol myristate acetate) and the well was filled with 5 ml of medium. The culture was left at 37°C, 5% CO_2 for 48 hours to achieve confluence. After 48 hours, the medium containing PMA was changed to standard medium and the disc was left for a further 7 days. The disc was rinsed with PBS to ensure that any cells not adhered would be removed from the surface; subsequently, the cells were fixed and stained with 555 Phalloidin and H33352 (ThermoFisher Scientific, UK). Images of the disc under a laser scanning confocal microscope (Leica TCS SP2) showed that the cells had adhered to the disc surface (Figure 5-16).

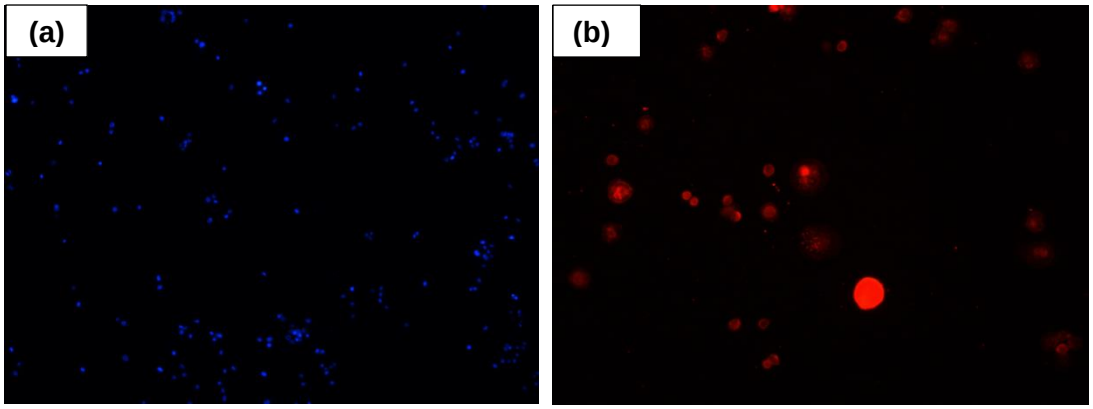

Figure 5-16 Confocal microscope image showing H33352 and 555 Phalloidin uptake on fixed cells

After confirming that the cells adhered to the disc, a further test was carried out to measure the effect of attached macrophages on the Co ion release in the medium. Cells were seeded onto 2 polished CoCr discs, with 3 controls namely an identical disc without cells seeded (only the CoCr disc in medium), a well containing seeded cells in medium and medium only. Media was changed at 2 time points and stored for Co ion release measurements on the GFAAS (2.4.1). The first sample point for ion concentration measurement was taken after the medium containing PMA had been removed. The 2nd time point was taken after a period of 7 days when the medium was changed. The 3rd time point was after 14 days. The medium with the cells was collected and spun at 2000 rpm to allow any ingested ions to be released into the supernatant.

After the study, the discs were imaged using SEM (Inspect F, FEI, Eindhoven, NL) coupled with energy dispersive X-ray analysis (EDX) (INCA Energy 350, Oxford Instruments, Oxfordshire, UK) to identify any cell induced corrosive features.

5.5.3.1.1 Results

All 3 control conditions evaluated had a cobalt release which was less than the detection limit of the instrument (5 ppb). The cobalt ion release from seeding the disc with macrophages was 11.2 ppb.

5.5.3.2 Study 2: Hip simulator evaluation of taper fluids

6 40 (+0) mm CoCr heads on Ti-6Al-4V trunnions were assembled and run on the orbital hip simulator for 160 000 cycles. 3 fluids were evaluated: $FeCl_3$ (n=2, pH 0.95), PBS [H+] (n=2, pH 1.67) and 25 % serum (n=2).

Prior to the impaction of the head on the trunnion, 0.5 ml of each fluid was injected into the head taper with a silicone isolation chamber already attached to the basal rim of the femoral head and the taper was mated in an inverted position. Subsequently, the head was impacted on the trunnion using a femoral impactor and hammer. The distal end of the silicone chamber was sealed by bolting onto the adaptable trunnion base. The isolation chamber was filled with approximately 5 ml of the same fluid in the taper so that 2 head taper-trunnion assemblies each had $FeCl_3$, PBS [H+] and 25 % serum (1 % w/v sodium azide) in and around the taper. All 6 assemblies were run using 500 ml of 25 % serum (1 % w/v sodium azide) as the bearing surface lubricant. The hip simulator was stopped after 100 000 cycles and 2 ml of fluid was taken out of the isolation chamber for ion analysis. This was replaced with approximately the same amount of fluid. The test was stopped after 160 000 cycles which constituted another time point for ion analysis using GFAAS (2.4.1).

5.5.3.2.1 Results

The concentration of fluids reported is the total concentration of taper fluid and surrounding chamber. Comparatively, when the $FeCl_3$ and PBS [H+] were used in the taper microenvironment on the hip simulator, the Co released was at least 2 orders of magnitude higher than the 25% serum and cell culture conditions. The difference between Co release in $FeCl_3$ and PBS [H+] was not statistically significant either at 100 000 cycles or the end of testing (Table 5-3).

Table 5-3 Cumulative Co concentration in taper microenvironment (mean ± stdev), † one of the two taper junctions with $FeCl_3$ underwent fatigue failure at 122 000 cycles

		Co concentration / ppb		
		$FeCl_3$	25 % serum	PBS[H+]
Number of cycles	100 000	10267 ± 14293	27.5 ± 0.07	2405 ± 40
	160 000	28832 ± 32113†	54.1 ± 0.49	43529 ±1249

Although confocal imaging showed that the cells had adhered to the disc (Figure 5-16), SEM images did not reveal etched features representative of a cell's morphology (Figure 5-17). Also, EDX analysis showed that on the polished surface, no Fe was detected. However, on the edges (not polished), Fe was detected in small amounts (Figure 5-17).

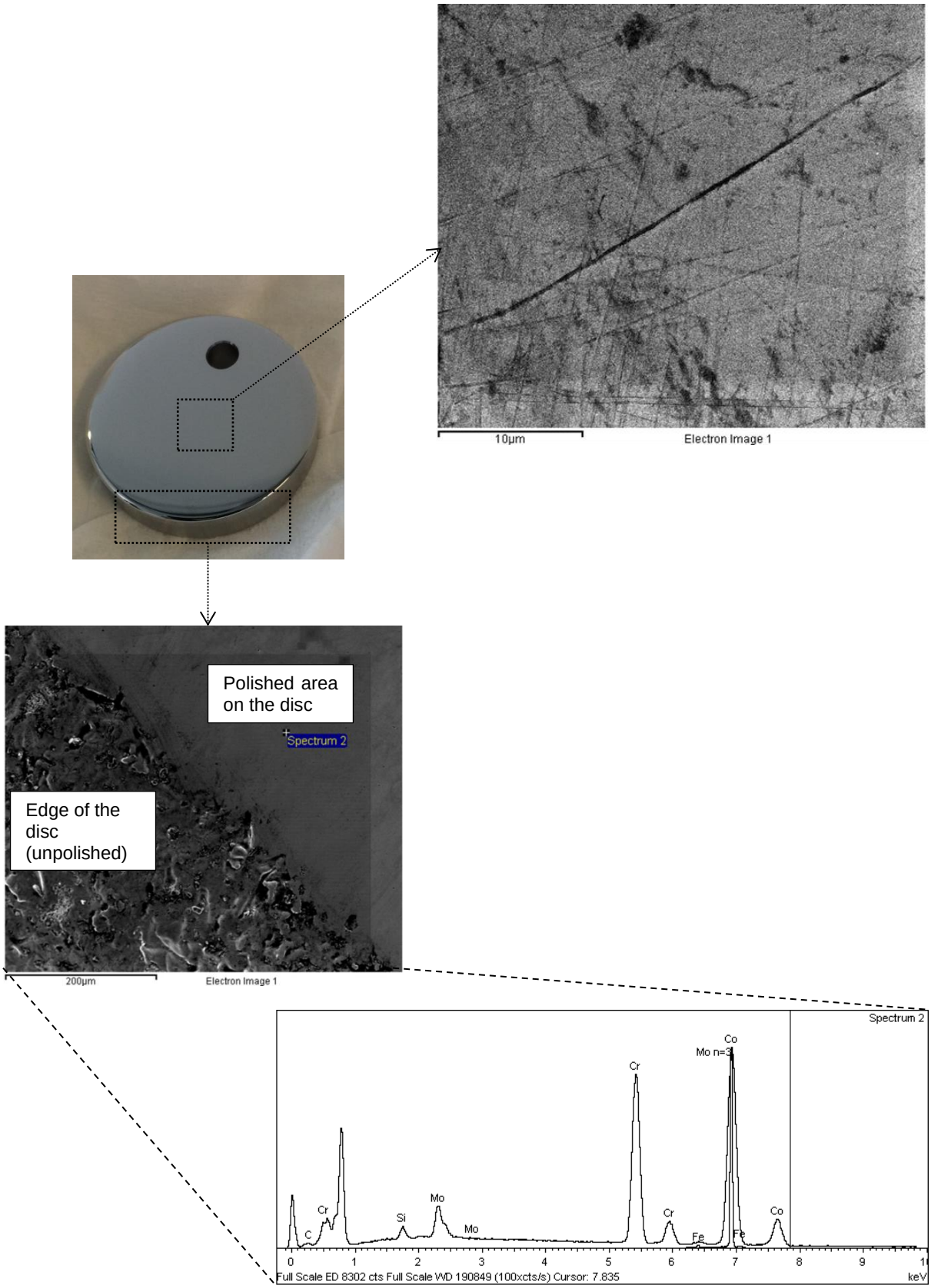

Figure 5-17 SEM images of CoCr disc after the end of the cell culture study and EDX analysis of the unpolished region showing small amounts of Fe

5.5.3.3 Discussion

The results from the cell culture study were comparable to a static dissolution study performed by Royle (2012) without the use of cells where the mean Co release in serum over 7 days was less than 10ppb. SEM analysis did not show signs of the cells' morphology etched onto the polished surface as reported by Gilbert et al. (2015b) and Cerquiglini et al. (2016). Gilbert and colleagues attributed the presence of Fe nodules on the retrieved devices to the cell corrosion process (Cerquiglini et al., 2016, Gilbert et al., 2015); although Fe was detected in small amounts in the unpolished region of the disc, it could be an artefact of the manufacturing process. The cobalt concentration released into the cell medium is considerably less than the taper and chamber fluid concentrations from the hip simulator evaluation. Further, since the report by Gilbert et al. (2015b), Aldinger and Pawar (2017) have attributed the supposed cell corrosion features to electrosurgery. Of the 3 fluids evaluated on the hip simulator, the highest concentration of Co ions around the taper microenvironment at the end of the test (160 000 cycles) was measured in acidified PBS.

5.6 Outcomes

It was concluded that the experimental evaluation should combine 2 contact conditions with 2 peak surface roughness values to yield 4 taper test conditions:

i. 5° head tapers with rough 5° trunnions (XER)

ii. 5° head tapers with smooth 5° trunnions (XES)

iii. 5° head tapers with rough 8° trunnions (XDR)

iv. 5° head tapers with smooth 8° trunnions (XDS)

Test samples evaluated subsequently, were identified with the suffix ER and ES for rough and smooth proximally contacting trunnions respectively and DR and DS for rough and smooth distally contacting trunnions respectively.

All taper assemblies will be tested in a fluid environment containing acidified PBS isolated in a silicone bellow designed with sampling ports to allow for the monitoring of ion release at time intervals.

Chapter 6. Experimental evaluation of ion release from taper junctions

6.1 Introduction

Corrosion mechanisms which may be initiated at the taper junction include galvanic, crevice, dissolution or mechanically assisted crevice corrosion (MACC) (Espallargas et al., 2015, Cooper et al., 2012a). The result is the release of ionic and particulate species; although it has been suggested that galvanic corrosion is not a primary mechanism for ion release in a taper junction with dissimilar metals (Levine et al., 2013).

The presence of metal ions is used in conjunction with other symptoms such as unexplained pain, a thickened pseudocapsule, bone marrow oedema, or muscular insufficiency to diagnose MACC of taper junctions (McGrory et al., 2017, Cooper et al., 2012a). Accordingly, a cobalt concentration of more than 1 ppb has been suggested as a threshold for confirming MACC along with a ratio of Co to Cr which is greater than 1 (McGrory et al., 2017). Although, Co and Cr concentrations can be used to indicate taper corrosion, the measures do not correctly predict the severity of MACC nor soft tissue destruction (McGrory et al., 2017). The release of Ti ions does not initiate aggressive reactions hence, it is not often clinically evaluated to evaluate taper corrosion (Cross et al., 2017).

There have been reports suggesting that taper junction design will influence the occurrence and observation of taper corrosion (Collier et al., 1992). Therefore, the measurement of metal ions released from the taper junction in a laboratory setting from different taper junction designs could identify susceptible designs prior to implantation. Also, the effect of variables of taper junction design on metal ion release could be evaluated. In

taper junctions with MoM bearings, the Co ions released from the taper junction were 2 orders of magnitude lower than the bearing (Pamu et al., 2012). However, such an evaluation has not been carried out on MoP devices which constitute over 50 % of primary THR devices implanted (National Joint Registry of England, 2016).

The aim of this study was to investigate the ion release from CoCr/Ti taper junctions on an orbital hip simulator with metal-on-polyethylene bearings. The use of the designed silicone chamber (Chapter 5) to encapsulate the junction ensured that the taper products were not influenced by release from the bearing surface.

6.2 Materials and Methods

6.2.1 Hip simulator testing

Prior to testing, all test components: CoCr femoral heads, HXLPE liners, Ti-6Al-4V acetabular shells and Ti-6Al-4V trunnion inserts were cleaned according to in ISO 14242-2 (2000). The silicone chamber was ultrasonicated in detergent and ultrapure distilled and deionised water whilst the adaptable taper bases were cleaned with detergent and ultrapure water. All components were dried using a jet of nitrogen gas.

17 taper assemblies were evaluated; the sample characteristics are given in Table 6-1; 2 head offsets were required to correctly locate the head centre to the centre of rotation of the hip simulator. In the assembly of the taper (Figure 6-3), the female taper was filled with 0.5 ml of acidified PBS (pH 1.7) hereafter referred to as the internal taper fluid. The taper was locked in an inverted position by hand by the application of pressure to the bottom surface of the adaptable taper base and the femoral head. Subsequently, the taper assembly was impacted with 5 standard blows using a hammer and femoral head impactor. The taper environment was isolated as described in Chapter 5, with the silicone chamber containing 5 ml of acidified PBS (pH 1.7). The fluid around the taper is hereafter referred to

as the external taper fluid. Half of the external taper fluid was sampled daily (on average every 70 000 cycles) and an equal volume of fresh PBS [H+] was replaced. As mentioned in 5.4.1 and 5.5.3, the very acidic saline was chosen because of increased susceptibility of CoCr to pH lower than 3; likewise the pH inside taper junctions has been reported to be as low as 1. Therefore, the pH used in the current test could create an aggressive taper environment since. The bearing surface was lubricated with 25 % bovine serum with sodium azide to prevent microbial contamination. The bearing lubricant was not changed throughout the duration of the test. To replenish the fluid lost due to evaporation, the bearing lubricant was topped up with ultrapure distilled and deionised water (resistivity, 18.0 MΩ.cm) every 8 hours.

Tests were run to 0.5 Mc except where the taper failed before this time point.

Table 6-1 Characteristics of samples evaluated on the hip simulator; Rough: Rz 16 + 3 µm, Smooth: Rz 6 + 3 µm, all heads were CoCr

Sample ID	Features		Contact condition	Femoral head offset
	Angle	Topography		
1ER	5°	Rough	Proximal	+0 mm
2ER				
3ER				
4ER				
5ER				
7ES		Smooth		
8ES				
1DR	8°	Rough	Distal	-4 mm
2DR				
3DR				
4DR				
5DR				
6DR				
1DS		Smooth		
3DS				
4DS				
7DS				

Figure 6-1 A smooth 5° trunnion and a smooth 8° trunnion

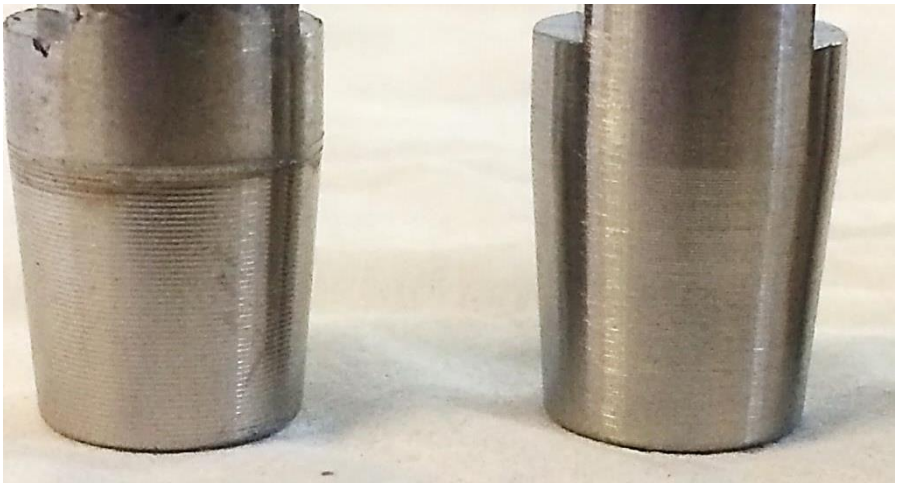

Figure 6-2 A rough 8° trunnion and a smooth 8° trunnion

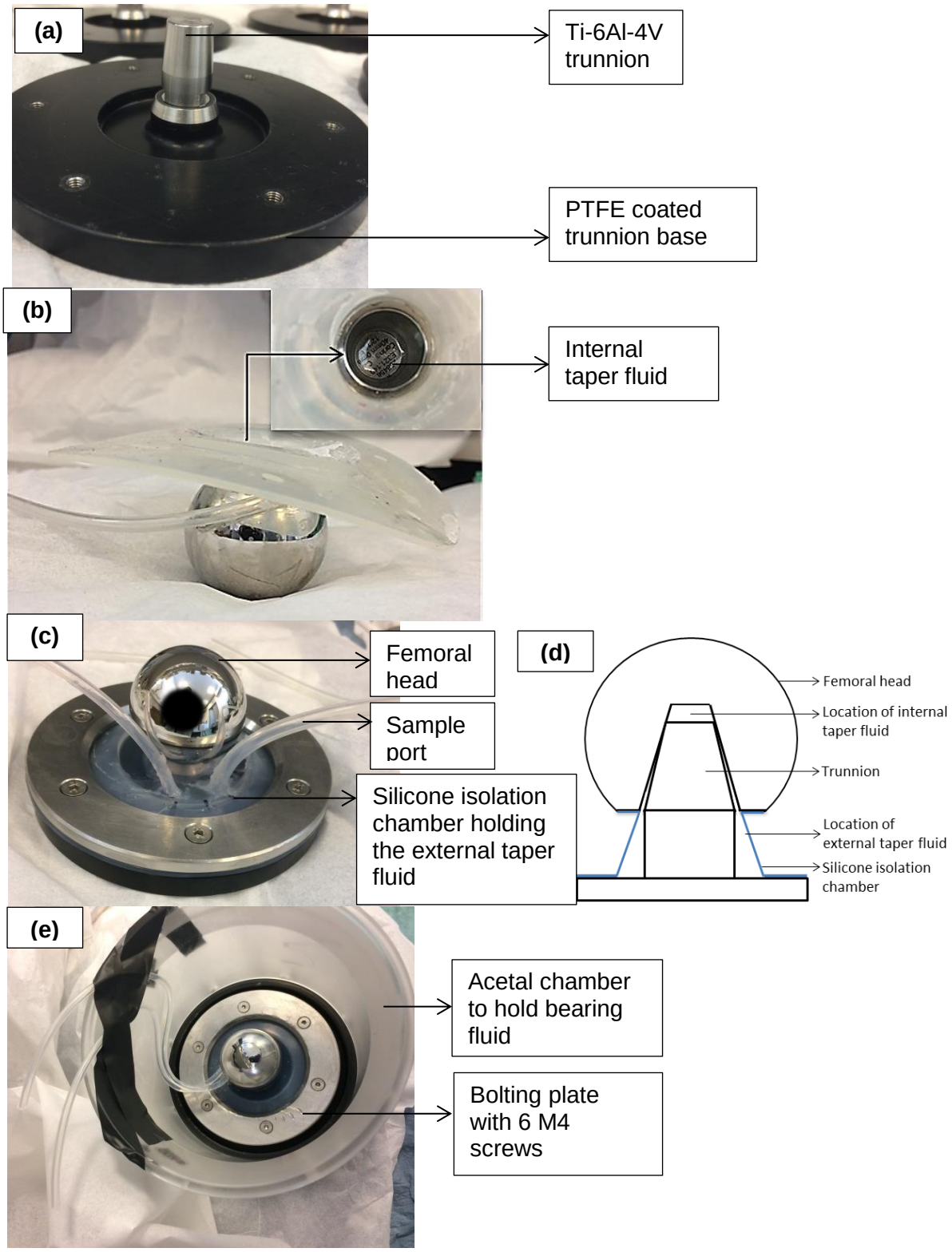

Figure 6-3 Assembly of taper prior to experimental evaluation (a) assembled trunnion insert and base, (b) inverted femoral head containing internal taper fluid, (c) head-trunnion assembly with silicone chamber for the external fluid (black circle drawn to block light reflection), (d)Schematic of (c), (e) Final assembly with acetal chamber for the bearing lubricant

6.2.2 Surface Analysis

6.2.2.1 Macroscopic imaging

A handheld USB microscope (VMS-004 Discovery Series 400x, Veho, Hampshire, UK) was used to image the male and female taper surfaces.

The taper surfaces were imaged after testing, prior to and after subjecting them to a cleaning protocol in ISO 14242-2 (2000) (see Appendix A.5). The components were subsequently imaged on the SEM.

6.2.2.2 Scanning electron microscopy of the male and female tapers

SEM (Inspect F, FEI, Eindhoven, NL) with energy dispersive X-ray analysis (EDX) (INCA Energy 350, Oxford Instruments, Oxfordshire, UK) was used to image the male and female taper surfaces and to identify elemental composition of features observed. An accelerating voltage of 20.0 keV was used and the working distance was set to 10 mm.

The heads were inverted to have a partial view of the female taper surface and to identify interesting surface features. This was achieved by placing a femoral head in a sample specimen cup (cylinder holder) in an inverted position and tilted at an angle to allow viewing of the surface of the head taper bore. Surface features on the trunnions were also imaged. Each trunnion was imaged by placing it horizontally on a carbon adhesive disc which was adhered to an SEM stub.

6.2.3 Metal ion measurement

The Co ions in the bearing lubricant (serum), isolation chamber environment and taper fluid as well as the Cr ions released into the isolation chamber environment and internal and external taper fluid were measured using graphite furnace atomic absorption spectrometry (GFAAS) (2.4.1) (SpectrAA 220FS atomic absorption spectrometer with a GTA-110

autosampler, Varian, Oxfordshire, UK). All GFAAS measurements were performed using pyrolytically coated graphite partition tubes (Agilent, California, US).

Metal concentrations were measured in the serum and internal taper fluid at the end of the test in addition to the external taper fluid samples taken at intervals described in 6.2.1.

6.2.4 Data Analysis

Statistical analysis was performed using a two-tailed student's t-test; significance was set at $p<0.05$.

6.3 Results

12 of the 17 samples tested on the hip simulator experienced fatigue failure (Table 6-2) at the left hand M6 thread before 0.5 Mc despite the incorporation of the undercut feature described in Chapter 5, Figure 5-13. 4 of the 5 samples which remained intact were 5° proximally contacting tapers. One 8° distally contacting taper was evaluated for more than 0.5 Mc; fatigue failure of this sample occurred after 0.8 Mc. On average the 5° tapers failed 100 000 cycles after the 8° tapers; however, the difference was not statistically significant ($p = 0.3$). When the contact conditions were disregarded, the smooth trunnions ($R_z = 6 + 3$ µm) failed significantly earlier than the rough trunnions ($R_z = 16 + 3$ µm) ($p < 0.001$).

Table 6-2 Details of trunnions run on the hip simulator including the test duration

Sample ID	Features		Contact condition	Test duration / cycles
	Angle	Topography		
1ER	5°	Rough	Proximal	511,925
2ER				511,925
3ER				511,925
4ER				512,628
5ER				326,852
7ES		Smooth		87,843
8ES				140,340
1DR	8°	Rough	Distal	232,721
2DR				214,204
3DR				775,485
4DR				297,772
5DR				307,906
6DR				246,909
1DS		Smooth		95,839
3DS				83,530
4DS				277,839
7DS				111,253

6.3.1 Macroscopic features

Following testing, it was observed that the 5° trunnion combinations showed more signs of damage than the 8° combinations. Macroscopically, corrosion was identified as discolouration of interfacing taper components or deposition of dark deposits at the taper interface. Some features were observed after the taper was disassembled including:

i. Discolouration or black deposits on femoral heads

ii. White deposits and burnishing marks on trunnions

Also, imprint of rough trunnions onto femoral heads was observed; where imprinting occurred on the femoral heads, it was used to confirm the proximal and distal engagement of the 5° and 8° combinations respectively (Figure 6-4). The engagement position of the 5° trunnions was inside the taper bore at approximately a third of the length (Figure 6-4a). In comparison, the distal trunnions showed that the position of taper engagement was at the entrance of the taper junction adjacent to the rim of the femoral head (Figure 6-4b)

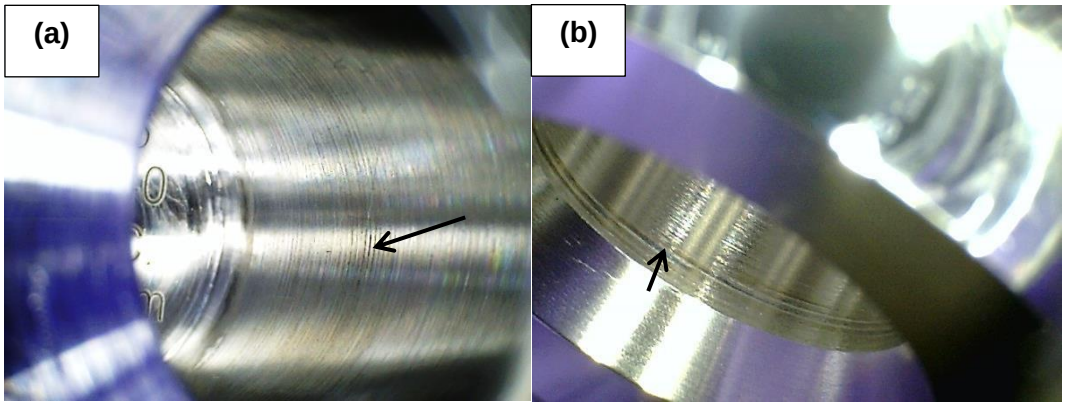

Figure 6-4 Taper engagement positon on (a) a head paired with a 5 ° trunnion in proximal contact and (b) a head paired with an 8 ° trunnion in distal contact

6.3.1.1 Corrosion features on femoral heads

The observation of black deposits on the femoral heads as well as discolouration was associated with the corrosion process. These features were most prominent in the region over which the trunnion engaged with the femoral heads. Where rough trunnions had been used, regardless of the location of contact (proximal or distal), the corrosion features were seen in the grooves created by imprinting of the trunnion onto the femoral head (Figure 6-4b). The occurrence of the black deposits was also seen in the fillet at the base of the femoral head taper bore (Figure 6-5 c and d). Imaging of the femoral heads after cleaning showed that the features persisted (Figure 6-5 e and f).

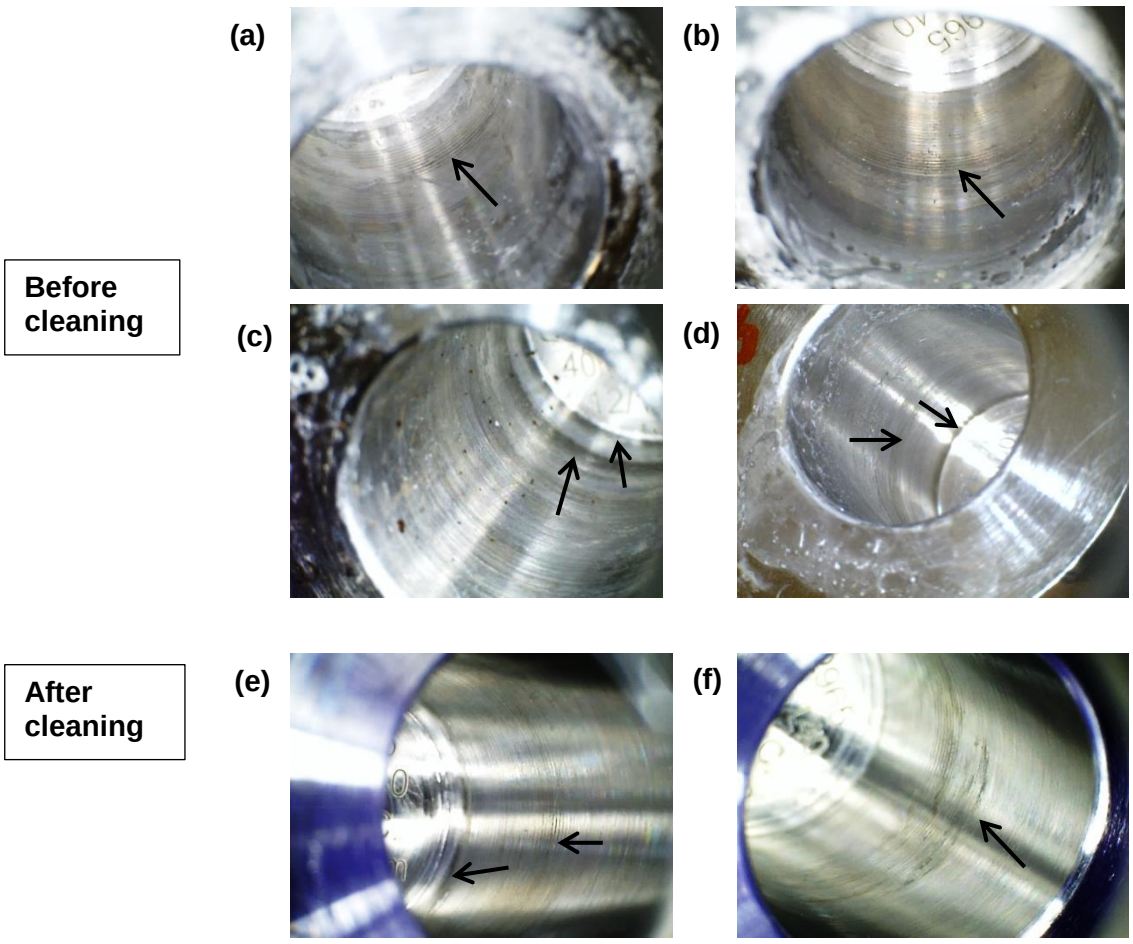

Figure 6-5 Corrosion features observed on femoral heads paired with rough trunnions (a and b) and smooth trunnions (c and d) prior to cleaning; figures e and f show the persistence of corrosion features after cleaning of components shown in a and b

6.3.1.2 Burnishing and white deposits on trunnions

Discolouration was also observed on the trunnions; these features were identified as burnishing marks. The burnishing marks were accompanied by white deposits on rough trunnions; these deposits were seemingly located in the grooves (Figure 6-6). Their location correlated with the position of taper engagement; hence, they were either located proximally on the 5° trunnions (Figure 6-6a) or distally on the 8° trunnions (Figure 6-6b). On the smooth trunnions, the white deposits occurred together with burnishing or alone (Figure 6-7). Also, it was observed that on the proximal tapers the location of the white deposits varied, with the furthest located at 8 mm from the top of the trunnion (Figure 6-8). This suggested a larger range of engagement positions than the distal tapers which consistently engaged at the most distal part of the trunnion which was also the widest. Further, subjecting the components to cleaning did not eliminate the white deposits.

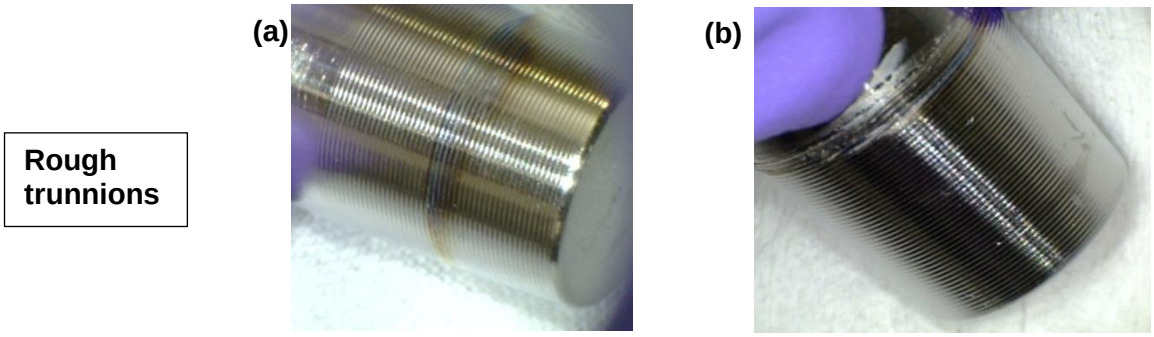

Figure 6-6 Discolouration and deposition of a whitish substance on (a) rough 5° trunnion (2ER) (b) rough 8° trunnion (3DR)

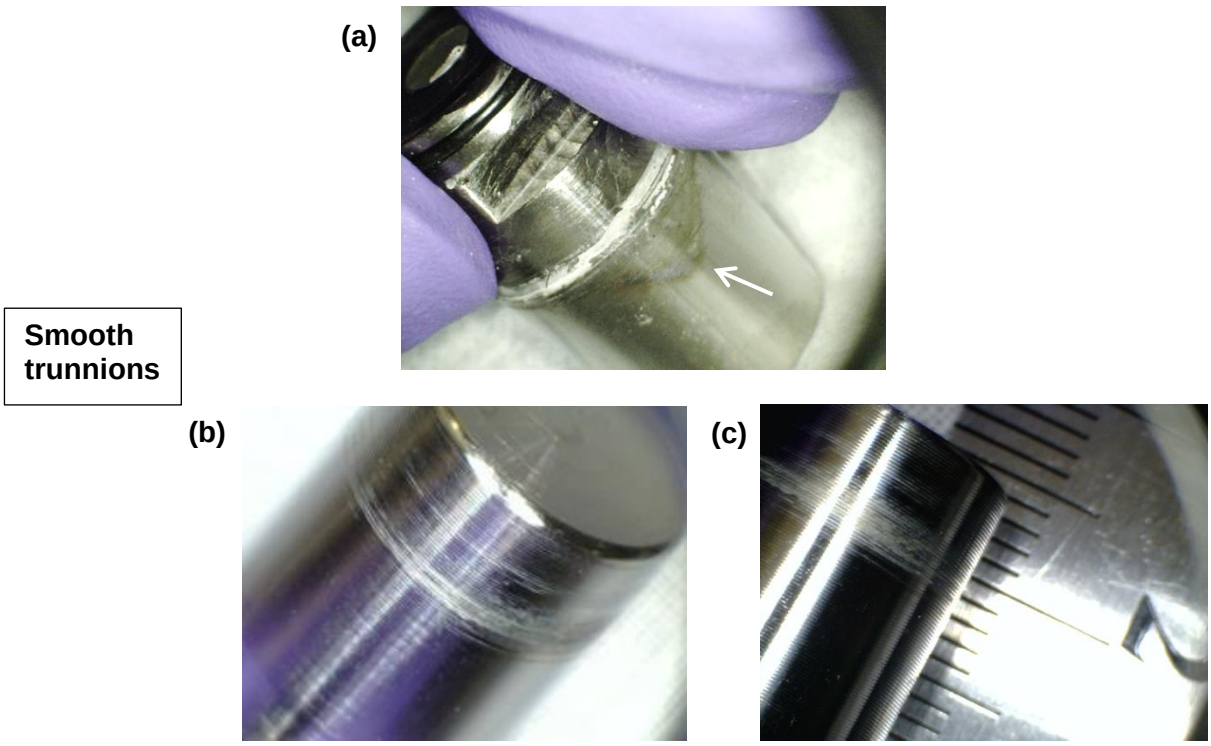

Figure 6-7 (a) Burnishing on a smooth 8° trunnion (7DS), white deposits seen on (b) a smooth 5° trunnion (6ES) prior to cleaning and (c) the same trunnion after cleaning

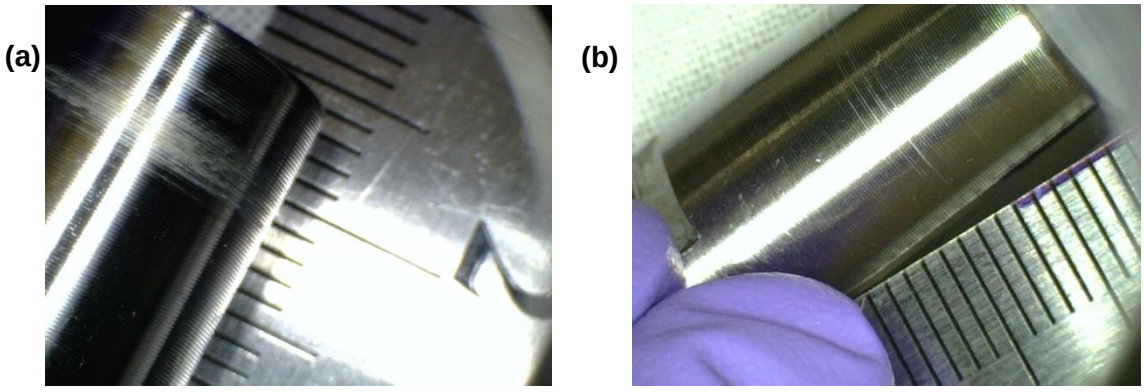

Figure 6-8 (a) a smooth 5° trunnion (6ES) with white deposits 5mm from the top (b) a smooth 5° trunnion (8ES) with white deposits 8 mm from the top

6.3.2 Microscopic evaluation

Imprinting of the rougher Ti alloy trunnion surface on the femoral head taper was clearly visible in the SEM images (Figure 6-9). Deformation of the peaks occurred in two ways where the peak was either inverted (Figure 6-10) or it was flattened (Figure 6-11); some trunnions showed both (Figure 6-10 and Figure 6-12). It was difficult to ascertain if the deformation occurred during taper impaction or disassembly.

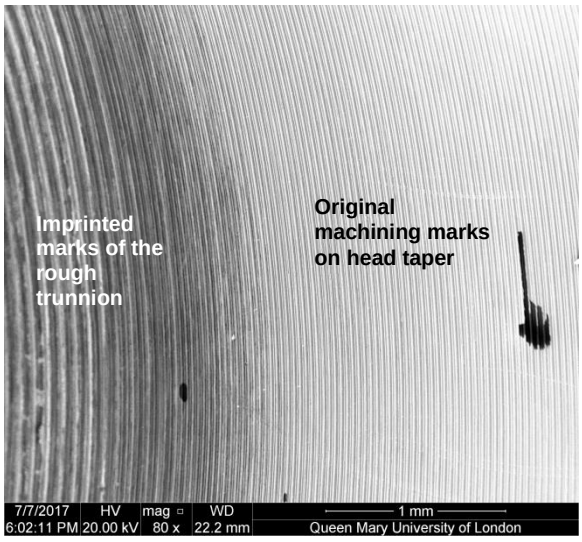

Figure 6-9 SEM image of a femoral head paired with a rough trunnion showing the original machining mark as well as the imprinting of the rough trunnion

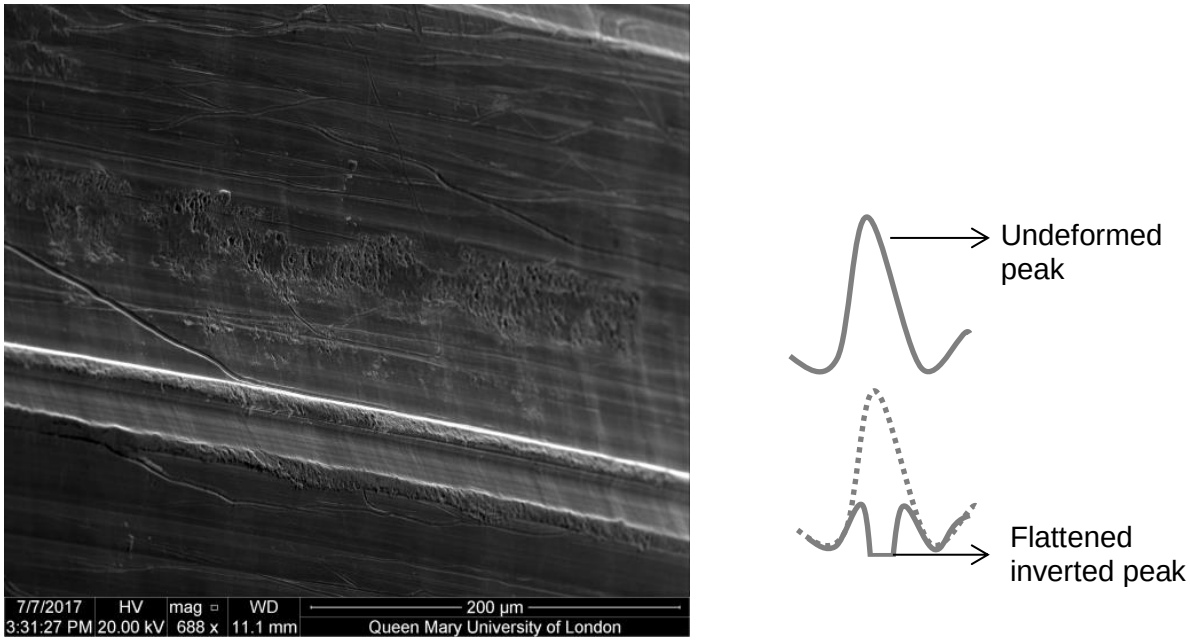

Figure 6-10 SEM image of inverted peak on a rough 8° trunnion (4DR) and schematic of feature

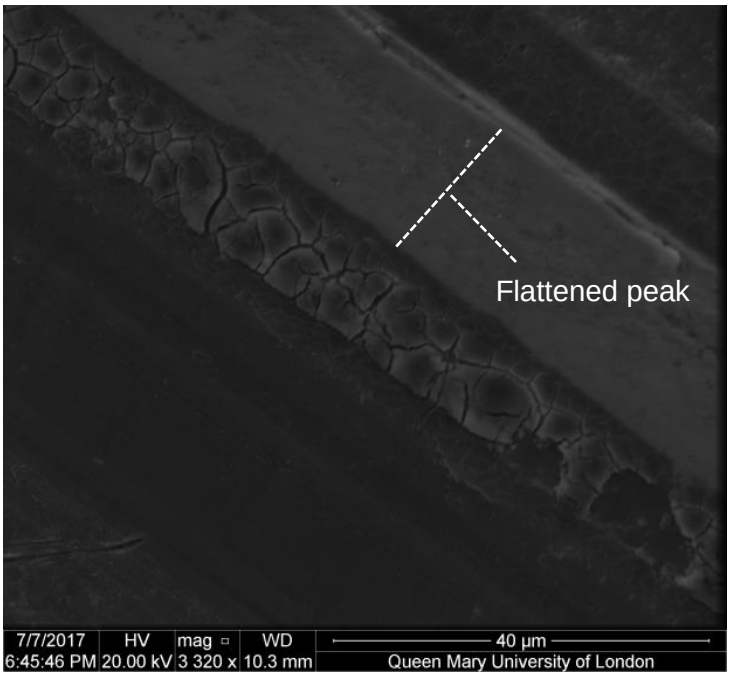

Figure 6-11 Flattened peak on a smooth 8° trunnion (7DS)

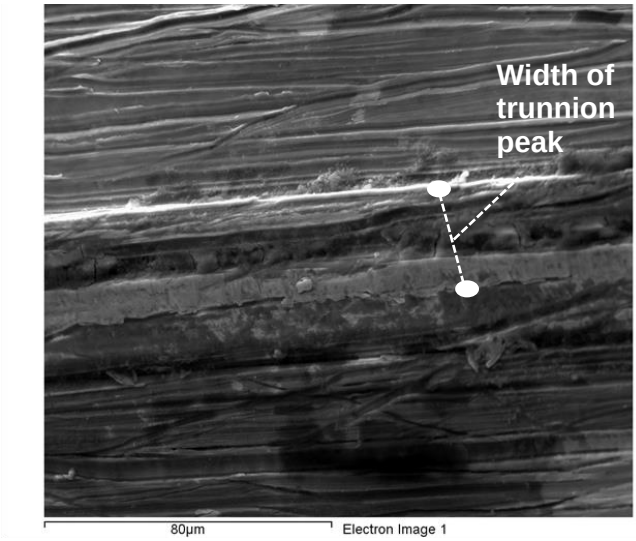

Figure 6-12 inverted peak with flattened features on a rough 5° trunnion (3ER)

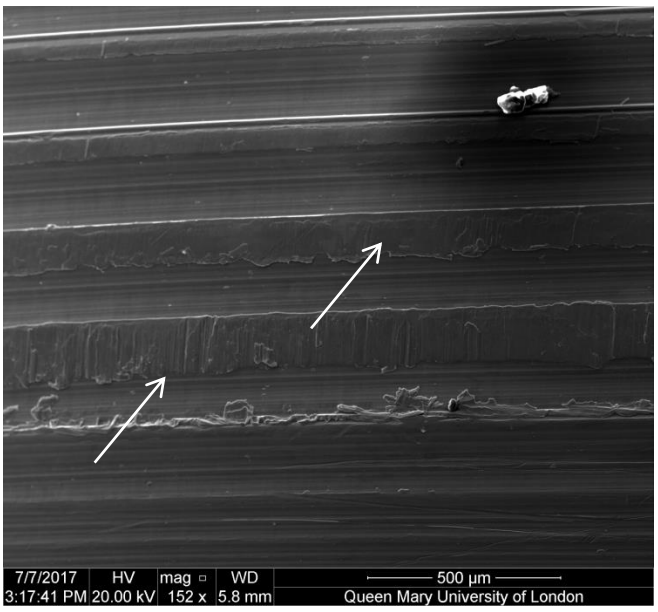

Figure 6-13 Flattened peaks on the trunnion shown in Figure 6-10

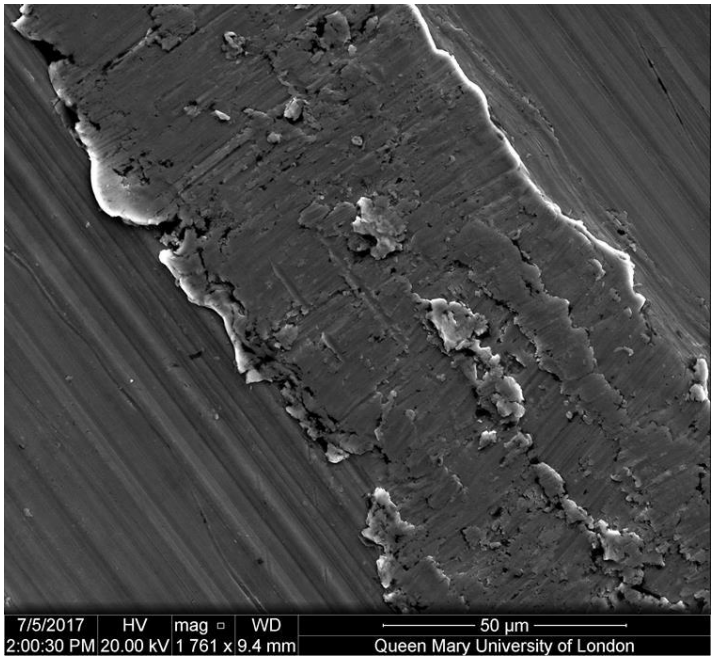

Figure 6-14 Flattened peak on a smooth 5° trunnion (8ES)

Material deposition was also observed regardless of trunnion angles and surface finish. The deposits were confined to the titanium alloy trunnions and were often found either side of peaks (Figure 6-15a and b) or between successive peaks (Figure 6-15c). Elemental mapping of the trunnions showed that the deposits were composed of Cr, P, O and occasionally K or Ca (Figure 6-16 and Figure 6-17).

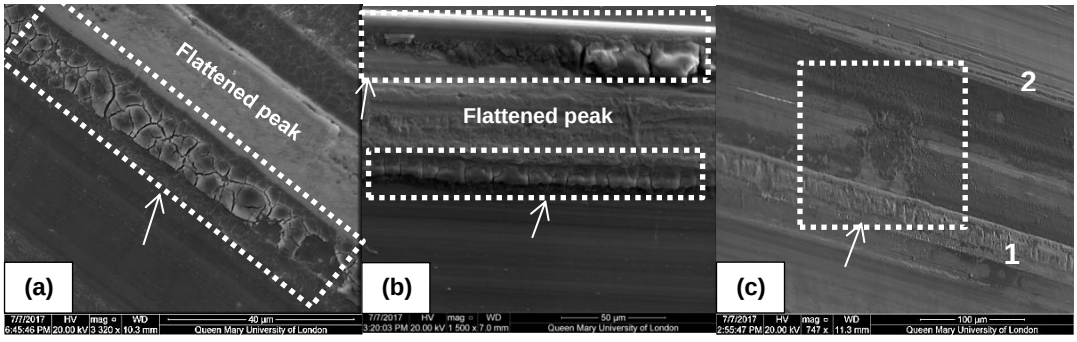

Figure 6-15 Deposits seen on trunnions tested (a) 7DS= smooth 8° trunnion, (b) 4DR = rough 8° trunnion, (c) 5DS= smooth 8° trunnion successive peaks (numbered on the image)

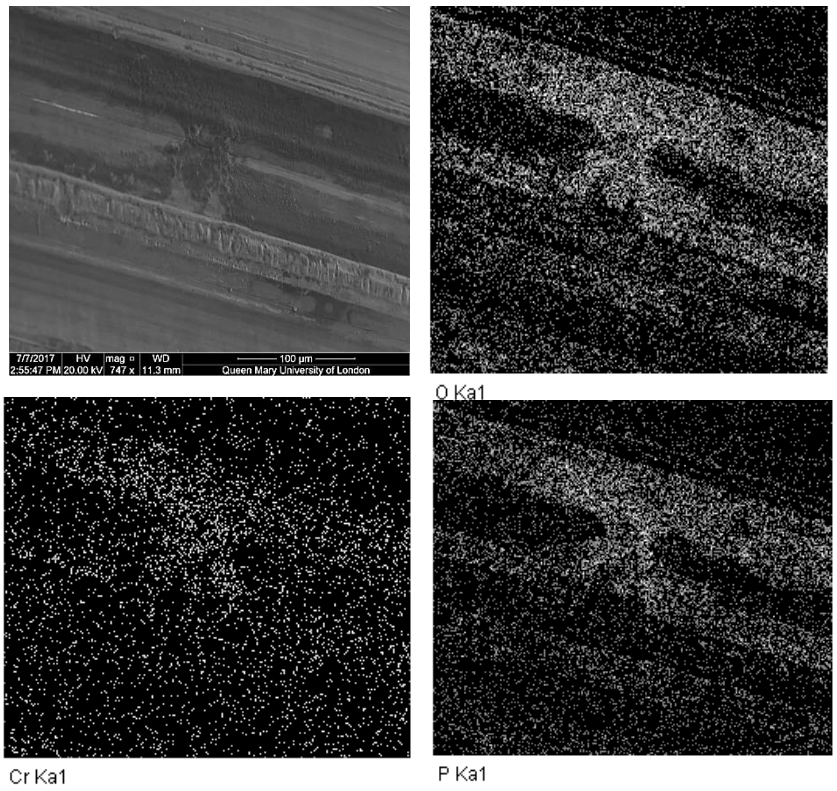

Figure 6-16 Elemental mapping of deposits on a smooth 8° distally contacting trunnion; sample ID - 5DS

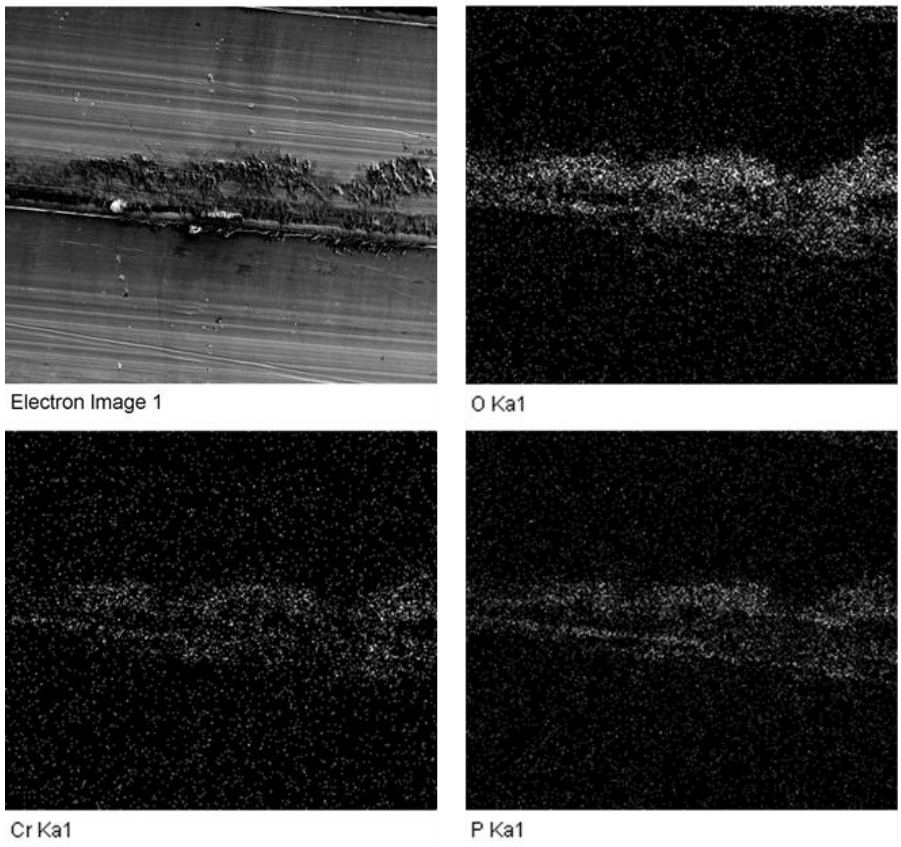

Figure 6-17 Elemental mapping of deposits on a rough 5° proximally contacting trunnion; sample ID - 1ER

Further, the SEM images revealed features suggestive of pitting on the trunnions; these features were located between successive ridges on trunnions with both smooth and rough surface finishes (Figure 6-18). These pit-like features were also observed on the femoral head tapers as well as fretting marks (Figure 6-19 and Figure 6-20). Fretting was identified as parallel marks along the taper axis. In addition, features indicative of etching were observed on the femoral head which was evaluated for the longest time period (0.8 Mc), wherein considerable surface damage was observed and machining marks were no longer visible at the entry of the taper junction distal to where the paired trunnion would have engaged (Figure 6-20). Finally, EDX analysis of an area on a femoral head where the trunnion is thought to have imprinted on the head taper, confirmed the transfer of Ti onto the femoral head (Figure 6-21).

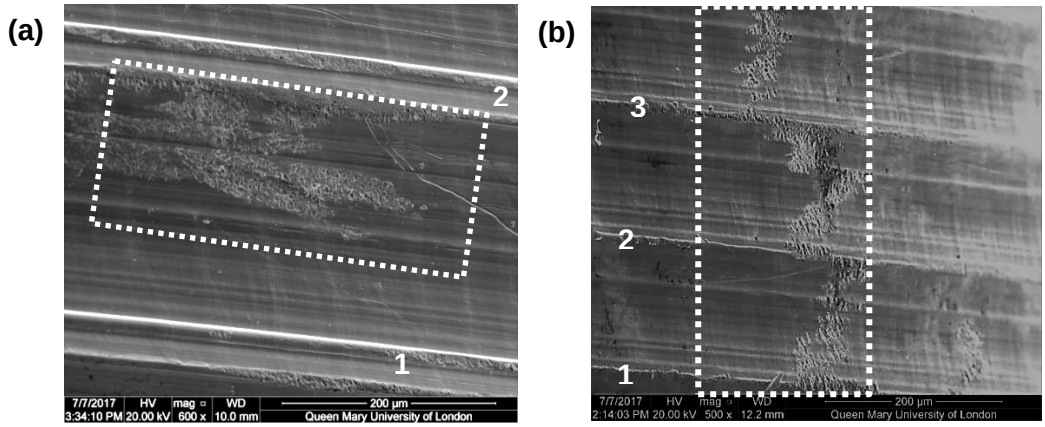

Figure 6-18 SEM images showing pits between successive peaks (numbered on the image) on (a) a rough trunnion (4DR) (b) a smooth trunnion (7DS)

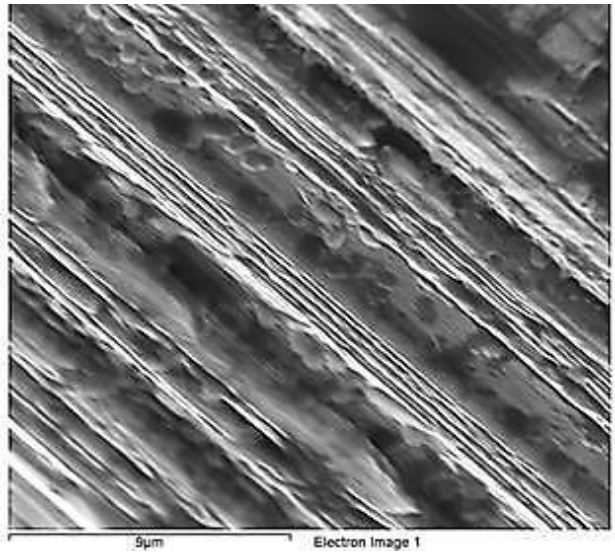

Figure 6-19 Pit-like features on a femoral head

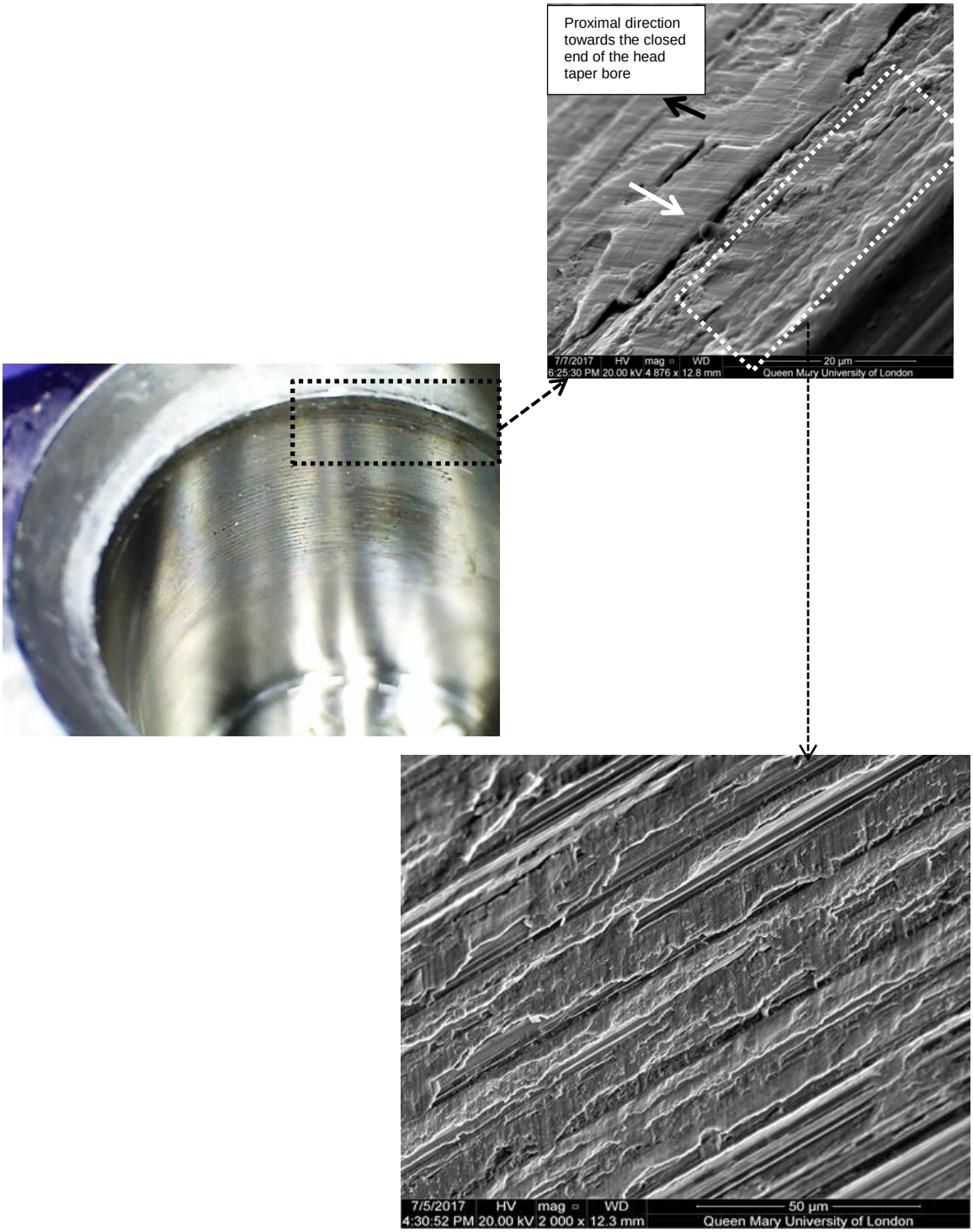

Figure 6-20 Fretting and surface damage on a femoral head; parallel marks along the taper axis suggestive of fretting (white arrow) and surface damage (rectangle) showing discontinuity in machining lines

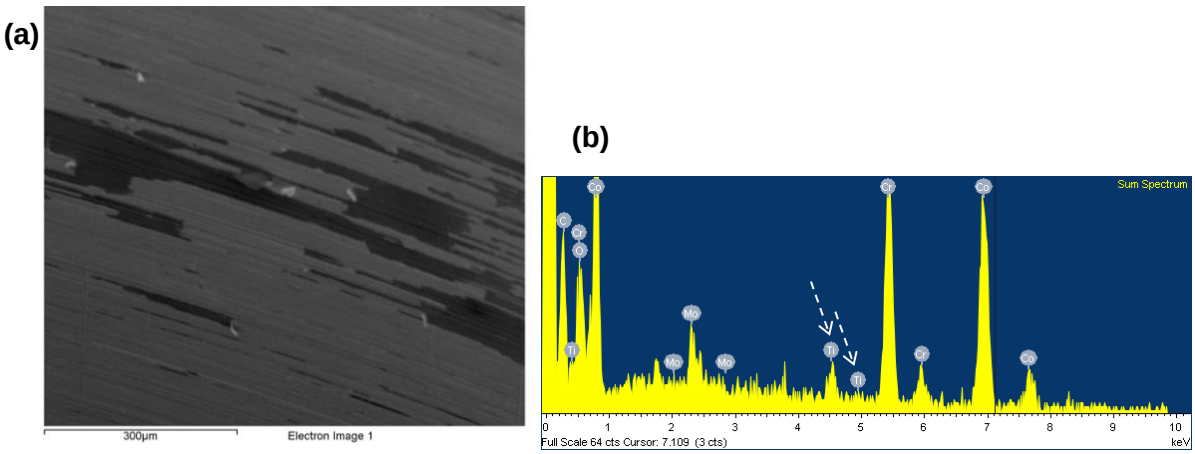

Figure 6-21 (a) SEM image of imprinted trunnion on the femoral head taper (b) EDX of the image in (a) confirming Ti transfer

6.3.3 Co and Cr ion release results

The ion release results were presented as cumulative values of Co and Cr release as well as an evaluation of the Co to Cr ratios (Co/Cr ratio). In presenting this, the ratio of the base alloy and a threshold value of 1 were highlighted. This threshold value represents the minimum value beyond which there is an elevation of Co over Cr; this is a feature thought to be indicative of a corroding taper (Plummer et al., 2016, Nodzo et al., 2017, McGrory et al., 2017).

6.3.3.1 Cumulative ion release in external taper fluids

The concentrations of ions measured on the GFAAS were corrected for serial dilutions due to fluid sampling. Sampling half of the fluid corresponded to a dilution factor of 2 and successive dilutions yielded a dilution factor of 2^n; where n was the number of times the initial fluid volume had been diluted (Appendix A.3).

Taking into account the gradient of the cumulative ion release profiles, the median Cr release rate into the external taper fluid for the proximally contacting tapers was 0.06295 (range: 0.0065 – 0.1306) ppb/cycle (Figure 6-22) and the median Co release rate 0.0118 (range: 0.0071 – 0.0648) ppb/cycle (Figure 6-23). Whereas, for distally contacting tapers, the median Cr release rate into the external taper fluid for the distally contacting tapers was 0.022 (range: 0.0005 – 0.0802) ppb/cycle (Figure 6-24) and the median Co release rate in the same set of tapers was 0.0109 (range: 0.0009 – 0.0331) ppb/cycle (Figure 6-25).

6.3.3.2 Proximal contact

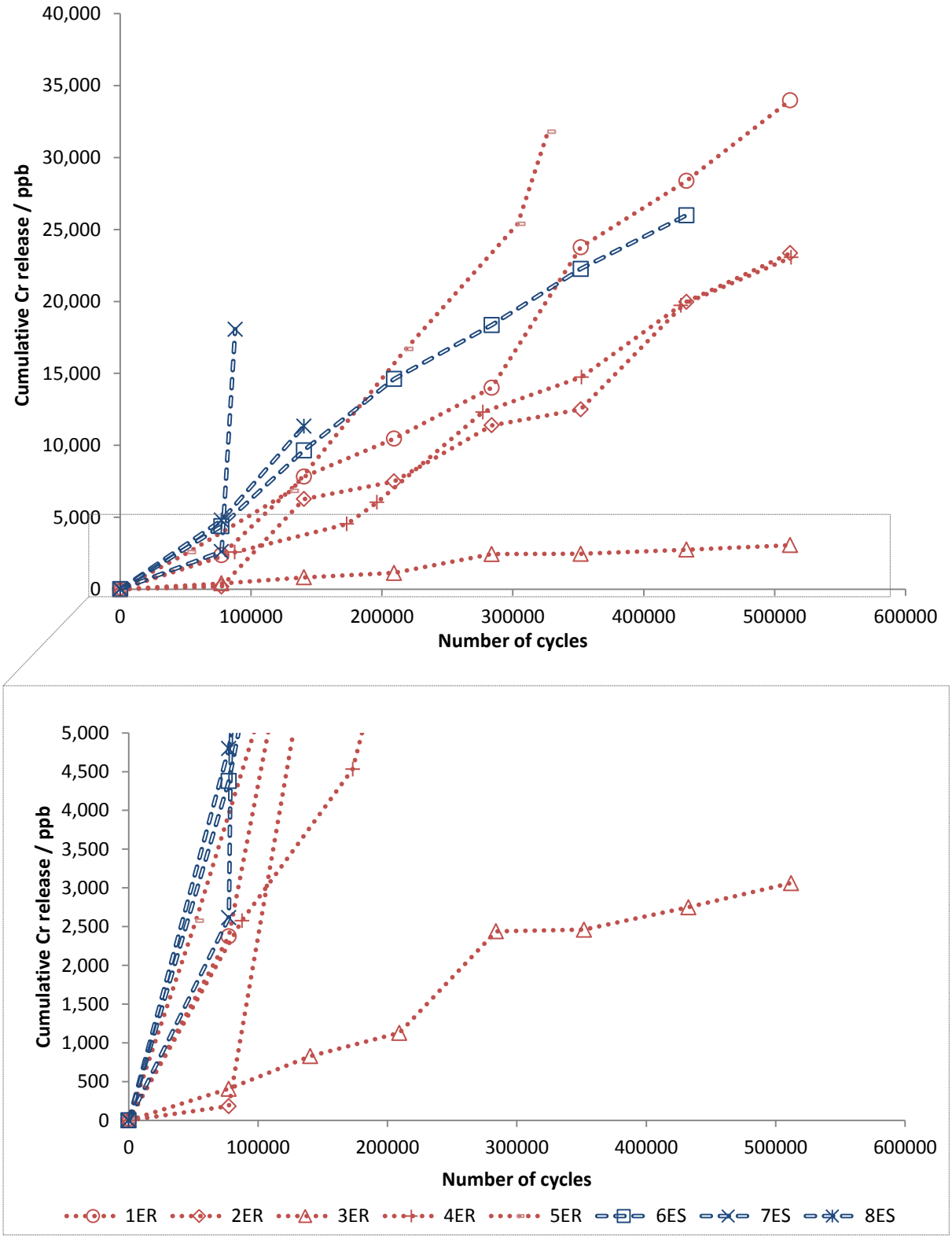

Figure 6-22 Cumulative Cr release in the external taper fluid for the 5° proximally contacting trunnions; R=rough, S=smooth

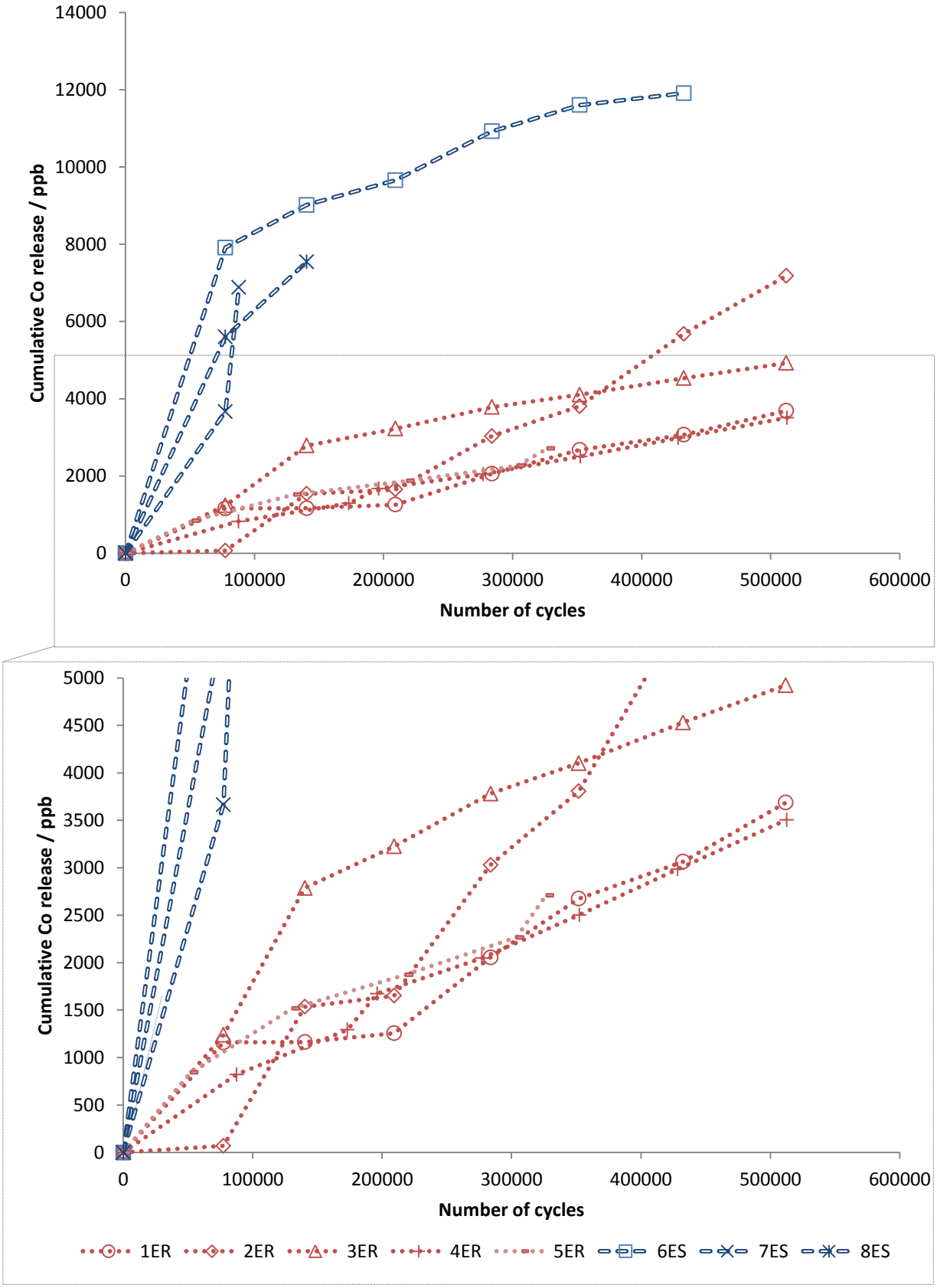

Figure 6-23 Cumulative Co release in the external taper fluid for the 5° proximally contacting trunnions; R=rough, S=smooth

6.3.3.3 Distal contact

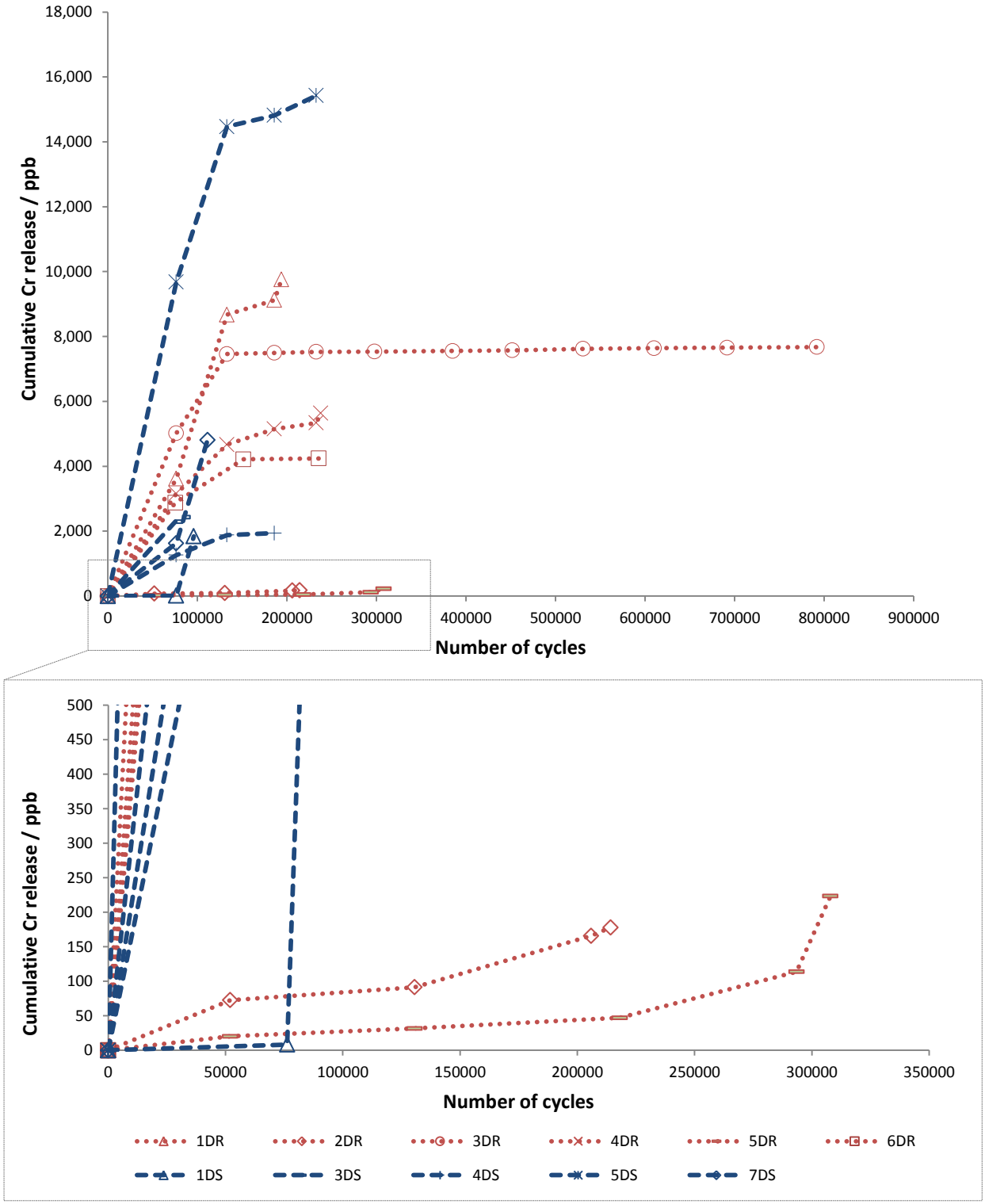

Figure 6-24 Cumulative Cr release in the external taper fluid for the 8° distally contacting trunnions; R=rough, S=smooth

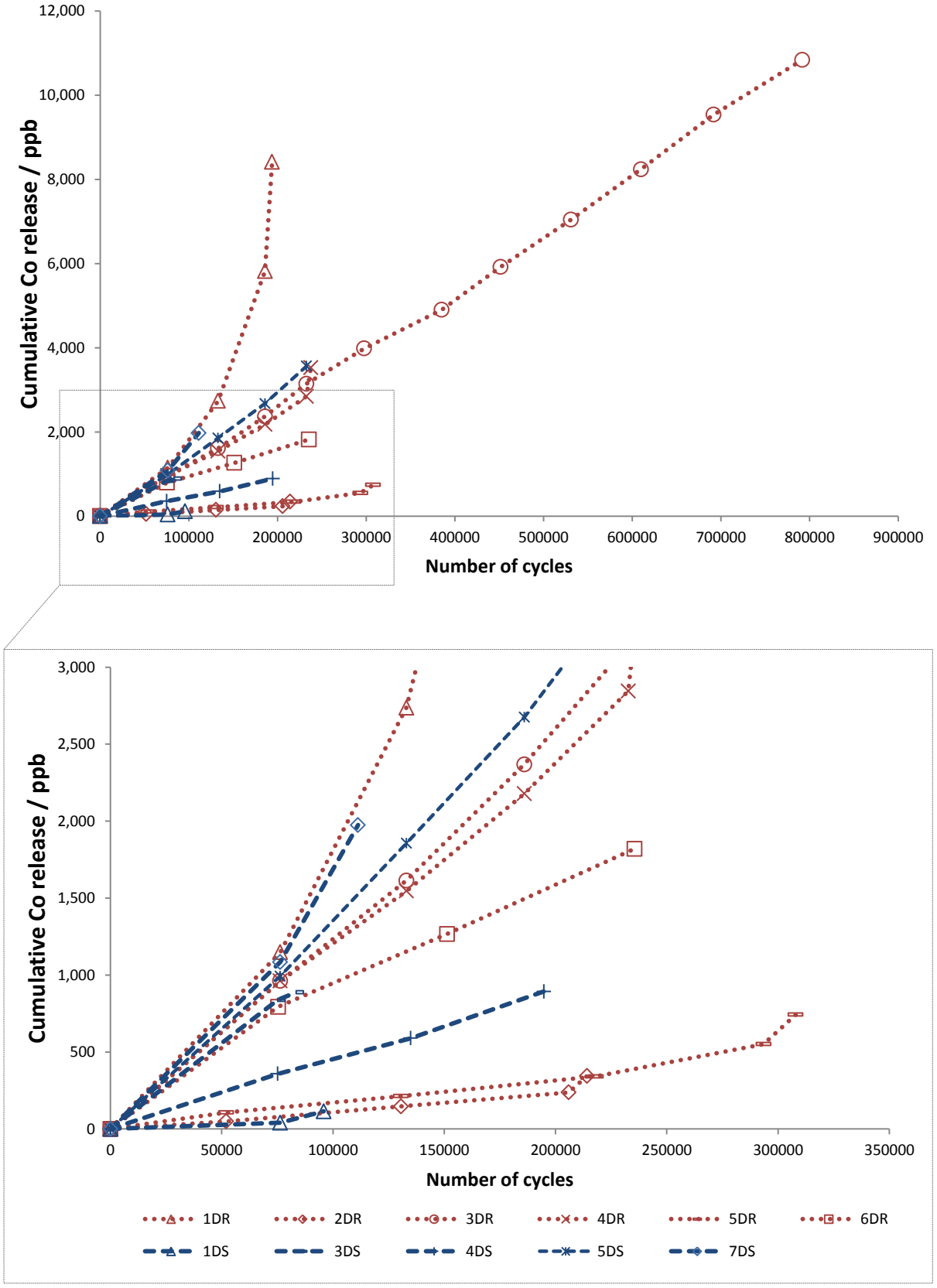

Figure 6-25 Cumulative Co release in the external taper fluid for the 8° distally contacting trunnions; R=rough, S=smooth

Trunnion 2ER with the highest cumulative Cr released was found to have black deposits in the samples taken from the external taper fluid (Figure 6-26).

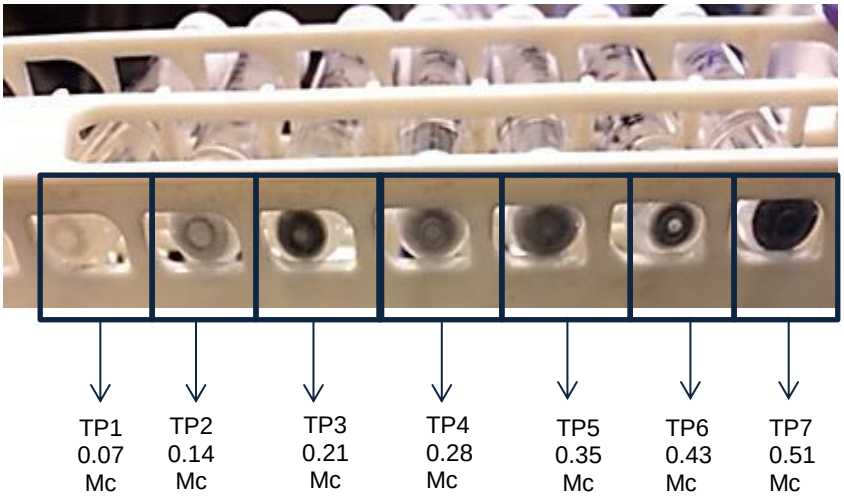

Figure 6-26 Fluid collected from the taper environment on samples 2ER with a rough 5 ° trunnion showing black deposits

6.3.3.4 Comparison of ion release in internal and external taper fluids and bearing lubricant

To compare across the different fluid volumes used in the current study, the concentrations were converted to volume of ions. A greater volume of Co than Cr was released into the head taper for both 5 and 8° trunnions. This was significant for both trunnion angles ($p<0.05$). Considering the effect of trunnion surface texture on the volume of Co and Cr released into the internal taper fluid, there was no statistically significant difference between the rough and smooth trunnions for both 5° proximal and 8° distal contact conditions (Figure 6-27). The increase in the volume of Co and Cr released in the internal taper fluid for the 8° trunnions relative to the 5° trunnion was attributed to the larger surface area of the head taper exposed to the taper fluid in the 8° trunnion combinations as compared to the 5° trunnions.

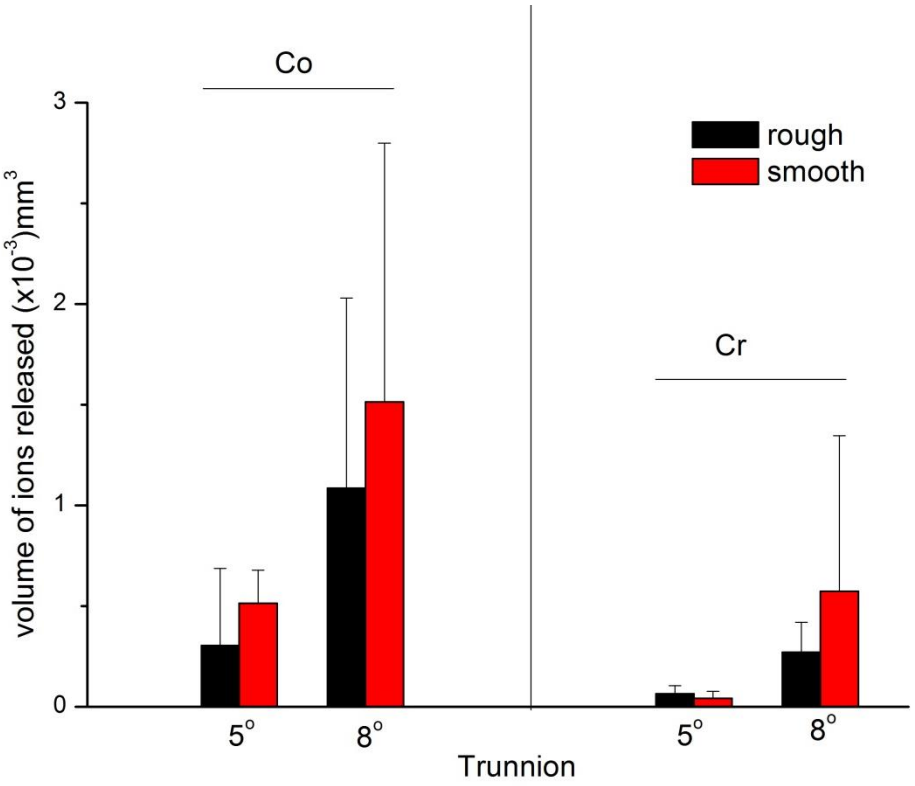

Figure 6-27 Volume of cobalt and chromium ions released in the internal taper fluid

The volume of cobalt released into the external taper fluid was greater than in the internal taper and bearing fluids in the 5° trunnion condition (Table 6-3). In comparison, the 8° trunnions showed higher cobalt release in the bearing relative to the external taper fluid; relative to the internal taper fluid, the bearing fluid had more cobalt for the rough trunnions but less cobalt for the smooth trunnions. The volume of Cr released into the external taper fluid was consistently higher than the internal taper fluid regardless of surface texture and trunnion angle (Table 6-3).

Table 6-3 Comparison of mean volume of ions released between the bearing fluid (at the end of the test), internal (at the end of the test) and external taper fluids (cumulative value)

	Volume of Co released (x 10^{-3}) mm^3					
	5°			8°		
	Internal taper fluid	External taper fluid	Bearing fluid	Internal taper fluid	External taper fluid	Bearing fluid
Rough	0.30	2.03	3.00	1.10	2.40	3.10
Smooth	0.51	2.77	2.40	1.50	0.84	1.70
	Volume of Cr released (x 10^{-3}) mm^3					
	5°			8°		
	Internal taper fluid	External taper fluid		Internal taper fluid	External taper fluid	
Rough	0.06	12.9		0.27	2.56	
Smooth	0.04	10.4		0.57	2.97	

6.3.3.5 Co/Cr ratios

The Co/Cr ratio varied in the external taper environment over the duration of testing in both proximal and distal taper contact conditions (Figure 6-28 and Figure 6-29). With respect to the distal (8°) tapers, the fluid samples evaluated were equally distributed between a ratio greater than 1 and less than 1 (Figure 6-29). In contrast, over the duration of hip simulator testing in the proximal contact (5°) condition, over 80 % of fluid samples evaluated had a Co/Cr ratio of 1 or lower (Figure 6-28).

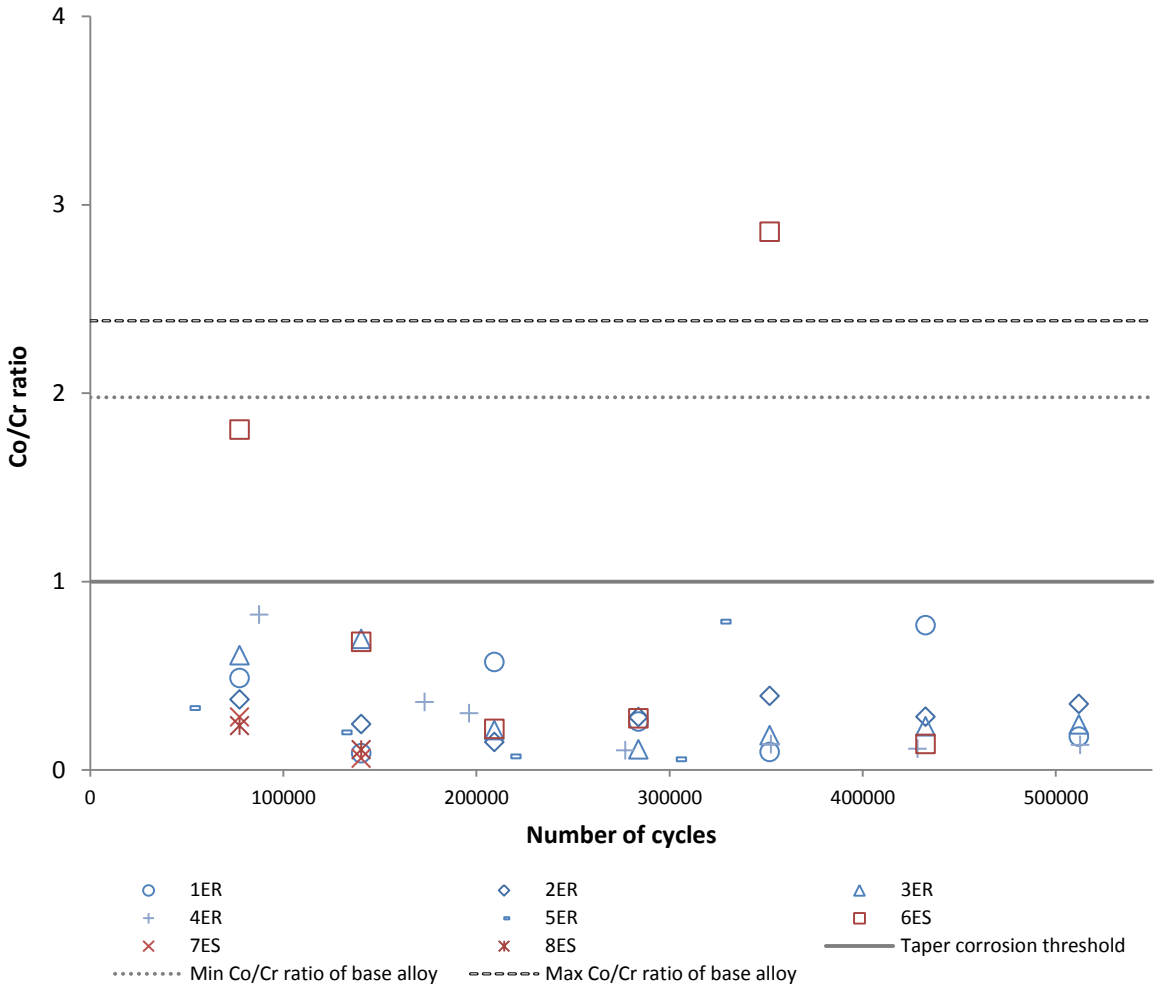

Figure 6-28 Variation of Co/Cr ratio in external taper fluid samples taking over the duration of testing in the hip simulator for proximally contacting 5° tapers; in figure legend, R represents rough trunnions, S represents smooth trunnions

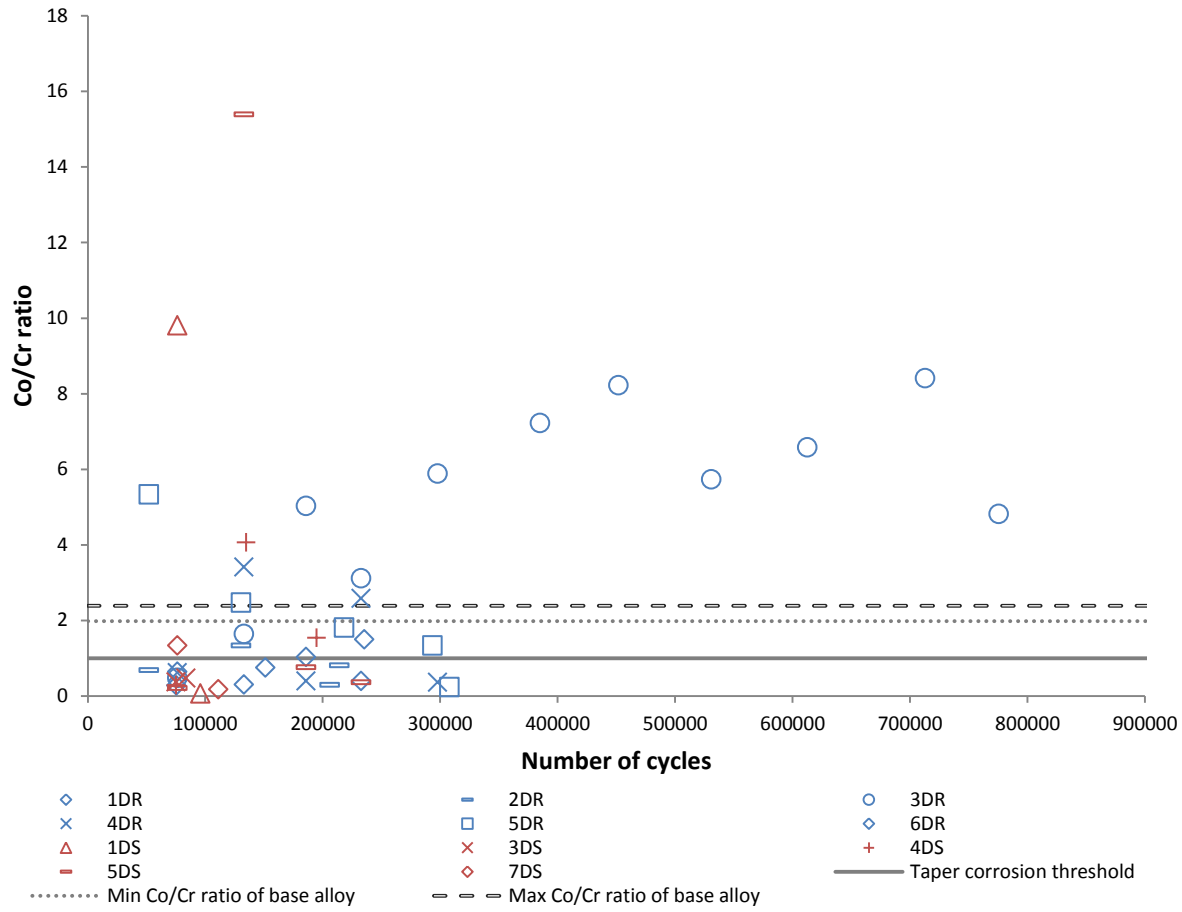

Figure 6-29 Variation of Co/Cr ratio in external taper fluid samples taking over the duration of testing in the hip simulator for distally contacting 8° tapers; in figure legend, R represents rough trunnions, S represents smooth trunnions

The surface topography of the trunnion had no significant effect ($p > 0.05$) on the ratio of Co to Cr measured (Figure 6-30).

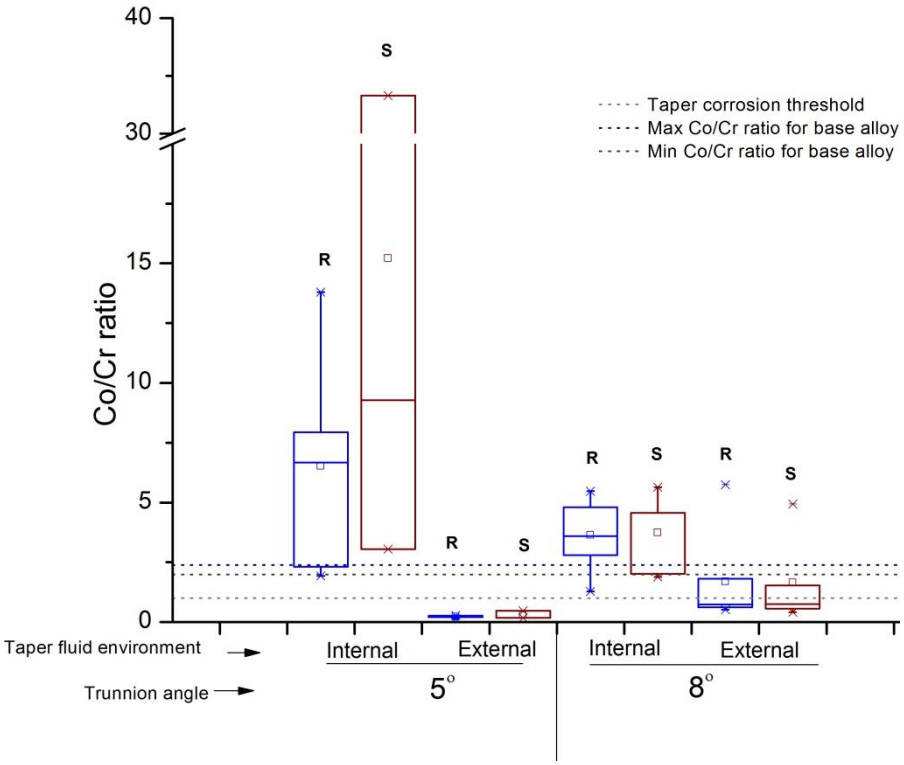

Figure 6-30 Effect of trunnion surface texture on the Co/Cr ratio; internal taper fluids represent samples collected after hip simulator testing and external taper fluid values are the median Co/Cr ratios across the sampling time points throughout the duration of testing

When the surface texture was disregarded and both smooth and rough trunnions were grouped together, the lowest mean ratio of cobalt to chromium was measured in the proximal external taper fluid. The mean value was less than the base alloy and the threshold value of 1. Comparatively, the mean ratio in the proximal internal taper fluid was the highest but also exhibited the largest variability. Considering the external taper fluids, the mean Co/Cr ratio was significantly higher around distal tapers than proximal; also, the mean value was greater than 1 but less than the ratio of Co to Cr in the base alloy. Regardless of the contact conditions, all internal taper fluid samples had a Co/Cr ratio greater than the base alloy (Figure 6-31).

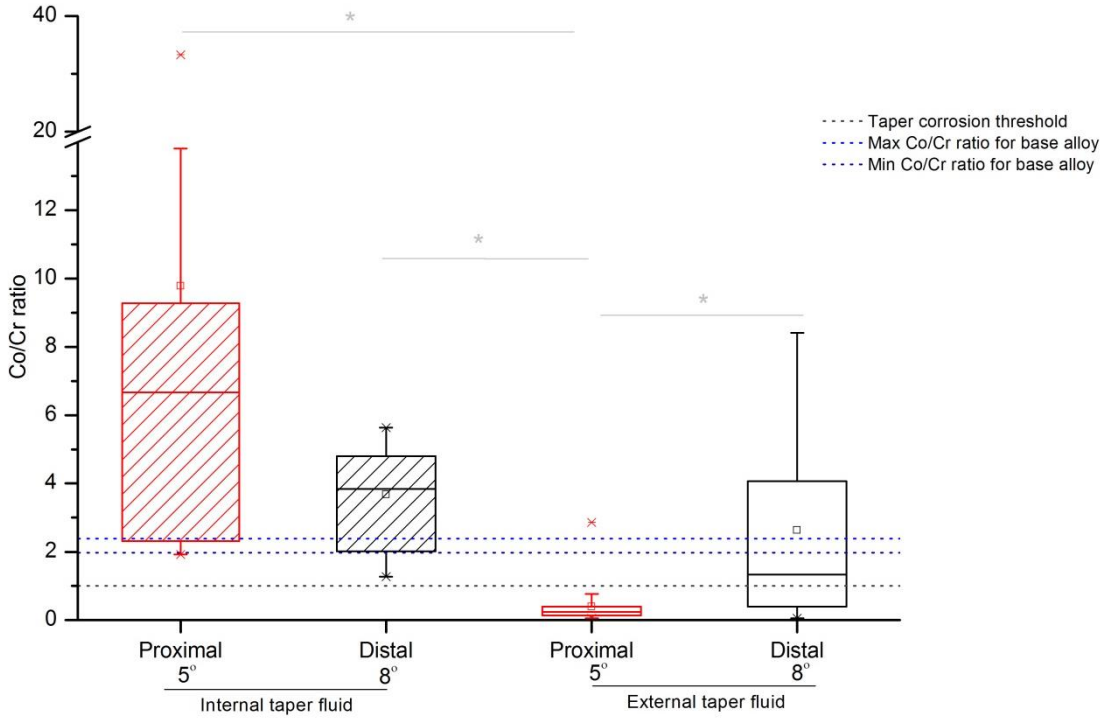

Figure 6-31 Graph showing Co/Cr ratio for the internal and external taper fluids on both proximal and distal contact conditions (rough and smooth) (* p<0.05) with annotated values for the Co/Cr of the base alloy for the femoral heads and reported clinical threshold for corroding taper

6.4 Discussion

This study is the first to evaluate the ions released from taper junctions utilising MoP articulations on a hip simulator. The effects of trunnion surface topography, location of taper contact and the location of taper fluid (internal or external) on Co and Cr release were also analysed.

Despite the short tests conducted significant amounts of Co and Cr were released around the fluid surrounding the taper. Previously in the literature, much longer periods have been reported; Li et al. (2015) reported corrosion features after 45 Mc. The taper junctions experienced fretting on the hip simulator and the use of saline with a low pH appeared to have resulted in etching and pitting of the surfaces although the etching was only observed in the longest running sample (3DR). These features have been observed in explants (Figure 6-32).

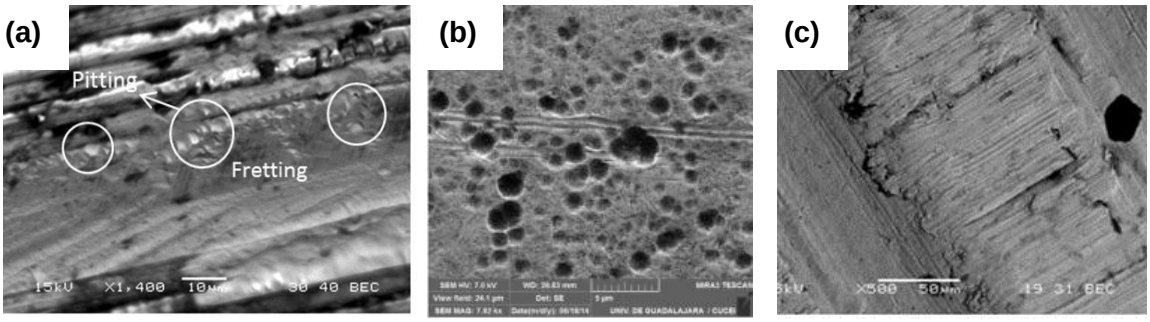

Figure 6-32 Images of some corrosion features reported in the literature (a) Pitting and fretting on a femoral head (Kocagöz et al., 2013) (b) Pitting in retrievals of corroded surface of CoCr alloy (Alemón et al., 2015) (c) Fretting damage on a Ti-6Al-4V taper (Kurtz et al., 2013)

In addition to visual features, the detection of a combination of chemical compounds has been used to confirm the occurrence of corrosion (Munir et al., 2016). The occurrence of Cr, P and O as indicated in the elemental mapping analysis of the deposits found on the trunnions, could be associated with $CrPO_4$ which has been reported to be a particulate corrosion product. However, when it is observed around corroded tapers, it is seen as green deposits (Urban et al., 1994, Jacobs et al., 1998). Green deposits were not observed on any

of the components evaluated on the hip simulator. This may be because chromium phosphate is soluble in acids which would prevent precipitation.

The observation of white deposits was associated with the formation of TiO_2. Willert et al. (1996) report white deposits thought to be titanium corrosion deposits. EDX analysis could not be used to confirm the compound because if $CrPO_4$ was indeed present, it would result in a conflict in identifying the source of the oxygen. The presence of the white deposits was restricted to the suspected engagement position of the tapers; this reinforces that the hip simulator motion is able to generate fretting at the taper junction because the compound is formed in response to cyclic motion (Munir et al., 2016). Further, EDX spectrum of a feature suspected to be imprints conferred by a rough titanium trunnion on a femoral head in Figure 6-21a showed Ti peaks; this reinforced the report by Moharrami et al. (2013) that the softer Titanium alloy is able to abrade the CoCr alloy because its oxide is harder than the oxide of CoCr.

6.4.1 Comparison of internal taper, external taper and bearing fluids

In acidic conditions, Cr is preferentially released; Dufils et al. (2015) showed that relative to neutral conditions (pH 7.6), the concentration of Co released increased by 2 folds in acidic conditions (pH 4.5) whilst Cr release quadrupled thus reducing the Co/Cr ratio from 4.5 to 1.8. The cumulative ion release results (Figure 6-22 - Figure 6-25) show that Cr was indeed released at an increased rate relative to Co for both proximal and distal contact conditions; the median Cr release rate for proximal trunnions was 5 times more, whilst median Cr release rate was 2 times that of Co for distal trunnions.

The current work showed that the volume of cobalt released from the taper in an acidic environment could be more than the bearing surface (Table 6-3). This is in contrast to the result obtained by Pamu et al. (2012) which showed that the volume of ions released into the

LHMoM bearing lubricant was at least 24 times greater than the volume of ions from the taper after 2 Mc of hip simulator testing. The volume of Cr in the bearing lubricant was not measured because the fluid was in contact with stainless steel fixtures that may have been sources of Cr release. However, these fixtures were not in contact with the taper fluids.

The volume of Co released in the internal taper fluid was less than the external taper fluid with the exception of the smooth 8° trunnions (Table 6-3). Replenishing the external taper fluid following sampling would have increased the oxygen content whereas the internal taper fluid would not have this renewed oxygen. However, the distally contacting tapers also had the fluid replenished but the trend was not observed for the smooth 8° trunnions which had less cobalt in the external taper fluid than internal. Although it is possible that the volume of Co could have been higher, but failure of the isolation chamber released some of the cobalt volume in the external taper fluid into the bearing surface lubricant. However, this would have been restricted to the last time point and would suggest that the smooth 8° trunnions were particularly more susceptible to this; it is not certain why this would have been. The effect of oxygen is also apparent in the observation of elevated volume of Cr released in the external taper fluid as compared to the internal taper fluid. It is likely that as the acidic environment was encouraging the breakdown of the Cr_2O_3 passive layer, the presence of oxygen continuously facilitated attempts at repassivation. However, the persistent acidity would act to continuously breakdown the reformed layer thus increasing the chromium measured.

The considerably elevated level of Cr in the external taper fluid of the proximal tapers relative to the distal tapers may have occurred due to the presence of a crevice in the former. In the proximal contact condition, the engagement position was approximately 5 mm from the top of the trunnion (although it was 8 mm on sample 8ES). Consequently, for a 13.5 mm long trunnion, a 9 mm crevice extends from the position of taper engagement to the

opening of the taper junction (Figure 6-33). Therefore, fluid ingress into the crevice may have occurred and the movement of the agitation of the external taper fluid due to the hip simulator motion would facilitate mixing of the highly concentrated crevice fluid with the external taper fluid. It is known that mass transport facilitates the corrosion process (Shreir, 1976). Conversely, the 8° trunnions engaged at the opening of the taper junction thus preventing the formation of any crevices at the junction (Figure 6-33). This suggestion is reinforced by the observation by Grostefon and Nelson (2017) that ingress into a crevice-like environment is crucial to a corroding taper. The implication of this result is to infer that in evaluating the performance of a taper junction as it relates to corrosion and ion release, Cr should be the distinguishing factor. Crucially, a distally contacting taper construct might open up to allow fluid ingress under other activities of daily living such as stair climb where toggling could occur. However stair climb was not evaluated in the current experimental study.

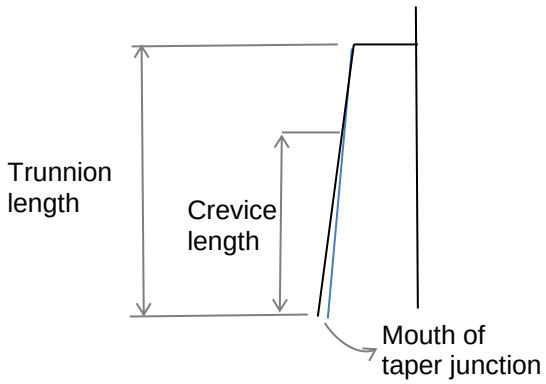

Figure 6-33 Crevice length relative to trunnion length in proximal taper contact

In evaluating the ion release from the taper junction, the experiment was run at room temperature. The human body maintains a steady temperature of 37°C and temperatures greater than 42 °C have been measured during gait (Kung et al., 2015). Corrosion rates have been reported to increase at elevated temperatures (Fontana, 2005). However, a large part of a THR is metallic (at least the femoral stem) which is able to dissipate heat and the

use of a constant elevated temperature in the current study, could have overestimated the effect of temperature (Kung et al., 2015).

6.4.2 Co/Cr ratios

The results from the current study showed that there was a marked increase in the release of Cr over Co in samples where crevice corrosion was suspected to have been occurring. This is in apparent contradiction with reports of a disproportionate elevation of Co over Cr in taper corrosion (McGrory and McKenney, 2016). However, the conclusions or trend associated with Co/Cr ratio is not consistent. *In vivo* samples from patients with hip resurfacing and total hip replacements have shown to have Co/Cr ratios less than and greater than 1 from bearing surface. Comparatively, hip simulator studies of MoM bearings have reported Co/Cr ratio between 2.2 and 3.1 (Royle, 2012). In an analysis of MoM and resurfacing explants, severely corroded tapers from MoM devices, showed the highest median Co/Cr ratio of 1.86 when whole blood samples were evaluated, although the resurfacing devices which have no tapers also had Co/Cr greater than 1 as did THR devices with corrosion scores of 2 and 3; although they were all significantly lower than the taper with severe corrosion (Hothi et al., 2016a).

Although, all conditions evaluated were exposed to the same acidic fluid, the mean Co/Cr ratio was greater than 1 for the internal taper fluids in both the 5° proximal and 8° distal taper contact conditions and the external taper fluid for the distal 8° taper (Figure 6-30). Further, relative to the percentage of constituent elements that make up the femoral head (Table 6-4), the Co to Cr ratio of the bulk alloy should range between 1.9 and 2.4. Therefore, the proportion of Cr released into the external taper fluid is higher than the bulk alloy at lower pH for 5° proximal tapers. It may be suggested that the same mechanism is occurring for all 3 conditions where the mean Co/Cr ratio is greater than 1.

Table 6-4 Chemical composition of femoral heads tested; data supplied by Corin Group plc

Element	Cr	Mo	Fe	Mn	Si	C	Ni	N	Co
Composition (%)	27.0 – 30.0	5.0 – 7.0	0.75 max	1.0 max	1.0 max	0.14 max	0.5 max	0.25 max	Balance

A suggestion that different mechanisms give rise to different Co/Cr ratios has been reported in the literature. Sidaginamale et al. (2016) showed that the size of debris resulted in a variation of median Co/Cr ratio between 0.4 and 3. However, the mean Co/Cr ratio of the internal taper fluids is significantly greater than the Co/Cr ratio of the external taper fluid of the 8° distal taper. This may have been modulated by the oxygen availability; an acidic environment would result in an unstable oxide layer which is eventually broken down resulting in Co release from the base alloy (Cartner et al., 2016). The absence of oxygen in the internal taper fluids would have prevented the chromium rich oxide layer from reforming as there is more cobalt in the base alloy than chromium, the ratio is more than 1. In comparison, oxygen is available in the external taper fluid around the distal tapers which would encourage repassivation; it is apparent that there is a delicate balance of oxygen presence and acidic conditions in the corrosion process. The proposed explanation for this is that for the 5° contact condition which had more Cr released than Co, the presence of a crevice where there is already reduced pH would reduce the oxygen locally and unlike what occurs in the internal taper fluid where oxygen depletion prevents oxide reformation, the replenishment of fluid would add oxygen which could be transported by the movement of the simulator; this could initiate the continuous attempt at repassivation therefore releasing more Cr over Co. The continuous oxide layer damage would be expected to be exacerbated by the micromotion at the interface.

6.4.3 Influence of trunnion surface topography

Within the trunnion angles tested, there was no statistically significant difference in ion release between the rough and smooth trunnions. However, it was apparent that the

increased Rz provided more stability at the taper junction thus significantly prolonging the fatigue life of the rougher trunnions. The lack of correlation between ion release and trunnion surface topography, was in agreement with the retrieval analysis of 400 trunnions by Arnholt et al. (2015) where it was concluded that surface topography did not influence fretting and corrosion at the taper interface. The drawbacks associated with rough trunnions are related to the elevated localised stresses at the peaks with increased likelihood of oxide layer damage. Elevated stresses at peaks may only occur if the peaks fail to plastically deform. The results in 6.3.2 show that there was deformation at the peaks. Moreover, it is possible that in a highly acidic environment such as the one in the current study, the oxide layer on the femoral head would be compromised anyway regardless of the surface texture. Therefore, any benefits of a smoother trunnion would not be realised. The deformation of peaks has also been reported to result in areas of increased lattice defects which are more prone to corrosion (Lundberg et al., 2015); it is possible that the effect of this is more long term and could be observed over a longer time period than was evaluated in the current study.

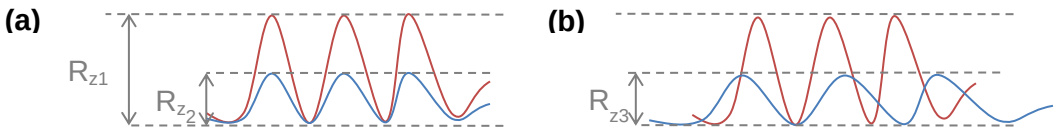

Figure 6-34 Schematic of variations in surface roughness profile of trunnions (a) showing a variaition in peak height and same pitch (b) showing variaitons in both peak height and pitch

In designing the trunnions for the current study, trunnion roughness was specified as would be commercially, based on the Rz (Figure 6-34). Susceptibility to crevice corrosion is defined by a scaling factor which is related to the square of a crevice depth divided by its width (Van Citters et al., 2015). If the surface profile of the trunnions used in the current study is as shown in Figure 6-34, and assuming the depth is not a factor because there is no valley below the reference line, then the scaling factor would be equal for both rough and

smooth trunnions. Hence, despite the smaller peaks in the smoother trunnions, the propensity for crevice corrosion based on surface texture alone would be the same. If however, the profile of the smoother trunnions used in the current study is as depicted in Figure 6-34b, then the scaling factor would be greater in the 'rougher' trunnion thus increasing its susceptibility to corrosion. The fact that $R_{z2}=R_{z3}$ (Figure 6-34) but would result in different scaling factors, reflects the need for standardisation of roughness parameters which define the surface features of male and female tapers.

Chapter 7. Final Discussion

THR is one of the most successful orthopaedic surgery of the last decade (Affatato et al., 2006). With the increasing life expectancy and obesity rates, the number of procedures is estimated to increase by 174%, 62% and 45% in the US, UK and Sweden by the year 2030 relative to 2005 (Kurtz et al., 2007, National Joint Registry of England and Wales, 2005, Culliford et al., 2015, Nemes et al., 2014, Swedish Hip Arthroplasty Register, 2005). The increase in the number of THR patients will inevitably increase the number of people affected by taper corrosion. If it is symptomatic, it will result in the need for revision surgery which increases the cost of care at a time when healthcare costs are escalating (Wilson et al., 2008); if asymptomatic and diagnosed late, it results in poor outcomes due to extensive soft tissue damage (Cooper et al., 2012a, McGrory and McKenney, 2016) and ever higher costs.

Although initially recognised as a problem in large headed metal-on-metal (LHMoM) devices (Cook et al., 2013, Scully and Teeny, 2013), the findings of the current study, increasing torque with head size, as well as the development of torques for MoP bearings comparable to MoM, suggests that this may also become a problem with larger diameter MoP devices. Indeed, there have been a number of reports of pseudotumour formation secondary to head-neck taper corrosion in MoP devices (Table 7-1). These reports started shortly after the LHMoM concerns arose in 2010 (Morlock, 2015), and cut across head sizes and offsets, taper types and trunnion material. It has been highlighted that peculiar features in the blood vessels of pseudotumours from MoP devices, encourage the accumulation of ions in the joint space (Eltit et al., 2017) and are associated with highly destructive lesions which elicit reactions worse than the reactions observed in MoM bearing combinations. Similarly, Nodzo et al. (2017) found the median volumes of pseudotumours with MoP was almost 3 times larger than associated with MoM resurfacing pseudotumours. It appears that,

adverse tissue reactions in MoP are potentially problematic and may start to become more prevalent in the coming years.

Table 7-1 Retrieval studies reporting the incidence of ALTR in MoP devices (CoCr heads)

	Head size	Offsets	Trunnion material*	Taper size*
Lindgren et al. (2011)	28	+4	TMZF	V40
Cooper et al. (2012a)	28 to 36	-3.5 to +10.5	CoCr TMZF	10/12 12/14 V40
Walsh et al. (2012)	36	NR	CoCr	12/14
Mao et al. (2012)	32	NR	TMZF	V40
Fricka et al. (2012)	36	NR	CoCr	12/14
Khair et al. (2013)**	36	-5	TMZF	NR
Clyburn (2013)	32	+4	TMZF	V40
Scully and Teeny (2013)	32	+4	TMZF	NR -
Cook et al. (2013)	40 44	0	TMZF	V40
Bisseling et al. (2013)	28	+10.5	Ti-6Al-7Nb	12/14
Whitehouse et al. (2015)	26 to 36	-3.5 to +7	CoCr TMZF	6 12/14
Carli et al. (2015)	28 36	+12 +15.5	CoCr	12/14
Banerjee et al. (2015)	32 40	+4 +6	TMZF Ti-6Al-4V	V40 12/14
Watanabe et al. (2015)	28	NR	CoCr	NR
Plummer et al. (2016)	28 to 40	-3.5 to +13	CoCr Ti***	NR
Manthe et al. (2016)	32 36	-5 to +3.5	Ti-6Al-4V TMZF	12/14 V40
Eltit et al. (2017)	28 to 54	-	Ti-6Al-4V TMZF	12/14 V40
Nodzo et al. (2017)	28 to 36	-6 to +7	CoCr TMZF	Type II 12/14 V40 Type I

*some taper sizes and trunnion materials were inferred from Porter et al. (2014) based on the name of the femoral stem

**components reported in the table are of the 2nd revision surgery; details of the components of the initial revision were not given

***precise Titanium alloy not stated

NR not reported

Understanding the torque transmitted across the taper junction is important. Although methods reported in the literature describe a positive correlation with head size, the torque values quoted are not comparable across test setups (Figure 7-1). The torque values found in the current study ranged from 0.2 – 1.1 Nm which was lower than most studies reported. However, the friction generated at the bearing surface for the 28 mm head on the pendulum simulator (3.3.5) was comparable to the result reported by Brockett et al. (2007) utilising the same test facility (Figure 7-2). Torque measurements are subject to factors such as cup inclination, acetabular material, acetabular deformation, load, lubrication and the condition of the bearing surface, axis of measurement (Scholl et al., 2016a, Saikko, 2008), as well as differences in the mechanics of the testing device. The strain gauge measurement carried out in the current work, is most similar to the studies by Saikko (2008); both utilised a 23° biaxial rocking motion and a similar axis of measurement (taper axis). However, comparisons between (28 mm, 1 kN) (Saikko, 2008) and 28 mm (+3.5 and +7 mm) at 1.25 kN in the current study found lower torque values. This might be due to the floating bearing in the orbital bearing simulator being positioned superior to the cup holder, in order to facilitate alignment of the centres of the head and cup (Kurtz, 2010). This would allow passive movement in the M-L plane and A-P plane in comparison to a seemingly rigid acetabular setup utilised in (Saikko, 2008). This passive movement may have reduced the torque measured in the current study.

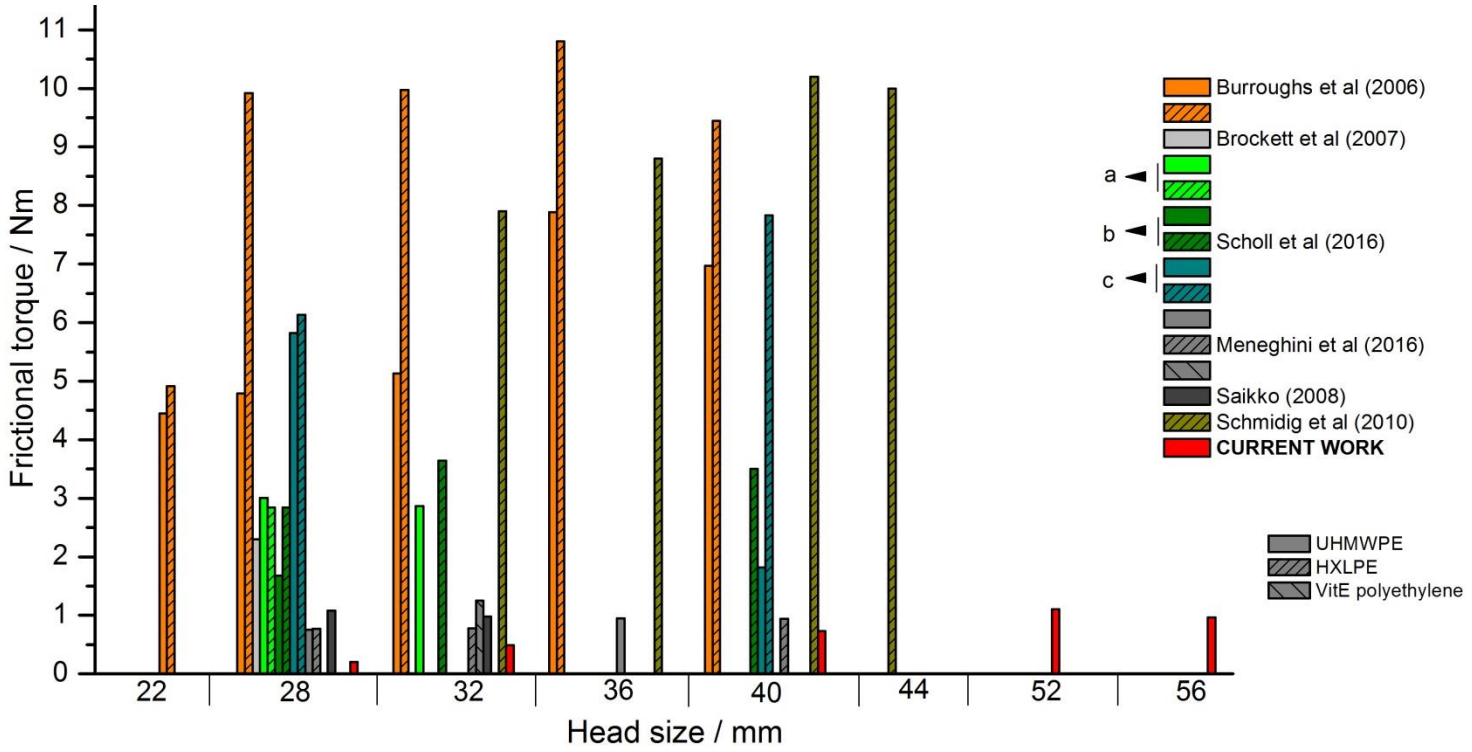

Burroughs et al (2006)	Mini-Bionix MTS 858,100 % bovine serum, 3 kN, ±15°
Brockett et al (2007)	Pendulum friction simulator, 100% bovine calf serum, maximum load 2± 0.1 kN, swing phase 0.3 kN, ±25° (±1°) F/E, 1 Hz
Scholl et al (2016)	a: ±23° biaxial rocking, 50% bovine serum, 2450 N, 1 Hz, 20 cycles
	b: Bionix 858, 25% bovine serum, 2450 N, ±20°IER
	c: 25% bovine serum, 2450 N, ±20°F/E, 0.75 Hz
Meneghini et al (2016)	Mini-Bionix 858 MTS, 100% alpha calf Serum, 650 N, ±20°IER, 1 Hz, 2000 cycles
Saikko (2008)	Novel torque system incorporated into a ±23° biaxial rocking simulator,50% alfa calf serum, 2kN static load
Schmidig et al (2010)	50% bovine alfa calf serum, 2450 N, ±20°,0.5 Hz, 20 cycles
Current work	±23° biaxial rocking, 25% bovine serum, 3000 N, 1 Hz

Figure 7-1 Reported frictional torque values for different CoCr heads

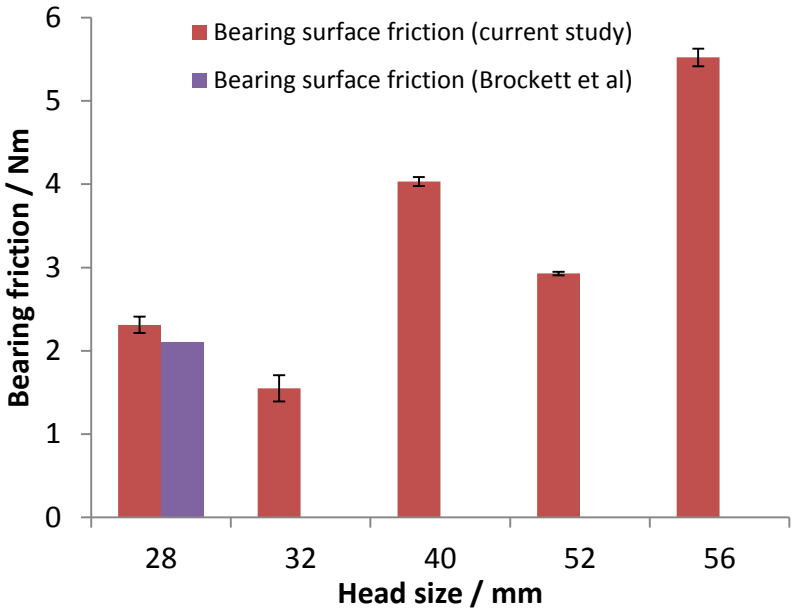

Figure 7-2 Comparison of the bearing surface friction measurements from the current study and a study by Brockett et al. (2007)

Large friction from the bearing surface has been described as contributing to taper corrosion by increasing micromotion and causing large torques to be transmitted to the taper junction, thereby destabilising it (Langton et al., 2012, Toni et al., 2012, Dyrkacz et al., 2013). However, measuring the bearing surface friction independent of the torque adjacent to the taper junction does not allow the contribution of friction to taper instability to be determined. Ideally, bearing friction and torque adjacent to the taper junction measurements would be taken simultaneously, however this has not been reported in the literature and indeed was not possible in the current work.

The advantage of using a hip simulator to evaluate the performance of taper junctions was that torques were generated at the taper junction, in addition to bending moments as applied in the ASTM F1875 fretting test (3.4.3). Both the FE evaluation in the current study and the experimental ion release study indicated that micromotion occurs at the taper junction under loading. Indeed the magnitude of micromotion parallel to the taper surfaces recorded in the FE study was found to be similar to values reported from experimental setups (Table 7-2).

Table 7-2 Magnitudes of micromotion for different taper material combinations

Material combination	Micromotion / μm	Load / N	References
CoCr/SS	25	3000	Gilbert et al. (2009)
Ceramic*/Ti-6Al-4V	6	5340	Grupp et al. (2010)
CoCr/CoCr	3	2300	Jauch et al. (2011)
CoCr/Ti-6Al-4V	4.5		
CoCr/CoCr	2	4000	Mali and Gilbert (2015)
CoCr/TMZF	12.5	3200	Swaminathan et al. (2015)
CoCr/Ti-6Al-4V	6.6		
CoCr/Ti-6Al-4V	**4.4 ± 0.12**	**3000**	**Current study**

*type of ceramic not specified

The FE study modelled taper clearances up to 0.28° although anecdotally, the largest clinically relevant clearance declared by manufacturers is 0.2°. Results in Chapters 3 and 4 indicated that larger head sizes resulted in an increase in torques being transmitted through the taper and also that increasing taper clearances increased the gap formed at the taper junction under loading. Therefore, it may be concluded that the use of larger heads should be controlled by tighter taper clearances, if the benefits of increased stability and reduced dislocation are to be fully exploited.

The ions release results in the current study are representative of early conditions around the taper environment. The short time periods evaluated in this study are more representative of the early postoperative phase where inflammation is still occurring in an acidic environment (Posada et al., 2015, Chen et al., 2012). It has been previously suggested in MoM wear tests that 50 % of the total Co and Cr is released from these bearings over the initial 500 000 cycles (Royle, 2012). However, this has not been established for taper ion release; the only previous study evaluating the taper junction on the hip simulator (Pamu et al., 2012) showed that the ion release in Ringer's solution continued to increase from 0 to 2 Mc without steady state conditions ever being reached. From the results generated in this study, it was not possible to establish any further details on whether a steady state was ever generated.

7.1 Understanding the experimental ion release at the taper junction

MoP devices have been thought to be a more attractive bearing option due to their lower metal ion release compare to MoM (Tiusanen et al., 2013). However, the results in the current work indicate that considerable ion release will occur at the taper under acidic conditions. For the external taper fluid, the mean cumulative Co at the end of testing (0.5 Mc or the point of taper failure) for proximal and distal taper contact conditions, were 4.1 and 3.0 ppm respectively, whilst for Cr, the ionic concentration it was 21.3 and 4.9 ppm respectively for the same conditions. To contextualise these results, mean Co and Cr concentrations of 4.9 ppm and 2.1 ppm from synovial fluid samples have been recorded in hips at retrieval with MoP articulations (Eltit et al., 2017). The average volume of synovial fluid in asymptomatic hips is 2.7 ml (Moss et al., 1998). Considering the proximal and distal contact as a single population would result in a mean cumulative Co concentration of 3.5 ppm and a mean cumulative Cr concentration of 11.8 ppm; hence the mean cumulative concentrations measured in the current study can be adjusted for the synovial fluid volume, to suggest that the concentration of Co would be 6.4 ppm and for Cr, it would be 21.9 ppm. Relative to 2.7 ml of joint fluid, *in vitro* Co ion release evaluations for roughened MoP bearings established maximum concentrations of 220 ppm released from the bearing surface after 5 Mc (de Villiers et al., 2015). Royle (2012) measured mean Co and Cr concentrations of approximately 9100 and 3100 ppm at 4 Mc from roughened MoM.

The results in 6.4.1 suggested that in understanding taper corrosion through ion release, Cr is a more discriminating factor, in contrast to the apparent focus on cobalt release. This increased focus is probably due to the increased toxicity of Co^{2+} relative to Cr^{3+} (Catelas et al., 2003) and its increased solubility which makes it easier to measure systemically; also, the rate of Co production can be estimated because the rates of excretion and production

are equal (Cobb and Schmalzreid, 2006). Cobalt and chromium levels in THR patients are measured from whole blood or its derivatives such as serum, plasma or erythrocytes and urine (Daniel et al., 2007a, Tiusanen et al., 2013, Daniel et al., 2007b) and these values are recorded in the ppb range. Clinically, metal concentrations in the serum are not useful as a surrogate measure of systemic metal ion exposure (Daniel et al., 2007b) and can only be used as a predictor with moderate specificity and sensitivity (Vundelinckx et al., 2013).

A Co/Cr ratio less than 1 (mean = 0.4) was observed in the external taper fluid of proximal tapers whilst the distal tapers had a mean Co/Cr ratio of 2.9 in the external taper fluid (Figure 6-31). The observation in the proximal tapers is in contrast to reports of a Co/Cr ratio in serum of greater than 1 being suggestive of a corroding taper (Plummer et al., 2016, Nodzo et al., 2017). The Co/Cr ratio does not provide an accurate understanding of ion release from taper junctions. Certainly, serum ion levels do not highlight the high concentrations found in tissues adjacent to the joint replacement. Relative to joint fluid samples, serum samples are between 1 and 3 orders of magnitude lower (Kwon et al., 2009, Catelas et al., 2003, Eltit et al., 2017). Serum measurements are more commonly used as samples because they are more easily obtained and analysed than joint fluids (Daniel et al., 2007b, McGrory et al., 2017). Further, Figure 6-28 and Figure 6-29 show that the Co/Cr ratio was not always consistent across sampling points over the duration of testing. Synovial fluid is turned over daily (Levick and McDonald, 1995). In the experimental evaluation, new fluid was added daily. However, the entire fluid could not be replaced because it would have depleted the air in the chamber thus making it impossible to refill. Nonetheless, if the variation of Co/Cr ratio is a phenomenon that also occurs *in vivo*, then the time point where the patient sample is taken would impact the concentrations measured.

All metal ions are subject to the excretion and/or dilution mechanisms that occur systemically. Within blood and its derivatives, there will be differences in Cr concentration

measured because Cr exists in 2 valence states. Cr^{6+} binds strongly to cells and is not detectable in serum samples, whilst Cr^{3+} is excluded from cells (Milošev, 2012, MacDonald et al., 2003); therefore, neither serum nor erythrocyte measurements provide a true evaluation of implant chromium release. In addition, chromium has a propensity to precipitate (Sidaginamale et al., 2016), meaning that lower values of chromium are measured systemically than is actually released. Whilst joint fluid samples are better at highlighting the elevated concentrations in surrounding tissues, it is also unlikely that they will account for precipitation of chromium unless taken at a very early time point postoperatively; reports on joint fluid ion analyses have taken samples no earlier than 9 months after initial implantation (Lass et al., 2014, Davda et al., 2011, Langton et al., 2010). Immediately postoperatively however, the corrosion process may just be initiated and samples evaluated at a later time point may be influenced by precipitation as well as transport away from the joint fluid.

7.2 Influence of the taper environment

PBS[H^+] was used to accelerate the corrosion. As indicated in Chapter 5, representative physiological fluids are often used for evaluating implant responses to electrolytes found in the body. However, the *in vivo* taper environment has not been characterised previously. The nature of the surface of corroding CoCr alloys depends upon its surrounding environment and the fracture properties of oxide layers is dependent upon the electrolyte conditions (Gilbert, 2012, Lewis et al., 2006). McGrory et al. (2017) suggested that the fluid in contact with the taper is synovial fluid. Synovial fluid and its components have previously been studied relative to bearing lubrication but not to the taper environment.

Synovial fluid (SF) and PBS have similar inorganic composition (Lewis et al., 2005) but PBS has no protein content. Release of Co and Cr from CoCr alloys showed that synovial fluid induced higher Cr release than PBS and water (Lewis et al., 2005) as proteins may

have impeded the formation of the protective oxide film (Royhman et al., 2013). It has also been reported that an organic ligand with a high affinity for Cr^{3+} is present in synovial fluid; the effect of this is to attract chromium ions through the pores of oxide layers and promote dissolution due to cationic conductivity (Lewis et al., 2005, Lewis et al., 2006). Hence, SF could be more corrosive than PBS at neutral condition. Under acidic conditions however, synovial fluid may confer protection by repelling corrosive anions such as Cl^- (Lewis et al., 2005). To that end, the prevailing pH around the joint space is not clear. It is believed that the inflammatory phase of healing immediately post implantation could persist for more than 6 weeks (Chen et al., 2012). Likewise, it is also thought that Co and Cr release from the implant, not related to the taper junction can initiate Fenton-like reactions (2.5.2) which could sustain an inflammatory response. Both acute and chronic inflammation are thought to create acidification (Posada et al., 2015). However, it is also known that physiological fluids *in vivo* have a buffering capacity; Milošev et al. (2016) showed that the change in mean pH of the synovial fluid was small in patients revised for aseptic and septic loosening (pH 7.6 and 7.55 respectively), compared to osteoarthritic joints prior to joint replacement (pH 7.78) despite the increase in metal ions at revision. Also, if the entire joint space was acidic for prolonged periods, precipitates of $CrPO_4$ would be unlikely in adjacent tissues. Therefore, it is more likely that the acidic conditions *in vivo,* are actually confined to crevices.

If synovial fluid was to be used in *in vitro* evaluations, aside from being difficult to obtain and its associated expense for its use in a multiple station hip simulator with continuous sampling, the SF analysed in the literature is sourced from arthritic hips. The total protein content of healthy synovial fluid is lower at 19-22 mg/ml compared to 40-68 mg/ml for the diseased fluid (Roba, 2009). Protein concentration has an effect on the electrochemical behaviour of implant metals (Karimi, 2014). Moreover, after THR, the synovial capsule reforms and produces a lubricant that has been termed pseudosynovial fluid (PSF)(Roba, 2009, Kung et al., 2015). Both are blood dialysates (Takakubo et al., 2013) but PSF is lower

in viscosity (lower hyaluronic acid content) than pre-arthroplasty fluids (Kung et al., 2015). PSF will vary in protein content as different failure mechanisms such as implant loosening and wear will alter the protein content as a result of the associated inflammation (Roba, 2009). Further, the torque transferred to the taper junction due to bearing surface friction will be a function of protein concentration (Roberts et al., 1982). All of these may alter the corrosion observed at head-neck tapers *in vivo*.

7.3 Future work

This study has corroborated the suggestions and findings in the literature that an increase in head size is accompanied by an increase in frictional torque. However, the ion release profile was only determined for 40 mm heads and there has been no evaluation of the effect of head size on the production of ionic matter at the taper junction. A hip simulator evaluation showed that increasing head sizes led to an increase in metal ions in the bearing surface lubricant (de Villiers et al., 2015), although the reports in clinical evaluation with respect to ion release have been inconsistent. Craig et al. (2014) observed a significant rise in mean levels of Co ions in the blood of patients with 36 mm heads relative to patients with 28 mm diameter heads but the increase in with 40 mm heads was smaller and less significant in comparison with the 28 mm group. Conversely, Hallows et al. (2011) found no difference in serum Co concentrations between small (28-32 mm) and large heads (> 38 mm); however, elevated serum Cr levels were reported for the large heads compared to the small heads. Nonetheless, neither the hip simulator study nor the clinical studies would have distinguished between bearing surface and taper ion release and there may have been variations in the relative contribution of the taper and bearing to the total concentration of ions measured. As long as the design of the rim of the femoral head remains the same, the current isolation setup could be used to evaluate the effect of head size on taper ion release. In addition, isolating the taper on heads of different sizes may help to elucidate why, despite

a positive correlation between torque and head size, there have been considerable reports of corrosion observed *in vivo* on smaller heads (28 – 32 mm) (Lombardi et al., 2016, McGrory et al., 2017).

Adverse conditions at bearing surfaces such as 3rd body abrasion may be expected to disrupt lubrication, increase the bearing surface friction and thus increase torque at the taper junction. The study in Chapter 6 evaluated a CoCr/Ti-6Al-4V junction; clinically, other metallic combinations are widely utilised including CoCr/CoCr and CoCr/SS. Although galvanic corrosion is not thought to be a significant factor in taper corrosion, it would be interesting to study the different metallic taper combinations under hip simulator loading. This is especially true of CoCr/SS taper interfaces because they have been shown to generate lower fretting currents than CoCr/Ti. Also, a study by Chaplin et al. (2004) evaluating 20 retrieved SS trunnions which were *in situ* for at least 1 year showed no signs of corrosion. It should be noted that the group did not specify nor evaluate the femoral heads paired with the trunnions. However, in evaluating SS trunnions without the complete stem fixation, it is possible that an incomplete picture of taper corrosion results. Some of the non-titanium femoral stems are fixed using bone cement; bone cement as well as its accompanying additives such as antibiotics and radiopaque agents have been reported to affect stem electrochemistry (Bryant et al., 2013). This raises concerns about the so-called cathodic polarisation effect results such that corrosion at the head-neck taper may be reduced due to the occurrence of corrosion at the stem-bone cement interface (McGrory et al., 2017).

The current taper isolation design can be used to isolate taper debris as the cytotoxic effect is also dependent on particulate products (Kwon et al., 2009). Accordingly, even at Co and Cr concentrations of 3 and 5 ppm respectively in local tissue, nano particles generated minimal or no inflammatory response in mice unlike micron sized particles (Madl et al.,

2015). Reports of more aggressive reactions associated with taper debris relative to bearing surface debris (Langton, 2014, Hart et al., 2013) is likely to be due to differences in morphology and characteristics of metallic particles. Therefore, generating clinically relevant taper debris would facilitate cytotoxicity studies to elucidate factors contributing to its increased potency. This may also help to explain if particular features of taper corrosion are responsible for whether a patient is symptomatic or otherwise (Fehring et al., 2014, McGrory et al., 2017) outside of individual patient sensitivities (Eltit et al., 2017, Jacobs, 2016).

This study showed the profile of ion release from the taper junction at the early stages post implantation. A retrospective evaluation using FEA (4.4.9) showed that the distal contact (8°) trunnions failed earlier than the proximal contact (5°) trunnions due to markedly lower contact area with the distal contact conditions and consequently, less stability at the junction. It might be suggested that this instability created larger displacements and was transferred to the thread causing fatigue failure. Nonetheless, some proximal trunnions also failed which suggests there was also load bearing by the threads. The current standard for wear testing is 5 Mc (Trommer and Maru, 2017). It would be ideal to establish the release profile from the taper junction over an equal timeframe to determine if an equilibrium state is reached. At 0.5 Mc, the corrosion observed at the femoral head taper was only mild or moderate according to the Goldberg scale. Running the hip simulator test for longer would be more likely recreate severe taper corrosion which has been observed in retrieved specimens (Hothi et al., 2017a, Jennings et al., 2016). This would require that the trunnion be redesigned to prevent fatigue fracture, indeed, the titanium trunnions could be manufactured as a single unit.

Despite the benefits of evaluating taper junctions using the simplified walking cycle on the hip simulator, simulators could be used to evaluate the taper junction under stair climb loading since the FE results in this thesis suggest that the gap and stresses will be larger

under stair climb loading. Although the stair climb loading condition is not currently mandated in testing THR devices, its use may be beneficial to 'beyond compliance' initiatives to improve implant performance.

References

ABDULLAH, K. 2010. Study of factors affecting taper joint failures in modular hip implant using finite element modelling. *Modeling simulation and optimization—focus on applications. InTech.(ISBN: 978-953-307-055-1)*.

AFFATATO, S., LEARDINI, W. & ZAVALLONI, M. 2006. Hip Joint Simulators: State of the Art. *In:* BENAZZO, F., FALEZ, F. & DIETRICH, M. (eds.) *Bioceramics and Alternative Bearings in Joint Arthroplasty.* Steinkopff.

AFFATATO, S., SPINELLI, M., ZAVALLONI, M., MAZZEGA-FABBRO, C. & VICECONTI, M. 2008. Tribology and total hip joint replacement: Current concepts in mechanical simulation. *Medical Engineering & Physics,* 30**,** 1305-1317.

AFOLARANMI, G. A., TETTEY, J., MEEK, R. M. D. & GRANT, M. H. 2008. Release of Chromium from Orthopaedic Arthroplasties. *The Open Orthopaedics Journal,* 2**,** 10-18.

ALDINGER, P., CARTNER, J. & JONES, B. 2015. Validating a Simplified Method for Assessing Total Hip Arthroplasty Taper Corrosion Susceptibility with a 15-Year Retrieval Database. *In:* A, G., STEVEN, K., JACK, L. & WILLIAM, M. (eds.) *Modularity and Tapers in Total Joint Replacement Devices STP1591.* West Conshohocken, PA: ASTM International

ALDINGER, P. & PAWAR, V. 2017. Similarities between Reported Inflammatory Cell-Induced Corrosion Features and Electrocautery Damage. *Bone & Joint Journal* 99-B**,** 9.

ALEMÓN, B., FLORES, M., RAMÍREZ, W., HUEGEL, J. C. & BROITMAN, E. 2015. Tribocorrosion behavior and ions release of CoCrMo alloy coated with a TiAlVCN/CNx multilayer in simulated body fluid plus bovine serum albumin. *Tribology International,* 81**,** 159-168.

ALTIMED JSC. 2012. *Ceramic Femoral Head* [Online]. Available: http://www.altimed.by/en/products/hips/heads/biolox_delta_head/ [Accessed 30/12/2016 2016].

ANTONIOU, R. A. & RADTKE, T. C. 1997. Mechanisms of fretting-fatigue of titanium alloys. *Materials Science and Engineering: A,* 237**,** 229-240.

ARNHOLT, C., UNDERWOOD, R. J., MACDONALD, D. W., HIGGS, G. B., CHEN, A. F., KLEIN, G. R., HAMLIN, B. R., LEE, G.-C., MONT, M. A., CATES, H. E., MALKANI, A. L., KRAAY, M. J., RIMNAC, C. M. & KURTZ, S. M. 2015. Microgrooved Surface Topography Does Not Influence Fretting Corrosion of Tapers in Total Hip Arthroplasty: Classification and Retrieval Analysis. *In:* A, G., STEVEN, K., JACK, L. & WILLIAM, M. (eds.) *Modularity and Tapers in Total Joint Replacement Devices STP1591.* West Conshohocken, PA: ASTM International

ARNHOLT, C. M., MACDONALD, D. W., TOHFAFAROSH, M., GILBERT, J. L., RIMNAC, C. M., KURTZ, S. M., KLEIN, G., MONT, M. A., PARVIZI, J., CATES, H. E., LEE, G.-C., MALKANI, A. & KRAAY, M. 2014. Mechanically Assisted Taper Corrosion in Modular TKA. *The Journal of Arthroplasty,* 29**,** 205-208.

ASHKANFAR, A. 2015. *A Computational Approach to Fretting Wear Prediction in Total Hip Replacements.* PhD, Liverpool John Moores.

ASHKANFAR, A., LANGTON, D. J. & JOYCE, T. J. 2017. A large taper mismatch is one of the key factors behind high wear rates and failure at the taper junction of total hip replacements: A finite element wear analysis. *Journal of the Mechanical Behavior of Biomedical Materials,* 69**,** 257-266.

ASTMF1875 1998. Standard Practice for Fretting Corrosion Testing of Modular Implant Interfaces: Hip Femoral Head-Bore and Cone Taper Interface. West Conshohocken, PA: ASTM International

AZOM 2012. Stainless Steel - Grade 17-4.

BANERJEE, S., CHERIAN, J. J., BONO, J. V., KURTZ, S. M., GEESINK, R., MENEGHINI, R. M., DELANOIS, R. E. & MONT, M. A. 2015. Gross Trunnion Failure After Primary Total Hip Arthroplasty. *The Journal of Arthroplasty,* 30**,** 641-648.

BEADLING, A. 2017. *Biotribocorrosion of orthopaedic hip replacements.* PhD, Leeds.

BERGMANN, G., BENDER, A., DYMKE, J., DUDA, G. & DAMM, P. 2016. Standardized Loads Acting in Hip Implants. *PLOS ONE,* 11**,** e0155612.

BERGMANN, G., DEURETZBACHER, G., HELLER, M., GRAICHEN, F., ROHLMANN, A., STRAUSS, J. & DUDA, G. N. 2001. Hip contact forces and gait patterns from routine activities. *Journal of Biomechanics,* 34**,** 859-71.

BERRY, D. J., ABDEL, M. P. & CALLAGHAN, J. J. 2014. What are the current clinical issues in wear and tribocorrosion? *Clinical Orthopaedics and Related Research,* 472**,** 3659-64.

BISHOP, N., WITT, F., POURZAL, R., FISCHER, A., RÜTSCHI, M., MICHEL, M. & MORLOCK, M. 2013. Wear patterns of taper connections in retrieved large diameter metal-on-metal bearings. *Journal of Orthopaedic Research,* 31**,** 1116-1122.

BISSELING, P., TAN, T., LU, Z., CAMPBELL, P. A. & SUSANTE, J. L. V. 2013. The absence of a metal-on-metal bearing does not preclude the formation of a destructive pseudotumor in the hip-a case report. *Acta Orthopaedica,* 84**,** 437-441.

BITTER, T., JANSSEN, D., SCHREURS, B. W., KHAN, I. & VERDONSCHOT, N. 2013. The Effect of Head Impaction on Contact Stress and Micromotions at the Head-Taper Connection. *Bone & Joint Journal Orthopaedic Proceedings Supplement,* 95-B**,** 241.

BOBYN, J. D., TANZER, M., KRYGIER, J. J., DUJOVNE, A. R. & BROOKS, C. E. 1994. Concerns with modularity in total hip arthroplasty. *Clinical Orthopaedics and Related Research***,** 27-36.

BONE, M. C., SIDAGINAMALE, R. P., LORD, J. K., SCHOLES, S. C., JOYCE, T. J., NARGOL, A. V. & LANGTON, D. J. 2015. Determining material loss from the femoral stem trunnion in hip arthroplasty using a coordinate measuring machine. *Proceedings of the Institution of Mechanical Engineers, Part H: Journal of Engineering in Medicine,* 229**,** 69-76.

BOWSHER, J. G. 2001. *Accelerated wear testing methodologies for total hip replacements.* PhD, Queen Mary, University of London.

BOWSHER, J. G. & SHELTON, J. C. 2001. A hip simulator study of the influence of patient activity level on the wear of crosslinked polyethylene under smooth and roughened femoral conditions. *Wear,* 250**,** 167-179.

BROCK, T. M., SIDAGINAMALE, R., RUSHTON, S., NARGOL, A. V., BOWSHER, J. G., SAVISAAR, C., JOYCE, T. J., DEEHAN, D. J., LORD, J. K. & LANGTON, D. J. 2015. Shorter, rough trunnion surfaces are associated with higher taper wear rates than longer, smooth trunnion surfaces in a contemporary large head metal-on-metal total hip arthroplasty system. *Journal of Orthopaedic Research,* 33**,** 1868-74.

BROCKETT, C., WILLIAMS, S., JIN, Z., ISAAC, G. & FISHER, J. 2007. Friction of total hip replacements with different bearings and loading conditions. *Journal of Biomedical Materials Research - Part B Applied Biomaterials,* 81**,** 508-15.

BROWN, S. A., FARNSWORTH, L. J., MERRITT, K. & CROWE, T. D. 1988. In vitro and in vivo metal ion release. *Journal of Biomedical Materials Research,* 22**,** 321-338.

BRYANT, M., HU, X., FARRAR, R., BRUMMITT, K., FREEMAN, R. & NEVILLE, A. 2013. Crevice corrosion of biomedical alloys: a novel method of assessing the effects of

bone cement and its chemistry. *Journal of Biomedical Materials Research Part B: Applied Biomaterials,* 101**,** 792-803.
BRYANT, M. & NEVILLE, A. 2016. Corrosion and mechanical properties. *Orthopaedics and Trauma,* 30**,** 176-191.
BUENTE, D., HUBER, G. & MORLOCK, M. 2016. Bottoming-out as the ultimate failure mode of the neck taper of a bi-modular THR stem design *Bone & Joint Journal Orthopaedic Proceedings Supplement,* 98-B**,** 59.
BUNDY, K. J. 2005. Corrosion Testing in In Vivo Environments. *In:* BABOIAN, R. (ed.) *Corrosion Tests and Standards: Application and Interpretation* ASTM International.
BURROUGHS, B. R., MURATOGLU, O. K., BRAGDON, C. R., WANNOMAE, K. K., CHRISTENSEN, S., LOZYNSKY, A. J. & HARRIS, W. H. 2006. In vitro comparison of frictional torque and torsional resistance of aged conventional gamma-in-nitrogen sterilized polyethylene versus aged highly crosslinked polyethylene articulating against head sizes larger than 32 mm. *Acta Orthopaedica,* 77**,** 710-718.
BUTCHER, D. J. & SNEDDON, J. 1998. *A Practical Guide to Graphite Furncae Atomic Absorption Spectrometry,* New York, John Wiley & Sons, Inc.
CADOSCH, D., AL-MUSHAIQRI, M. S., GAUTSCHI, O. P., MEAGHER, J., SIMMEN, H. P. & FILGUEIRA, L. 2010. Biocorrosion and uptake of titanium by human osteoclasts. *Journal of Biomedical Matererials Research Part A,* 95**,** 1004-10.
CADOSCH, D., CHAN, E., GAUTSCHI, O. P., SIMMEN, H. P. & FILGUEIRA, L. 2009. Bio-corrosion of stainless steel by osteoclasts--in vitro evidence. *Journal of Orthopaedic Research,* 27**,** 841-6.
CALES, B. & STEFANI, Y. 1998. Risks and advantages in standardization of bores and cones for heads in modular hip prostheses. *Journal of Biomedical Materials Research,* 43**,** 62-8.
CAMPBELL, P., YUAN, N., LUCK, J., COURPRON, P. & PARK, S. H. 2017. Re-Examining the Concept of Inflammatory Cell-Induced Corrosion. *Bone & Joint Journal* 99-B**,** 57.
CARLI, A., POLITIS, A., ZUKOR, D., HUK, O. & ANTONIOU, J. 2015. Clinically significant corrosion at the head-neck taper interface in total hip arthroplasty: a systematic review and case series. *HIP International,* 25**,** 7-14.
CARTNER, J., ALDINGER, P., FESSENDEN, M. & LI, C. 2013. Taper Damage Is Dependent Upon Material Combination: Correlation of 15 Years of Retrieved Devices. *Bone & Joint Journal Orthopaedic Proceedings Supplement,* 95-B**,** 260.
CARTNER, J., ALDINGER, P., LI, C. & COLLINS, D. 2016. Characterization of Femoral Head Taper Corrosion Features Using a 22-Year Retrieval Database. *HSS Journal* 1-7.
CATELAS, I., PETIT, A., ZUKOR, D. J., ANTONIOU, J. & HUK, O. L. 2003. TNF-α secretion and macrophage mortality induced by cobalt and chromium ions in vitro-Qualitative analysis of apoptosis. *Biomaterials,* 24**,** 383-391.
CERQUIGLINI, A., HENCKEL, J., HOTHI, H. S., DI LAURA, A., SKINNER, J. A. & HART, A. J. 2016. Inflammatory cell-induced corrosion in total knee arthroplasty: a retrieval study. *Journal of Biomedical Materials Research, Part B Applied Biomaterials***,** n/a-n/a.
CHAPLIN, R. P. S., LEE, A. J. C. & HOOPER, R. M. 2004. Assessment of wear on the cones of modular stainless steel Exeter hip stems. *Journal of Materials Science: Materials in Medicine,* 15**,** 977-990.
CHEN, X., BAI, C., XIE, L., ZHANG, Y. & WANG, K. 2012. Inflammatory response to orthopedic biomaterials after total hip replacement. *Journal of Orthopaedic Science,* 17**,** 407-412.

CHU, Y.-H., ELIAS, J. J., DUDA, G. N., FRASSICA, F. J. & CHAO, E. Y. S. 2000. Stress and micromotion in the taper lock joint of a modular segmental bone replacement prosthesis. *Journal of biomechanics,* 33**,** 1175-1179.

CHUMAKOV, A., BATALOVA, V., SLIZHOV, Y., GODYMCHUK, A. & RIEZNICHENKO, L. 2016. Electro-Fenton-like reactions of transition metal ions with electrogenerated hydrogen peroxide. *AIP Conference Proceedings,* 1772**,** 040004.

CLARK, G. C. F. & WILLIAMS, D. F. 1982. The effects of proteins on metallic corrosion. *Journal of Biomedical Materials Research,* 16**,** 125-134.

CLYBURN, T. A. 2013. Pseudotumor in Metal-on-Polyethylene Total Hip Arthroplasty. *Reconstructive Review,* 3.

COBB, A. G. & SCHMALZREID, T. P. 2006. The clinical significance of metal ion release from cobalt-chromium metal-on-metal hip joint arthroplasty. *Proceedings of the Institution of Mechanical Engineers, Part H: Journal of Engineering in Medicine,* 220**,** 385-98.

COLLIER, J. P., SURPRENANT, V. A., JENSEN, R. E. & MAYOR, M. B. 1991. Corrosion at the interface of cobalt-alloy heads on titanium-alloy stems. *Clinical Orthopaedics and Related Research***,** 305-12.

COLLIER, J. P., SURPRENANT, V. A., JENSEN, R. E., MAYOR, M. B. & SURPRENANT, H. P. 1992. Corrosion between the components of modular femoral hip prostheses. *Journal of Bone & Joint Surgery, British Volume,* 74**,** 511-7.

COLLINS, S. 2011. Hip prosthesis system. Google Patents.

COOK, R. B., BOLLAND, B. J. R. F., WHARTON, J. A., TILLEY, S., LATHAM, J. M. & WOOD, R. J. K. 2013. Pseudotumour formation due to tribocorrosion at the taper interface of large diameter metal on polymer modular total hip replacements. *The Journal of Arthroplasty,* 28**,** 1430-6.

COOK, R. B., MAUL, C. & STRICKLAND, A. M. 2015. Validation of an Optical Coordinate Measuring Machine for the Measurement of Wear at the Taper Interface in Total Hip Replacement. *In:* A, G., STEVEN, K., JACK, L. & WILLIAM, M. (eds.) *Modularity and Tapers in Total Joint Replacement Devices STP1591.* West Conshohocken, PA: ASTM International

COOK, S. D., BARRACK, R. L., BAFFES, G. C., CLEMOW, A. J., SEREKIAN, P., DONG, N. & KESTER, M. A. 1994. Wear and corrosion of modular interfaces in total hip replacements. *Clinical orthopaedics and related research,* 298**,** 80-88.

COOPER, H. J. 2014. The local effects of metal corrosion in total hip arthroplasty. *Orthopedic Clinics of North America,* 45**,** 9-18.

COOPER, H. J., DELLA VALLE, C. J., BERGER, R. A., TETREAULT, M., PAPROSKY, W. G., SPORER, S. M. & JACOBS, J. J. 2012a. Corrosion at the Head-Neck Taper as a Cause for Adverse Local Tissue Reactions After Total Hip Arthroplasty. *Journal of Bone & Joint Surgery. American volume,* 94**,** 1655-1661.

COOPER, H. J., DELLA VALLE, C. J. & JACOBS, J. J. 2012b. Biologic Implications of Taper Corrosion in Total Hip Arthroplasty. *Seminars in arthroplasty,* 23**,** 273-278.

CRAIG, P., BANCROFT, G., BURTON, A., COLLIER, S., SHAYLOR, P. & SINHA, A. 2014. Raised levels of metal ions in the blood in patients who have undergone uncemented metal-on-polyethylene Trident-Accolade total hip replacement. *Bone & Joint Journal,* 96-B**,** 43-7.

CROSS, M. B., TRIVELLAS, M. & JACOBS, J. J. 2017. Corrosion at the Modular Head–Neck Junction. *In:* ABDEL, M. P. & DELLA VALLE, C. J. (eds.) *Complications after Primary Total Hip Arthroplasty: A Comprehensive Clinical Guide.* Springer International Publishing.

CROWNINSHIELD, R. D., MALONEY, W. J., WENTZ, D. H., HUMPHREY, S. M. & BLANCHARD, C. R. 2004. Biomechanics of Large Femoral Heads: What They Do and Don't Do. *Clinical Orthopaedics and Related Research,* 429**,** 102-107.

CULLIFORD, D., MASKELL, J., JUDGE, A., COOPER, C., PRIETO-ALHAMBRA, D. & ARDEN, N. K. 2015. Future projections of total hip and knee arthroplasty in the UK: results from the UK Clinical Practice Research Datalink. *Osteoarthritis and Cartilage,* 23**,** 594-600.

DAMM, P., DYMKE, J., ACKERMANN, R., BENDER, A., GRAICHEN, F., HALDER, A., BEIER, A. & BERGMANN, G. 2013. Friction in Total Hip Joint Prosthesis Measured In Vivo during Walking. *PLoS ONE,* 8**,** e78373.

DANIEL, J., ZIAEE, H., PRADHAN, C., PYNSENT, P. B. & MCMINN, D. J. W. 2007a. Blood and urine metal ion levels in young and active patients after Birmingham hip resurfacing arthroplasty. *Journal of Bone & Joint Surgery, British Volume,* 89-B**,** 169.

DANIEL, J., ZIAEE, H., PYNSENT, P. B. & MCMINN, D. J. W. 2007b. The validity of serum levels as a surrogate measure of systemic exposure to metal ions in hip replacement. *Journal of Bone & Joint Surgery, British Volume,* 89-B**,** 736.

DAVDA, K., LALI, F. V., SAMPSON, B., SKINNER, J. A. & HART, A. J. 2011. An analysis of metal ion levels in the joint fluid of symptomatic patients with metal-on-metal hip replacements. *Journal of Bone & Joint Surgery, British Volume,* 93-B**,** 738-745.

DAVIES, A. P., WILLERT, H. G., CAMPBELL, P. A., LEARMONTH, I. D. & CASE, C. P. 2005. An unusual lymphocytic perivascular infiltration in tissues around contemporary metal-on-metal joint replacements. *Journal of Bone & Joint Surgery, American Volume,* 87**,** 18-27.

DAVIS, J. R. 2003. Handbook of Materials for Medical Devices. ASM International.

DAY, J. S. & ABBOUD, J. A. 2016. Implant Retrieval. *In:* FRANKLE, M., MARBERRY, S. & PUPELLO, D. (eds.) *Reverse Shoulder Arthroplasty: Biomechanics, Clinical Techniques, and Current Technologies.* Cham: Springer International Publishing.

DE VILLIERS, D. 2014. *Accelerated wear protocols for understanding clinical wear in modern hip prostheses.* PhD, Queen Mary, University of London.

DE VILLIERS, D. & SHELTON, J. C. 2016. Measurement outcomes from hip simulators. *Proceedings of the Institution of Mechanical Engineers, Part H: Journal of Engineering in Medicine,* 230**,** 398-405.

DE VILLIERS, D., TRAYNOR, A., COLLINS, S. N. & SHELTON, J. C. 2015. The increase in cobalt release in metal-on-polyethylene hip bearings in tests with third body abrasives. *Proceedings of the Institution of Mechanical Engineers. Part H, Journal of Engineering in Medicine,* 229**,** 611-618.

DEL BALSO, C., TEETER, M. G., TAN, S. C., LANTING, B. A. & HOWARD, J. L. 2015. Taperosis: Does head length affect fretting and corrosion in total hip arthroplasty? *Bone & Joint Journal,* 97-B**,** 911-6.

DERAR, H. & SHAHINPOOR, M. 2015. Recent Patents and Designs on Hip Replacement Prostheses. *The Open Biomedical Engineering Journal,* 9**,** 92-102.

DI LAURA, A., HOTHI, H. S., MESWANIA, J. M., WHITTAKER, R. K., DE VILLIERS, D., ZUSTIN, J., BLUNN, G. W., SKINNER, J. A. & HART, A. J. 2017. Clinical relevance of corrosion patterns attributed to inflammatory cell-induced corrosion: A retrieval study. *Journal of Biomedical Materials Research - Part B Applied Biomaterials,* 105**,** 155-164.

DI PRIMA, M. A., VESNOVSKY, O., KOVACS, P., HOPPER, R. H., HO, H., ENGH, C. A. & TOPOLESKI, L. D. T. 2015. Comparison of Visual Assessment Techniques for Wear and Corrosion in Modular Hip Replacement Systems. *In:* A, G., STEVEN, K., JACK, L. & WILLIAM, M. (eds.) *Modularity and Tapers in Total Joint Replacement Devices STP1591.* West Conshohocken, PA: ASTM International

DONALDSON, F. E., COBURN, J. C. & SIEGEL, K. L. 2014. Total hip arthroplasty head-neck contact mechanics: A stochastic investigation of key parameters. *Journal of Biomechanics,* 47**,** 1634-41.

DOS SANTOS, C. T., BARBOSA, C., MONTEIRO, M. J., ABUD, I. C., CAMINHA, I. M. V. & ROESLER, C. R. M. 2016. Characterization of the fretting corrosion behavior, surface and debris from head-taper interface of two different modular hip prostheses. *Journal of the Mechanical Behavior of Biomedical Materials,* 62**,** 71-82.

DROUIN, J. M. & CALES, B. 1994. Yttria-Stabilized Zirconia Ceramic for Improved Hip Joint Head *In:* ANDERSSON, O. H., HAPPONEN, R.-P. & YLI-URPO, A. (eds.) *Bioceramics* Oxford: Butterworth-Heinemann Ltd.

DUDA, G. N., KONIG,C., BERGMANN, G., TOHTZ, S., PERKA, C., HELLER, M.O.W 2013. Biomechanics of the Artificial Hip. *In:* BERRY, D. M. L., JAY. (ed.) *Surgery of the Hip.* Saunders.

DUFILS, J., LAURENT, M. P., KUNZE, J., ROYHMAN, D., MATHEW, M. T., FRIDRICI, V. & WIMMER, M. A. 2015. A Servoelectric Apparatus with Potentiostat to Study the Fretting Corrosion of Cobalt-Chromium–Titanium Alloy Couples. *In:* A, G., STEVEN, K., JACK, L. & WILLIAM, M. (eds.) *Modularity and Tapers in Total Joint Replacement Devices STP1591.* West Conshohocken, PA: ASTM International

DYRKACZ, R. M. R., BRANDT, J.-M., OJO, O. A., TURGEON, T. R. & WYSS, U. P. 2013. The Influence of Head Size on Corrosion and Fretting Behaviour at the Head-Neck Interface of Artificial Hip Joints. *The Journal of arthroplasty,* 28**,** 1036-1040.

ELKINS, J., CALLAGHAN, J. & BROWN, T. 2014. Stability and Trunnion Wear Potential in Large-diameter Metal-on-Metal Total Hips: A Finite Element Analysis. *Clinical Orthopaedics and Related Research,* 472**,** 529-542.

ELTIT, F., ASSIRI, A., GARBUZ, D., DUNCAN, C., MASRI, B., GREIDANUS, N., BELL, R., SHARMA, M., COX, M. & WANG, R. 2017. Adverse reactions to metal on polyethylene implants: Highly destructive lesions related to elevated concentration of cobalt and chromium in synovial fluid. *Journal of Biomedical Materials Research, Part A,* 105**,** 1876-1886.

ENGLISH, R., ASHKANFAR, A. & ROTHWELL, G. 2016. The effect of different assembly loads on taper junction fretting wear in total hip replacements. *Tribology International,* 95**,** 199-210.

ESPALLARGAS, N., TORRES, C. & MUÑOZ, A. I. 2015. A metal ion release study of CoCrMo exposed to corrosion and tribocorrosion conditions in simulated body fluids. *Wear,* 332**,** 669-678.

ESPOSITO, C. I., WRIGHT, T. M., GOODMAN, S. B., BERRY, D. J., THE CLINICAL, B. & BIOENGINEERING STUDY GROUPS FROM THE CARL, T. B. W. 2014. What is the Trouble With Trunnions? *Clinical Orthopaedics and Related Research,* 472**,** 3652-3658.

ESSNER, A. & WANG, A. 2010. Tribological Assessment of UHMWPE in the Hip. *In:* KURTZ, S. M. (ed.) *UHMWPE Biomaterials Handbook - Ultra-High Molecular Weight Polyethylene in Total Joint Replacement and Medical Devices* Elsevier.

EXATECH 2012. The Dangers of Big Femoral Heads on Thin Polyethylene: The Missing Part of the Equation. *Technical Profiles,* 711-12-81 Rev. A.

FARHOUDI, H., OSKOUEI, H. R., PASHA ZANOOSI, A. A., JONES, F. C. & TAYLOR, M. 2016. An Analytical Calculation of Frictional and Bending Moments at the Head-Neck Interface of Hip Joint Implants during Different Physiological Activities. *Materials,* 9.

FDA 1995. Guidance Document for the Preparation of Premarket Notification for Ceramic Ball Hip Systems. Rockville, MD.

FEHRING, K. A. & FEHRING, T. K. 2015. Modes of Failure in Metal-on-Metal Total Hip Arthroplasty. *Orthopedic Clinics of North America,* 46**,** 185-92.

FEHRING, T. K., ODUM, S., SPROUL, R. & WEATHERSBEE, J. 2014. High frequency of adverse local tissue reactions in asymptomatic patients with metal-on-metal THA. *Clinical Orthopaedics and Related Research,* 472**,** 517-22.

FERBER, R. & MACDONALD, S. 2014. *Running Mechanics and Gait Analysis,* Illinois, Human Kinetics.

FISHER, J. 2011. Bioengineering reasons for the failure of metal-on-metal hip prostheses, an Engineer's perspective. *Bone & Joint Journal,* 93-B**,** 1001-1004.

FONTANA, M. G. 2005. *Corrosion engineering*, Tata McGraw-Hill Education.

FORD, M. C., HARKESS, J. W. & MIHALKO, W. M. 2015. Orthopaedic Surgeon Modularity Utilization and Surgical Technique Considerations in the Face of Implant Corrosion. *In:* A, G., STEVEN, K., JACK, L. & WILLIAM, M. (eds.) *Modularity and Tapers in Total Joint Replacement Devices STP1591.* West Conshohocken, PA: ASTM International

FRICKA, K. B., HO, H., PEACE, W. J. & ENGH, C. A. 2012. Metal-on-Metal Local Tissue Reaction Is Associated With Corrosion of the Head Taper Junction. *The Journal of Arthroplasty,* 27**,** 26-31.e1.

GADELMAWLAA, E. S., KOURAB, M. M., MAKSOUDC, T. M. A., ELEWA, I. M. & SOLIMAN, H. H. 2002. Roughness parameters. *Journal of Materials Processing Technology* 123**,** 133-145.

GILBERT, J. L. (ed.) 2012. *Mechanically Assisted Corrosion of Metallic Biomaterials*: ASM International

GILBERT, J. L., BUCKLEY, C. A. & JACOBS, J. J. 1993. In vivo corrosion of modular hip prosthesis components in mixed and similar metal combinations. The effect of crevice, stress, motion, and alloy coupling. *Journal of Biomedical Materials Research,* 27**,** 1533-1544.

GILBERT, J. L., MALI, S. A. & SIVAN, S. 2015a. Corrosion of Modular Tapers in Total Joint Replacements: A Critical Assessment of Design, Materials, Surface Structure, Mechanics, Electrochemistry, and Biology. *In:* A, G., STEVEN, K., JACK, L. & WILLIAM, M. (eds.) *Modularity and Tapers in Total Joint Replacement Devices STP1591.* West Conshohocken, PA: ASTM International

GILBERT, J. L., MEHTA, M. & PINDER, B. 2009. Fretting crevice corrosion of stainless steel stem–CoCr femoral head connections: comparisons of materials, initial moisture, and offset length. *Journal of Biomedical Materials Research Part B: Applied Biomaterials,* 88**,** 162-173.

GILBERT, J. L., SIVAN, S., LIU, Y., KOCAGOZ, S. B., ARNHOLT, C. M. & KURTZ, S. M. 2015b. Direct in vivo inflammatory cell-induced corrosion of CoCrMo alloy orthopedic implant surfaces. *J Biomed Mater Res A,* 103**,** 211-23.

GIRARD, J. 2015. Femoral head diameter considerations for primary total hip arthroplasty. *Orthopaedics & Traumatology: Surgery & Research,* 101**,** S25-S29.

GOLDBERG, J. R., BUCKLEY, C. A., JACOBS, J. J. & GILBERT, J. L. 1997. Corrosion Testing of Modular Hip Implants. *In:* MARLOWE, D. E., PARR, J. E. & MAYOR, M. B. (eds.) *Modularity of Orthopedic Implants STP1301.* West Conshohocken, PA: ASTM

GOLDBERG, J. R. & GILBERT, J. L. 1997. Electrochemical response of CoCrMo to high-speed fracture of its metal oxide using an electrochemical scratch test method. *Journal of Biomedical Materials Research,* 37**,** 421-31.

GOLDBERG, J. R. & GILBERT, J. L. 2003. In vitro corrosion testing of modular hip tapers. *Journal of Biomedical Materials Research, Part B Applied Biomaterials,* 64B**,** 78-93.

GOLDBERG, J. R., GILBERT, J. L., JACOBS, J. J., BAUER, T. W., PAPROSKY, W. & LEURGANS, S. 2002. A multicenter retrieval study of the taper interfaces of modular hip prostheses. *Clinical Orthopaedics and Related Research***,** 149-61.

GOYAL, N., HO, H., FRICKA, K. B. & ENGH, C. A., JR. 2014. Do you have to remove a corroded femoral stem? *The Journal of Arthroplasty,* 29**,** 139-42.
GROSTEFON, J. & NELSON, W. 2017. HIP TAPER CORROSION STUDY OF SEALED TAPERS. *Bone & Joint Journal Orthopaedic Proceedings Supplement,* 99-B**,** 146.
GRUPP, T. M., WEIK, T., BLOEMER, W. & KNAEBEL, H.-P. 2010. Modular titanium alloy neck adapter failures in hip replacement - failure mode analysis and influence of implant material. *BMC Musculoskeletal Disorders,* 11**,** 3.
HADLEY, M., HARDAKER, C., WILLIAMS, S., JIN, Z., ISAAC, G. & FISHER, J. 2013. Development of a Stop-Dwell-Start (SDS) Protocol for In Vitro Wear Testing of Metal-on-Metal Total Hip Replacements. *In:* KURTZ, S. M., GREENWALD, A. S., MIHALKO, W. M. & LEMONS, J. E. (eds.) *Selected Technical Papers STP1560 Metal-On-Metal Total Hip Replacement Devices.* West Conshohocken, PA: ASTM International.
HADLEY, M. J. F. 2012. *Long term functional simulation of large diameter metal on metal hip implants.* PhD, University of Leeds.
HALL, D. J., POURZAL, R., DELLA VALLE, C. J., GALANTE, J. O., JACOBS, J. J. & URBAN, R. M. 2015. Corrosion of Modular Junctions in Femoral and Acetabular Components for Hip Arthroplasty and Its Local and Systemic Effects. *In:* A, G., STEVEN, K., JACK, L. & WILLIAM, M. (eds.) *Modularity and Tapers in Total Joint Replacement Devices STP1591.* West Conshohocken, PA: ASTM International
HALLOWS, R. K., PELT, C. E., ERICKSON, J. A. & PETERS, C. L. 2011. Serum Metal Ion Concentration: Comparison Between Small and Large Head Metal-on-Metal Total Hip Arthroplasty. *The Journal of Arthroplasty,* 26**,** 1176-1181.
HAMROCK, B. J. & DOWSON, D. 1978. Elastohydrodynamic Lubrication of Elliptical Contacts for Materials of Low Elastic Modulus I—Fully Flooded Conjunction. *Journal of Lubrication Technology,* 100**,** 236-245.
HANSEN, D. C. 2008. Metal corrosion in the human body: The ultimate bio-corrosion scenario. *The Electrochemical Society Interface* 17**,** 31-34.
HARMAND, M. F. 1995. In vitro study of biodegradation of a Co-Cr alloy using a human cell culture model. *Journal of Biomaterials Science, Polymer Edition,* 6**,** 809-14.
HART, A. J., MATTHIES, A., BILLS, P. J., RACASAN, R., BLUNN, G., BLUNT, L. & SKINNER, J. 2013. The taper junction contributes one third of the total volumetric material loss in large diameter metal-on-metal hip arthroplasties. *American Academy of Orthopaedic Surgeons Annual Meeting.* Chicago, IL, USA.
HENTHORN, M. 1981. *Localized Corrosion- Cause of Metal Failure STP 516*, American Society for Testing and Materials.
HERNIGOU, P., QUEINNEC, S. & FLOUZAT, L. C. H. 2013. One hundred and fifty years of history of the Morse taper: from Stephen A. Morse in 1864 to complications related to modularity in hip arthroplasty. *International Orthopaedics,* 37**,** 2081-2088.
HESKETH, J., HU, X., YAN, Y., DOWSON, D. & NEVILLE, A. 2013. Biotribocorrosion: Some electrochemical observations from an instrumented hip joint simulator. *Tribology International,* 59**,** 332-338.
HEXTER, A., PANAGIOTIDOU, A., SINGH, J., SKINNER, J. & HART, A. 2013. Corrosion at the head-trunnion taper interface in large diameter head metal-on-metal total hip arthroplasty: A comparison of five manufacturers. *Bone & Joint Journal Orthopaedic Proceedings Supplement,* 95-B**,** 3.
HIGGS, G. B., HANZLIK, J. A., MACDONALD, D. W., GILBERT, J. L., RIMNAC, C. M. & KURTZ, S. M. 2013. Is increased modularity associated with increased fretting and corrosion damage in metal-on-metal total hip arthroplasty devices?: a retrieval study. *The Journal of Arthroplasty,* 28**,** 2-6.

HIGGS, G. B., MACDONALD, D. W., GILBERT, J. L., RIMNAC, C. M., KURTZ, S. M., CHEN, A. F., KLEIN, G. R., HAMLIN, B. R., LEE, G.-C., MONT, M. A., CATES, H. E., MALKANI, A. L. & KRAAY, M. J. 2016. Does Taper Size Have an Effect on Taper Damage in Retrieved Metal-on-Polyethylene Total Hip Devices? *The Journal of Arthroplasty,* 31**,** 277-281.

HIROMOTO, S., NODA, K. & HANAWA, T. 2002. Development of electrolytic cell with cell-culture for metallic biomaterials. *Corrosion Science,* 44**,** 955-965.

HOLZWARTH, U. & COTOGNO, G. 2012. Total hip arthroplasty : State of the art, prospects and challenges. European Commision Joint Research Centre.

HOTHI, H. S., BERBER, R., WHITTAKER, R. K., BLUNN, G. W., SKINNER, J. A. & HART, A. J. 2016a. The Relationship Between Cobalt/Chromium Ratios and the High Prevalence of Head-Stem Junction Corrosion in Metal-on-Metal Total Hip Arthroplasty. *The Journal of Arthroplasty,* 31**,** 1123-1127.

HOTHI, H. S., ESKELINEN, A. P., BERBER, R., LAINIALA, O. S., MOILANEN, T. P., SKINNER, J. A. & HART, A. J. 2016b. Factors Associated With Trunnionosis in the Metal-on-Metal Pinnacle Hip. *The Journal of Arthroplasty,* 32**,** 286-290.

HOTHI, H. S., KENDOFF, D., LAUSMANN, C., HENCKEL, J., GEHRKE, T., SKINNER, J. & HART, A. 2017a. Clinically insignificant trunnionosis in large-diameter metal-on-polyethylene total hip arthroplasty. *Bone & Joint Research,* 6**,** 52-56.

HOTHI, H. S., PANAGIOTOPOULOS, A. C., WHITTAKER, R. K., BILLS, P. J., MCMILLAN, R. A., SKINNER, J. A. & HART, A. J. 2017b. Damage Patterns at the Head-Stem Taper Junction Helps Understand the Mechanisms of Material Loss. *The Journal of Arthroplasty,* 32**,** 291-295.

HOTHI, H. S., WHITTAKER, R. K., MESWANIA, J. M., BLUNN, G. W., SKINNER, J. A. & HART, A. J. 2015. Influence of stem type on material loss at the metal-on-metal pinnacle taper junction. *Proceedings of the Institution of Mechanical Engineers, Part H: Journal of Engineering in Medicine,* 229**,** 91-97.

HUBER, M., REINISCH, G., TRETTENHAHN, G., ZWEYMÜLLER, K. & LINTNER, F. 2009. Presence of corrosion products and hypersensitivity-associated reactions in periprosthetic tissue after aseptic loosening of total hip replacements with metal bearing surfaces. *Acta Biomaterialia,* 5**,** 172-180.

HUGHES, P. J., BROWN, S. A., PAYER, J. H. & MERRITT, K. 1990. The effects of heat treatments and bead size on the corrosion of porous F75 in saline and serum. *Journal of Biomedical Materials Research,* 24**,** 79-94.

HUSSENBOCUS, S., KOSUGE, D., SOLOMON, L. B., HOWIE, D. W. & OSKOUEI, R. H. 2015. Head-Neck Taper Corrosion in Hip Arthroplasty. *BioMedical Research International,* 2015**,** 9.

ISAAC, G. H., THOMPSON, J., WILLIAMS, S. & FISHER, J. 2006. Metal-on-metal bearings surfaces: Materials, manufacture, design, optimization, and alternatives. *Proceedings of the Institution of Mechanical Engineers, Part H: Journal of Engineering in Medicine,* 220**,** 119-133.

JACOBS, J. J. 2016. Corrosion at the Head-Neck Junction: Why Is This Happening Now? *The Journal of Arthroplasty,* 31**,** 1378-80.

JACOBS, J. J., GILBERT, J. L. & URBAN, R. M. 1998. Corrosion of metal orthopaedic implants. *Journal of Bone & Joint Surgery, American Volume,* 80-A**,** 268-282.

JANI, S., SAUER, W., MCLEAN, T., LAMBERT, R. & KOVACS, P. 1997. Fretting Corrosion Mechanisms at Modular Implant Interfaces. *In:* MARLOWE, D., PARR, J. & MAYOR, M. (eds.) *Modularity of Orthopedic Implants STP1301.* West Conshohocken, PA: ASTM International.

JAUCH-MATT, S. Y., MILES, A. W. & GILL, H. S. 2017. Effect of trunnion roughness and length on the modular taper junction strength under typical intraoperative assembly forces. *Medical Engineering & Physics,* 39**,** 94-101.

JAUCH, S. Y., HUBER, G., HOENIG, E., BAXMANN, M., GRUPP, T. M. & MORLOCK, M. M. 2011. Influence of material coupling and assembly condition on the magnitude of micromotion at the stem-neck interface of a modular hip endoprosthesis. *Journal of Biomechanics,* 44**,** 1747-51.

JAUCH, S. Y., HUBER, G., SELLENSCHLOH, K., HASCHKE, H., BAXMANN, M., GRUPP, T. M. & MORLOCK, M. M. 2013. Micromotions at the Taper Interface Between Stem and Neck Adapter of a Bimodular Hip Prosthesis During Activities of Daily Living. *Journal of Orthopaedic Research,* 31**,** 1165-71.

JENNINGS, J. M., DENNIS, D. A. & YANG, C. C. 2016. Corrosion of the Head-neck Junction After Total Hip Arthroplasty. *Journal of the American Academy of Orthopaedic Surgeons,* 24**,** 349-56.

JIN, Z. M., FISHER, J. & INGHAM, E. 2006a. Biotribology: Material Design, Lubrication, and Wear in Artificial Hip Joints. *In:* TOTTEN, G. E. (ed.) *Handbook of Lubrication and Tribology: Volume I Application and Maintenance.* Second ed.: CRC Press.

JIN, Z. M., STONE, M., INGHAM, E. & FISHER, J. 2006b. (v) Biotribology. *Current Orthopaedics,* 20**,** 32-40.

JOHNSTON, I. D., MCCLUSKEY, D. K., TAN, C. K. L. & TRACEY, M. C. 2014. Mechanical characterization of bulk Sylgard 184 for microfluidics and microengineering. *Journal of Micromechanics and Microengineering,* 24**,** 035017.

JOHNSTON, R. C., NOBLE, P. C., HURWITZ, D. E. & ANDRIACCHI, T. P. 2007. Biomechanics of the Hip. *In:* CALLAGHAN, J. J., ROSENBERG, A. G. & RUBASH, H. E. (eds.) *The Adult Hip.* Baltimore: Lippincott Williams & Wilkins.

KAO, Y.-Y. J., KOCH, C. N., WRIGHT, T. M. & PADGETT, D. E. 2016. Flexural Rigidity, Taper Angle, and Contact Length Affect Fretting of the Femoral Stem Trunnion in Total Hip Arthroplasty. *The Journal of Arthroplasty,* 31**,** 254-258.

KARIMI, S. 2014. *Corrosion Behaviour of Metallic Bio-implant Alloys.* PhD, University of British Columbia.

KARIMI, S., NICKCHI, T. & ALFANTAZI, A. M. 2012. Long-term corrosion investigation of AISI 316L, Co–28Cr–6Mo, and Ti–6Al–4V alloys in simulated body solutions. *Applied Surface Science,* 258**,** 6087-6096.

KASSI, J. P., HELLER, M. O., STOECKLE, U., PERKA, C. & DUDA, G. N. 2005. Stair climbing is more critical than walking in pre-clinical assessment of primary stability in cementless THA in vitro. *Journal of Biomechanics,* 38**,** 1143-54.

KHAIR, M. M., NAM, D., DICARLO, E. & SU, E. 2013. Aseptic Lymphocyte Dominated Vasculitis-Associated Lesion Resulting From Trunnion Corrosion in a Cobalt-Chrome Unipolar Hemiarthroplasty. *The Journal of Arthroplasty,* 28**,** 196.e11-196.e14.

KHAN, M. A., WILLIAMS, R. L. & WILLIAMS, D. F. 1999. The corrosion behaviour of Ti–6Al–4V, Ti–6Al–7Nb and Ti–13Nb–13Zr in protein solutions. *Biomaterials,* 20**,** 631-637.

KNUTSEN, A., PARK, S.-H., EBRAMZADEH, E. & CAMPBELL, P. 2015. The Importance of Cleaning Modular Parts on Visual Scores of Taper Damage. *In:* A, G., STEVEN, K., JACK, L. & WILLIAM, M. (eds.) *Modularity and Tapers in Total Joint Replacement Devices STP1591.* West Conshohocken, PA: ASTM International

KOCAGOZ, S. B., UNDERWOOD, R. J., MACDONALD, D. W., GILBERT, J. L. & KURTZ, S. M. 2016. Ceramic Heads Decrease Metal Release Caused by Head-taper Fretting and Corrosion. *Clinical Orthopaedics and Related Research,* 474**,** 985-994.

KOCAGÖZ, S. B., UNDERWOOD, R. J., SIVAN, S., GILBERT, J. L., MACDONALD, D. W., DAY, J. S. & KURTZ, S. M. 2013. Does taper angle clearance influence fretting and

corrosion damage at the head–stem interface? A matched cohort retrieval study. *Seminars in Arthroplasty,* 24**,** 246-254.
KOPER, M. C., MATHIJSSEN, N. M. C., WITT, F., MORLOCK, M. M. & VEHMEIJER, S. B. W. 2015. Severe Wear and Pseudotumor Formation Due to Taper Mismatch in a Total Hip Arthroplasty. *JBJS Case Connector,* 5**,** e29.
KRISHNAN, H., KRISHNAN, S. P., BLUNN, G., SKINNER, J. A. & HART, A. J. 2013. Modular neck femoral stems. *Bone & Joint Journal,* 95-B**,** 1011-21.
KRULL, A., MORLOCK, M. M. & BISHOP, N. E. 2017. The Influence of Contamination and Cleaning on the Strength of Modular Head Taper Fixation in Total Hip Arthroplasty. *The Journal of Arthroplasty***,** 1-6.
KUNG, S. M., MARKANTONIS, J., NELSON, D. S. & CAMPBELL, P. 2015. The Synovial Lining and Synovial Fluid Properties after Joint Arthroplasty. *Lubricants,* 3**,** 394-412.
KURTZ, S., K, O., LAU, E., MOWAT, F. & HALPERN, M. 2007. Projections of primary and revision hip and knee arthroplasty in the United States from 2005 to 2030. *Journal of Bone & Joint Surgery, American Volume,* 89**,** 780-5.
KURTZ, S. M. 2010. UHMWPE Biomaterials Handbook - Ultra-High Molecular Weight Polyethylene in Total Joint Replacement and Medical Devices 2nd ed.: Elsevier.
KURTZ, S. M., KOCAGÖZ, S. B., HANZLIK, J. A., UNDERWOOD, R. J., GILBERT, J. L., MACDONALD, D. W., LEE, G.-C., MONT, M. A., KRAAY, M. J., KLEIN, G. R., PARVIZI, J. & RIMNAC, C. M. 2013. Do Ceramic Femoral Heads Reduce Taper Fretting Corrosion in Hip Arthroplasty? A Retrieval Study. *Clinical Orthopaedics and Related Research,* 471**,** 3270-3282.
KWON, Y. M., XIA, Z., GLYN-JONES, S., BEARD, D., GILL, H. S. & MURRAY, D. W. 2009. Dose-dependent cytotoxicity of clinically relevant cobalt nanoparticles and ions on macrophages in vitro. *Biomedical Materials,* 4**,** 025018.
LANGTON, D. J. (ed.) 2014. *Are Metal Ion Levels a Triggest for Surgical Intervention?*: Springer-Verlag New York.
LANGTON, D. J., JAMESON, S. S., JOYCE, T. J., HALLAB, N. J., NATU, S. & NARGOL, A. V. F. 2010. Early failure of metal-on-metal bearings in hip resurfacing and large-diameter total hip replacement, A Consequence of Excess Wear. *Bone & Joint Journal,* 92-B**,** 38-46.
LANGTON, D. J., SIDAGINAMALE, R., LORD, J. K., NARGOL, A. V. & JOYCE, T. J. 2012. Taper junction failure in large-diameter metal-on-metal bearings. *Bone & Joint Research,* 1**,** 56-63.
LANGTON, D. J., SIDAGINAMALE, R. P., AVERY, P., WALLER, S., TANK, G., LORD, J., JOYCE, T., COOKE, N., LOGISHETTY, R. & NARGOL, A. V. F. 2016. Retrospective cohort study of the performance of the Pinnacle metal on metal (MoM) total hip replacement: a single-centre investigation in combination with the findings of a national retrieval centre. *BMJ Open,* 6**,** e007847.
LANTING, B., NAUDIE, D. D. & MCCALDEN, R. W. 2016. Clinical Impact of Trunnion Wear After Total Hip Arthroplasty. *JBJS Reviews,* 4**,** e4.
LASS, R., GRÜBL, A., KOLB, A., STELZENEDER, D., PILGER, A., KUBISTA, B., GIUREA, A. & WINDHAGER, R. 2014. Comparison of synovial fluid, urine, and serum ion levels in metal-on-metal total hip arthroplasty at a minimum follow-up of 18 years. *Journal of Orthopaedic Research,* 32**,** 1234-1240.
LATHAM, J., COOK, R., BOLLAND, B. & YASEN, S. 2013. Big Heads on Stems - What Have We Learned? *Bone & Joint Journal Orthopaedic Proceedings Supplement,* 95-B**,** 115.
LAVERNIA, C. J., BAERGA, L., BARRACK, R. L., TOZAKOGLOU, E., COOK, S. D., LATA, L. & ROSSI, M. D. 2009. The effects of blood and fat on Morse taper disassembly forces. *American Journal of Orthopedics (Belle Mead NJ).* 38**,** 187-277.

LAVERNIA, C. J., EMERSON, C. P., VILLA, J. M. & COOK, S. D. 2015. Trunnion Options in Primary Total Hip Arthroplasty in 2014. *In:* GREENWALD, A., KURTZ, S., LEMONS, J. & MIHALKO, W. (eds.) *Modularity and Tapers in Total Joint Replacement Devices STP1591.* West Conshohocken, PA: ASTM International

LEE, D. W. & HWANG, S. K. 2014. Primary Total Hip Arthroplasty Using Third Generation Ceramic-Ceramic Articulation: Results after a Minimum of Three-years of Follow-up. *Hip & Pelvis,* 26**,** 84-91.

LEVICK, J. R. & MCDONALD, J. N. 1995. Fluid movement across synovium in healthy joints: role of synovial fluid macromolecules. *Annals of the Rheumatic Diseases,* 54**,** 417-423.

LEVINE, B. R., HSU, A. R., SKIPOR, A. K., HALLAB, N. J., PAPROSKY, W. G., GALANTE, J. O. & JACOBS, J. J. 2013. Ten-Year Outcome of Serum Metal Ion Levels After Primary Total Hip Arthroplasty: A Concise Follow-up of a Previous Report. *Journal of Bone & Joint Surgery, American volume,* 95**,** 512-518.

LEVINSON, R. 2001. *More Modern Chemical Techniques*, Royal Society of Chemistry

LEWIS, A., KILBURN, M., PAPAGEORGIOU, I., ALLEN, G. & CASE, C. 2005. Effect of synovial fluid, phosphate‐buffered saline solution, and water on the dissolution and corrosion properties of CoCrMo alloys as used in orthopedic implants. *Journal of Biomedical Materials Research Part A,* 73**,** 456-467.

LEWIS, A. C., KILBURN, M. R., HEARD, P. J., SCOTT, T. B., HALLAM, K. R., ALLEN, G. C. & LEARMONTH, I. D. 2006. The entrapment of corrosion products from CoCr implant alloys in the deposits of calcium phosphate: a comparison of serum, synovial fluid, albumin, EDTA, and water. *Journal of Orthopaedic Research,* 24**,** 1587-96.

LI, C., PARIKH, A., SPRAGUE, J. & PAWAR, V. 2015. Mechanically Assisted Crevice Corrosion on CoCrMo Heads after Long-term Hip Simulator Wear Testing. *Orthopaedic Research Society Annual Meeting* Nevada, Las Vegas.

LIAO, Y., HOFFMAN, E., WIMMER, M., FISCHER, A., JACOBS, J. & MARKS, L. 2013. CoCrMo Metal-on-Metal Hip Replacements. *Physical Chemistry Chemical Physics* 15**,** 746-56.

LIEBERMAN, J. R., RIMNAC, C. M., GARVIN, K. L., KLEIN, R. W. & SALVATI, E. A. 1994. An analysis of the head-neck taper interface in retrieved hip prostheses. *Clinical Orthopaedics and Related Research,* 300**,** 162-167.

LIN, H.-Y. & BUMGARDNER, J. D. 2004. In vitro biocorrosion of Co□Cr□Mo implant alloy by macrophage cells. *Journal of Orthopaedic Research,* 22**,** 1231-1236.

LINDGREN, J. U., BRISMAR, B. H. & WIKSTROM, A. C. 2011. Adverse reaction to metal release from a modular metal-on-polyethylene hip prosthesis. *Journal of Bone & Joint Surgery, British Volume,* 93-B**,** 1427-30.

LIODAKIS, E., CARLI, A., ZUKOR, D., HUK, O. & ANTONIOU, J. 2015. Corrosion at the Head-Neck Taper Interface Affects the Prognosis of Hip Revision Surgery. *In:* A, G., STEVEN, K., JACK, L. & WILLIAM, M. (eds.) *Modularity and Tapers in Total Joint Replacement Devices STP1591.* West Conshohocken, PA: ASTM International

LIU, Y. & GILBERT, J. L. 2017. The effect of simulated inflammatory conditions and Fenton chemistry on the electrochemistry of CoCrMo alloy. *Journal of Biomedical Materials Research Part B: Applied Biomaterials***,** n/a-n/a.

LOMBARDI, A. V., BEREND, K. R., ADAMS, J. B. & SATTERWHITE, K. L. 2016. Adverse Reactions to Metal on Metal Are Not Exclusive to Large Heads in Total Hip Arthroplasty. *Clinical Orthopaedics and Related Research,* 474**,** 432-440.

LUNDBERG, H. J., HA, N. Q., HALL, D. J., URBAN, R. M., LEVINE, B. R. & POURZAL, R. 2015. Contact Mechanics and Plastic Deformation at the Local Surface Topography Level After Assembly of Modular Head-Neck Junctions in Modern Total Hip Replacement Devices. *In:* A, G., STEVEN, K., JACK, L. & WILLIAM, M. (eds.)

Modularity and Tapers in Total Joint Replacement Devices STP1591. West Conshohocken, PA: ASTM International

MACDONALD, S. J., MCCALDEN, R. W., CHESS, D. G., BOURNE, R. B., RORABECK, C. H., CLELAND, D. & LEUNG, F. 2003. Metal-on-Metal Versus Polyethylene in Hip Arthroplasty: A Randomized Clinical Trial. *Clinical Orthopaedics and Related Research,* 406**,** 282-296.

MACLEOD, A. R., SULLIVAN, N. P., WHITEHOUSE, M. R. & GILL, H. S. 2016. Large-diameter total hip arthroplasty modular heads require greater assembly forces for initial stability. *Bone & Joint Research,* 5**,** 338-46.

MADL, A. K., KOVOCHICH, M., LIONG, M., FINLEY, B. L., PAUSTENBACH, D. J. & OBERDÖRSTER, G. 2015. Toxicology of wear particles of cobalt-chromium alloy metal-on-metal hip implants Part II: Importance of physicochemical properties and dose in animal and in vitro studies as a basis for risk assessment. *Nanomedicine: Nanotechnology, Biology and Medicine,* 11**,** 1285-1298.

MALI, S. A. 2016. Mechanically assisted crevice corrosion in metallic biomaterials: a review. *Materials Technology,* 31**,** 732-739.

MALI, S. A. & GILBERT, J. L. 2015. Correlating fretting corrosion and micromotions in modular tapers: Test method development and assessment. *In:* A, G., STEVEN, K., JACK, L. & WILLIAM, M. (eds.) *Modularity and Tapers in Total Joint Replacement Devices STP1591.* West Conshohocken, PA: ASTM International

MALIK, S. S. & MALIK, S. S. 2015. *Orthopaedic Biomechanics Made Easy*, Cambridge Univeristy Press.

MANTHE, M., BLASSER, K., BEAUCHAMP, C. & O'CONNOR, M. I. 2016. Trunnion Corrosion Causing Failure in Metal-on-Polyethylene Total Hip Arthroplasty with Monolithic Femoral Components *Reconstructive Review,* 6.

MAO, X., TAY, G. H., GODBOLT, D. B. & CRAWFORD, R. W. 2012. Pseudotumor in a well-fixed metal-on-polyethylene uncemented hip arthroplasty. *The Journal of Arthroplasty,* 27**,** 493.e13–493.e17.

MARTIN, J. R., CAMP, C. L., WYLES, C. C., TAUNTON, M. J., TROUSDALE, R. T. & LEWALLEN, D. G. 2016. Increased Femoral Head Offset is Associated With Elevated Metal Ions in Asymptomatic Patients With Metal-on-Polyethylene Total Hip Arthroplasty. *The Journal of Arthroplasty,* 31**,** 2814-2818.

MATHARU, G. S., NANDRA, R. S., BERRYMAN, F., JUDGE, A., PYNSENT, P. B. & DUNLOP, D. J. 2017. Risk factors for failure of the 36 mm metal-on-metal Pinnacle total hip arthroplasty system, a retrospective single-centre cohort study. *Bone & Joint Journal,* 99-B**,** 592-600.

MATTEI, L., DI PUCCIO, F., PICCIGALLO, B. & CIULLI, E. 2011. Lubrication and wear modelling of artificial hip joints: A review. *Tribology International,* 44**,** 532-549.

MATTHIES, A. K., RACASAN, R., BILLS, P., BLUNT, L., CRO, S., PANAGIOTIDOU, A., BLUNN, G., SKINNER, J. & HART, A. J. 2013. Material loss at the taper junction of retrieved large head metal-on-metal total hip replacements. *Journal of Orthopaedic Research,* 31**,** 1677-1685.

MCCANN, L., INGHAM, E., JIN, Z. & FISHER, J. 2009. Influence of the meniscus on friction and degradation of cartilage in the natural knee joint. *Osteoarthritis and Cartilage,* 17**,** 995-1000.

MCGRORY, B. J. & MCKENNEY, B. R. 2016. Revision for taper corrosion at the head-neck junction: pearls and pitfalls. *Current Reviews in Musculoskeletal Medicine,* 9**,** 97-102.

MCGRORY, B. J., PAYSON, A. M. & MACKENZIE, J. A. 2017. Elevated Intra-Articular Cobalt and Chromium Levels in Mechanically Assisted Crevice Corrosion in Metal-on-Polyethylene Total Hip Arthroplasty. *The Journal of Arthroplasty,* 32**,** 1654-1658.

MCTIGHE, T., BRAZIL, D., CLARKE, I., KEPPLER, L., KEGGI, J., TKACH, T. & MCPHERSON, E. 2015. Metallic Modular Taper Junctions in Total Hip Arthroplasty. *Reconstructive Review,* 5.

MEADE, C. L. 1999. Accelerated corrosion testing. *Metal Finishing,* 97**,** 526-531.

MENEGHINI, R. M., LOVRO, L. R., WALLACE, J. M. & ZIEMBA-DAVIS, M. 2016. Large Metal Heads and Vitamin E Polyethylene Increase Frictional Torque in Total Hip Arthroplasty. *The Journal of Arthroplasty,* 31**,** 710-714.

MEYER, H., MUELLER, T., GOLDAU, G., CHAMAON, K., RUETSCHI, M. & LOHMANN, C. 2012. Corrosion at the Cone/Taper Interface Leads to Failure of Large-diameter Metal-on-metal Total Hip Arthroplasties. *Clinical Orthopaedics and Related Research,* 470**,** 3101-3108.

MILOŠEV, I. 2012. CoCrMo Alloy for Biomedical Applications. *In:* DJOKIĆ, S. S. (ed.) *Biomedical Applications* Springer

MILOŠEV, I., LEVAŠIČ, V., VIDMAR, J., KOVAČ, S. & TREBŠE, R. 2016. pH and metal concentration of synovial fluid of osteoarthritic joints and joints with metal replacements. *Journal of Biomedical Materials Research Part B: Applied Biomaterials***,** n/a-n/a.

MOGA, I., HARRINGTON, M. A., ISMAILY, S. & NOBLE, P. 2013. Trunnion Surface Damage in THR: MPE vs MOM Articulations. *Bone & Joint Journal Orthopaedic Proceedings Supplement,* 95-B**,** 140.

MOHARRAMI, N., LANGTON, D. J., SAYGINER, O. & BULL, S. J. 2013. Why does titanium alloy wear cobalt chrome alloy despite lower bulk hardness: A nanoindentation study? *Thin Solid Films,* 549**,** 79-86.

MONTASER, A. 1998. *Inductively Coupled Plasma Mass Spectrometry,* New York, Wiley-VCH.

MOORE, K. D., BECK, P. R., PETERSEN, D. W., CUCKLER, J. M., LEMONS, J. E. & EBERHARDT, A. W. 2008. Early Failure of a Cross-Linked Polyethylene Acetabular Liner: A Case Report. *Journal of Bone & Joint Surgery, American volume,* 90**,** 2499-2504.

MORLEY, D., STARKS, I. & LIM, J. 2012. A Case of a C-Stem Fracture at the Head-Neck Junction and a Review of the Literature. *Case Reports in Orthopedics,* 2012**,** 4.

MORLOCK, M., BÜNTE, D., GÜHRS, J. & BISHOP, N. 2016. Corrosion of the Head-Stem Taper Junction—Are We on the Verge of an Epidemic? *HSS Journal* 1-8.

MORLOCK, M. M. 2015. The taper disaster - how could it happen? *HIP International,* 25**,** 339-46.

MORLOCK, M. M., BISHOP, N. & HUBER, G. 2011. Biomechanics of Hip Arthroplasty. *In:* KNAHR, K. (ed.) *Tribology in Total Hip Arthroplasty.* Springer Berlin Heidelberg.

MOSKAL, J. & STOVER, M. 2015. Mechanically assisted crevice corrosion of the head-neck taper in a large head metal-on-metal total hip arthroplasty. *Arthroplasty Today,* 1**,** 103-106.

MOSS, S. G., SCHWEITZER, M. E., JACOBSON, J. A., BROSSMANN, J., LOMBARDI, J. V., DELLOSE, S. M., CORALNICK, J. R., STANDIFORD, K. N. & RESNICK, D. 1998. Hip joint fluid: detection and distribution at MR imaging and US with cadaveric correlation. *Radiology,* 208**,** 43-48.

MU, Y., KOBAYASHI, T., SUMITA, M., YAMAMOTO, A. & HANAWA, T. 2000. Metal ion release from titanium with active oxygen species generated by rat macrophages in vitro. *Journal of Biomedical Materials Research,* 49**,** 238-43.

MUNIR, S., IMBULDENIYA, A. & WALSH, W. W. W. 2013. Variations in the Trunnion Surface Topography Between Different Commercially Available Hip Replacement Stems. *Bone & Joint Journal Orthopaedic Proceedings Supplement,* 95-B**,** 197.

MUNIR, S., OLIVER, R. A., ZICAT, B., WALTER, W. L., WALTER, W. K. & WALSH, W. R. 2016. The histological and elemental characterisation of corrosion particles from taper junctions. *Bone & Joint Research,* 5**,** 370-378.

NADKARNI, R. A. 1991. A Review of Modern Instrumental Methods of Elemental Analysis of Petroleum Related Material: Part II—Analytical Techniques. *In:* NADKARNI, R. A. (ed.) *Modern Instrumental Methods of Elemental Analysis of Petroleum Products and Lubricants* Philadelphia, PA 19106: ASTM International.

NAMBU, S., OBERT, R., ROARK, M., LINTON, D., BIBLE, S. & MOSELEY, J. 2015. Accelerated Fretting Corrosion Testing of Modular Necks for THA. *In:* GREENWALD, A., KURTZ, S., LEMONS, J. & MIHALKO, W. (eds.) *Modularity and Tapers in Total Joint Replacement Devices STP1591.* West Conshohocken, PA: ASTM International

NASSIF, N. A., NAWABI, D. H., STONER, K., ELPERS, M., WRIGHT, T. & PADGETT, D. E. 2014. Taper Design Affects Failure of Large-head Metal-on-metal Total Hip Replacements. *Clinical Orthopaedics and Related Research,* 472**,** 564-571.

NATIONAL JOINT REGISTRY OF ENGLAND AND WALES 2005. 3rd Annual Clinical Report.

NATIONAL JOINT REGISTRY OF ENGLAND, W. A. N. I. 2016. 13th Annual Report.

NEMES, S., GORDON, M., ROGMARK, C. & ROLFSON, O. 2014. Projections of total hip replacement in Sweden from 2013 to 2030. *Acta Orthopaedica,* 85**,** 238-43.

NGANBE, M., LOUATI, H., KHAN, U., SPEIRS, A. & BEAULE, P. E. 2010. Retrieval analysis and in vitro assessment of strength, durability, and distraction of a modular total hip replacement. *Journal of Biomedical Materials Research, Part A,* 95**,** 819-27.

NODZO, S. R., ESPOSITO, C. I., POTTER, H. G., RANAWAT, C. S., WRIGHT, T. M. & PADGETT, D. E. 2017. MRI, Retrieval Analysis, and Histologic Evaluation of Adverse Local Tissue Reaction in Metal-on-Polyethylene Total Hip Arthroplasty. *The Journal of Arthroplasty,* 32**,** 1647-1653.

OBERG, E., JONES, F. D., HORTON, H. L. & RYFFEL, H. H. 2012. Machinery's Handbook (29th Edition) & Guide to Machinery's Handbook. Industrial Press.

OEHY, J. & BIDER, K. 2004. Design parameter to improve range of motion (ROM) in total hip arthroplasty. *In:* LAZENNEC, J. Y. & DIETRICH, M. (eds.) *Bioceramics in Joint Arthroplasty.* Springer-verlag.

OLESIK, J. W. 2000. *Inorganic Mass Spectrometry: Fundamentals and Applications* New York, Marcel Dekker, Inc.

ONG, K. L., RUNDELL, S., LIEPINS, I., LAURENT, R., MARKEL, D. & KURTZ, S. M. 2009. Biomechanical modeling of acetabular component polyethylene stresses, fracture risk, and wear rate following press-fit implantation. *Journal of Orthopaedic Research,* 27**,** 1467-1472.

PAMU, J., HUSSAIN, A., DANIEL, J., KAMALI, A. & LI, C. 2012. Metal Ion Release at the Taper Junction in Metal on Metal (MoM) Devices. *Journal of Bone & Joint Surgery, British Volume,* 94-B**,** 84.

PANAGIOTIDOU, A., MESWANIA, J., HUA, J., MUIRHEAD-ALLWOOD, S., HART, A. & BLUNN, G. 2013. Enhanced wear and corrosion in modular tapers in total hip replacement is associated with the contact area and surface topography. *Journal of Orthopaedic Research,* 31**,** 2032-2039.

PANAGIOTIDOU, A., MESWANIA, J., OSMAN, K., BOLLAND, B., LATHAM, J., SKINNER, J., HADDAD, F. S., HART, A. & BLUNN, G. 2015. The effect of frictional torque and bending moment on corrosion at the taper interface : an in vitro study. *Bone Joint J,* 97-B**,** 463-72.

PANSARD, E., FOUILLERON, N., DEREUDRE, G., MIGAUD, H. & GIRARD, J. 2012. Severe corrosion after malpositioning of a metallic head over the Morse taper of a

cementless hip arthroplasty. A case report. *Orthopaedics & Traumatology: Surgery & Research,* 98**,** 247-50.
PANSU, M., GAUTHEYROU, J. & J-Y, L. 2001. *Soil Analysis: Sampling Instrumentation Quality control,* Lisse, A.A. Balkema Publishers.
PAREKH, J., CHAN, N. & NOBLE, P. 2016. How do positive and negative taper mismatches affect the interface mechanics of modular head-neck junctions? *Bone & Joint Journal Orthopaedic Proceedings Supplement,* 98-B**,** 86.
PASTIDES, P. S., DODD, M., SARRAF, K. M. & WILLIS-OWEN, C. A. 2013. Trunnionosis: A pain in the neck. *World Journal of Orthopedics,* 4**,** 161-6.
PENNOCK, A. T., SCHMIDT, A. H. & BOURGEAULT, C. A. 2002. Morse-type tapers: Factors that may influence taper strength during total hip arthroplasty. *The Journal of Arthroplasty,* 17**,** 773-778.
PIVEC, R., MENEGHINI, R. M., HOZACK, W. J., WESTRICH, G. H. & MONT, M. A. 2014. Modular Taper Junction Corrosion and Failure: How to Approach a Recalled Total Hip Arthroplasty Implant. *The Journal of arthroplasty,* 29**,** 1-6.
PLUMMER, D. R., BERGER, R. A., PAPROSKY, W. G., SPORER, S. M., JACOBS, J. J. & DELLA VALLE, C. J. 2016. Diagnosis and Management of Adverse Local Tissue Reactions Secondary to Corrosion at the Head-Neck Junction in Patients With Metal on Polyethylene Bearings. *The Journal of Arthroplasty,* 31**,** 264-268.
PORTER, D. A., URBAN, R. M., JACOBS, J. J., GILBERT, J. L., RODRIGUEZ, J. A. & COOPER, H. J. 2014. Modern Trunnions Are More Flexible: A Mechanical Analysis of THA Taper Designs. *Clinical Orthopaedics and Related Research,* 472**,** 3963-3970.
POSADA, O. M., TATE, R. J. & GRANT, M. H. 2015. Toxicity of cobalt-chromium nanoparticles released from a resurfacing hip implant and cobalt ions on primary human lymphocytes in vitro. *Journal of Applied Toxicology,* 35**,** 614-22.
POURZAL, R., HALL, D. J., HA, N. Q., URBAN, R. M., LEVINE, B. R., JACOBS, J. J. & LUNDBERG, H. J. 2016. Does Surface Topography Play a Role in Taper Damage in Head-neck Modular Junctions? *Clinical Orthopaedics and Related Research,* 474**,** 2232-42.
RACASAN, R., BILLS, P., BLUNT, L., HART, A. & SKINNER, J. 2015. Method for Characterization of Material Loss from Modular Head-Stem Taper Surfaces of Hip Replacement Devices. *In:* A, G., STEVEN, K., JACK, L. & WILLIAM, M. (eds.) *Modularity and Tapers in Total Joint Replacement Devices STP1591.* West Conshohocken, PA: ASTM International
RAJPURA, A., KENDOFF, D. & BOARD, T. N. 2014. The current state of bearing surfaces in total hip replacement. *Bone & Joint Journal,* 96-B**,** 147-56.
RAJU, S., CHINNAKKANNU, K., PUTTASWAMY, M. K. & PHILLIPS, M. J. 2017. Trunnion Corrosion in Metal-on-Polyethylene Total Hip Arthroplasty: A Case Series. *JAAOS - Journal of the American Academy of Orthopaedic Surgeons,* 25**,** 133-139.
RECLARU, L., LERF, R., ESCHLER, P.-Y., BLATTER, A. & MEYER, J.-M. 2002. Pitting, crevice and galvanic corrosion of REX stainless-steel/CoCr orthopedic implant material. *Biomaterials,* 23**,** 3479-3485.
REHMER, A., BISHOP, N. E. & MORLOCK, M. M. 2012. Influence of assembly procedure and material combination on the strength of the taper connection at the head-neck junction of modular hip endoprostheses. *Clinical Biomechanics (Bristol, Avon),* 27**,** 77-83.
RICCIARDI, B. F., NOCON, A. A., JERABEK, S. A., WILNER, G., KAPLOWITZ, E., GOLDRING, S. R., PURDUE, P. E. & PERINO, G. 2016. Histopathological characterization of corrosion product associated adverse local tissue reaction in hip implants: a study of 285 cases. *BMC Clinical Pathology,* 16**,** 3.

ROBA, M. 2009. *Interaction of Synovial Fluid Components with Artificial Hip-Joint Materials* PhD, ETH Zurich.
ROBERTS, B. J., UNSWORTH, A. & MIAN, N. 1982. Modes of lubrication in human hip joints. *Annals of the Rheumatic Diseases,* 41**,** 217-224.
RODRIGUEZ, J. A. & RATHOD, P. A. 2012. Large diameter heads. *Journal of Bone & Joint Surgery, British Volume,* 94-B**,** 52-54.
ROYHMAN, D., RADHAKRISHNAN, R., YUAN, J. C.-C., MATHEW, M. T., MERCURI, L. G. & SUKOTJO, C. 2014. An electrochemical investigation of TMJ implant metal alloys in an artificial joint fluid environment: The influence of pH variation. *Journal of Cranio-Maxillofacial Surgery,* 42**,** 1052-1061.
ROYHMAN, D., YUAN, J. C., SHOKUHFAR, T., TAKOUDIS, C., SUKOTJO, C. & MATHEW, M. T. 2013. Tribocorrosive behaviour of commonly used temporomandibular implants in a synovial fluid-like environment: Ti–6Al–4V and CoCrMo. *Journal of Physics D: Applied Physics,* 46**,** 404002.
ROYLE, M. 2012. *Influence of coatings on ion release from large diameter metal-on-metal hip bearings.* Doctor of Philosophy, Queen Mary, University of London.
SAIKKO, V. 2008. Friction Measurement in the Biaxial Rocking Motion Hip Joint Simulator. *Journal of Tribology,* 131**,** 011201-011201-8.
SCHAAFF, P. 2004. The role of fretting damage in total hip arthroplasty with modular design hip joints -evaluation of retrieval studies and experimental simulation methods. *Journal of Applied Biomaterials & Biomechanics,* 2**,** 121-35.
SCHAAFF, P. & HOLZWARTH, U. 2003. *Characterisation of loading and damage modes of fretting and the role of fretting damage in medical implants : a literature report,* Ispra, Institute for Health and Consumer Protection, Joint Research Centre, European Commission.
SCHAFER, R., SOLTESZ, U. & BERNARD, P. F. 1998. Friction in hip-joint prostheses and its influence on the fixation of the artificial head. *Journal of Materials Science: Materials in Medicine,* 9**,** 687-90.
SCHEUBER, L. F., USBECK, S. & PETKOW, F. 2014. The Neck Taper in Hip Arthroplasty: What does the surgeon have to consider? : Ceramtec.
SCHLEMMER, G. & RADZIUK, B. 1999. *Analytical Graphite Furnace Atomic Absorption Spectrometry: A Laboratory Guide,* Basel, Birkhauser Verlag.
SCHNEIDER, M., FEY, D., WENZEL, K. & MACHLEIDT, T. A Generic Approach for Analysis of White-Light Interferometry Data via User-Defined Algorithms. *In:* MURGANTE, B., MISRA, S., ROCHA, A. A. C., FALCAO, M. I., TANIR, D., APDUHAN, B. O. & GERVASI, O., eds. International Conference Computational Science and its Applications 2014 Guimaraes, Portugal Springer.
SCHOLES, S. C. & UNSWORTH, A. 2000. Comparison of friction and lubrication of different hip prostheses. *Proceedings of the Institution of Mechanical Engineers, Part H: Journal of Engineering in Medicine,* 214**,** 49-57.
SCHOLL, L., LONGARAY, J., RAJA, L., LEE, R., FAIZAN, A., HERRERA, L., THAKORE, M. & NEVELOS, J. 2016a. Friction in modern total hip arthroplasty bearings: Effect of material, design, and test methodology. *Proceedings of the Institution of Mechanical Engineers, Part H: Journal of Engineering in Medicine,* 230**,** 50-57.
SCHOLL, L., SCHMIDIG, G., FAIZAN, A., TENHUISEN, K. & NEVELOS, J. 2016b. Evaluation of surgical impaction technique and how it affects locking strength of the head–stem taper junction. *Proceedings of the Institution of Mechanical Engineers, Part H: Journal of Engineering in Medicine,* 230**,** 661-667.
SCHWACHMEYER, V., DAMM, P., BENDER, A., DYMKE, J., GRAICHEN, F. & BERGMANN, G. 2013. In Vivo Hip Joint Loading during Post-Operative Physiotherapeutic Exercises. *PLoS ONE,* 8**,** e77807.

SCULLY, W. F. & TEENY, S. M. 2013. Pseudotumor associated with metal-on-polyethylene total hip arthroplasty. *Orthopedics,* 36**,** e666-70.
SHAREEF, N. & LEVINE, D. 1996. Effect of manufacturing tolerances on the micromotion at the Morse taper interface in modular hip implants using the finite element technique. *Biomaterials,* 17**,** 623-630.
SHEN, M. C., RIEKER, C. B., GNEPF, P., LIEBENTRITT, G. & SCHÖN, R. 2005. Effect of clearance on frictional torque characteristics of metal-on-metal THA. *ORS Annual Meeting.* Washington DC.
SHREIR, L. L. (ed.) 1976. *Corrosion Testing and Corrosion Rates*: Newnes-Butterworths.
SIDAGINAMALE, R. P., JOYCE, T. J., BOWSHER, J. G., LORD, J. K., AVERY, P. J., NATU, S., NARGOL, A. V. F. & LANGTON, D. J. 2016. The clinical implications of metal debris release from the taper junctions and bearing surfaces of metal-on-metal hip arthroplasty: joint fluid and blood metal ion concentrations. *Bone & Joint Journal,* 98-B**,** 925-933.
SIVAN, S., PIERI, K. G. & GILBERT, J. L. 2015. Cell-Induced Corrosion on Titanium Alloys. *ORS Annual Meeting* Las Vegas, Nevada.
SMITH, S. L. & JOYCE, T. J. 2017. A hop, skip, and a jump: Towards better wear testing of hip implants. *In:* FRIIS, E. (ed.) *Mechanical Testing of Orthopaedic Implants.* Woodhead Publishing.
SMITH, S. L. & UNSWORTH, A. 2000. Simplified motion and loading compared to physiological motion and loading in a hip joint simulator. *Proceedings of the Institution of Mechanical Engineers, Part H: Journal of Engineering in Medicine,* 214**,** 233-8.
SNEDDON, J. & BUTCHER, D. J. 2002. Application of graphite furnace atomic absorption spectrometry in biological and clinical samples *In:* SNEDDON, J. (ed.) *Advances in Atomic Spectroscopy.* Amsterdam: Elsevier Science B.V.
SRIDHAR, N., DUNN, D. S., BROSSIA, C. S., CRAGNOLINO, G. A. & KEARNS, J. R. 2005. Crevice corrosion. *In:* BABOIAN, R. (ed.) *Corrosion Tests and Standards: Application and Interpretation* 2nd ed.: ASTM International.
STOHS, S. J. & BAGCHI, D. 1995. Oxidative mechanisms in the toxicity of metal ions. *Free Radical Biology and Medicine,* 18**,** 321-336.
SWAMINATHAN, V. & GILBERT, J. L. 2012. Fretting corrosion of CoCrMo and Ti6Al4V interfaces. *Biomaterials,* 33**,** 5487-503.
SWAMINATHAN, V., SCHOLL, L., LEE, R., FAIZAN, A., THAKORE, M., TENHUISEN, K. & NEVELOS, J. 2015. Simultaneous Hip Head-Stem Taper Junction Measurements of Electrochemical Corrosion and Micromotion: A Comparison of Taper Geometry and Stem Material. *In:* A, G., STEVEN, K., JACK, L. & WILLIAM, M. (eds.) *Modularity and Tapers in Total Joint Replacement Devices STP1591.* West Conshohocken, PA: ASTM International
SWEDISH HIP ARTHROPLASTY REGISTER 2005. Annual Report
TADDEI, P., TOZZI, S., CARMIGNATO, S. & AFFATATO, S. 2016. May the surface roughness of the retrieved femoral head influence the wear behavior of the polyethylene liner? *Journal of Biomedical Materials Research Part B: Applied Biomaterials,* 104**,** 1374-1385.
TAKAKUBO, Y., BERCE, A., TREBŠE, R., TAMAKI, Y., MILOŠEV, I., AL-SAMADI, A., TIAINEN, V.-M., ORTON & KONTTINEN, Y. T. 2013. Wear and corrosion in the loosening of Total Joint Replacements (TJRs). *In:* YAN, Y. (ed.) *Bio-Tribocorrosion in Biomaterials and Medical Implants.* PA, USA: Woodhead Publishing.
TAN, S. C., TEETER, M. G., DEL BALSO, C., HOWARD, J. L. & LANTING, B. A. 2015. Effect of Taper Design on Trunnionosis in Metal on Polyethylene Total Hip Arthroplasty. *The Journal of Arthroplasty,* 30**,** 1269-1272.

TAS, A. C. 2014. The use of physiological solutions or media in calcium phosphate synthesis and processing. *Acta Biomaterialia,* 10**,** 1771-1792.
TATEIWA, T., CLARKE, I. C., SHIRASU, H., MASAOKA, T., SHISHIDO, T. & YAMAMOTO, K. 2006. Effect of low protein concentration lubricants in hip simulators. *Journal of Orthopaedic Science,* 11**,** 204-211.
TENGVALL, P., LUNDSTRÖM, I., SJÖQVIST, L., ELWING, H. & BJURSTEN, L. M. 1989. Titanium-hydrogen peroxide interaction: model studies of the influence of the inflammatory response on titanium implants. *Biomaterials,* 10**,** 166-175.
THEODORE, W., PIERREPONT, J., B, M. & LI, Q. 2013. A Finite Element Investigation into the Effects of Head Size and Taper Design on the Micromotion at the Head/Neck Interface in Total Hip Replacement. *21st Annual Symposium on Computational Methods in Orthopaedic Biomechanics.* University of Texas, San Antonio.
THERMOELEMENTAL 2001. AAS, GFAAS, ICP or ICP-MS? Which technique should I use?: An elementary overview of elemental analysis. *In:* THERMOELEMENTAL (ed.). USA.
THOMAS, C., MACKEY, M. M., DIAZ, A. A. & COX, D. P. 2009. Hydroxyl radical is produced via the Fenton reaction in submitochondrial particles under oxidative stress: implications for diseases associated with iron accumulation. *Redox Report,* 14**,** 102-108.
THOMAS, R. 2004. *Practical Guide to ICP-MS: A Tutorial for Beginners,* Gaithersburg, Maryland, Marcel Dekker.
TIUSANEN, H., MÄKELÄ, K., KIILUNEN, M., SARANTSIN, P., SIPOLA, E. & PESOLA, M. 2013. The Effect Of Different Bearing Surfaces On Metal Ion Levels In Urine Following 28 mm Metal-On-Metal And 28 mm Metal-On-Polyethylene Total Hip Arthroplasty. *Scandinavian Journal of Surgery,* 102**,** 197-203.
TONI, A., BALEANI, M., BORDINI, B., STEA, S., PILLA, F. & SUDANESE, A. 2012. "Trunionitis": A Cause for Concern? *Seminars in Arthroplasty,* 23**,** 248-250.
TRIANTAFYLLOPOULOS, G. K., ELPERS, M. E., BURKET, J. C., ESPOSITO, C. I., PADGETT, D. E. & WRIGHT, T. M. 2016. Otto Aufranc Award: Large Heads Do Not Increase Damage at the Head-neck Taper of Metal-on-polyethylene Total Hip Arthroplasties. *Clinical Orthopaedics and Related Research,* 474**,** 330-338.
TROMMER, R. M. & MARU, M. M. 2017. Importance of preclinical evaluation of wear in hip implant designs using simulator machines. *Revista Brasileira de Ortopedia (English Edition),* 52**,** 251-259.
TUCKER, K., PICKFORD, M., NEWELL, C., HOWARD, P., HUNT, L. P. & BLOM, A. W. 2015. Mixing of components from different manufacturers in total hip arthroplasty: prevalence and comparative outcomes. *Acta Orthopaedica,* 86**,** 671-7.
TURITTO, V. & SLACK, S. M. 2016. Blood and Related Fluids. *In:* MURPHY, W., BLACK, J. & HASTINGS, G. (eds.) *Handbook of Biomaterial Properties.* New York: Springer
ULLMARK, G. 2016. The unstable total hip arthroplasty. *EFORT Open Reviews,* 1**,** 83.
UNDERWOOD, R. J., SAYLES, R. S. & CANN, P. M. 2012. A Protocol to Measure the Wear of Large Head Metal-on-Metal Total Hip Replacement Head Neck Taper Junctions *ORS Annual Meeting* San Francisco.
URBAN, R. M., JACOBS, J. J., GILBERT, J. L. & GALANTE, J. O. 1994. Migration of corrosion products from modular hip prostheses. Particle microanalysis and histopathological findings. *Journal of Bone & Joint Surgery, American Volume,* 76**,** 1345-59.
VALKO, M., MORRIS, H. & CRONIN, M. T. 2005. Metals, toxicity and oxidative stress. *Current Medicinal Chemistry,* 12**,** 1161-208.
VAN CITTERS, D. W., MARTIN, A. J., CURRIER, J. H., PARK, S.-H. & EDIDIN, A. A. 2015. Factors Related to Imprinting Corrosion in Modular Head-Neck Junctions. *In:* A, G.,

STEVEN, K., JACK, L. & WILLIAM, M. (eds.) *Modularity and Tapers in Total Joint Replacement Devices STP1591.* West Conshohocken, PA: ASTM International
VANHAECKE, F. 2012. *Isotopic Analysis: Fundamental and Applications using ICP-MS,* Weinheim, Germany, Wiley-VCH.
VICECONTI, M., BALEANI, M., SQUARZONI, S. & TONIL, A. 1997. Fretting wear in a modular neck hip prosthesis. *Journal of Biomedical Materials Research,* 35**,** 207-216.
VICECONTI, M., RUGGERI, O., TONI, A. & GIUNTI, A. 1996. Design-related fretting wear in modular neck hip prosthesis. *Journal of Biomedical Materials Research* 30**,** 181-6.
VIDELA, H. A. & HERRERA, L. K. 2005. Microbiologically influenced corrosion: looking to the future. *International Microbiology,* 8**,** 169-80.
VIRTANEN, S., MILOŠEV, I., GOMEZ-BARRENA, E., TREBŠE, R., SALO, J. & KONTTINEN, Y. T. 2008. Special modes of corrosion under physiological and simulated physiological conditions. *Acta Biomaterialia,* 4**,** 468-476.
VUNDELINCKX, B. J., VERHELST, L. A. & SCHEPPER, J. 2013. Taper corrosion in modular hip prostheses: analysis of serum metal ions in 19 patients. *The Journal of Arthroplasty,* 28**,** 1218-1223.
WALKER, P., CAMPBELL, D., TORRE, P. D., BRAZIL, D. & MCTIGHE, T. 2016. Trunnion Corrosion and Early Failure in Monolithic Metal-on-Polyethylene TMZF Femoral Components: A Case Series. *Reconstructive Review,* 6.
WALSH, A. J., NIKOLAOU, V. S. & ANTONIOU, J. 2012. Inflammatory Pseudotumor Complicating Metal-On-Highly Cross-Linked Polyethylene Total Hip Arthroplasty. *The Journal of Arthroplasty,* 27**,** 324.e5-324.e8.
WANG, A., ESSNER, A. & SCHMIDIG, G. 2004. The effects of lubricant composition on in vitro wear testing of polymeric acetabular components. *Journal of Biomedical Materials Research Part B: Applied Biomaterials,* 68B**,** 45-52.
WANG, A., STARK, C. & DUMBLETON, J. H. 1995. Role of cyclic plastic deformation in the wear of UHMWPE acetabular cups. *Journal of Biomedical Materials Research,* 29**,** 619-626.
WANG, K. 1996. The use of titanium for medical applications in the USA. *Materials Science and Engineering: A,* 213**,** 134-137.
WANG, W. 2010. *Reverse Engineering: Technology of Reinvention* Boca Raton, FL, CRC Press.
WATANABE, H., TAKAHASHI, K., TAKENOUCHI, K., SATO, A., KAWAJI, H., NAKAMURA, H. & TAKAI, S. 2015. Pseudotumor and deep venous thrombosis due to crevice corrosion of the head–neck junction in metal-on-polyethylene total hip arthroplasty. *Journal of Orthopaedic Science,* 20**,** 1142-1147.
WEISSE, B., AFFOLTER, C., STUTZ, A., TERRASI, G. P., KÖBEL, S. & WEBER, W. 2008. Influence of contaminants in the stem—ball interface on the static fracture load of ceramic hip joint ball heads. *Proceedings of the Institution of Mechanical Engineers, Part H: Journal of Engineering in Medicine,* 222**,** 829-835.
WHITEHOUSE, M. R., ENDO, M., ZACHARA, S., NIELSEN, T. O., GREIDANUS, N. V., MASRI, B. A., GARBUZ, D. S. & DUNCAN, C. P. 2015. Adverse local tissue reactions in metal-on-polyethylene total hip arthroplasty due to trunnion corrosion. *Bone & Joint Journal,* 97-B**,** 1024-30.
WHITTAKER, R. K., HOTHI, H. S., ESKELINEN, A., BLUNN, G. W., SKINNER, J. A. & HART, A. J. 2016. Variation in taper surface roughness for a single design effects the wear rate in total hip arthroplasty. *Journal of Orthopaedic Research,* 35**,** 1784-1792.
WILLERT, H. G., BROBACK, L. G., BUCHHORN, G. H., JENSEN, P. H., KOSTER, G., LANG, I., OCHSNER, P. & SCHENK, R. 1996. Crevice corrosion of cemented titanium alloy stems in total hip replacements. *Clinical Orthopedic and Related Research***,** 51-75.

WILSON, N. A., SCHNELLER, E. S., MONTGOMERY, K. & BOZIC, K. J. 2008. Hip And Knee Implants: Current Trends And Policy Considerations. *Health Affairs,* 27**,** 1587-1598.

WITT, F., BOSKER, B. H., BISHOP, N. E., ETTEMA, H. B., VERHEYEN, C. C. & MORLOCK, M. M. 2014. The relation between titanium taper corrosion and cobalt-chromium bearing wear in large-head metal-on-metal total hip prostheses: a retrieval study. *Journal of Bone & Joint Surgery, American Volume,* 96**,** e157(1)-e157(9).

WITT, F., GUHRS, J., MORLOCK, M. M. & BISHOP, N. E. 2015. Quantification of the Contact Area at the Head-Stem Taper Interface of Modular Hip Prostheses. *PLoS One,* 10**,** e0135517.

WROBLEWSKI, B. M., SINEY, P. D. & FLEMING, P. A. 2012. Microseparation, fluid pressure and flow in failures of metal-on-metal hip resurfacing arthroplasties. *Bone & Joint Research,* 1**,** 25-30.

YAVARI, M. R. & IDRIS, M. H. 2016. Effect of surface roughness and taper angle on junction strength of modular biomedical implant. *International Journal of Mechanical and Mechatronics Engineering,* 16**,** 42-47.

ZARTMAN, K. C., BERLET, G. C., HYER, C. F. & WOODARD, J. R. 2011. Combining dissimilar metals in orthopaedic implants: revisited. *Foot Ankle Specialist,* 4**,** 318-23.

ZENG, P., RAINFORTH, W. M. & COOK, R. B. 2015. Characterisation of the oxide film on the taper interface from retrieved large diameter metal on polymer modular total hip replacements. *Tribology International,* 89**,** 86-96.

ZHENG, Y. 2016. *Magnesium Alloys as Degradable Biomaterials,* Boca Raton, FL, CRC Press Taylor & Francis Group.

ZHU, M. & WINDLER, M. 2003. Fretting and anodic current of the taper interface of stainless steel hip stems/cobalt-chromium femoral heads. *ASTM SPECIAL TECHNICAL PUBLICATION,* 1438**,** 235-248.

ZYGO. 2017. *Optical Profiler Basics* [Online]. Available: https://www.zygo.com/?/met/profilers/opticalprofilersabout.htm [Accessed 21/12/2017 2017].

Appendices

A.1 Test component drawings

Final isolation design

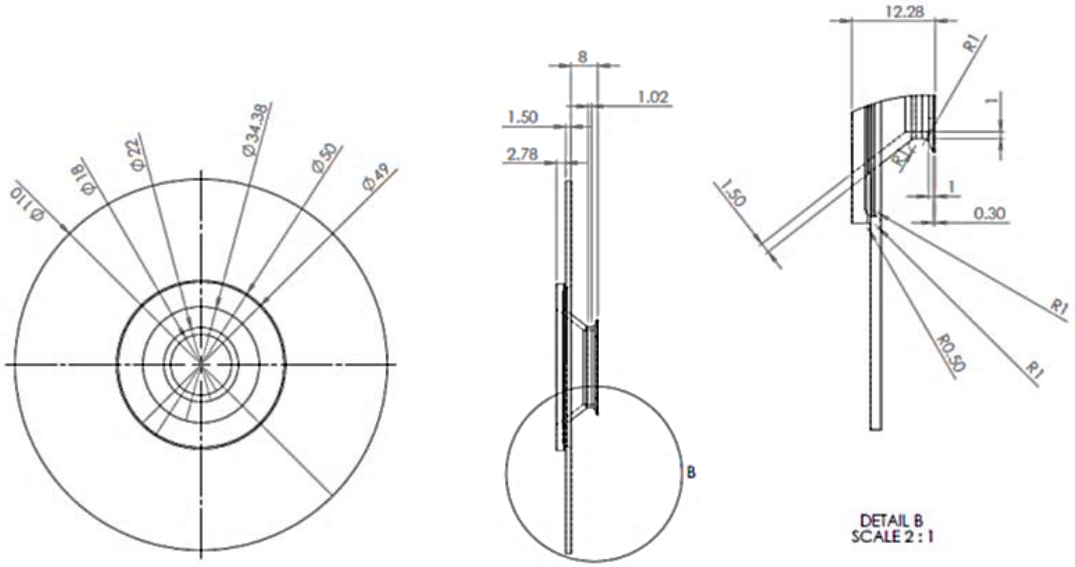

Figure A-0-1 Final isolation design

(a)

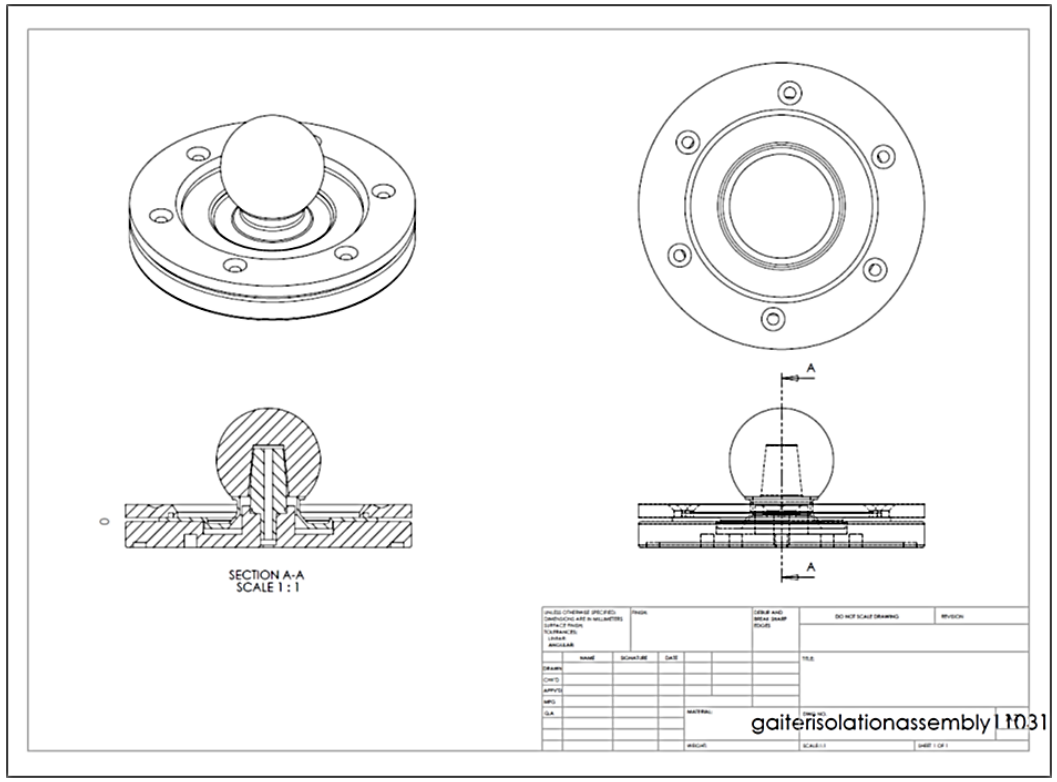

(b)

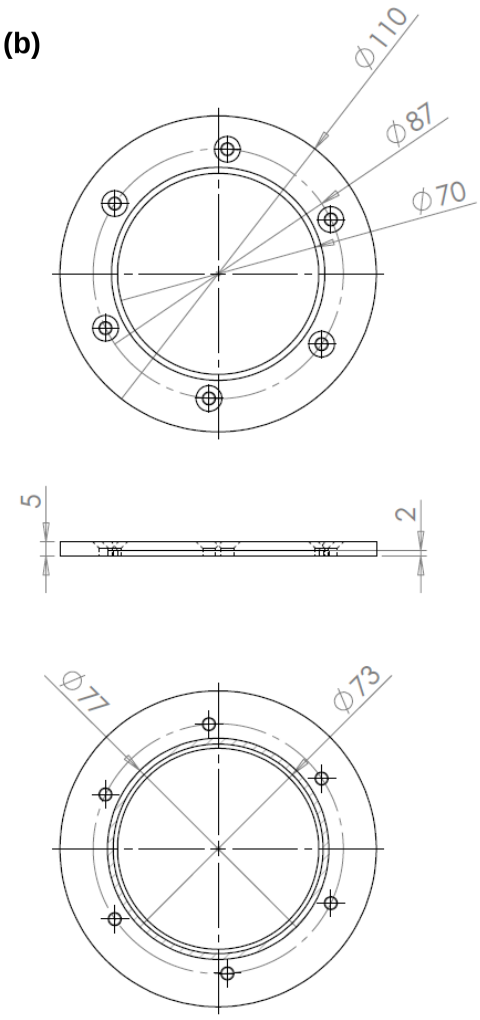

Figure A-0-2(a) Assembly of taper isolation setup (b) Drawing and dimensions of bolting plate

Acetabular component modification

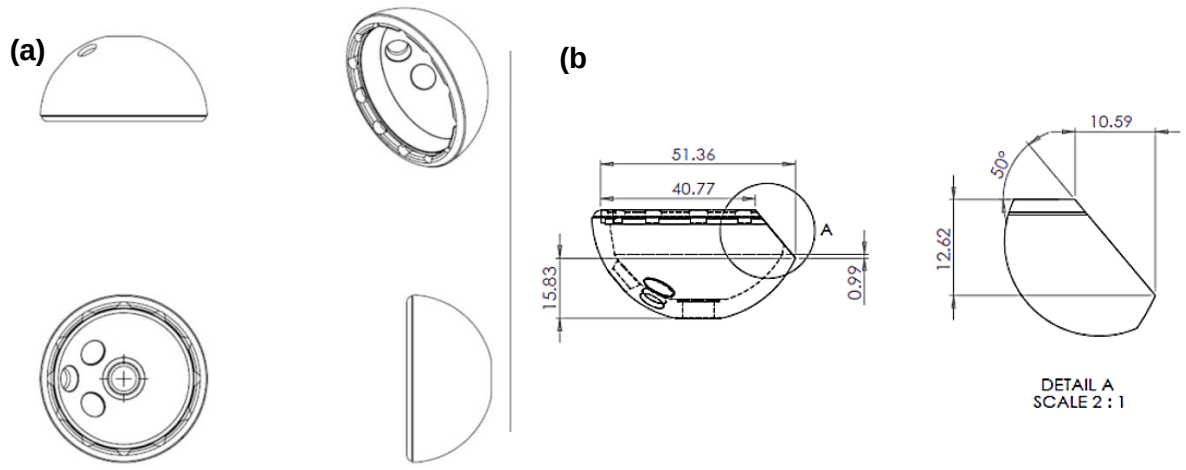

Figure A-0-3(a) Unmodified actabular shell (b) Details showing sectioning features

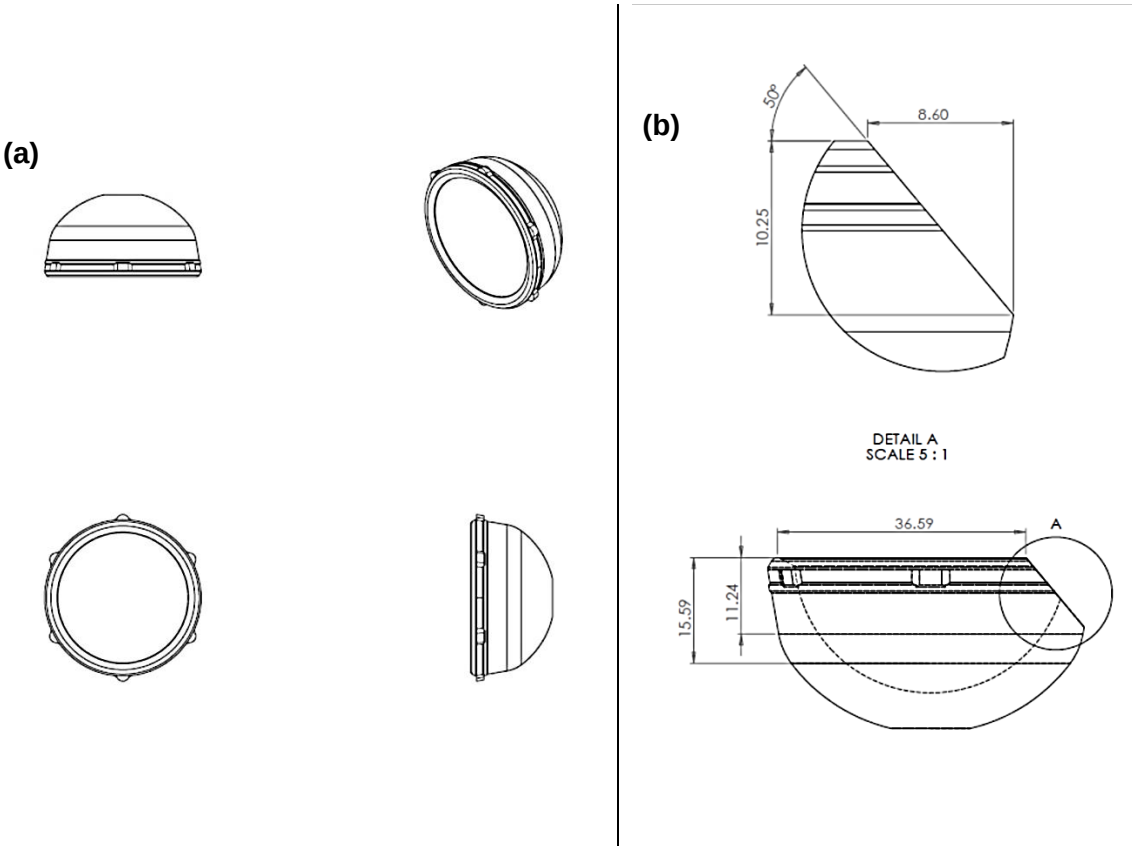

Figure A-0-4 (a) Unmodified acetabular liner (b) Details showing sectioning features

A.2 Experimental evaluation of taper engagement position

To determine the position of taper engagement, a range CoCr heads (28, 32, 40, 52, 56 mm) were impacted onto a 17-4 steel trunnion with 5 hits using a hammer and a femoral head impactor. After impaction, each assembly was measured using a height gauge. This was compared to the height prescribed in the specifications. A total of 3 repeats were recorded per head size.

Results:

When impaction blows were applied to lock a taper, it was found that the 56 mm taper assembly engaged at a position outside of the tolerance defined in the design specification; in comparison, the rest of the taper assemblies were within tolerance with respect to the engagement position.

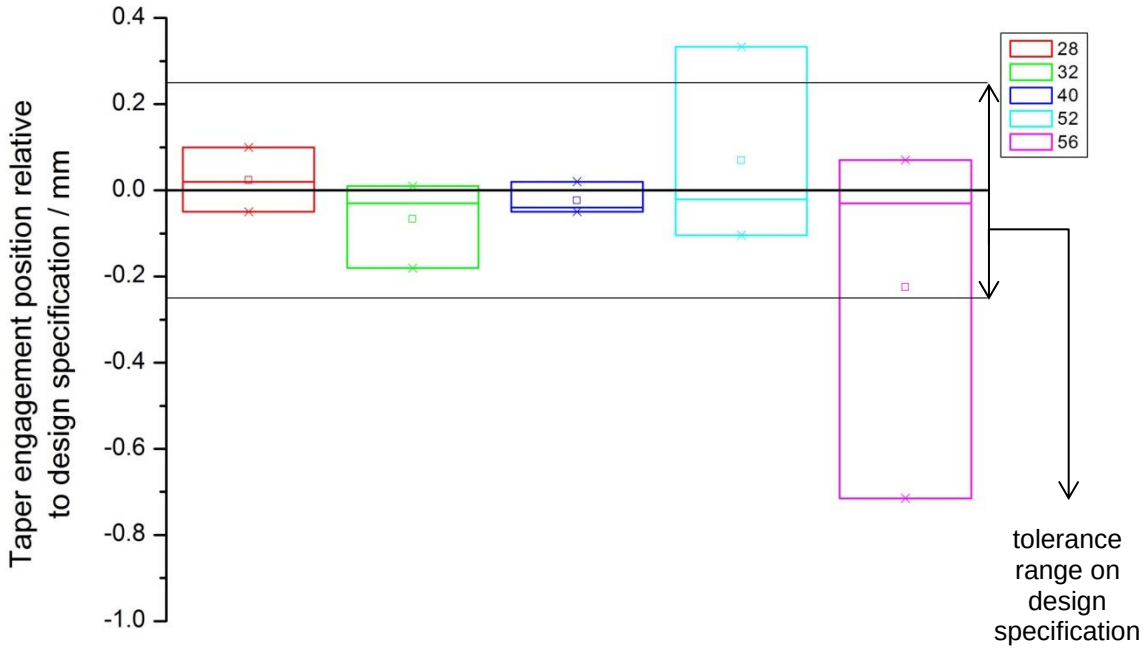

Figure A-0-5 Measured position of taper engagement for a range of head sizes; negative value representative of femoral head sitting lower than the specified engagement position

A.3 Dilution factor analysis

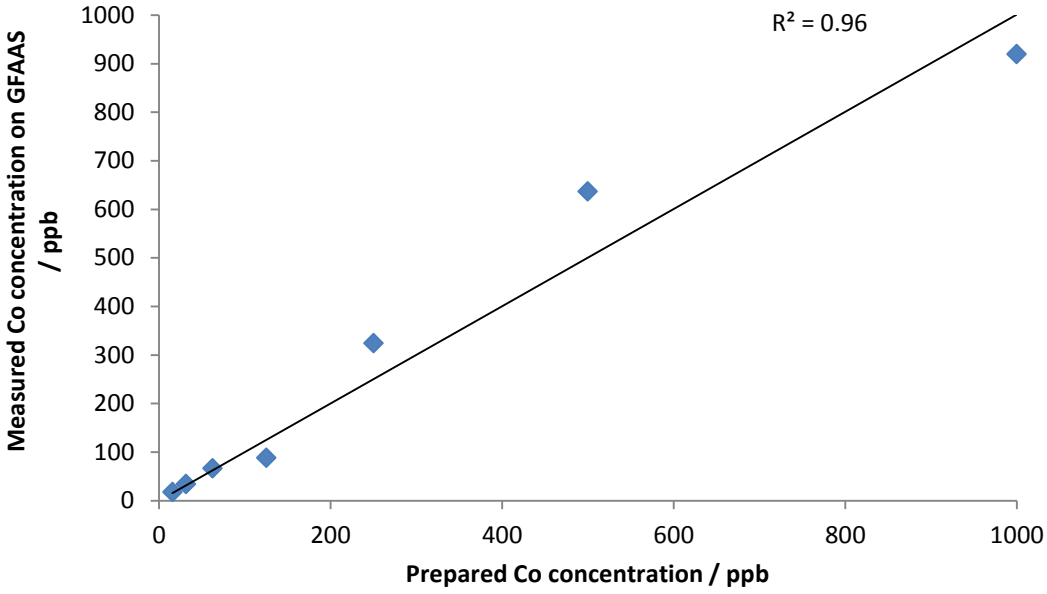

Figure A-0-6 Concentrations measured in dilution analysis

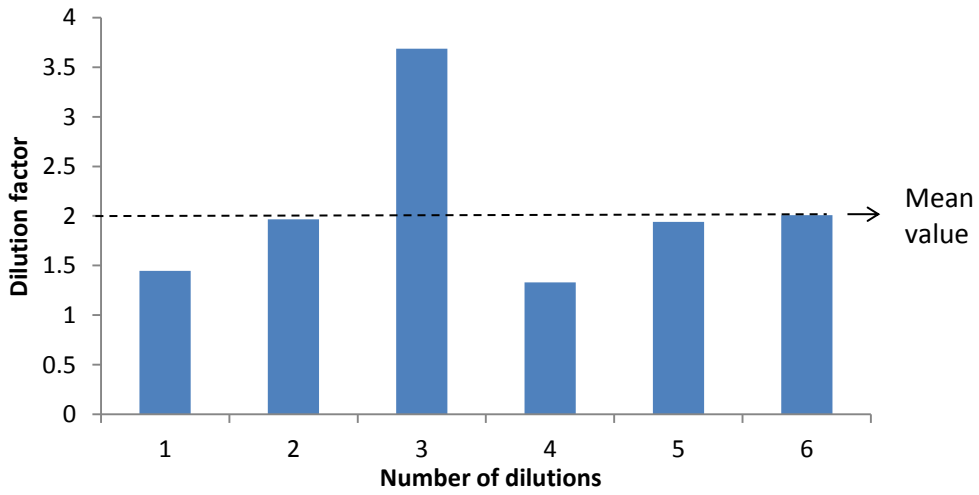

Figure A-0-7 Dilution factor for serial dilutions from 1000 ppb to 15.625 ppb on the GFAAS; dilution 6 corresponds to diluting 31.25 ppb to 15.625 ppb

A.4 Equations for calculating torques, bending moments and strains

Principal strains

$$\varepsilon_{1,2} = \frac{\varepsilon_a+\varepsilon_c}{2} \pm \frac{1}{\sqrt{2}}\sqrt{(\varepsilon_a - \varepsilon_b)^2 + (\varepsilon_b - \varepsilon_c)^2} \quad (17)$$

Full bridge configuration: $\Delta_e = \varepsilon G_F V$ (18)

Torque:

Trunnion fixture: $T = \pi G \varepsilon R^3$ (19)

Femoral stem: $T = \frac{G\varepsilon a^2 b}{3+1.8^{a}/_{b}}$ (20)

Half bridge configuration: $\Delta_e = {\varepsilon G_F V}/_2$ (21)

Bending moment $M = {E\varepsilon I}/_y$ (22)

Where: T = torque, G = shear modulus, R = radius of shaft

Δ_e= output voltage, V= excitation voltage, G_F = gauge factor, E= Young's modulus

I =second moment of area ε = measured strain

a= width, b=length

y= distance from the neutral axis to region of maximum stress

A.5 Component cleaning protocol

1. Rinse with ultrapure water.
2. Using an electric toothbrush clean the bearing surface using a solution of ultrapure water and Decon 90 detergent for 5 minutes.
3. Rinse with ultrapure water.
4. Vibrate in ultrasonic tank in ultrapure water for 10 minutes.
5. Rinse with ultrapure water.
6. Vibrate in ultrasonic tank in a solution of ultrapure water and detergent for 10 minutes.
7. Rinse with ultrapure water.
8. Vibrate in ultrasonic tank in ultrapure water for 10 minutes.
9. Rinse with ultrapure water.
10. Vibrate in ultrasonic tank in ultrapure water for 3 minutes.
11. Rinse with ultrapure water.
12. Dry with a jet of clean nitrogen gas.
13. Soak in propan-2-ol for 5 minutes.
14. Dry with jet of clean nitrogen gas.
15. Leave to air dry for a minimum of 12 hours prior to weighing*

* Not required for current methodology

A.6 Publications

Papers

- *'Prediction of in vivo taper performance: The influence of loading and taper design variables'* Submitted to Journal of Biomedical Materials Research: Part B Applied Biomaterials, September 2017

Poster Presentations

- *'FE analysis of changes in taper to reduce corrosion in vivo'* - Annual Meeting, Orthopaedic Research Society, San Diego, California, 2017
- *'Is Increased Torque Measured At Taper Junction For Larger Head Diameters?'*- Annual Meeting, Orthopaedic Research Society, Orlando, Florida, 2016

Prediction of in vivo taper performance: The influence of loading and taper design variables

H. Y. Raji[1], JC Shelton[1]

1 School of Engineering and Materials Science, Queen Mary University of London, E1 4NS, UK

ABSTRACT

The head-neck taper junction has been widely reported to corrode leading to adverse tissue reactions. Taper corrosion is a poorly understood phenomenon but has been associated with oxide layer damage and ingress of corrosive physiological fluids. Micromotion may damage the oxide layer; although little is understood about the prevailing stresses which cause this, whilst the ingress of fluid around the joint space into the taper will depend on the taper contact position and the separation of the interfaces during loading. The current work reports on the effect of taper clearances and trunnion length on the taper surface stresses and the taper gap opening. These were determined for CoCr/Ti taper interfaces using FEA under loading conditions including walking and stair climb as well as hip simulator load profiles.

Shorter trunnions and stair climb loading were shown to generate the greatest taper gaps (80μm) and also the largest surface stresses (1200 MPa) on the head taper. The largest taper gaps were associated with smaller taper contact areas. Clearances within ±0.1° had no effect on the taper gaps generated, as the tapers engaged over comparable lengths; the taper gap opening was dependent upon the taper engagement length rather than location (proximal or distal) of contact. The walking profile or variants applied by hip simulators, was insufficient to differentiate between taper designs and evaluate differences

in the magnitudes of taper gaps. The use of more demanding activity such as stair climb during *in vitro* evaluations could provide better predictions of taper performance *in vivo*.

1. Introduction

Total Hip Replacements (THRs) comprise a femoral stem connected to a spherical head which articulates with an acetabular cup. A modular femoral stem and head was introduced during the 1970s in order to introduce ceramic heads in combination with metal femoral stems (Hernigou et al., 2013), although modular THRs now widely utilise metallic heads. The head-neck junction features a Morse taper enabling the components to be held together by frictional forces, originally designed with a relatively small taper angle of 2.8° (Hernigou et al., 2013) whilst more recent designs utilise angles of 2, 5 or 8°. The precise taper angles as specified by individual manufacturers exhibit inherent variability such that a nominal taper angle of 5° may range between 5.525° and 5.975° dependant on the manufacturer (Kocagöz et al., 2013, Brock et al., 2015). Indeed, even tapers supplied from a single manufacturer exhibit head taper angles which may vary between 5.575° and 5.800° (Langton et al., 2012).

A taper junction can necessarily create a crevice between components with the potential for relative motion (micromotion) along the surfaces at the junction, resulting in mechanically assisted crevice corrosion (MACC) (Hussenbocus et al., 2015). The standard test for evaluating the components at the head-neck junction involves fretting, defined in ASTM F1875, which utilises uniaxial test rigs to apply cyclical forces to the taper junction along the taper axis. Analysis of retrieved specimens however has demonstrated toggling described as a mechanism which creates the opening of the taper junction allowing ingress of corrosive fluids (Langton et al., 2012). It indicates relative movement perpendicular to the taper surface, or taper gap opening. This mechanism has motivated an interest in evaluating tapers under moving load vectors, and the use of hip joint simulators. Such systems vary in complexity but broadly apply loads representative of those during steady state gait, although

some have simulated more demanding loading conditions involved in, for example, stair climb (Affatato et al., 2006).

There has been an increased interest in corrosion at the head neck junction as a result of the failure rates associated with large head metal-on-metal (LHMoM) devices, and other bearing material combinations (Kurtz et al., 2013, Moga et al., 2013). The severity of *in vivo* taper corrosion has been found to be mild to severe over a range of head sizes (Hothi et al., 2017, Whitehouse et al., 2015, Tan et al., 2015). Research has focused on issues related to taper surface topography, assembly conditions, trunnion flexural rigidity and changes in taper geometry (Morlock et al., 2016, Jacobs, 2016, Hussenbocus et al., 2015).

Machined profiles on trunnions used with ceramic heads were introduced to reduce tensile stresses at the taper interface (Drouin and Cales, 1994), but trunnions with threaded stems are now commonly mated with either ceramic or metal head tapers (Arnholt et al., 2014, Munir et al., 2013). In addition surgical factors such as low impaction force (less than 4 kN), off-axis impaction and taper contamination coupled with an increase in trunnion flexibility, due to the use of lower elastic modulus alloys, have all been reported to facilitate crevice corrosion (Lavernia et al., 2009, Jauch et al., 2011, Rehmer et al., 2012, Jauch-Matt et al., 2017, Brock et al., 2015, Porter et al., 2014). Taper geometry itself has evolved, including a reduction in both taper diameter and trunnion length (Morlock, 2015, Pastides et al., 2013, Langton et al., 2012). The reduction in taper length from 20 mm to below 10 mm has resulted in an increased impingement-free range of motion (ROM) although it has also reduced the surface area available for taper contact (Langton et al., 2012, Panagiotidou et al., 2015). This change is reported to reduce the stability of the taper and increase relative motion of the mating taper under load (Hussenbocus et al, 2015). Instability at the taper, resulting from suboptimal contact, leads to the possibility of gaps forming at the taper junction (Parekh et al., 2016). Indeed, Grostefon and Nelson (2017) have recently demonstrated that fluid ingress-egress is an important process in the so-called MACC by

demonstrating that the presence of a sealant resulted in no change in corrosion currents for CoCr/Ti tapers.

Taper clearance, also known as angular or taper mismatch, is the difference between the head and trunnion taper angles. A positive difference results in the taper components engaging towards the closed end of the taper (termed proximal or throat contact), leaving it is readily open to the joint environment (Figure 1). The reverse case generates distal or mouth contact with taper engagement occurring towards the open end of the junction. Under a loading condition such that the vector changes direction relative to the taper, both proximal and distal contact conditions could result in separation at the taper junction and subsequent ingress of corrosive fluids into the taper. Fluid ingress in conjunction with hypoxic conditions prevalent at the junction would exacerbate corrosion (Collier et al, 1991). Thus, a taper junction that does not permit fluid ingress may be considered a desirable design feature. Despite their apparent importance, no standard has been developed for the control of taper clearances. Indeed ASTM F1636-95e2 with specifications covering the dimensions and tolerances of male and female tapers was withdrawn with no replacement (Parekh et al., 2016, Ashkanfar et al., 2017). In a retrieval analysis of THRs Kocagöz et al. (2013) reported a taper clearance range of ±0.125° while there is anecdotal evidence that clinically, values up to 0.2° are possible. The impact of clearances has been evaluated with respect to interface micromotion and stresses, establishing that within a relatively narrow (±0.015°) clearance, the interface micromotion, or fretting, did not change between proximal and distal contacts (Parekh et al. 2016).

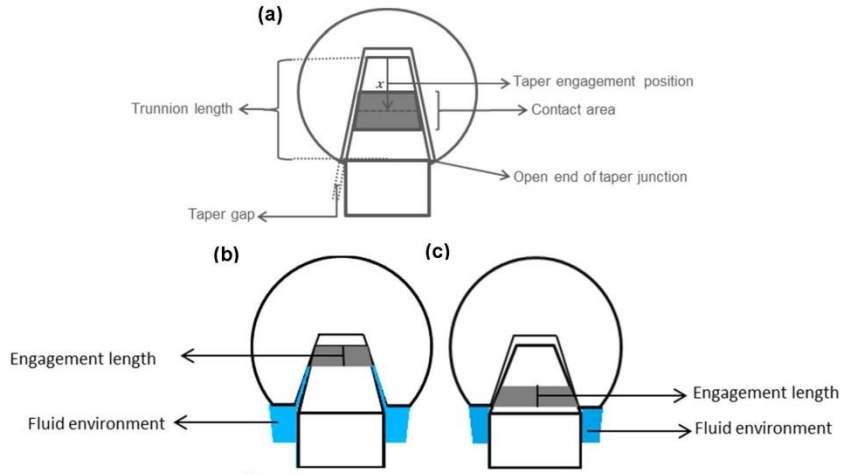

Figure 1 Schematic of taper junctions showing (a) taper contact variables, and contact regions described as (b) proximal and (c) distal

.

The current study is designed to evaluate the effects of loading and clearances on the taper gap formation and surface stresses at the taper junction, using a computational approach. This can inform taper design and evaluation of taper performance, with recognition of the parameters that may influence corrosion. The influence of varying taper clearance on gap formation, defined as the relative movement at the entry of the taper interface normal to the taper surface (Figure 1), which may influence fluid ingress, has not been previously studied. This leads to the following test hypotheses namely: (i) low taper clearance and distal contact can generate conditions which would reduce corrosion (ii) loading profiles applied by a hip simulator can create toggling at the taper junction.

2. Method

2.1 Model

A 3D FE model of a 40 mm (+0 mm head offset) CoCrMo head and a Titanium alloy trunnion was created using Abaqus/CAE 6.14-1. The components of the model were assigned individual material properties, as indicated in Table 1, and meshed using 2nd order tetrahedral elements (C3D10). An approximate mesh density of 0.19 mm^3 was found to provide convergence for all test conditions. The contact interaction between the head taper and trunnion was modelled using a finite sliding formulation with a surface-to-surface discretisation and a constant friction coefficient of 0.21 (English et al, 2016).

Table 1 Material properties used in the FE model

Part	Material	E / MPa	v	ρ / kgm^{-3}
Femoral head	CoCrMo	230 000	0.30	8290
Trunnion	Ti-6Al-4V	116 000	0.31	4430

2.2 Loading conditions

A load of 4 kN was applied to a node on top of the femoral head to mate the taper (Figure 2a) followed by functional loads representative of activities of daily living as well as profiles applied by commercial hip simulators. When loading was applied, the trunnion base (Figure 2a) was constrained in all 6 degrees of freedom over an area of 115 mm^2.

Four load profiles were modelled; 'walking' and 'stair climb' loading profiles were representative of activities of daily living measured by an instrumented THR implant (Hadley, 2012). The 'orbital hip sim' load profile represented the loading cycle applied by an orbital hip simulator which undergoes biaxial rocking motion with angular displacements in flexion/extension (F/E) and abduction/adduction (Abd/Add) (Essner and Wang, 2010). The 'prosim' load profile simulated the loading profile exerted by a hip simulator which applies dual axes rotations, namely, F/E and internal/external rotation (IER) (Hadley et al., 2013). The loads for each of these profiles were applied to a reference point, coupled to the head

taper and trunnion surfaces, located in the centre of the head (English et al., 2016) (Figure 2b). For all loading conditions, the assembly was constrained by creating a second reference point in the head centre, constraining it in 3 degrees of translation (U_1=U_2=U_3=0) and kinematically coupling it to the bearing surface of the femoral head, thereby precluding the need to include an acetabular liner in the model (English et al., 2016).

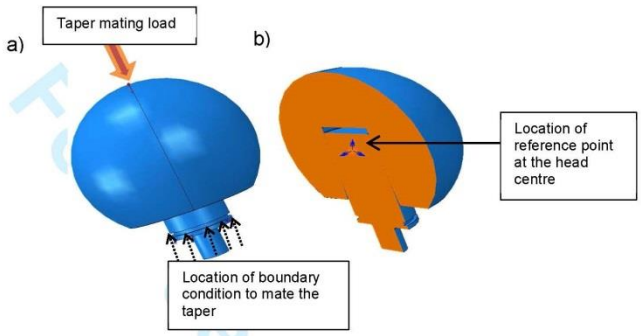

Figure 2 Location of loads and boundary conditions on the model

2.3 Variation of taper gap with activities

The gap formed at the junction for 9 trunnion angles (5.46° - 5.74°) paired with a female taper at 5.76° was evaluated for loading activities simulating a: (1) walking cycle, (2) profile of a walking cycle applied by hip simulators and (3) stair climb (Figure 3). The taper angular variations chosen were representative of commercially available designs reported in the literature (Kao et al., 2016, Triantafyllopoulos et al., 2016, Kocagöz et al., 2013, Langton et al., 2012, Hernigou et al., 2013, Brock et al., 2015). A maximum taper gap was defined as the maximum normal separation between the two taper contact surfaces, measured at the open end of the taper junction over a load cycle, Figure 1. Mean contact areas under loading and the peak von Mises stresses on the surface of the head and trunnion were compared for the different activities. The contact area was defined as the sum of regions on the surface elements at the taper interface for which there was a contact force. This was recorded

following mating of the taper as well as determining the mean contact area over the entire loading cycle.

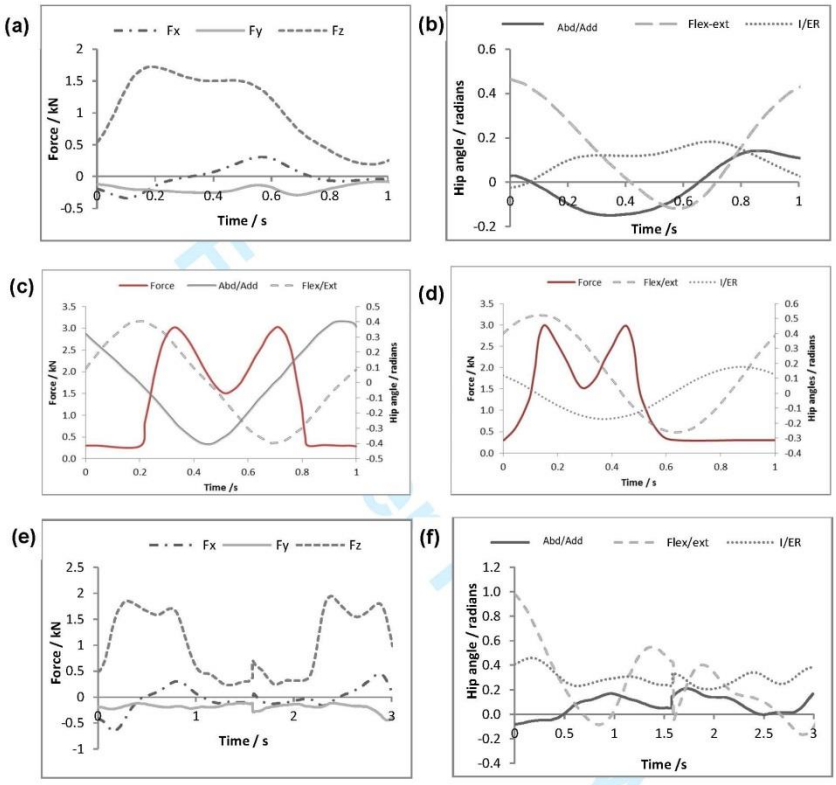

Figure 3 Forces and rotations applied to the femoral head during the simulation of (a and b) walking (c) Orbital Hip simulator (d) Prosim and (e and f) Stair climb (Hadley, 2012)

2.4 Effect of trunnion length taper angles and clearances on taper gap

The taper gap generated was evaluated for 3 representative trunnion lengths, namely 10.5, 13.5 and 18 mm, Kao et al. (2016). The taper angles were kept constant using the same female taper angle of 5.76° (with a 40 mm head diameter) and a male taper angle of 5.66°. Each taper was subject to the range of loading profiles, described in section 2.3.

The effect of taper design on the taper gap using only stair climb as the functional activity was compared for the 2, 5 and 8° tapers at a range of angular clearances 0.02 – 0.28° (Figure 4). The variables evaluated were taper gap and taper engagement position, the latter defined as the distance between the top of the trunnion and the midpoint of the resultant contact region after the taper was mated (Figure 1).

Comparisons between proximal and distal taper contact were modelled using clearance angles of -0.02° to -0.25°on a single 5.76° head taper under stair climb loading conditions only.

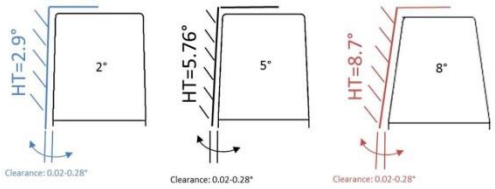

Figure 4 Schematic representation of taper angles and clearances modelled HT= head taper

3. Results

3.1 Effect of activity on taper gap and surface stresses

Changing the taper clearances led to a range of contact areas as indicated in Figure 5. There was a clear reduction in mean contact area at the taper junction following loading conditions of both simulated stair climb and walking compared to the contact area after the taper was mated. By contrast, the hip simulator conditions resulted in either an equivalent or an increase in the mean contact area (Figure 5). The contact area at the taper interface developed with stair climb loading, displayed an asymmetric contact pattern (Figure 6a) while during walking an axisymmetric profile was evident (Figure 6b). The mean contact area was positively correlated to the contact area of the mated taper (Figure 7a). Stair climb loading created the largest gap and the smallest area at the largest taper clearance of 0.28° (Table 2). When compared across the taper clearances modelled with the 5.76° head taper, it was observed that there was an inverse relationship with the taper gap formed (Figure 7b).

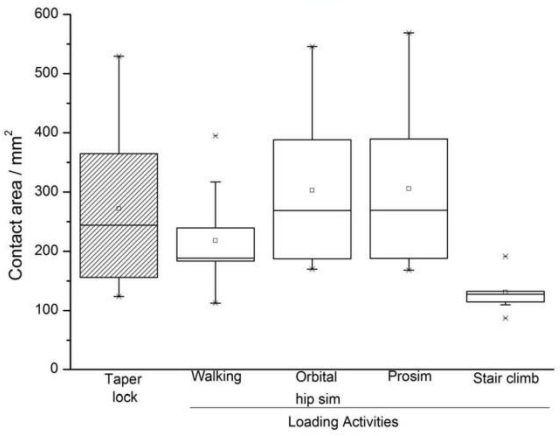

Figure 5 Influence of loading on the mean contact area after a loading cycle compared to the contact area generated at taper lock, presented for all taper clearances

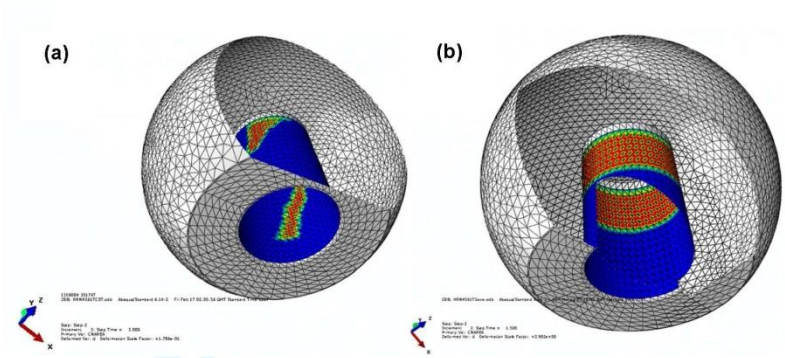

Figure 6(a) Asymmetric contact area on the femoral head during stair climb (b) Axisymmetric contact area under 'walking' load profile (similar contact pattern for both simulator profiles)

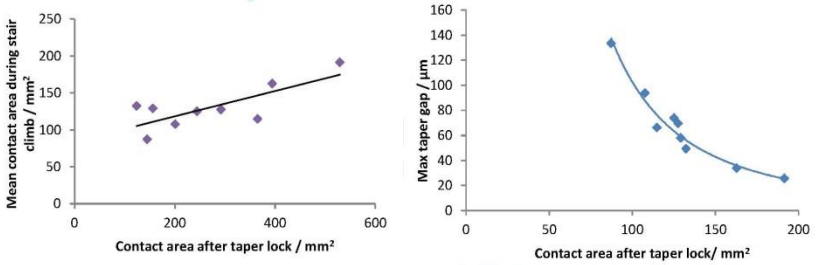

Figure 7 Relationships developed under simulated stair climb loading for a) contact area once the taper was mated with mean contact area at the taper junction after taper lock for all 5° proximal taper contact conditions (b) maximum gap developed at the taper junction with mean contact area after taper lock for all taper clearances for a 5.76° head taper

Stair climb loading resulted in elevated surface stresses on the head taper compared to the other loading conditions (Table 2). The mean peak surface stresses at the trunnion were two orders of magnitude lower than the mean peak female head taper stress. Further, it was observed that the plane of the maximum taper opening was the same as that of the highest surface head taper stresses. This, combined with the asymmetric contact pattern at the junction indicated that a toggling mechanism was being simulated.

Table 2 Results for proximal taper contact conditions

Activity	Max von Mises stress / MPa		Max taper gap / μm	Mean contact area / mm^2
	Head taper	Trunnion		
Walking	250	86	13	219
Orbital hip sim	138		9	303
Prosim	107		9	306
Stair climb	950		67	131

3.2 *Influence of trunnion length on taper conditions*

Under walking and hip simulator loading profiles, the shortest trunnion length generated the lowest taper gap for the three trunnions evaluated with comparable head taper stresses and contact areas. In comparison, under stair climb loading, the shortest trunnion generated a considerably larger maximum taper gap and peak head taper stress than the longer trunnions as well as the lowest contact area (Figure 8).

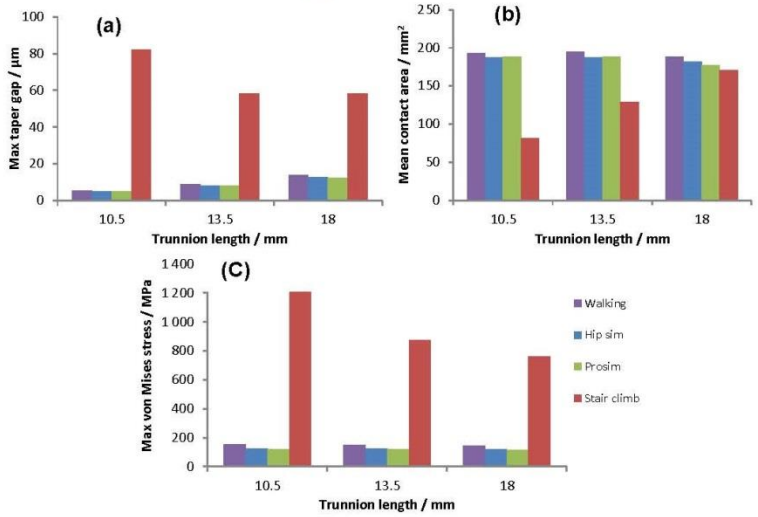

Figure 8 Effect of trunnion length on (a) maximum taper gap (b) corresponding contact area under physiological walking, 2 hip simulator profiles and stair climb activity (c) maximum surface stress at the head taper. All data relates to a taper assembly with a head taper angle of 5.76° and a trunnion angle of 5.66°, utilising a clearance of 0.1°

3.3 *Influence of taper clearance on engagement position and taper gap*

The taper engagement position, evaluated under stair climb loading, showed that for each of the 3 taper angles modelled, the more distal the taper engagement position, the smaller the maximum taper gap generated, Figure 9.

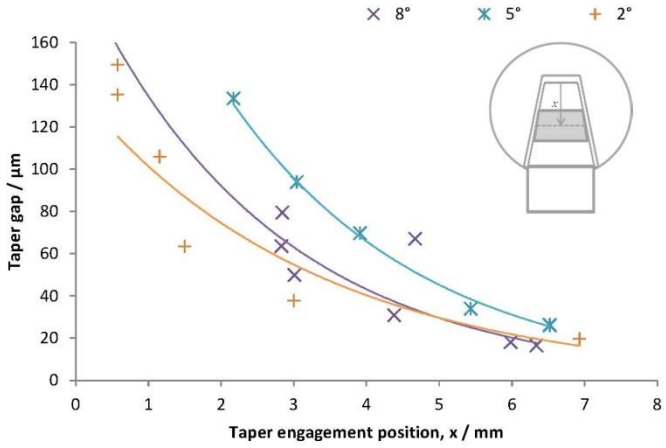

Figure 9 Relationship between taper engagement position and taper gap under stair climb loading for proximal contact angles

3.4 *Variation in taper gap under proximal and distal contact conditions*

Gaps were generated at the taper under both proximal and distal contact conditions under stair climb loading. The maximum taper gap generated reduced with the taper clearance for both contact conditions along with the taper engagement lengths (Figure 10). Within a range of ±0.1°, similar gaps were generated because the tapers engaged over comparable lengths.

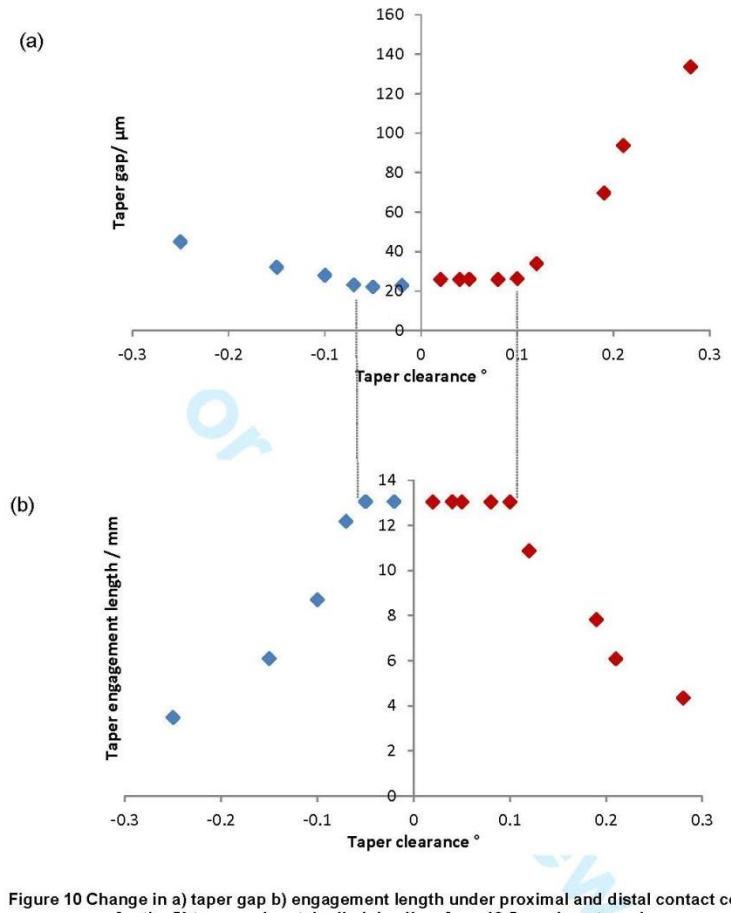

Figure 10 Change in a) taper gap b) engagement length under proximal and distal contact conditions for the 5° taper under stair climb loading, for a 13.5 mm long trunnion

4. Discussion

The FE modelling approach has proved successful in evaluating the effects of loading and taper clearances on both gap formation and surface stresses. The findings can be related to previously reported experimental and clinical findings. As an example, in retrieval studies (Hothi et al 2017) toggling has been demonstrated to both allow fluid ingress and produce 'tilting' of the trunnion in the head taper thus generating high surface stresses which exacerbates the potential for corrosion (Chu et al., 2000). In the present work evidence of the simulation of conditions that produce a toggling effect were observed in tapers. A large range of gap opening values (9 – 150 μm) at the mouth of the tapers were observed depending on factors associated with trunnion length, taper engagement position, taper angle and taper clearance. Significantly the effects were greatest under the simulated conditions of stair climbing.

It has been well established that orthopaedic metals develop corrosion resistant thin passive oxide layers (of the order of 1 – 4 nm) (Mali, 2016, Goldberg and Gilbert, 1997). However if this layer is compromised in a biological environment, the rate of corrosion can be increased by a factor of 10^8 (Goldberg et al., 2002). Although the premise of MACC is that micromotion due to cyclic loading, may abrade or fracture these oxide films (Gilbert et al., 1993), little is understood about these stress-induced mechanisms. The elevated von Mises surface stresses established in the present work on the head taper (Figure 8c) may create the conditions where this oxide layer is compromised thereby exposing the underlying metal to the corrosive fluid which penetrates the taper junction. The introduction of rougher trunnions may further raise concerns about fracture of the oxide layer by increasing local surface stresses due to the surface peaks at the head taper; a multiscale FE study (Lundberg et al., 2015), confirmed that the largest stresses were observed at the peaks of surface topography features. Further, the study established that trunnion stresses did not change substantially under either loading or design variations. This implies that whereas, changing conditions at the taper could have a detrimental impact on the passive layer on the

head taper, the trunnion oxide layer may remain intact. This could provide an explanation for why head tapers are seen to corrode preferentially over trunnions in retrieved components (Higgs et al., 2013).

The use of a simulated walking cycle load on a hip simulator is advantageous in order to evaluate the response of a taper junction under a changing load vector. However, the present work has suggested that this loading condition may not provide a complete evaluation. Indeed while the walking cycle can be successfully used to estimate bearing surface wear, it is not capable of discriminating between different taper designs. For this a more challenging activity is required, for example stair climbing with its inherent inclusion of torsional loading (Bergmann et al, 2001), which has previously been reported to differentiate the stability of different designs of cemented stems in the laboratory (Kassi et al., 2005). In the current study, stair climb generated the largest taper gaps and maximum surface von Mises stresses at the head taper (Table 2), as well as generating a movement that could be interpreted as representing toggling at the taper junction.

Trunnion lengths have been reduced in current modular THRs providing impingement free range of motion (ROM) (Langton et al., 2012, Oehy and Bider, 2004). However, shorter trunnions have been reported to be associated with increased corrosion at the taper junction particularly at their base, which may be attributed to increased stresses at this location (Tan et al., 2015, Langton et al., 2012). The results of the present study showed that for a constant head and trunnion angle, the stresses at the base of the shortest trunnion were indeed the largest and that under stair climb, the shortest taper (10.5 mm) produced a large taper gap and the highest maximum von Mises surface stresses (Figure 8) raising concerns about short trunnion designs.

Engineering drawings of tapers specify gauge points coincident on both male and female tapers. Although it is assumed that the taper will engage at this location, it is not known where the taper will engage after surgical impaction, due to manufacturing tolerances which

lead to variability. The original design of tapers using ceramic heads was implemented for proximal contact to prevent large tensile stresses thereby reducing the risk of head fracture (Cales and Stefani, 1998). However, metal taper junctions can be designed to engage distally (Kocagöz et al., 2013). The present findings indicate that regardless of taper angle, moving the taper engagement point more distally, reduced the gap formed at the distal taper (Figure 9). This arrangement reduces the transport of fluid into the junction and thereby would minimise corrosion when compared to a more proximally contacting taper.

Retrieval analysis has not found any correlation between taper clearance and damage due to fretting (Kocagöz et al., 2013), although this may be due to the multiple factors that influence conditions in THRs. Under certain clearances, both proximal and distal contact conditions generate similar taper gaps if the length over which the taper engages is equivalent. Consequently, for the 5° tapers modelled in this study, a clearance of up to 0.1° maximised the engagement along the length of the trunnion, and thereby retained a maximum taper gap of approximately 20 μm. Ashkanfar et al. (2017) concluded that a similar taper mismatch (no more than 6´ (0.1°)) would minimise taper wear. In the present work increasingly negative clearances resulted in increasing taper gaps (Figure 10a) as a result of the toggling mechanism which reduced contact area at the taper junction (Figure 11) and thus increased the maximum taper gap generated under stair climbing. This would be interpreted as detrimental to the likely taper performance.

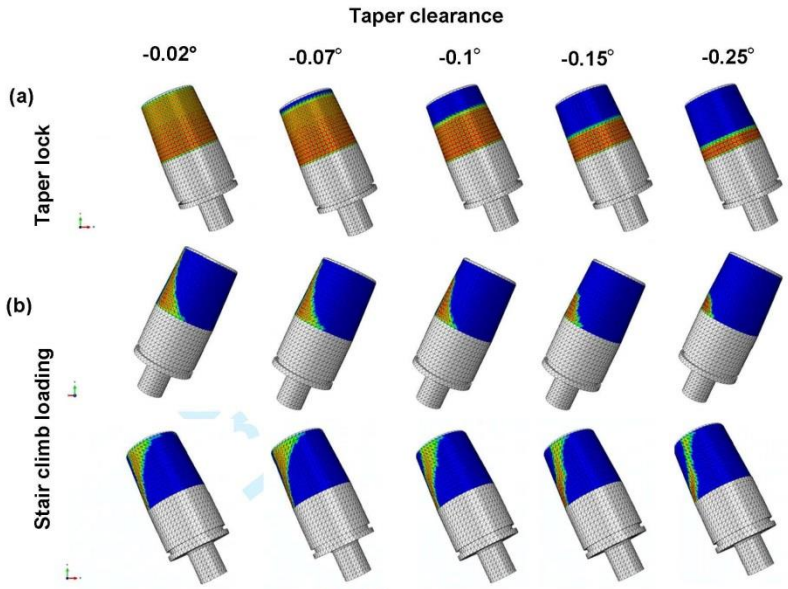

Figure 11 Change in contact area distribution from (a) symmetric after taper lock to (b) asymmetric under stair climb loading for the 5° taper with negative taper clearances

Maximising the engagement length at a taper junction, thereby maximising the contact area, reduces the gaps that may be developed during physical activity. Increased contact area over the taper junction has been reported to be beneficial as it increases the stability at the taper junction (Hussenbocus et al., 2015). However, there has been no design limit for the contact area formed at the taper junction. A 1995 FDA recommendation for ceramic head tapers suggested that a stem taper must be in direct contact with at least than 50% of the vertical length of the taper (FDA, 1995). Yet, in a study assessing the contact area at the taper interface, the proportion of area in contact for a 11 mm long trunnion, 12/14 taper was reported to be less than 20 % even utilising impact loads of 8 kN (Witt et al., 2015). These values are analogous to the contact area generated following mating reported in the current study but do not represent the contact area that may occur during loading. However, the contact area under loading was found to be directly proportional to the area after taper mating under the most severe loading condition (Figure 7). Accordingly, it may be deduced that the FDA recommendation would result in a contact area of 130 mm^2 whilst a 20 % area in contact at a mated taper interface could result in a contact area of 100 mm^2. These values would be predicted to generate taper gaps of over 50 μm. Further experimental work is required to understand whether a threshold value of maximum taper gap generation under loading could reduce the onset of corrosion.

5. Conclusions

Consideration of design features at the taper junction is important if hip implants longevity is to be improved. The application of a single axis load vector along the taper axis as applied in the ASTM F1875 fretting test does not generate taper gap opening. In the current work, even the standard walking profile, or its simplified variants, has been shown to be insufficient to differentiate features that occur at taper junctions with relevant taper design variables. The mechanism that could be described as toggling was simulated during stair climb loading, as shown by differentiated maximum taper gap opening values and high localised von Mises surface stresses on the trunnion. The taper mean contact area may

provide a design criterion that can indicate taper performance; contact areas below 220 mm^2 over a stair climb loading cycle, lead to large gaps at the distal taper junction, may be detrimental to taper performance. The taper gap opening is dependent on the length over which the taper engages and not its location of contact i.e. proximal or distal; for 5° tapers, the engagement length was maximised and thus taper gap minimised within a clearance range of ±0.1°. These findings are significant in the future design evolution of taper junctions for use in the orthopaedic industry and their evaluation prior to implantation, impacting significantly on the benefits for patients.

AFFATATO, S., LEARDINI, W. & ZAVALLONI, M. 2006. Hip Joint Simulators: State of the Art. *In:* BENAZZO, F., FALEZ, F. & DIETRICH, M. (eds.) *Bioceramics and Alternative Bearings in Joint Arthroplasty.* Steinkopff.

ARNHOLT, C. M., MACDONALD, D. W., TOHFAFAROSH, M., GILBERT, J. L., RIMNAC, C. M., KURTZ, S. M., KLEIN, G., MONT, M. A., PARVIZI, J., CATES, H. E., LEE, G.-C., MALKANI, A. & KRAAY, M. 2014. Mechanically Assisted Taper Corrosion in Modular TKA. *The Journal of Arthroplasty,* 29, 205-208.

ASHKANFAR, A., LANGTON, D. J. & JOYCE, T. J. 2017. A large taper mismatch is one of the key factors behind high wear rates and failure at the taper junction of total hip replacements: A finite element wear analysis. *Journal of the Mechanical Behavior of Biomedical Materials,* 69, 257-266.

ASTMF1875 1998. Standard Practice for Fretting Corrosion Testing of Modular Implant Interfaces: Hip Femoral Head-Bore and Cone Taper Interface. West Conshohocken, PA: ASTM International

BROCK, T. M., SIDAGINAMALE, R., RUSHTON, S., NARGOL, A. V., BOWSHER, J. G., SAVISAAR, C., JOYCE, T. J., DEEHAN, D. J., LORD, J. K. & LANGTON, D. J. 2015. Shorter, rough trunnion surfaces are associated with higher taper wear rates than longer, smooth trunnion surfaces in a contemporary large head metal-on-metal total hip arthroplasty system. *Journal of Orthopaedic Research,* 33, 1868-74.

CALES, B. & STEFANI, Y. 1998. Risks and advantages in standardization of bores and cones for heads in modular hip prostheses. *Journal of Biomedical Materials Research,* 43, 62-8.

CHU, Y.-H., ELIAS, J. J., DUDA, G. N., FRASSICA, F. J. & CHAO, E. Y. S. 2000. Stress and micromotion in the taper lock joint of a modular segmental bone replacement prosthesis. *Journal of biomechanics,* 33, 1175-1179.

DROUIN, J. M. & CALES, B. 1994. Yttria-Stabilized Zirconia Ceramic for Improved Hip Joint Head *In:* ANDERSSON, O. H., HAPPONEN, R.-P. & YLI-URPO, A. (eds.) *Bioceramics* Oxford: Butterworth-Heinemann Ltd.

ENGLISH, R., ASHKANFAR, A. & ROTHWELL, G. 2016. The effect of different assembly loads on taper junction fretting wear in total hip replacements. *Tribology International,* 95, 199-210.

ESSNER, A. & WANG, A. 2010. Tribological Assessment of UHMWPE in the Hip. *In:* KURTZ, S. M. (ed.) *UHMWPE Biomaterials Handbook - Ultra-High Molecular Weight Polyethylene in Total Joint Replacement and Medical Devices* Elsevier.

FDA 1995. Guidance Document for the Preparation of Premarket Notification for Ceramic Ball Hip Systems. Rockville, MD.

GILBERT, J. L., BUCKLEY, C. A. & JACOBS, J. J. 1993. In vivo corrosion of modular hip prosthesis components in mixed and similar metal combinations. The effect of crevice, stress, motion, and alloy coupling. *Journal of Biomedical Materials Research,* 27, 1533-1544.

GOLDBERG, J. R. & GILBERT, J. L. 1997. Electrochemical response of CoCrMo to high-speed fracture of its metal oxide using an electrochemical scratch test method. *Journal of Biomedical Materials Research,* 37, 421-31.

GOLDBERG, J. R., GILBERT, J. L., JACOBS, J. J., BAUER, T. W., PAPROSKY, W. & LEURGANS, S. 2002. A multicenter retrieval study of the taper interfaces of modular hip prostheses. *Clinical Orthopaedics and Related Research*, 149-61.

HADLEY, M., HARDAKER, C., WILLIAMS, S., JIN, Z., ISAAC, G. & FISHER, J. 2013. Development of a Stop-Dwell-Start (SDS) Protocol for In Vitro Wear Testing of Metal-on-Metal Total Hip Replacements. *In:* KURTZ, S. M., GREENWALD, A. S., MIHALKO, W. M. & LEMONS, J. E. (eds.) *Selected Technical Papers STP1560 Metal-On-Metal Total Hip Replacement Devices.* West Conshohocken, PA: ASTM International.

HADLEY, M. J. F. 2012. *Long term functional simulation of large diameter metal on metal hip implants.* PhD, University of Leeds.

HERNIGOU, P., QUEINNEC, S. & FLOUZAT, L. C. H. 2013. One hundred and fifty years of history of the Morse taper: from Stephen A. Morse in 1864 to complications related to modularity in hip arthroplasty. *International Orthopaedics,* 37, 2081-2088.

HIGGS, G. B., HANZLIK, J. A., MACDONALD, D. W., GILBERT, J. L., RIMNAC, C. M. & KURTZ, S. M. 2013. Is increased modularity associated with increased fretting and corrosion damage in metal-on-metal total hip arthroplasty devices?: a retrieval study. *The Journal of Arthroplasty,* 28, 2-6.

HOTHI, H. S., PANAGIOTOPOULOS, A. C., WHITTAKER, R. K., BILLS, P. J., MCMILLAN, R. A., SKINNER, J. A. & HART, A. J. 2017. Damage Patterns at the Head-Stem Taper Junction Helps Understand the Mechanisms of Material Loss. *The Journal of Arthroplasty,* 32, 291-295.

HUSSENBOCUS, S., KOSUGE, D., SOLOMON, L. B., HOWIE, D. W. & OSKOUEI, R. H. 2015. Head-Neck Taper Corrosion in Hip Arthroplasty. *BioMedical Research International,* 2015, 9.

JACOBS, J. J. 2016. Corrosion at the Head-Neck Junction: Why Is This Happening Now? *J Arthroplasty,* 31, 1378-80.

JAUCH-MATT, S. Y., MILES, A. W. & GILL, H. S. 2017. Effect of trunnion roughness and length on the modular taper junction strength under typical intraoperative assembly forces. *Medical Engineering & Physics,* 39, 94-101.

JAUCH, S. Y., HUBER, G., HOENIG, E., BAXMANN, M., GRUPP, T. M. & MORLOCK, M. M. 2011. Influence of material coupling and assembly condition on the magnitude of micromotion at the stem-neck interface of a modular hip endoprosthesis. *Journal of Biomechanics,* 44, 1747-51.

KAO, Y.-Y. J., KOCH, C. N., WRIGHT, T. M. & PADGETT, D. E. 2016. Flexural Rigidity, Taper Angle, and Contact Length Affect Fretting of the Femoral Stem Trunnion in Total Hip Arthroplasty. *The Journal of Arthroplasty,* 31, 254-258.

KASSI, J. P., HELLER, M. O., STOECKLE, U., PERKA, C. & DUDA, G. N. 2005. Stair climbing is more critical than walking in pre-clinical assessment of primary stability in cementless THA in vitro. *Journal of Biomechanics,* 38, 1143-54.

KOCAGÖZ, S. B., UNDERWOOD, R. J., SIVAN, S., GILBERT, J. L., MACDONALD, D. W., DAY, J. S. & KURTZ, S. M. 2013. Does taper angle clearance influence fretting and corrosion damage at the head–stem interface? A matched cohort retrieval study. *Seminars in Arthroplasty,* 24, 246-254.

KURTZ, S. M., KOCAGÖZ, S. B., HANZLIK, J. A., UNDERWOOD, R. J., GILBERT, J. L., MACDONALD, D. W., LEE, G.-C., MONT, M. A., KRAAY, M. J., KLEIN, G. R.,

PARVIZI, J. & RIMNAC, C. M. 2013. Do Ceramic Femoral Heads Reduce Taper Fretting Corrosion in Hip Arthroplasty? A Retrieval Study. *Clinical Orthopaedics and Related Research,* 471, 3270-3282.

LANGTON, D. J., SIDAGINAMALE, R., LORD, J. K., NARGOL, A. V. & JOYCE, T. J. 2012. Taper junction failure in large-diameter metal-on-metal bearings. *Bone & Joint Research,* 1.

LAVERNIA, C. J., BAERGA, L., BARRACK, R. L., TOZAKOGLOU, E., COOK, S. D., LATA, L. & ROSSI, M. D. 2009. The effects of blood and fat on Morse taper disassembly forces. *American Journal of Orthopedics (Belle Mead NJ).* 38, 187-277.

LUNDBERG, H. J., HA, N. Q., HALL, D. J., URBAN, R. M., LEVINE, B. R. & POURZAL, R. 2015. Contact Mechanics and Plastic Deformation at the Local Surface Topography Level After Assembly of Modular Head-Neck Junctions in Modern Total Hip Replacement Devices. *In:* A, G., STEVEN, K., JACK, L. & WILLIAM, M. (eds.) *Modularity and Tapers in Total Joint Replacement Devices STP1591.* West Conshohocken, PA: ASTM International

MALI, S. A. 2016. Mechanically assisted crevice corrosion in metallic biomaterials: a review. *Materials Technology,* 31, 732-739.

MOGA, I., HARRINGTON, M. A., ISMAILY, S. & NOBLE, P. 2013. Trunnion Surface Damage in THR: MPE vs MOM Articulations. *Bone & Joint Journal Orthopaedic Proceedings Supplement,* 95-B, 140.

MORLOCK, M., BÜNTE, D., GÜHRS, J. & BISHOP, N. 2016. Corrosion of the Head-Stem Taper Junction—Are We on the Verge of an Epidemic? *HSS Journal ®,* 1-8.

MORLOCK, M. M. 2015. The taper disaster - how could it happen? *HIP International,* 25, 339.

MUNIR, S., IMBULDENIYA, A. & WALSH, W. W. W. 2013. Variations in the Trunnion Surface Topography Between Different Commercially Available Hip Replacement Stems. *Bone & Joint Journal Orthopaedic Proceedings Supplement,* 95-B, 197.

OEHY, J. & BIDER, K. 2004. Design parameter to improve range of motion (ROM) in total hip arthroplasty. *In:* LAZENNEC, J. Y. & DIETRICH, M. (eds.) *Bioceramics in Joint Arthroplasty.* Springer-verlag.

PANAGIOTIDOU, A., MESWANIA, J., OSMAN, K., BOLLAND, B., LATHAM, J., SKINNER, J., HADDAD, F. S., HART, A. & BLUNN, G. 2015. The effect of frictional torque and bending moment on corrosion at the taper interface : an in vitro study. *Bone Joint J,* 97-B, 463-72.

PAREKH, J., CHAN, N. & NOBLE, P. 2016. How do positive and negative taper mismatches affect the interface mechanics of modular head-neck junctions? *Bone & Joint Journal Orthopaedic Proceedings Supplement,* 98-B, 86.

PASTIDES, P. S., DODD, M., SARRAF, K. M. & WILLIS-OWEN, C. A. 2013. Trunnionosis: A pain in the neck. *World Journal of Orthopedics,* 4, 161-6.

PORTER, D. A., URBAN, R. M., JACOBS, J. J., GILBERT, J. L., RODRIGUEZ, J. A. & COOPER, H. J. 2014. Modern Trunnions Are More Flexible: A Mechanical Analysis of THA Taper Designs. *Clinical Orthopaedics and Related Research,* 472, 3963-3970.

REHMER, A., BISHOP, N. E. & MORLOCK, M. M. 2012. Influence of assembly procedure and material combination on the strength of the taper connection at the head-neck junction of modular hip endoprostheses. *Clinical Biomechanics (Bristol, Avon),* 27, 77-83.

TAN, S. C., TEETER, M. G., DEL BALSO, C., HOWARD, J. L. & LANTING, B. A. 2015. Effect of Taper Design on Trunnionosis in Metal on Polyethylene Total Hip Arthroplasty. *The Journal of Arthroplasty,* 30, 1269-1272.

TRIANTAFYLLOPOULOS, G. K., ELPERS, M. E., BURKET, J. C., ESPOSITO, C. I., PADGETT, D. E. & WRIGHT, T. M. 2016. Otto Aufranc Award: Large Heads Do Not Increase Damage at the Head-neck Taper of Metal-on-polyethylene Total Hip Arthroplasties. *Clinical Orthopaedics and Related Research,* 474, 330-338.

WHITEHOUSE, M. R., ENDO, M., ZACHARA, S., NIELSEN, T. O., GREIDANUS, N. V., MASRI, B. A., GARBUZ, D. S. & DUNCAN, C. P. 2015. Adverse local tissue reactions in metal-on-polyethylene total hip arthroplasty due to trunnion corrosion. *Bone & Joint Journal,* 97-B, 1024.

WITT, F., GUHRS, J., MORLOCK, M. M. & BISHOP, N. E. 2015. Quantification of the Contact Area at the Head-Stem Taper Interface of Modular Hip Prostheses. *PLoS One,* 10, e0135517.

Source of funding:

Corin Group plc sponsored PhD studentship for HY Raji

FE Analysis of Changes in Taper Design to Reduce Corrosion *in vivo*

Halimat Y. Raji[1], Julia C. Shelton[1]
[1]Queen Mary University of London, UK

Disclosures: Corin Group plc, MatOrtho Ltd

INTRODUCTION

Modularity in total hip replacements (THRs) facilitates the management of individual patient variability. However, the head-neck taper junction has been widely reported to corrode leading to adverse tissue reactions [1]. Passivating oxide films, typically of the order of 5-70 Å, provide a kinetic barrier to corrosion [2] but mechanically assisted crevice corrosion theory suggests that micromotion damages the oxide layer causing corrosion if fluid ingress into the taper occurs [3]. Although it is believed that fretting and micromotion may abrade or fracture oxide films, little is understood about the prevailing stresses which cause this. Further, the ingress of fluid around the joint space into the taper will depend on the taper contact position and the separation of the interface during loading. *In vivo* taper corrosion could be reduced by reducing surface stresses on the head taper and designing the taper to engage distally. The aim of this study is to consider taper design parameters to reduce taper gap opening and maximise distal taper contact area.

METHOD

FE analysis was carried out on a 40 mm CoCr femoral head (E=230 GPa, ν=0.3) and 17-4 SS trunnions (E=200 GPa, ν=0.29) at varying taper angles using Abaqus CAE 6.14-1. A 4 kN impact load was applied instantaneously along the taper axis to lock the taper [3]. A vertical load combined with rotations representative of flex/ext and abd/add (as shown in fig 1) were applied to the head. The loading point was coupled to the trunnion [4]. 9 taper combinations (first number represents the head taper angle and the second the trunnion angle) were modelled: (i) 5.73°,5.71° (ii) 5.76°,6.66° (iii) 5.76°,7.66° (iv) 5.76°,8.66° (v) 5.76°,5.66° (vi) 5.78°,5.66° (vii) 5.79°,5.66° (viii) 5.79°,5.64° (ix) 5.81°,5.63°. The head and trunnion were meshed with 2nd order tetrahedral elements (C3D10). The taper contact was modelled as finite sliding using the penalty contact formulation and a friction coefficient of 0.21 [3]. The variables of interest were taper gap (separation of taper surfaces), maximum contact area and von Mises stresses at the taper surface.

RESULTS

The first 4 taper combinations listed resulted in distal contact with a mean maximum contact area of 314 mm^2 compared to 209 mm^2 for proximal contact. Femoral head taper stresses were seen to reduce with increase in contact area whereas the trunnion stresses remained largely the same (fig 2). Also, progressing from distal to proximal contact led to increasing gap opening between the taper contact surfaces (fig 3).

DISCUSSION

The results showed that a more proximal contact at the taper increases the taper gap generated during physiological loading (fig 3). As such, a proximally contacting taper may be more likely to corrode since the junction is open to fluid ingress. However, there has been no difference in fretting corrosion reported between taper contact conditions [6]. Thus, taper corrosion is possibly not a function of contact position alone but rather contact position in combination with contact area. It has been suggested that increased surface stresses at the taper could damage the oxide layer of the interface materials at the junction [7]. Increasing the contact area at the taper will potentially prevent the damage to the oxide layer at the head taper since it results in reduced stresses as shown in fig 2. Therefore, it is reasonable to prescribe that the worst condition at the taper junction is a proximally contacting taper with submaximal contact area and thus large head taper stresses; under such conditions, bodily fluids may enter the junction and encounter an exposed metal substrate at the head taper. In contrast, the oxide layer at the trunnion may not be compromised since surface stresses here remain constant (fig 2). This may account for the observation in retrievals where fewer trunnions corrode in comparison to head tapers. Further work is required to confirm these trends across a range of activities.

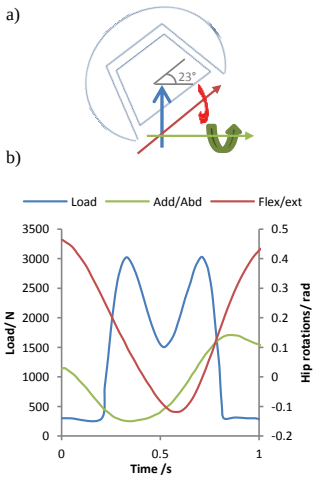

Figure 1 Load and rotations schematic (a) and variation (b)

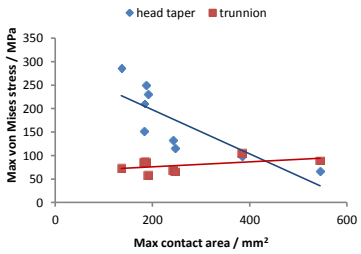

Figure 2 Relationship between maximum contact area at the taper junction and von Mises stresses at the taper surface

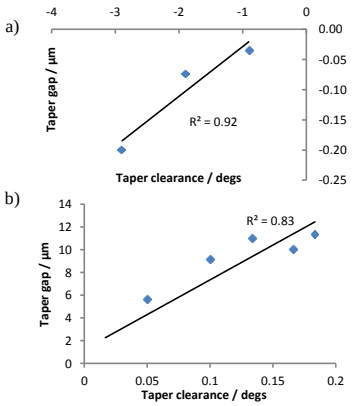

Figure 3 Variation of taper gap with taper clearance for (a) distal and (b) proximal taper contacts where taper clearance is the positive difference between head and trunnion angles

SIGNIFICANCE

A proximal taper with minimal contact area will lead to larger separation generated between the taper interface during physiological loading in addition to damaging the oxide layer; therefore exposing the substrate metal to corrosive fluid. Corrosion at the taper junction could be reduced if tapers were designed for distal contact whilst maximising contact area.

REFERENCES

1] Langton et al (2016) *BMJ Open* **6**:e007847
2] Hallab et al *(2004)* Orthopedic Applications in *ISBN 0-12-582463-7*:526-554
3] Goldberg et al (1997) *ASTM STP 1301*:157–76
4] English et al (2016) *Tribology Intl* **95**:199-210
5] Bicqué et al (2006) *Wear* **260**(3): 231-242
6] Kocagoz et al (2013) *Semin Arthroplasty* **24**(4): 246–254
7] Hothi et al (2016) *J Arthroplasty* S0883-5403(16)30327-8

Is increased torque measured at taper junction for larger head diameters?

Halimat Y Raji [1], Silvia Suñer[2], Julia C Shelton[1]
[1]Queen Mary University of London, UK, [2]Corin Group PLC

Disclosures: Halimat Y. Raji (N). Silvia Suñer (3C-Corin Group plc) Julia C. Shelton (2 - S&N, 5 – Corin Group plc)

INTRODUCTION

Torque is generated at a hip implant bearing surface during activities which load the implant, as a result of friction at the bearing surface, which is transmitted through the implant. Of particular interest is the torque generated at the head-stem taper junction; it has been suggested that this leads to instability and increased corrosion [1]. Torques generated from friction at the bearing surface have been quantified using a range of methodologies, including friction simulators. The stability of tapers has been evaluated using standard test protocols. However, the torque experienced by implants is a function of 3 axes of motion of a hip joint [2]. The friction simulator and ISO standard tests, often apply loads and motion in one plane only. The hip simulator incorporates multiple axes of motion as well as realistic dynamic loading cycles. Bearing surface torque tests have previously been evaluated in relation to either acetabular or stem loosening; the magnitude of the torque transmitted through the taper junction has not been fully evaluated. The aim of this study was to determine the influence of relevant loading and bearing design parameters on the torque transmitted through the taper.

METHOD

Testing was carried out on an orbital hip simulator (MTS Systems, USA). The acetabular cup was inclined at 35o to the horizontal and the head was mounted on a male taper which formed part of the trunnion fixture. A pair of 3 axis stacked rectangular rosettes (UFRA-1-17-3L, Technimeasure, UK) was placed diametrically opposed around the circumference of the fixture, close to the taper and coated in a polysulphide coating (M-coat-J; Vishay, UK) for moisture resistance. The -45° and 45° gauges were connected to the other pair diametrically opposite in a full bridge configuration to measure torque, whilst the vertical gauges in the rosette were connected in a half bridge configuration to measure bending. Tests were carried out on commercially available 28 and 40 mm and prototype 52 mm diameter metal on polyethylene bearings (Corin Group PLC, Cirencester, UK). Each component was subjected to a typical walking cycle with a maximum load of 3.0 kN using a lubricant of 25 % (v/v) newborn calf serum. Tests were run for 1 hour with strains recorded at 10 Hz; each test was repeated at least twice, with multiple sets of data recorded at each setup. The components were subjected to sinusoidal loads of 250 - 3850 N at rotational speeds of 5, 10, 30 and 60 rpm. Mean peak torque and peak bending moments were determined. Statistical analysis was performed using a student's t-test; significance was set at $p \leq 0.05$.

RESULTS

The mean peak torque measured on the 28, 40 and 52 mm diameter bearings was 1.95±0.25, 0.73±0.18 and 1.04±0.13 Nm respectively which were all statistically significantly different. The mean peak bending moment for the 40 and 52 mm diameter heads was 12.70 and 12.76 Nm respectively; this was not significantly different despite the change in offset. The torque increased with load (Fig. 1), although increases in rotational speed did not affect the peak torque recorded ($p > 0.05$).

DISCUSSION

Larger bending moments than torsional moments were found, in agreement with the study by Schwachmeyer et al. (2013) for patients monitored using instrumented implants, in level walking [5]. The bending moments were not significantly influenced by head. The torque obtained from this study however was an order of magnitude smaller than values previously reported for ceramic on polyethylene prostheses *in vivo* [5]. This might be explained by the absence of muscle forces underestimating torsional moments [3]. A larger head size is advantageous because it provides increased stability and range of motion, whilst providing greater entraining velocity and increasing the minimum film thickness for lubrication. However, the recent reported increase in the incidence of taper corrosion has been linked to increasing head sizes [3], which may result from the instability initiated by large torques at the taper junction, as suggested by observations from retrievals demonstrating increased corrosion scores for larger heads [4]. This study appears to support these findings for large heads. The torque for the 28 mm diameter head however was higher than the torque measured at 40 or
52 mm. This may be explained by the theoretical film thickness being an order of magnitude smaller for this head size, estimated from the Hamrock and Dowson equation [6], indicating that the lubrication regime is a more severe form of boundary lubrication, leading to an increase in torque, as shown in this study. The torque also increased with the load applied although it did not change with speed. The trend was the same for 28 mm and 52 mm heads. This could be because although the theoretical film thickness increased with speed, the lubrication regime remained as boundary lubrication. This study has evaluated torques generated during the walking cycle as well as for sinusoidal loads. To fully characterise torques around the taper junction, other activities should be considered along with other bearing designs and material combinations.

SIGNIFICANCE

This study has measured the torque adjacent to the taper junction on the hip simulator, confirming a sensitivity of the torque generated to the bearing diameter. This supports the observation that taper instability and corrosion may be attributed to torque at the taper, suggesting an optimum head size may lie close to 40 mm diameter.

REFERENCES

[1] Langton et al. 2012. *Bone and Joint Research,* 1**,** 56-63. [2] Damm et al. 2013. *PLoS ONE,* 8**,** e78373 [3] Duda et al. 2013. *In: Surgery of the Hip* [4] Dyrkacz et al. 2013. *Journal of Arthroplasty*, 28(6), 1036–1040. [5] Schwachmeyer et al. 2013. *PLoS ONE,* 8**,** e77807 [6] Scholes et al. 2003. *In:Friction, Lubrication and Wear of Artificial Joints.*

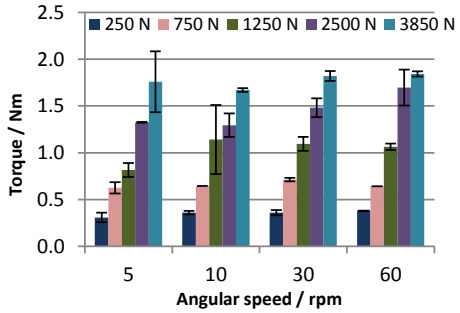

Fig 1: Max. torque developed as a function of angular speed and peak applied load, for a 52 mm MoP bearing (error bars ± SD)